An investigation into the aggregation of therapeutic peptides through adsorption to primary containers

Géraldine Yolande V Baekelandt

Newnham College

A thesis submitted for the degree of

Doctor of Philosophy

Department of Engineering

University of Cambridge

September 2019

Declaration

This dissertation is the result of my own work and includes nothing which is the outcome of work done in collaboration except as declared in the Preface and specified in the text.

It is not substantially the same as any that I have submitted, or, is being concurrently submitted for a degree or diploma or other qualification at the University of Cambridge or any other University or similar institution except as declared in the Preface and specified in the text. I further state that no substantial part of my dissertation has already been submitted, or, is being concurrently submitted for any such degree, diploma or other qualification at the University of Cambridge or any other University or similar institution except as declared in the Preface and specified in the text.

It does not exceed the prescribed word limit for the relevant Degree Committee.

- GB

Word Count: 49,795

Abstract

An investigation into the aggregation of therapeutic peptides through adsorption to primary containers.

Géraldine Yolande V Baekelandt

Therapeutic peptides are highly functional drugs currently being investigated for a number of diseases, due to their naturally occurrence in the body, their targeted mechanism and efficacy and tolerability.

The four therapeutic peptides under investigation in this thesis; glucagon, liraglutide, g797 and exendin-4 are all used or on trial for mediating blood glucose levels as a safe and effective treatment for type 2 diabetes. One of the largest drawbacks of peptides is their ability to aggregate and adsorb to surfaces that they come into contact with during their lifecycle; vials and syringes, causing loss of function, drug and toxicity.

A large, underexplored area of drug related research is investigation into the interface; in part due to its complexity. A plethora of different methods were used in order to investigate the peptide solutions ability to aggregate and adsorb to surfaces. The initial step was to investigate the stability of the four therapeutic peptides in solution, providing information on the aggregation of the peptides in bulk, investigated by the Atomic Force Microscope and Zeta Potential. Images of secondary structures formed in solution by each peptide were produced, as well as providing information on the charges of the solution and the colloidal stability, showing the need for an added lipidated chain for peptide stability.

Surface induced aggregation was then investigated through studying a variety of surfaces using the Quartz Crystal Microbalance with dissipation, giving both the wet mass adsorbed, as well as indications of the rigidity of the layer formed. The two most common surfaces used in the pharmaceutical industry; borosilicate glass and polystyrene, were amongst the surfaces investigated and were shown to cause the

highest adsorption of peptide, ranking as the least effective surfaces at preventing aggregation.

Another factor determining peptide adsorption to surfaces is roughness. Surfaces of different roughness were created through addition of gold nanoparticles, and using the QCM-D, adsorption was compared to that of flat gold surfaces. An increase of adsorption on flat surfaces compared to rougher surfaces was found, indicating a more intricate relationship than previously thought. E- beam lithography was then used to create different nanostructures on the gold surface.

Ultimately, the thesis aimed at tackling a large problem within the pharmaceutical industry, by providing alternative pathways to challenge the problem of aggregation through adsorption to primary containers.

Restriction Notice

The report contains unpublished and confidential data. Publication, duplication and transfer to third party is not allowed without permission by AstraZeneca plc.

Funding

This project is fully funded by AstraZenca Plc.

Acknowledgements

Thank you to all the wonderful people that I have met for the past four years, I would not have been able to do this without any of you. I would like to thank my supervisor, Prof Sir Mark Welland, for your expertise, and for being there when needed the most. My advisor, Dr Ana Dos Santos Gomez for being the peptide expert and giving me advice with biological systems.

Thank you to all of the Nanoscience staff, especially Sue Murkett who was always there for friendly chats and made sure the whole centre ran smoothly. To the technicians for helping me with any problems, and to always fix them quickly and with a friendly smile.

Thank you to all my nano-friends – without you the long hours at work and in the lab would have been so much more painful, and filled with a lot less laughter.

Thank you to my close family; Alex and Liz, for providing me with food and support during the most stressful times, but especially Mamie & Papie, who were always there for my highs, but mainly for my lows. Your support was exactly what I needed at the most trying times.

Thank you also to my other family; the Castle aka my kweens and Annie. You are the best friends anyone could ask for; my support system away from home, an eternally welcoming atmosphere when I needed it most.

And to two of the most important people in my life; Dr Nicole Weckman and Dr Yash Patel; without either of you I would have never made it this far. Thank you for everything.

Publications

There are currently two papers in preparation based on this thesis.

Glucagon and GLP-1 analogues adsorption to hydrophilic surfaces is determined by solution conditions, specific amino acid sequence and lipidation.' *In preparation, March 2019*

Authors: G. Baekelandt, N. E. Weckman, M. A. Bednarek, A. L Gomes Dos Santos, M. E. Welland.

'Increased surface roughness using gold nanoparticles, decreases Glucagon and GLP-1 adsorption to gold surfaces.' *In preparation, June 2019*

Authors: G. Baekelandt, J. A. Rubio, A. L Gomes Dos Santos, M. E. Welland.

Table of Contents

List of Figures

List of Tables

List of Equations

List of Abbreviations

Aβ -42 – Amyloid beta peptide (42)

AD patients – Alzheimer's Disease patients

AFM – Atomic Force Microscopy

Au – CH_3 - Functionalised gold sensor surface with hydrophobic group

Au – OH - Functionalised gold sensor surface with hydrophilic group

Au-NP – Functionalised gold sensor surface with gold nanoparticles

CMC – Critical micelle concentration

D_n – Normalized dissipation

DL – Double layer

DLS – Dynamic Light Scattering

DPI – Dual Polarization Interferometry

DPP- IV - Dipeptidyl peptidase 4

EBL – E – Beam Lithography

F_n - Normalized frequency

GLP-1 – Glucagon like peptide – 1

HAM – Hierarchal assembly model

Hb – Haemoglobin

NP – Nanoparticle

NSA – Non – specific adsorption

PC1–3 - Proprotein convertase 1

PC2 – Proprotein convertase 2

pI – Isoelectric point

PI – 3 - Phosphoinositide 3-kinase

PMMA - Poly(methyl methacrylate

PS - Polystyrene

Ra – Average roughness

RMS – Mean squared roughness

SAM – Self assembled monolayer

TD2M – Type 2 diabetes mellitus

TEM – Transmission Electron Microscopy

QCM-D – Quartz Crystal Microbalance with Dissipation

QSX 301 – Quartz crystal microbalance sensor chips, gold

QSX 303 - Quartz crystal microbalance sensor chips, silicon dioxide

QSX 305 - Quartz crystal microbalance sensor chips, polystyrene

QSX 336 – Quartz crystal microbalance sensor chips, borosilicate glass

ZP – Zeta Potential

1 Chapter

Literature Review

Therapeutic peptides are highly functional drugs which are currently being investigated for a number of diseases. Peptides are small proteins which specifically bind to cell surface receptors and act as signalling molecules between receptors. Due to their naturally occurring structure in the body, their targeted mechanism, their efficacy and tolerability, they are seen as a natural starting point for a new drug [1][2]. In fact, their tolerability in the human body is what differentiates them the most from other small chemically made molecules, and this was the initial starting point for insulin in its treatment for diabetes. Therapeutic peptides are usually seen as derivatives of one of three sources. The first being natural or bioactive peptides produced by plants, animal or human (derived from either larger protein fragments or naturally occurring peptide hormones.) (ii) Peptides isolated from genetic or recombinant libraries and (iii) peptides discovered from chemical libraries [3]. From this, more therapeutic peptides have been explored as a treatment for metabolic diseases.

Even though peptides are very effective, naturally made and hence tolerated in our body, they also have a plethora of disadvantages. The most pressing initial challenges encountered in therapeutic peptide drug development include low bioavailability, and quick renal clearance [4]. These problems have been worked on for years, and some progress has been made. However, even once the peptides have the right stereochemistry and longer half-lives, they still need to be made into a stable solution in order to be used.

The solution to be injected or administered has its own stability issues; the main one being aggregation of the peptide molecules. Aggregation is caused when the peptide molecules clump together, which occurs both in solution and on the surface interfaces [5]. Peptide aggregation in solution has been looked at in abundance by formulation chemists and biochemists, and hence peptides have been chemically changed as much as possible to limit the aggregation that they undergo in solution [6]. However, a large gap in aggregation research, is the ability of the drug to aggregate on interfaces, specifically on interfaces between the liquid peptide solution and the solid surface that they come into contact with on a daily basis, such as storage vials, and syringes [7]. It has been shown that aggregation of amphiphilic molecules on surfaces is directly linked to their ability to adsorb to the surface [8]–[10].

This chapter will give an overview of the use of therapeutic peptides in medicine and introduce several important therapeutic peptides that will be studied throughout the thesis. It will also present relevant theories underpinning the research of aggregation, adsorption and factors that facilitate these two mechanisms, and how surfaces play an important role in these biological processes.

1.1 Application of Therapeutic Peptides in Medicine

The use of therapeutic peptides in medicine and pharmaceuticals has seen a large increase over the past ten years. Peptides are seen as the answer, with billions of dollars in the glucose regulating market to try and combat diabetes, which has been steadily rising [4]. Insulin is the world's most renowned therapeutic peptide, used in the treatment of diabetes. Diabetes is a metabolic disease, defined by hyperglycaemia. There are several pathogenic processes involved in the development of diabetes, which range from resistance to the action of insulin to autoimmune destruction of the pancreatic β-cells that result in insulin deficiency [11]. In diabetes, the abnormalities in carbohydrate, fat, and protein

metabolism are due to the incomplete action of insulin on target tissues [12]. As a result of these complex mechanisms, it is usually difficult to distinguish exact causes for hyperglycaemia [13].

Insulin, which is naturally made in the body, and is a prime regulator of blood glucose in the body was seen as a natural starting point to exploring other therapeutic peptides, which play a role in blood glucose regulation [14]. Thus, therapeutic peptides, which regulate blood glucose were explored.

Due to the many advantages of therapeutic peptides, the peptide market has seen a huge increase in terms of value over the past few years. The global peptide drug market was estimated to have reached a value of US $25.4 billion in 2018 compared to US $14.1 billion in 2011, an almost 50% increase in just seven years. Notably, the category of novel innovative peptide drugs is one of the largest and is set to increase dramatically from an estimated value of US $8.6 billion in 2011 to US $17.0 billion in 2018, which would account for 66% of the peptide market globally. While the overall peptide market is steadily increasing in value, there are specific highlights in the field of lipidation of peptides. One of the most recent and relevant examples of a pioneering peptide drug class are the glucagon-like peptide-1 (GLP-1) agonists for the treatment of type 2 diabetes mellitus (TD2M) such as exendin-4 and liraglutide, whose sales totalled over US $2.6 billion in 2013 [15].

Despite the ever increasing sales numbers, peptides were not always seen as the 'holy grail' for the pharmaceutical markets. Peptides are notorious for their short half-life, as well as other physiochemical problems; largely their physical and chemical stability [16]. The principal reasons for the low oral bioavailability of peptide drugs are pre-systemic enzymatic degradation and poor penetration of the intestinal mucosa. Their in vivo plasma residence time can be increased chemically, through methods such as cyclization, bioisosteric replacement of

peptide bonds, or change of the stereochemistry of specific amino acids, and conjugation among others [17]. A very common and effective method of increasing the plasma residence time, is lipidation [18]. Lipidation of therapeutic peptides describes the process of adding a lipid group to the peptide chain in order to increase its circulation time, without hindering its therapeutic function [19]. However, lipidation does affect the hydrophobicity of the peptide, which in turn will also have a large effect on its overall properties, as will be seen in this thesis.

Another challenge of therapeutic peptides, is that they are poor candidates to move from the digestive tract to the circulatory system because of their physicochemical properties. Hence, another route of exploration is through different methods of administration of the drug [20]. Until recently, therapeutic peptides were usually administered by subcutaneous, intramuscular or intravenous routes (which inevitably cause discomfort for the patient) to circumvent the gut barrier. Consequently, alternative routes for the administration of peptide-based drugs have been improved in recent years, among which controlled release parenteral route; subcutaneous, intramuscular or intravenous or mucosal route (such as nasal spray or sublingual delivery)and transdermal route, such as patches [21]. Despite recent advances in oral delivery, the bioavailability of therapeutic peptides with these technologies is still much lower than that obtained by injection. In case of emergency, the low side effects, ease and speed of action from peptide injections is unbeaten [16].

In spite of some recent successes, the short half- life of these therapeutic peptides is still a major issue for drug companies [22][23]. However, another emerging issue is the stability of the therapeutic peptide solutions before treatment is administered [24]. This is highly dependent on both peptide structure and the surfaces and interfaces to which they are exposed, as rearrangement of peptides

occurs when in contact with surfaces, which can lead to surface induced aggregation.

Aggregates can cause loss of function of the drug, immunogenicity and other complications in the body. These side effects are undesirable, especially in therapeutic peptides used in the pharmaceutical industry. Peptides have many advantages, as described previously, over traditional medicine. Yet, much still has to be done in order to secure therapeutic peptides at the front of drug discovery. As well as calamitous side effects in the patient, aggregation of drugs also causes challenges in drug regulation, as well as a serious loss of stock and profits [25].

The following section will introduce the four peptides; glucagon, liraglutide, g797 and exendin-4 explored investigated in this thesis and their relevant applications in the pharmaceutical industry. The specific structures and amino acid sequences will be discussed in Chapter 3.

1.2 Therapeutic Peptides & Their Structure

1.2.1 Glucagon

Glucagon is a well-established therapeutic peptide in the pharmaceutical industry. Glucagon, a 29 amino amphipathic hormone, processed from proglucagon, is naturally produced in the body and is an excellent model for other therapeutic peptides [26]. Its backbone has been heavily used as a starting point for a plethora of other chemically modified peptides. The four peptides used in this thesis are all derived from a glucagon or lipidated glucagon backbone. The structure of glucagon is shown in Fig 1.1. below.

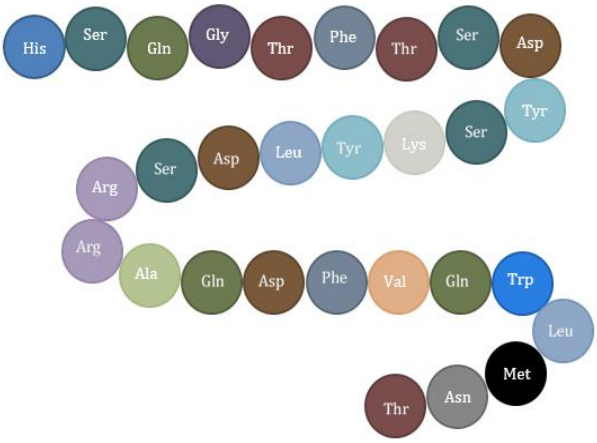

Figure 1.1: Structure of glucagon. Each amino acid is colour co-ordinated to distinguish them easily. Each individual amino acid contributes to glucagon's function as a core regulator of blood glucose in the body.

Pharmacologically, glucagon regulates blood sugar levels, in conjunction with insulin. Proglucagon, glucagons' precursor, is expressed in various tissues (such as the brain, pancreas, and intestine) and is proteolytically processed and results in multiple peptide hormones, which are tissue-specific. For example, in the intestine, proglucagon is processed into functional glucagon-like peptides-1 and -2 by subtilisin-like proprotein convertases PC1–3 in intestinal L cells [27]. In the pancreatic α-cells, proglucagon is processed into functional glucagon by PC2. Glucagon acts via a seven-transmembrane G protein-coupled receptor consisting of 485 amino acids [28]. To date, glucagon-binding sites have been identified in multiple tissues, including liver, brain, pancreas, kidney, intestine, and adipose tissues. When glucose levels are too low, glucagon is released. The first six amino acids of glucagon at the N-terminus bind to specific receptors on liver cells. This specific binding leads to the increase in cyclic monophosphate, which in turn assists the catabolism of stored glucagon and promotes gluconeogenesis and glycogenolysis. The immediate effect of this is an increase in glucose in the blood circulating the body [29][30].

Gluconeogenesis and glycogenolysis are two important mechanisms for increasing blood glucose. Gluconeogenesis is a metabolic pathway that results in the generation of glucose from non-carbohydrate carbon substrates e.g pyruvate, lactate, glycerol, and amino acids [31]. The pathway for gluconeogenesis is shown in Fig 1.2 below.

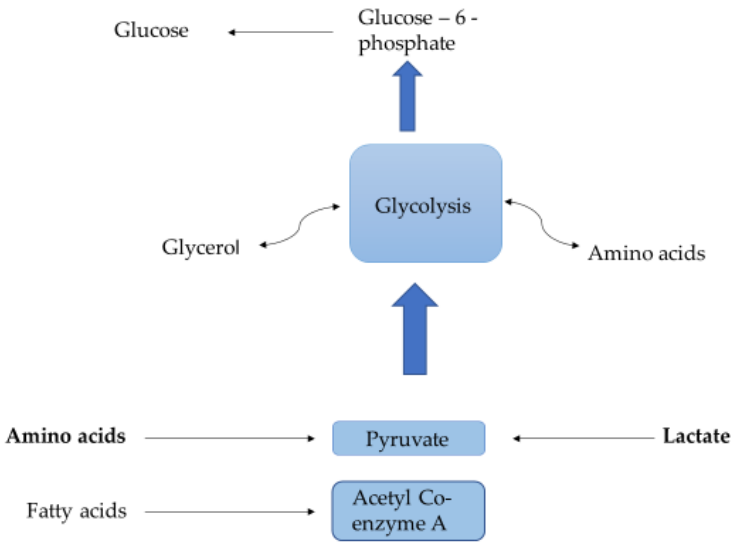

Figure 1.2: Gluconeogenesis pathway for the production of glucose from non-carbohydrate substances, in this case, amino acids, pyruvate and lactate.

Glycogenolysis is the mechanism in which glycogen is broken down into glucose-6-phosphate and glycogen. The overall reaction of this mechanism is shown below:

Glycogen(n) + Pi ↔ glycogen(n-1) + glucose-1-phosphate

The glucose-1-phosphate is firstly converted to glucose-6-phosphate by phosphoglucomutase, which is then immediately used as energy for muscle contractions [32]. This is shown in the figure below.

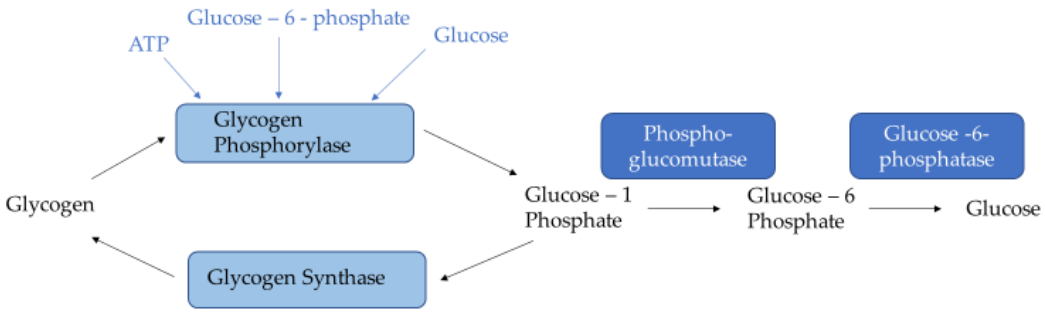

Figure 1.3: Diagrammatic representation of the glycogenolysis pathway described above. Glycogen, which is broken down through a series of biological pathways, is the starting material for glucose production.

Conversely, when glucose levels in the body are high, insulin circulation is triggered. The triggering of insulin allows glucose to be taken up and used by insulin-dependent tissues. Therefore, both glucagon and insulin are an essential part of the body's feedback system that keeps blood glucose at a stable level. This feedback system is accelerated by high stress levels and other environmental factors [33].

As well as its six amino acid sequence specific to liver cells, glucagon has a remarkable structure, which many other peptides are based on or related to and is discussed in depth in Chapter 3.

1.2.2 Liraglutide

Liraglutide, also known as Victoza, is another therapeutic peptide drug, based on the structure of glucagon like-peptide 1s (GLP-1), and a receptor agonist. GLP-1 is an aptly named glucagon – like peptide, as it is approximately 50% homologous to glucagon. GLP-1, like glucagon, also has insulinotropic activity, and is a tissue-specific posttranslational proteolytic product of the proglucagon gene that is released from intestinal L-cells in response to nutrient ingestion and enhances glucose-stimulated insulin secretion [34]. Unsurprisingly, therefore, the

closely related liraglutide peptide has been produced to combat type 2 diabetes (TD2M) via injection [35]. It's structure and added lipid chain are shown below.

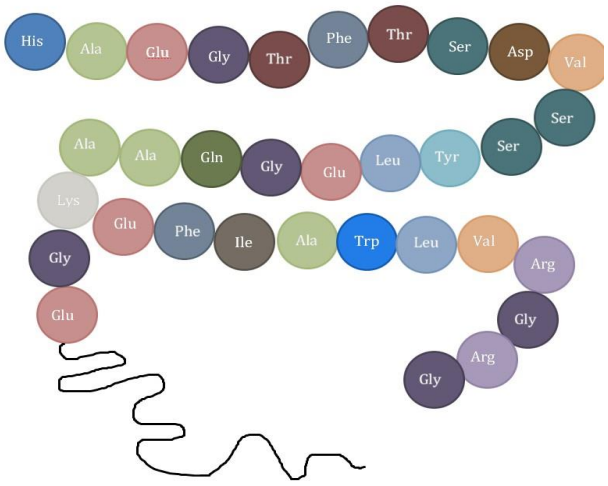

Figure 1.4: Structure of liraglutide, which has a GLP-1 backbone, with a C_{16} fatty acid chain at amino acid position 26.

Victoza, a drug produced by NovoNordisk, is currently on the market for the treatment of type 2 diabetes mellitus [36]. The current method of administration is subcutaneously, as an injection, which is one of the main drawback of therapeutic peptides, as discussed in Section 1.1.

1.2.3 Exendin-4

Exendin-4, commonly referred to as exenatide, is another therapeutic drug based on the structure of glucagon like-peptide 1s (GLP-1), and also a receptor agonist. As with liraglutide, exendin-4 also binds to the same receptors as GLP-1 does, which stimulates insulin secretion. Unsurprisingly, therefore, exedin-4 has also been commercially produced to combat type 2 diabetes (TD2M) via injection. It is sold under the brand names; Byetta and Bydureon which are produced by AstraZeneca [37]. It's amino acid sequence is shown below.

Figure 1.5: Structure of exendin-4, the largest of the therapeutic peptides investigated in this thesis, with an added 9C, referred to as the Trp cage, which stabilises the peptide.

The NMR structure of the peptide in aqueous trifluoroethanol (TFE) shows that the Trp-cage folds back onto the central helical part, forming the smallest known protein-fold which surrounds Trp25 [38].

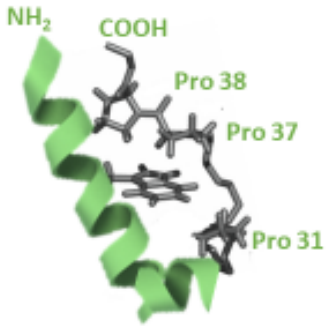

Figure 1.6: Trp cage of the exendin-4 molecule, displayed above. The NH_2 terminal and COOH terminal are labelled, and it can be seen that the molecule folds in on itself through electrostatic interactions. Adapted from [39].

Exendin-4 is a hormone found in the saliva of the Gila monster, and consists of 39 amino acids, which is slightly longer than the other GLP-1 based peptides. Exendin-4's glucose-dependent enhancement of insulin secretion can be mediated by its binding to the pancreatic GLP-1 receptor [40]. In animal models of diabetes and insulin secreting cell lines, GLP-1 and exendin-4 improved β-cell

function by increasing the expression of key genes involved in insulin secretion, and increasing insulin biosynthesis, through a PI-3-kinase mechanism [31]. This mechanism is also exendin-4's main advantage: it is resistant to degradation by DPP-IV, unlike all other peptides discussed in this thesis, which breaks down GLP-1 in mammals and is one of the main causes of short half-life of traditional therapeutic peptides.

Both liraglutide and exendin-4 (like many GLP-1 agonist receptors) have advantages over more traditional therapies for type 2 diabetes [42]: They act in a glucose-dependent manner, meaning they will stimulate insulin secretion only when blood glucose levels are higher than normal, which prevents overshoot, unlike conventional methods, where there is a risk of hypoglycaemia. Both liraglutide and exendin-4 also have the potential for inhibiting apoptosis and stimulating regeneration of β-cells (as seen in animal studies), decreasing appetite and lowering blood triglyceride levels [43].

Recently, it has been suggested that both liraglutide and exendin-4 can be used for their neuroprotective properties against Alzheimer's disease [44]. It has been shown that GLP-1 can act as a growth factor in the brain and induce neurite overgrowth to protect against oxidative injuries in neuronal cells. In addition, Abbas et al have demonstrated that the deletion of GLP-1 receptors impairs learning of new tasks [45]. As well as this concerning new evidence, there is also an indication that the deletion of GLP-1 receptors could be a factor in the development of long term potentiation of synaptic transmission in the hippocampus. Furthermore, both GLP-1 and exendin-4 have been revealed to reduce levels of beta amyloid in the brain. GLP-1 analogues have been shown to induce neuronal proliferation in mice; the increased proliferation could facilitate the reparation in neuronal networks, and therefore have beneficial effects in AD patients [46][47]. From these studies, it's evident that both these peptides are important for further investigation for a variety of different fields.

1.2.4 G797

G797 is an internally produced peptide by AstraZeneca, thanks to Dr Maria Bednarek. G797 was a peptide synthesized, as one of the many trial therapeutic peptide agents being looked at for more efficient type 2 diabetes treatment. As with the peptides mentioned above, which all aim to treat T2DM, G797 has a sequence based upon glucagon. G797 differs from the other three peptides in a few ways. Firstly, the C16 palmitoylated chain on G797 is located on its 10th amino acid, unlike liraglutide which has a side chain located on the 26th amino acid. Additionally, unlike both exendin-4 and liraglutide, the backbone of G797 is based on glucagon and not GLP-1. These differences made it a promising candidate for future therapeutic therapies. It's unique structure is shown below.

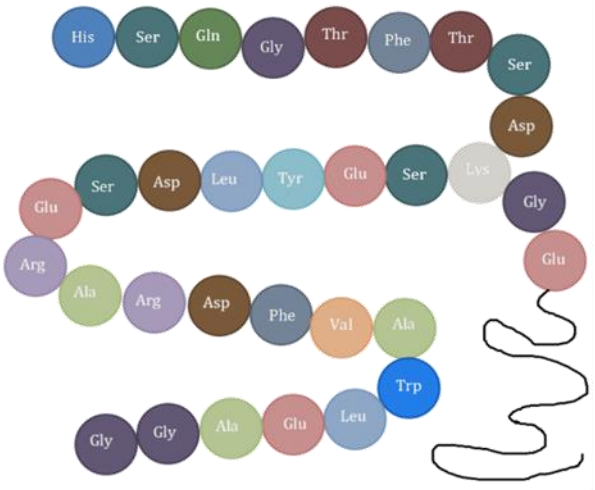

Figure 1.7: Structure of g797, with a glucagon backbone, and a lipidated palmitoyl chain (C_{16} fatty acid) at amino acid position 10, to prolong circulation in the body.

However, it should be noted that the supply of G797 was limited due to both funding and NDA issues, and hence was used both sparingly and no longer in use for Chapter 5.

The four peptides described above were the therapeutic drugs described in this thesis. All experiments were done on these four drugs, unless stated otherwise. These four peptides are crucial to the treatment of T2DM, and their interaction with solid surfaces is an area that should be explored fully in order to make a lasting impact.

1.3 Adsorption and Colloidal System

The four peptides previously described are amphiphilic molecules – they contain both hydrophilic and hydrophobic patches, depending on their amino acid sequence. The amphiphilic molecules can associate, in a dynamic and thermodynamically driven process which can be considered both a molecular solution and a true colloidal system. This makes peptides surface active agents – molecules (usually organic) that at low concentration, have the ability to adsorb at interfaces, altering the physical properties of those interfaces significantly [39]. Hence the interactions of the peptides with the solid/liquid interface are extremely interesting and require further investigation.

The adsorption behaviour of amphiphilic molecules at interfaces is attributed to the fact that they have a combination of polar and non-polar groups in one molecule. This results in the molecules, in this case the peptides, 'sitting' at the interfaces. The lyophilic moiety of the peptide remains in solution, whilst the lyophobic part positions itself away from the solvent interactions. Since water is the most common solvent, amphiphiles are usually described as having 'hydrophilic' heads and 'hydrophobic' tails [48].

The adsorption of the peptides to interfaces is associated with significant energy changes. The free energy of a peptide at the interface is lower than when the molecule is solubilised in either bulk phase. Therefore, as systems always strive towards lowest free energy, the accumulation of the amphiphile molecules at any

interface is a spontaneous process, which results in a decrease of the interfacial (surface) tension. For example, at the air–water surface, water molecules are subjected to unequal short-range attraction forces and, thus, undergo a net inward pull to the bulk phase [49].

When we consider the air–water boundary, the force driving adsorption is unfavourable hydrophobic interactions within the bulk phase, where water molecules interact with one another through hydrogen bonding [50]. As the peptides are amphiphilic, the presence of the hydrocarbon groups cause a distortion of the solvent structure, which, as stated before, increases the free energy of the system: this is known as the hydrophobic effect. In summation, both adsorption and aggregation phenomena result from the hydrophobic effect [51].

1.3.1 Micelles and Critical Micelle Concentration (CMC)

Amphiphilic peptides are capable of forming multiple different aggregation structures. One of the self-assembly structures of peptides are micelles, which form with the hydrophobic core inside, and hydrophilic moieties on the outside, facing the solution. As some of the peptides investigated in this thesis have an additional hydrophobic fatty acid chain, they are likely to form micelles in certain conditions. Depending on the individual peptide structures, adsorption can take place over various concentration ranges and rates. However, usually one can define this as above a specific concentration – the critical micelle concentration (CMC). Above or near the CMC is when micellisation or aggregation takes place [52]. Below the CMC, adsorption is at a dynamic equilibrium with, in this case, the peptide molecules continuously arriving and leaving the surface. At this critical micelle concentration, the interface is at almost maximum coverage and to minimise further free energy, the molecules start to aggregate in the bulk phase. Above the CMC, the system consists of free peptide monomers, an adsorbed monolayer, and micellised peptides in the bulk, all in equilibrium [53].

Micellisation is not a straight forward process and there are many factors that are known to strongly affect the CMC. One of the largest contributing factors is the structure of the surfactant, including the nature of both the hydrophobic tail and hydrophilic head group. The length of the hydrocarbon chain, otherwise known as the hydrophobic tail, is vitally important. For a homologous series of linear single-chain surfactants, it is well known that the CMC decreases logarithmically with carbon number [54]. Effect such as branching, double bonds and addition of polar and aromatic groups will have a noticeable effect on the CMC [55].

Additionally, the hydrophilic group also has an effect on the CMC – mainly whether its hydrophilic 'head' is ionic or non-ionic. For a C_{12} hydrocarbon, for example, which has an ionic head group, the CMC will lie in the range of 1×10^{-3} mol dm^{-3}, whilst for a C_{12} non-ionic material, the CMC will be closer to 1×10^{-4} mol dm^{-3}. The large discrepancy cannot be seen when it comes to the nature of the ionic group, as a major driving force for micelle formation is the entropy factor [56].

Counterion effects are another factor which influences the CMC. In ionic surfactants, micelle formation will be related to the interactions of ionic head group and the chosen solvent. When electrostatic repulsions are largest (ie at complete ionisation), there will be an increase in the degree of ion binding, and therefore a decrease in the CMC. In addition, varying counter ion valency produces a significant effect – for example, changing from monovalent to di-counter ions produces a noticeable decrease in the CMC [57].

The effect of adding a salt, usually an electrolyte, will cause a decrease in the CMC of most surfactants. The greatest effect is found for ionic materials, as the main contributing effect of the salt is to partially screen the electrostatic repulsion between the head groups. [58].

Micelles are just one form of aggregate structures that peptides can form, and hence the next section will tackle the exact mechanism of aggregation, and how different aggregate structures can be determined from individual peptide structure and solution conditions.

1.4 The Mechanism of Aggregation

Amphiphiles, such as peptides, have a pronounced propensity to adsorb to most surfaces [5]. This adsorption is due to a range of factors; from solution conditions such as temperature, pH and concentration, to peptide orientation and specific amino acid sequences and to the nature of the surface, physical and chemical [59], [60]. As peptides are not rigid molecules, adsorption and desorption at interfaces is complex giving rise to phenomena such as surface aggregation and structural rearrangement.

The aggregation of peptides is a common process, and one which can be found in most phases of drug development [61]. Aggregation is a term used to describe a process, which can be present in a variety of different forms. Aggregates can be amorphous [6] or highly structured, e.g. amyloid fibrils [62], and can form in solution or on surfaces due to adsorption [63], [64]. Not only are there many different structures of aggregates, but they can also arise from a plethora of different interactions. These include non-covalent association of polypeptide chains, or covalent linkage of chains, with some aggregates being reversible while others are irreversible. Whichever aggregate is formed, and however it is formed, it nevertheless reduces the physical stability of the peptide, which not only leads to a loss in activity, but also results in problems relating to toxicity and immunogenicity [58], [66].

Peptides have flexible backbones, which allows for side chains to place themselves in such a way as to be at a thermodynamic minimum. They are

folded into this stable state after synthesis at the ribosomes and have to pass through a variety of structural intermediates. As stated previously, the driving force for the chosen orientation of the peptides is the hydrophobic effect – the shielding of the hydrophobic amino acids side chains from the aqueous environment, creating a structure, which will be most stable due to favourable interactions with the solution [67]. The side chain interactions, moreover, stabilise the conformation, adding to its intrinsic stability [68].

Even though the initial triggering of aggregation of a peptide is still relatively ambiguous, extrinsic or environmental factors such as pH, light levels, ionic strength, temperature, roughness, charge and hydrophobicity influence the conformation of these proteins. Aggregation of peptides is widespread: an overabundance of studies have been done on analysis and molecular dynamics of aggregation [69], [70], [71]. Yet, after many years of research, there is mixed evidence of progress in terms of prevention of aggregation [72], [73].

Fig 1.8 below portrays the known information regarding peptide aggregation, and fibrillation.

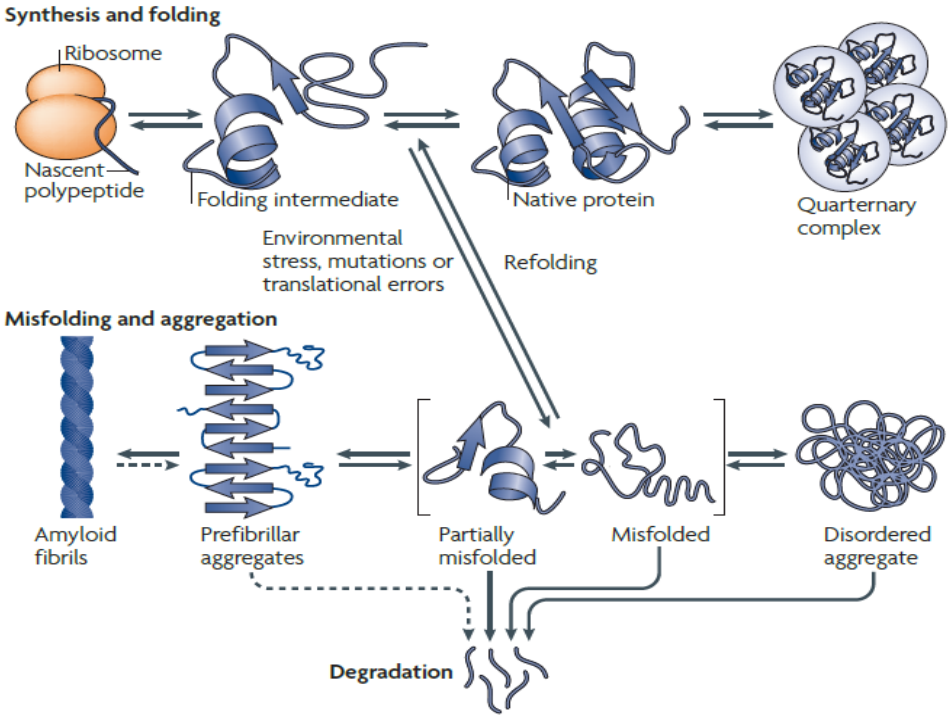

Figure 1.8: A diagrammatic representation of peptide folding. The different stages of peptide folding and misfolding are shown to be a delicate equilibrium. There is only a small energy difference between both the native state and the intermediate, which is another clear indication that peptides have a propensity to aggregate. One aggregate can also affect other aggregates, and hence create co-aggregates [74].

The discovery that any protein can aggregate at high enough protein concentration and under appropriate environmental conditions is not unexpected. Yet, noticeably, proteins and peptides that are not associated with diseases, can also form fibrils with the cross β-patterns that are characteristic of amyloid fibrils [75], [76]. Surprisingly, oligomers that form early in the aggregation process of non-disease-related proteins may also be cytotoxic [77]. The formation of aggregates, which are all similar in morphology, by a variety of

proteins, which are not related to one another either in sequence or structure, suggests that certain universal principles may govern fibrillation [78], [79]. Yet, the vastness of the countless different environmental factors, sequencing structure and intermolecular interactions of the peptides, makes deciphering the principles of protein aggregation challenging.

To further understand aggregation mechanisms, it is vital that the behaviour of individual parts of the peptide structures are investigated. Among the peptide chains, the alternating amine (NH) and carbonyl (CO) groups are highly polar and as a result, form hydrogen bonds between each other. These hydrogen bonds are additionally known to bind peptide chains together, which in turn give rise to the peptide secondary structures [80]. There are two core types of secondary structures formed by peptides, which are dependent on both the primary structure, and/or the amino acid sequence.

The two main forms of secondary structure are usually referred to as stable and unstable. The stable form of peptide secondary structures is made up of α-helices and β-sheets, whilst the unstable form contains random coils, loops and turns. The β-sheet interactions, which have been proven to form fibrillar morphologies, present an intricate link to the aggregation process [81]. The β-sheets are formed by individual peptides stacking parallel to each other, with the peptide backbone perpendicular to the fibril axis. The subsequent amyloid core is formed by a cross-β structure. As previously mentioned, hydrogen bonds are formed between the carbonyl oxygen atom and the amine group hydrogen atoms of the peptide backbone. The amino acid side chains lie on either side of the cross-beta sheet. The structure is stabilized by a large range of interactions: aromatic residue stacking, π-π-stacking, hydrophobic interactions and salt bridges between charged side chains [82].

The unstable form, which consists of the loops, turns and random coils, can associate with each other to form a tertiary structure, which, unlike the secondary structure, will include non – covalent interactions. The largest possible structure that peptides can form is the quaternary structure. The quaternary structure arises from a combination of two or more different chains of polypeptide, which then form a protein sub-unit. Creating these structures from an array of peptides is referred to as self-assembly [83].

Proteins consist of one or several amino acid chains, with each amino acid chain folding and moving independently from the other chains. The presence of molecular chaperones and the stable cellular environment prevents the formation of non-natively folded proteins [84]. However, newly formed proteins can occasionally misfold. It has been found that in E. coli, only 5-10% of all molecular proteins can afford to employ molecular chaperones to help them reach the folded state. Therefore, over 90% of proteins need to reach their native state by folding effectively and spontaneously without help from chaperones [85]. If the cell does not help re-fold the protein or degrade the protein, then aggregation can occur. This is due to hydrophobic patches of unfolded proteins interacting with other hydrophobic patches of unfolded proteins. Due to the patches being extremely hydrophobic, they tend to associate with each other as opposed to interacting with the solution as normal. Aggregation of peptides, therefore, can be defined as the process of misfolded peptides 'clumping' together.

The formation of these fibrillar aggregates can be undesirable due to the potential toxicity, as well as other pathological effects including depletion of a relevant protein, formation of toxic metabolites, or aggregate deposition. Proteins that undergo self-assembly have often been connected to protein misfolding diseases, such as Alzheimer's disease and Parkinson's disease. These diseases are caused by the formation of amyloid fibrils; the amyloid plaques in the brain are related

to the neuropathic diseases. Yet, recent findings suggest that the toxic effects of protein misfolding are not caused by the bulk aggregate, as previously thought, but by the earlier formations of toxic oligomers [86]. The toxicity of the early aggregates are said to be due to their capability to damage crucial cellular processes through interacting with membranes. This interaction leads to an increase in oxidative stress, which subsequently raises the levels of free Ca^{2+}, causing eventual cell death [87].

The two main types of fibrils formed in the aggregation process referred to as protofibrils and filaments. These are important as the type of fibril formed will be investigated in Chapter 3 of this thesis for each individual peptide. The amyloid protofibrils are composed of 2-4 fibril sheets, with peptides lying parallel to each other within a single sheet, and hence, anti-parallel to the opposite sheet. Cross-beta sheets characteristically have a ~4.7 Å reflection in the X-Ray diffraction pattern, with a corresponding distance to the peptide strands. Diffraction at ~10 Å indicates the presence of an opposing sheet. The opposing sheets can be formed by one of two ways: either distinct molecules or amyloid stacking of single peptides [88], [89].

For the maturing of fibrils, there are different theories on how fibrils associate. The first theory, which is referred to as HAM (Hierarchal assembly model). This theory broadly states that the fibrils associate through several cross-beta sheets which arrange with a head-to-tail arrangement, and/or by inter coiling of preassembled sheets. Typical amyloid fibrils are between 10 to 20 nm wide and can go up to several micrometres long, but average distances only reach a few nanometres [90]. Twisting of the individual peptide, or the fibril, is induced through side chain packing restrictions and electrostatic effects. The degree of twisting is reliant on the sequence of the peptide, the number and arrangement of associated sheets, and the solvent conditions (among other environmental factors) [83], [91], [92].

The second theory is drastically different, and forms filaments or protofibrils through addition of oligomers. Instead of lateral association, fibrils are matured by direct addition of oligomers to extend the fibril. This was shown to be the case for glucagon at 37°C incubation for different time frames using both in situ and ex-situ AFM techniques, as done by Zhang et al. This theory also corresponds with results found in this thesis (see Chapter 3), and can be seen in Fig 1.9 below. Henceforth, it is highly likely that the glucagon assembly process is simply the addition of oligomers to the ends of the extending and ever growing fibrils [93].

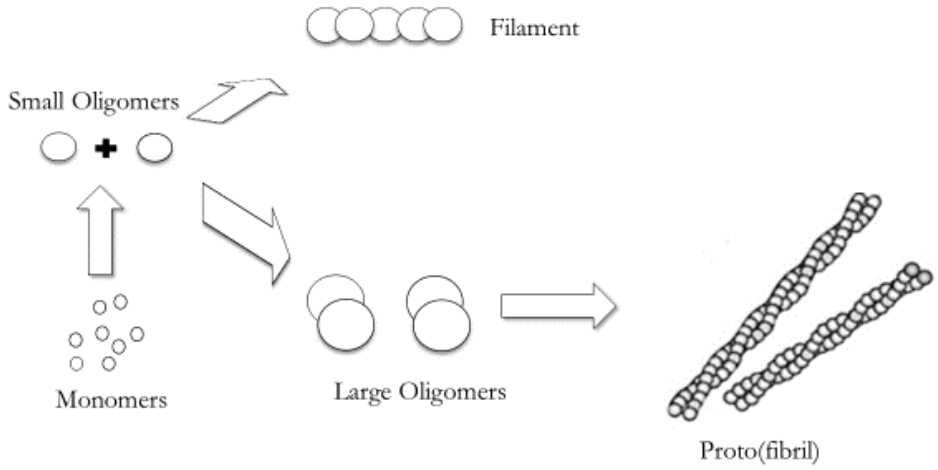

Figure 1.9: Diagrammatic representation of association of monomers to filaments and protofibrils. The fibrils are elongated directly by addition of monomers, which form small oligomers, which then add together to form a filament or form larger oligomers, which then form protofibrils. [94]. Adapted from [95].

Even though the formation of fibrils is reversible, the amyloid structure provides a protected environment for individual peptides. Amyloid peptide fibrils are stable in a wide range of temperatures and pHs, as well as in different solutions [96]. Additionally, the amyloid core protects the peptide sequence from enzymatic degradation [97]. Therefore, it is no surprise that amyloid fibrils show remarkable mechanical stability, as well as very high tensile strengths and stiffness (elastic modulus) [98].

Protein and peptide adsorption at interfaces (mainly the solid-liquid interface), is of great interest due to all its relevance in many areas of research; biosensors, biocompatibility, and drug delivery, to name a few. Proteins are large, and have numerous different structures (as previously described) making them difficult to use as a model system for peptide adsorption. On the other hand, peptides, which only comprise a small number of amino acids, provide a relatively simplistic model for protein adsorption. Solid-liquid interfaces are known to promote aggregation as they act as a template for nucleation [99]. Amyloid structures are formed by nucleated growth. In the peptide solution, individual molecules can arrange to form oligomers by thermodynamic fluctuations and intermolecular contacts. These early stage structures are not usually fibrillar in configuration, but can be composed of a variety of different aggregate types; ranging from unstructured to ring-shaped or spherical aggregates [100], [101]. A primary nuclei is produced, which can be elongated to form fibrils through either monomeric addition, or this nuclei can promote secondary nucleation by surface catalysis and fragmentation. The self-assembly process can only be stopped when an equilibrium is reached between monomer inclusion and monomer release [102], [103].

1.5 Surface Functionalization for aggregation

The previous sections have highlighted the need to discourage aggregation, but with much research going into the exact mechanisms and molecular dynamics of aggregation, little research has gone into preventing aggregation through adsorption. This is partly due to the complexity of surface factors that have to be considered, but also the large volume of different possible external factors at play. Considering aggregation is very environmentally dependent, if the right

environment can be created, the potential of increasing or decreasing aggregation can, in theory, be achieved.

Therapeutic peptides come into contact with containers for storage, transport and eventually with syringes for administration. These interactions are as integral to prevention of aggregation as the interactions within the peptide solution. Hence, this thesis will focus on the interface between the solution and the solid, focusing specifically on tailoring the surface to decrease adsorption of therapeutic peptides.

The occurrence of aggregates on the surface is thought to be due to either diffusion of surface bound peptides that act as a precursor for aggregation or because of direct adsorption of bulk peptides to other surface bound peptides [50]. Furthermore, cooperative effects can play a large role in the adsorption of peptides. Cooperative effects refer to peptides that are in close proximity to the surface, which are more likely to adsorb if there are already pre-adsorbed peptides present on the surface [51].

Therefore, protein–surface interactions are influenced by the surface properties of the material on one side, and protein's properties on the other side. Having discussed some of the peptide solution properties, such pH, temperature, and concentration, it is equally essential to discuss the properties relating to the adsorptive surface, such as surface induced aggregation, and co-operative effects. Both surface induced aggregation and co-operative effects are dependent upon a range of physiochemical factors; such as hydrophobicity, surface charge (wettability and surface energy), as well as substrate topography. The parameters that will be discussed in this thesis are therefore; hydrophobicity, charge and morphology and/or roughness of the surface [104].

1.5.1 Common interfacial surfaces in the peptide industry

Before tackling the parameters which affect surface adsorption of peptides, it is important to discuss the surfaces used for this thesis.

Peptides are stored, transported and administered in either plastic or glass vials, syringes or containers [105][106]. The studies done in this thesis, therefore, mainly focus on these two surfaces to determine whether they are indeed adequate surfaces to limit peptide adsorption and hence aggregation.

1.5.1.1 Borosilicate Glass

Borosilicate glass is a commonly used glass in the pharmaceutical industry due to its intrinsically stable properties. With its additional silica and boron trioxide added into the glass structure, it is known for its low thermal expansion coefficient and hence, its thermal resistance to shock. It's crystal lattice is shown below.

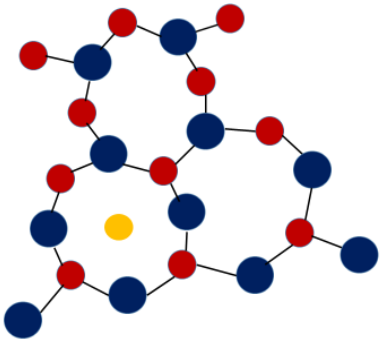

Figure 1.10: Structure of borosilicate glass with the blue spheres representing a silicon molecule, red spheres representing the oxygen molecules and the yellow sphere is the boron additive, to enhance the properties of the glass.

The common type of borosilicate glass used for laboratory glassware has a very low thermal expansion coefficient (3.3×10^{-6} K^{-1}), as previously stated. Compared to ordinary soda lime glass, this is about one-third of its thermal expansion coefficient which reduces material stresses caused by temperature gradients, which makes borosilicate a more suitable type of glass for most applications.

Other materials, such as fused quartzware have even lower thermal expansion coefficients (one-fifteenth the thermal expansion of soda-lime glass); however, are very difficult to work with and hence, make quartzware much more expensive, meaning borosilicate glass can be seen as the lower cost compromise [107].

Due to its high thermal and chemical resistance, and its good optical clarity, borosilicate glass is widely used in implantable medical devices such as artificial hip joints, prosthetic eyes, and dental composite materials (white fillings) [108]. One drawback of using this material is its ability to form sodium borohydride by reacting with sodium hydride upon heating, which is a common laboratory reducing agent.

This thesis looks at borosilicate glass as an interface for therapeutic drugs adsorption. Borosilicate tubing is used as the feedstock for the production of drug packaging and containers, such as the vials, which are used to store or transport the drug and pre-filled syringes, as well as, ampoules and even dental cartridges. The chemical resistance of borosilicate glass means it minimizes the migration of sodium ions from the glass matrix, hence making it well suited for injectable-drug applications compared to other standard glasses [109].

1.5.1.2 Polystyrene

Polystyrene is a polymer made from the monomer styrene. It is a synthetic, aromatic hydrocarbon polymer, which can come in various shapes and sizes. General-purpose polystyrene is brittle, clear and hard. Per unit weight, it is inexpensive and it is a poor barrier to oxygen and water vapour and additionally, has a relatively low melting point [110].

As a thermoplastic polymer, polystyrene presents at a solid state at room temperature but liquefies when heated above 100 °C, which is its glass transition temperature. In the polymerisation reaction to make polystyrene, the carbon–

carbon π bond in the monomer of styrene of the vinyl group is broken and a new carbon–carbon σ bond is formed [111]. The newly formed σ bond is stronger than the π bond that was broken, thus it is difficult to depolymerize polystyrene. Thousands of monomers typically comprise a chain of polystyrene, giving a molecular weight of 100,000–400,000 Da. It's structure is shown in Figure 1.11 below.

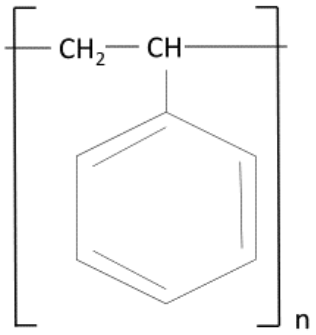

Figure 1.11: Molecular structure of polystyrene. Polystyrene contains a repeating unit of a cyclohexane ring, with CH-CH_2 repeating groups.

With polystyrene being one of the most widespread plastics, its production reaches several million tonnes per year. Its uses are varied and range from; protective packaging containers, lids, bottles, trays, tumblers, and disposable cutlery among many others [112]. Its main use of interest in this thesis is its use as a container for storage and transportation of therapeutic peptides.

Polystyrene, as well as many other plastics, is known to be a surface where there is a high rate of non- specific adsorption (NSA) [113], [114]. However, limited research has gone into alternatives as they can be expensive, difficult to manufacture and mass produce.

Both borosilicate glass and polystyrene are surfaces which enhance NSA. Non-specific adsorption is the result of electrostatic interactions, from both the ionic and hydrophobic adsorption of the molecule [115][116]. These two different

types of adsorption are dependent on the surface and the molecule itself. For example, the ionic adsorption is the interaction of the hydrophilic surface (e.g. glass) and ionic drugs (e.g., chloroquine), whilst the hydrophobic adsorption is the interaction of a hydrophobic surface (e.g., plastic) and hydrophobic drugs (e.g., paclitaxel, digoxin, verapamil). Recently, drug candidates have been becoming more hydrophobic and less soluble and the containers used in transportation, delivery and assays are also mainly made from hydrophobic plastics. Therefore, hydrophobic adsorption is mainly responsible for NSA [117][118].

1.5.2 Parameters that affect surface adsorption

The surfaces that therapeutic peptides come in contact with in an everyday scenario have been discussed in Section 1.5.1 above. The following section tackles the changes that can be made to adapt the level of adsorption, and hence aggregation, at the interface.

1.5.2.1 Hydrophobicity of the surface

The mechanism of interaction of peptides with solid surfaces strongly depends on the hydrophobicity and charge of the surface [119]. In general, proteins and peptides have a tendency to adhere more strongly to charged surfaces compared to uncharged, to nonpolar compared to polar, to high surface tension rather than to low surface tension. Belfort et al. states that non-polar surfaces may destabilize proteins which thereby facilitates any conformational reorientations, which in turn lead to strong inter protein and protein–surface interactions [120]. This clarifies the rather broad experimental findings that in the majority of cases, the affinity of proteins to surfaces decreases on hydrophilic substrates, and indeed increases on hydrophobic substrates [121]. An important exception to this 'rule' is the adsorption of an important class of proteins, the glycoproteins. Glycoproteins have their hydrophobic domains buried inside a shell of glycans.

Glycoproteins adsorb extensively on hydrophilic planar surfaces and sparsely on hydrophobic surfaces [122].

Numerous studies have shown similar results; that the peptide configuration will change depending on the surface it adsorbs to. Adsorption of $\alpha\beta(1–40)$ peptides on different surfaces (both hydrophobic and hydrophilic) caused conformational changes, which in turn, inhibited polymerization during incubation [123]. Peptide molecules adsorbed on hydrophobic surfaces promote an α- helix conformation due to the hydrogen bonding of the apolar part of the peptide, which is oriented towards the surface. This type of intra-molecular hydrogen bonding mimics the apolar trans membrane environment. In contrast, hydrophilic surfaces resemble the charged membrane surface, hence, β-sheet structures promote aggregation, mostly owing to electrostatic interactions, which can be promoted by the length of the carboxyl terminus [124].

As previously discussed, the folding of peptides is due to a variety of factors; and one of the most prominent factors is the hydrophobic effect [125]. An α-helix structure is commonly produced by dehydration of the apolar sites of the peptide, which is directly linked to the hydrophobic interactions and forming the local secondary structure. Nevertheless, in the absence of the electrostatic interactions, the binding of the hydrophobic tail of the peptide would be unable to form a stable peptide-solvent complex, which in turn wouldn't allow for the formation of a hydrophobic environment required for a stable helix formation. Consequently, adding hydrogenated complexes to the solution will enhance and induce fibril formation, as well as β- sheet formation. Protein aggregation directly stabilises β-sheet structures, and are directly related to fibrillogenesis [126]. It has, moreover, been shown that hydrogenated complexes also lead to amyloid formation. Silicon dioxide is a surface used in this thesis, and as silica is naturally very hydrophilic, the adsorption process on silica is also driven by electrostatic interactions. These interactions, as with other hydrophilic surfaces, result in

peptide molecules being adsorbed with the polar, and therefore, charged part toward the surface. As a result of the long range of electrostatic interactions, the peptide-surface contact is optimized by assisting the peptide residues on the surface and leaving the polar region more oriented towards the aqueous solution. To evade water contact, the neighbouring adsorbed molecules may aggregate, which, sequentially, induces intermolecular β-sheets structures.

It has been shown that on hydrophilic surfaces, fibrils grow upright like rods, and have a unique and uniform structure. This can be used in the future as a bio template for specifically tailored functional nanostructures [127][128].

Through much of biology, hydrophobicity has played a large role. When it comes to surface adsorption of peptides, this is no different. Hydrophobicity of a surface has a large effect on the adsorption of the peptide on the surface, which will lead to increased or decreased aggregation. In summation, highly hydrophobic surfaces are likely to cause increased adsorption compared to hydrophilic or neutral surfaces. Nonetheless, additional factors, such as charge, also play a substantial role.

1.5.2.2 Charge of the surface

Electrostatic interactions have a large effect on the adsorption of the peptide to the surface, as well as altering the peptide conformation on the surface compared to in solution.

In peptides, the isoelectric point (pI), is defined as the pH in which the protein has no net charge [129]. This varies from protein to protein depending on the specific amino acid sequence. Peptides adopt an unordered monomeric or dimeric structure when the charge distribution is large, and therefore, a net negative charge promotes electrostatic repulsion between the peptide molecules (the pH > pI). In contrast, when acidic residues are negatively charged, and basic residues positively charged, the aggregates change due to electrostatic

interactions, and form small oligomers with a β-sheet structure (pH < pI). At pH = pI, the peptide forms a mixture of structures as the interplay between electrostatic and hydrophobic interactions is equal [130]. This balanced ratio can be affected by a variety of different factors; one of which, is a hydrophobic surface. Once the peptide is adsorbed onto the hydrophobic surface, the random structure, as well as the β-sheet structure, are converted into an α- helical structures [131]. This in turn shows that the peptide- surface interaction is much preferable to an aggregated state in solution.

When peptide adsorption increases, single molecule surface interactions will develop into monolayer and then multilayer coverage. When monolayers adsorb to the surface, the packing density of monolayers have to be kept in mind. The packing layers depend on the strength of the electrostatic attraction between surface adsorbed peptides. When peptides have a high net charge, they are likely to assemble into a loose layer. Equally, if the peptides have a net neutral charge, they are more likely to form a densely packed layer [48][49].

As stated before, peptides prefer charged surfaces, with peptide adsorption increasing on highly charged surfaces compared to neutral surfaces [132]. Peptides that do carry a charge will prefer an oppositely charged surface compared to a surface of similar charge [133]. Additionally, one must think of the solution conditions relative to the surface charge. Using charged surfaces and oppositely charged peptides allows for the production of protein multilayer system. Multilayer protein films were made by more than one protein species. This was done through alternate electrostatic adsorption using the positively charged polyethylenimine (PEI), a protein layer of haemoglobin, lysozyme or myoglobin and then polystyrene sulfonate (PSS) as the negative surface [134].

Layering of peptides in vivo is a large body of research as is dependent on the Vroman effect. This effect states that pre-adsorbed proteins are replaced by

proteins which have higher binding affinities to the surface and hence are replaced. This causes an additional layer of complexity within biological systems.

The peptide conformations can also change according to both their charge and the charge of the surface. Silica particles and other negatively charged particles, which do not induce structural changes in the peptide, as their zeta potential is not negative enough to induce any kind of change. Conversely, hydrophobic Teflon particles are able to induce an α-helix. However, even though negatively charged particles and silica particles cannot take an active role, both can inhibit β-sheet formation. In order to stabilise the α-helix structure, and inhibit fibril formation, both hydrophobic groups and highly charged particles must be used [135].

As the charge of the surface determines levels of adsorption, positive and negative charged surfaces will also have an effect on the aggregation of peptides, and their configuration at the surface. As with the hydrophobicity of the surface, there is a clear trend towards increased or decreased aggregation according to the charge of the surface. Positively charged surfaces give little to no growth of fibrils, as with hydrophobic surfaces [136].

1.5.2.3 Roughness of the surface

Roughness of the surface, specifically for peptide aggregation, is a less researched area compared to hydrophilicity and charges of a surface. The hydrophobic and hydrophilic characters of surfaces are easy to tailor and have been investigated extensively. This volume of research on surface roughness and direct connection to aggregation has yet to be found.

However, much of the literature has focused on roughness of materials for biological implants due to its importance. For example, the field of tissue

engineering has determined that cells proliferation is heavily dependent on surface roughness of the scaffold, as the scaffold should be as close to the extracellular matrix (ECM) conditions as possible [137]. Numerous examples of the effect of surface roughness on cell function, shape and proliferation have been found, with some specific examples from Kunzler et al, who found that the proliferation human fibroblasts was decreased with increasing surface roughness, yet rat osteoblast proliferation increased significantly [138]. Another, more recent example, was Chehroudi et al, who found that micromachined implants with grooves and pits of between 30–120 μm depth showed better osseointegration results in vivo than a smooth control surface [139]. These are just a few examples of the key role that surface topography plays on cell viability and cell processes. These intricate links have yet to be established for peptide fibrillation, however, there have been some notable new developments in the field.

There has been a significant increase in new evidence to suggest that surface roughness influences the 2D diffusion of macromolecule chains by supplying changing topography of the surface [140]. As a result, the surface roughness could have a significant influence on the fibrillation process of peptides for surface-mediated fibrillation. Studies to date have focused on the effects of surface chemistry on peptide fibrillation. Increasing surface roughness increases the surface area to volume ratio. A clear argument is that with an increased surface area, a proportional effect will be seen for aggregation, and hence an increase in aggregation. Contrary to popular belief, Khurram Shezad et al have shown that Aβ42 fibrillation is inhibited on a surface with a high degree of roughness, processes slowly on a surface with a lower degree of roughness but occurs readily on a smooth surface [141]. However, Schwartz et al found that a rougher nanoscale topography obstructs surface diffusion of small polymers, which also corresponds with what Granick et al found; that a rough surface

weakens surface diffusion by causing hindrances [142]. This all points, predictably, to the fact that in order for fibrils to grow, peptide molecules need to be able to diffuse on the surface, which can be difficult if it is overly rough. Surfaces that show slight roughness decelerate the diffusion and therefore slow down the aggregation process, yet, very rough surfaces stop the diffusion altogether [143].

Above, we have seen that roughness can slow down and even halt the process of fibrillation. However, it is a more multifaceted problem than increased surface area is proportional to increased aggregation. With the addition of nanoparticles, will come an increase in the surface area to volume ratio of the surface. A recent study on C_{60} fullerenes has shown that the highly curved surface enhances enzyme and peptide stability in strongly denaturing environments (such as the very low pH's seen in this report). Additionally, it compares the stabilisation to flat surfaces, and found that the highly curved surfaces stabilised the enzyme and peptides to a much greater extent than the flat surfaces did [144]. Analogous results have been established with other nanoparticles such as silica and gold nanoparticles. The capacity to enhance protein stability by interfacing them with nanoparticles, and quantum dots, could impact a range of fields; from diagnostics to sensors and drug delivery [145]. However, interactions between the nanoparticles and peptides can be much more intricate. Nanoparticles are small (1 - 100 nm) spherical structures, and hence the interactions between the ever changing conformations of the peptide will be highly complex. The interaction between nanoparticles and other small particles (such as quantum-dots), with peptides is one of great interest for a variety of applications from bio sensing to new drug targeting techniques. Nanoparticles can also change peptide conformational structure; it was shown that haemoglobin (Hb)'s secondary structure changed drastically when in contact with CdS quantum dot [146]. Its secondary structure changed from 72.5% α-helix to 60%, confirmed through

Raman spectroscopy, fluorescence spectroscopy and synchronous fluorescence. Additionally, it was shown that the secondary structure changed due to direct chemical bonding between the cysteine residue of Hb and the sulphur on the QD Polystyrene nanoparticles had a similar effect on BSA. The adsorption and consequent desorption of BSA to the nanoparticles caused irreversible changes in the secondary structure of the protein. As with Hb, the α-helical content was reduced, whilst the β-sheet fraction of secondary structure was increased [147], [148].

Most recently, a highly related study was conducted, which showed that a range of different nanoparticles, ranging from polymer particles to carbon nanotubes, and PEG (poly(ethylene glycol)) -coated QDs, actually increased the rate of fibrillation of β-2-microglobulin protein at an acidic pH of 2.5 The fibrils, imaged by TEM (transmission electron microscopy), do not show growth out of the nanoparticles, and hence the suggested mechanism is that the concentration of the protein was locally increased in proximity to the nanoparticle surface [149]. An increase in peptide concentration increases the likelihood of the formation of oligomers. Other structures, have also been explored recently; Dendrimers interact with polypeptide conformations, and induce fibrillation through amyloid structures [150].

Furthermore, animal studies have demonstrated that C_{60} hydrated fullerene could have anti-amyloidogenic capacities. The C_{60} hydrated fullerene has been shown to inhibit the fibrillation of amyloid-β 25–35 peptide. At a dose of 7.2 n mol/ventricle, control rats were given a single injection of a C_{60} hydrated fullerene, which improved performance of a cognitive task. It was confirmed that this was due to the prevention of the fibrillation of the amyloid β 25-35 peptide through TEM studies [151].

All of the above suggests that there is a possible role for nanoparticles and nanoscale architecture in the development of a new surface for the prevention of aggregation of therapeutic peptides, and that there is still a plethora of research to be done in the field of surface roughness and adsorption and aggregation.

1.6 Objectives

Therapeutic peptides aggregating at surfaces is a challenging problem to tackle. From the literature presented, it is evident that there is not an easy solution to such a multifaceted problem; aggregation itself is a complex process, as is the interplay between the peptide properties and the interfacial surface. Investigating the interface between the peptide solution and the surface is an underexplored and vital area of research, especially as peptide solutions come into contact with solid surfaces throughout their lifetime; when stored in vials or administered using syringes [113], [152].

The main objective was to investigate aggregation of each peptide through adsorption to surfaces. Due to the complexity of the objective, three distinct areas of investigation were explored. The first was to explore the stability of the four therapeutic peptides in solution and to find common destabilising or stabilising mechanisms for the peptides in solution, which provides information on the aggregation of the peptides in bulk. Secondly, to investigate the surface induced aggregation of peptides through studying a variety of surfaces, and elucidate adsorptive mechanisms to each surface for individual peptides. Thirdly, to create surfaces of different roughness and asses their role in adsorption of the four peptides.

By looking at these three distinct areas, using a variety of different techniques, information can be gleamed about both the bulk solution, and the interface effects on aggregation of therapeutic peptides.

1.7 Overview

Chapter 2 explored the plethora of different techniques used in this thesis, ranging from imaging techniques, such as the Atomic Force Microscope, to solution techniques such as the DLS and Zeta Potential, to techniques to analyse wet mass adsorption to acoustic sensors. The background information on the techniques is crucial to the understanding of how each technique contributed to the investigation of the bulk solution and interface.

The first results chapter, Chapter 3, investigated the solution conditions to assess the stability of each individual peptide. This was done by looking at the individual secondary structures produced in destabilising conditions by each peptide; glucagon, liraglutide, g797 and exendin-4. The conditions explored ranged in pH (pH 2.4, pH 7.4 and pH 10.8) and concentration (0.5 mg/mL, 1.0 mg/mL, 2.5 mg/mL and 5.0 mg/mL). The Atomic Force Microscope was used to identify the peptides structures formed in solution and Zeta Potential to assess the overall charge of the peptide in solution conditions and their colloidal stability.

Once the stability of the peptides in solution were assessed, they were also investigated in relation to the surfaces which they adsorb to. The second results chapter, Chapter 4, focused on the adsorption of all four peptides; glucagon, liraglutide, g797 and exendin-4 to hydrophilic neutral, hydrophilic charged, hydrophobic neutral and hydrophobic charged surfaces, in order to assess the extent of adsorption and its dependency on both hydrophobicity and charge. The adsorption was investigated using the Quartz Crystal Microbalance with Dissipation, and a range of surfaces which were reflective of pharmaceutically relevant surfaces, such as borosilicate glass and polystyrene. Dynamic Light Scattering was also used to investigate further the sizes of aggregates formed in different solution conditions.

From the first two results chapters, the bulk solution and the surface was investigated. However, adsorption to surfaces is not solely dependent on charge and hydrophobicity, and hence a third surface factor was investigated, namely the surface roughness. As surface roughness is ill defined, the concept was difficult to tackle. The third results chapter, Chapter 5, focuses on different methods of changing the roughness of a surface, with special concentration on the addition of gold nanoparticles to the surface, investigated through the AFM and E-beam lithography to create tailored surfaces. The functionalised nanoparticle chips were then used for the same the QCM-D experiments to gauge the wet mass adsorbed in comparison to flat gold surfaces (< 1 nm roughness).

The last chapter tackles the main conclusions from the data and results presented in this thesis, and future works to be done in a field with many different avenues to explore.

2 Chapter

Methods and Techniques

This thesis explores the aggregation of peptides, especially through adsorption at the interface. In order to explore aggregation in solution and on the surface, a variety of different techniques were employed to get as clear a picture as possible. Certain techniques were used to study aggregates in the bulk solution, while techniques will have a focus on adsorption of peptides to surfaces, so surface techniques must also be utilized. The techniques described in this section were used in the experiments detailed in Chapter 3, 4 and 5.

2.1 Atomic Force Microscopy (AFM)

The AFM was one of the main techniques used in this thesis, as it gives a detailed image of the surface in nanometre resolution. Most fibrillation and aggregation studies of peptides use a high powered microscope, such as an SEM or AFM as there are a limited number of techniques that can image the detailed structures of aggregates, oligomers and fibrils in real time [153], [154].

The AFM is often used to study the relation between molecular conformations of peptides, as well as, the morphology of adsorbed films and fibrils on hydrophilic and hydrophobic surfaces. Aggregation, as described in Chapter 1, is the process of amphiphilic peptides self-assembling to form higher order structures. Kowalski et al. used the AFM to directly gauge its aggregation on both hydrophilic mica and hydrophobic graphite in real time [155]. The AFM was used to observe the initial stages of β-amyloid fibrillation in situ, and visualize the growth of individual β-amyloid protofibrils on a mica substrate over several

hours by Blackley and Sanders in 2000 [156]. Fibril growth patterns have also been observed using a time lapse – AFM, in which individual fibrils can be seen to grow on mica in real time [157]. The above examples are just some of the hundreds of papers using AFM as a valuable technique for imaging biological material [158]–[161]. The AFM has successfully managed to monitor individual fibrils and has proved a useful tool for detailed images of aggregation structures of macromolecules, as well as for surface manipulation and modification [162]–[164].

The Atomic Force Microscopy (AFM) is the predominant technique for imaging of biological macromolecules at the nanometre scale. In 1982, Binnig, Gerber, Rohrer and Weibel invented the Scanning Tunnelling Microscope, which could display individual surface atoms of a flat sample [165]. However, the STM had serious limitations for the study of the atomic scale - one of its main drawbacks was its inability to use non - conducting samples. In order for the Scanning Tunnelling Microscope to function, there must be a tunnelling current which flows between the tip and the sample, henceforth, only conducting materials could be used. To solve this problem, Binnig invented the AFM in 1986 - which can be used in ambient conditions, on any flat surface, and no sample preparation is required [166].

The AFM has a cantilever typically made of silicon or silicon nitride with a sharp tip, which probes the sample surface. The cantilevers have lateral dimensions of approximately 100 microns, with a thickness of the order of 1 micron. With these geometries, the spring constant of the cantilever will be in the range of 0.1 – 1 N/m, with resonant frequencies of 10-100 KHz, depending on the individual cantilever [167]. Once the tip approaches the surface, a range of attractive, close range forces between the tip and the surface result in a deflection of the cantilever towards the surface according to Hooke's Law [168]. Once the cantilever is in contact with the surface, repulsive forces become dominant, and the cantilever is

deflected away from the surface. Below in Fig 2.1, a diagram of the detection method is shown. The laser beam is used to detect the deflection of the cantilever, while the metallic cantilever provides a surface for the reflection of the laser beam. Any changes in the roughness of the surface will change the cantilever deflection and the change in reflection of the laser beam [169]. These subsequent changes are identified by a position- sensitive photodiode. The feedback loop controls the height of the tip, and in this manner, maintains a constant laser position. Through this feedback system, the AFM can generate a precise topographical map of the surface. Using this principle, the AFM can take clear, precise images with nm scale spatial resolution and pN force sensitivity [170].

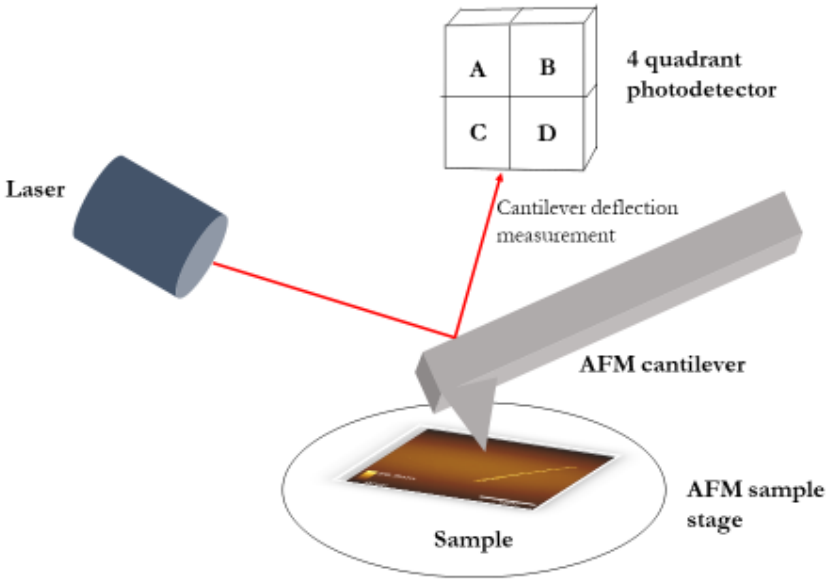

Figure 2.1: A diagrammatic representation of the AFM setup. The laser is directly reflected off the back of the cantilever and into the photodiode. Once this reflection has been detected, a feedback loop is used to keep the tip at a constant height to refrain from breakage.

The Atomic Force Microscope has three different modes; contact mode non-contact mode and tapping mode. Contact mode is the mode when the tip is dragged along the surface, and hence contours are measured. The image is then formed through direct deflection of the cantilever, or through the feedback signal

which keeps the cantilever at a constant position. This mode is often damaging to the sample surface, and can be more prone to noise and drifting [171]. Contact mode is at a repulsive distance to the surface, due to steric repulsion between the sample and the tip. When the tip approaches the sample to a few nanometres distance, van der Waals forces act upon it, snapping it towards the sample [172], [173].

Non – contact mode is when the tip is not in contact with the surface, but instead oscillated at its resonance frequency above the surface. The decrease in resonant frequency combined with the feedback loop system of the AFM means a constant oscillation amplitude or frequency is maintained by adjusting the average tip-to-sample distance. Measuring the tip-to-sample distance at each (x,y) data point allows the scanning software to construct a topographic image of the sample surface [174], [175].

The third and most common mode on the Atomic Force Microscope is tapping mode. The frequency and amplitude are kept constant, and the cantilever oscillates near resonance frequency in order to keep the probe tip close enough to the sample for short-range forces to become detectable whilst simultaneously preventing the tip from attaching to the surface. The stable amplitude signal is used as the parameter that goes into the electronic servo that controls the height of the cantilever above the sample [176], [177]. The forces (van der Waals, dipole-dipole interactions, electrostatic forces and capillary forces) acting on the AC magnetic cantilever when the tip comes close to the surface result in the amplitude of the cantilever's oscillation decreasing as the tip gets closer to the sample [178]. Tapping mode is the mode used for all the experiments described in this thesis, due to most samples developing a liquid meniscus layer in ambient conditions.

The Atomic Force Microscope does come with inherent drawbacks; such as scanning size. Scanning samples cannot have a larger area than 100 μm, as the

AFM requires high mechanical stability, any larger areas would take too long [179]. The relative slowness of the AFM technique also means it's more susceptible to thermal drift [180]. Additionally, the AFM can suffer from creep or hysteresis, and cannot identify overhangs or steep walls [181]. For this thesis, one of the main problems with AFM, however, is that it is difficult to quantify the amount of peptides adsorbed at an interface via only imaging methods. It is no surprise, therefore, that it is suggested to employ a complimentary technique in combination with the AFM, for more quantitative results [182], [183]. One of the more successful techniques for doing this, is by using the quartz crystal microbalance-dissipation (QCM-D).

2.2 Quartz Crystal Microbalance with Dissipation (QCM-D)

The Quartz Crystal Microbalance with Dissipation was first developed by Sittel, Rouse and Bailey in 1954 [184]. The QCM-D is a technique which functions as a highly sensitive mass detector, sensing hydrated masses in nanograms per cm^2.

The QCM is based on the inverse piezoelectric effect, which discovered that the application of voltage results in mechanical deformation of the material. When an alternating applied voltage is applied, a cyclical deformation occurs, leading to an oscillatory motion. If the frequency of the applied voltage matches the crystal's resonance frequency (or multiples of the resonance frequency named overtones), a standing wave is generated. Electrodes are patterned on either side of the AT-cut crystals. The patterned crystal vibrates in the thickness-shear mode, which is where the two surfaces move in an antiparallel fashion.

In order to be able to determine the mass adsorbed to the crystal, an equation can be used, which links the change in frequency to change in mass.

The Sauerbrey equation (below) is applicable for rigid homogenous layers, and is considered an appropriate model for extraction of hydrated mass if the dissipation is less than 2×10^{-6} [185].

$$\Delta f_n = -\frac{n}{C} m_f$$

Equation 2.1: The Sauerbrey equation, where m_f is the areal mass density of the adsorbed film, n is the number of overtone and c is the conversion factor (which is 17.89 ng $Hz^{-1}cm^{-2}$ for a 5MHz QCM-D crystal used in this thesis).

The quartz crystal that oscillates at a resonance frequency when an AC voltage is applied is shown below in Fig 2.2. The gold contact electrodes are shown, and the sample is deposited onto the highly sensitive area in the middle of the sensing chip.

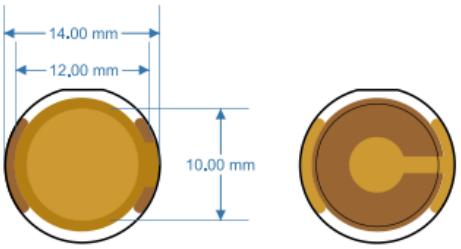

Figure 2.2: The QCM-D sensor chip used in this thesis, with its measurements. The image on the left is the top of the chip, whilst the image on the right is the bottom. The sensing area of the QCM-D is the 10 mm inner diameter of the electrode, and the bottom side has a 10mm area to achieve resonance frequency (f0).

QCMs have typical resonance frequencies in the order of MHz, and there is always a trade-off between the frequency (relating to the sensitivity) and the thickness (relating to the usability) of QCMs; the thinner the crystal, the higher the resonant frequency. The common frequency (f0) of a 5 MHz crystal has a corresponding thickness of ~ 330 μm. This is the crystal that will be used in this thesis, due to its wide availability, as well as its mechanical stability.

The additional property that the QCM-D provides over the QCM is the dissipation measurement, which can be described by a "ring-down" technique. This technique is made possible due to the external driving voltage which is turned off intermittently and the oscillation is left to decay freely. Given that quartz is piezoelectric, a voltage is generated during these decaying mechanical oscillations. This signal is recorded, which yields two parameters for each overtone; the resonance frequency F_n and the dissipation D_n. Additionally, the QCM-D is capable of viscoelastic characterization (via energy dissipation measurements) of bound masses [186]. The dissipation can be defined as:

$$D = \frac{E_{lost}}{2\pi E_{stored}}$$

Equation 2.2: Dissipation equation, where D is the dissipation, E_{lost} is the energy (or dissipation) lost in each cycle, and E_{stored} is the total energy of the system.

In Fig 2.3 below, a diagram has been constructed in order to understand the importance of both the change in frequency and the change in dissipation that occurs when using the QCM-D. An oscillating AC signal is applied to one contact electrode whereas the electrode in contact with the sample solution is grounded. Once peptide adheres to the surface, the resonance frequency will decrease due to the added hydrated mass, and the dissipation will increase due to a layer being formed on the surface of the electrode, which dissipates energy.

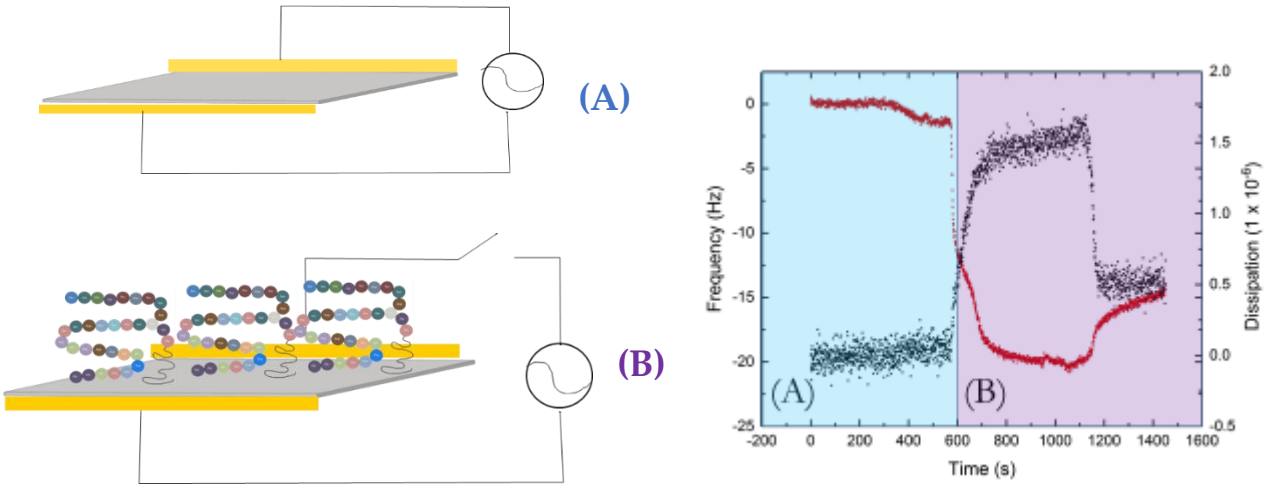

Figure 2.3: The QCM-D principle. (A) Shows the sensor electrode without any peptide. The frequency and dissipation shown in the box in the left have been normalized by the chosen buffer. (B) The crystal once mass is adsorbed, and hence the change in normalized frequency and dissipation in the purple box on the right, which can then be used to determine hydrated mass.

The resolution of frequency and dissipation in liquids is in the order of ± 0.1 Hz and 1 × 10^{-7}, respectively, with typical f and D responses for protein, vesicle, or cell adsorption being of the order of tens to hundreds of Hz and 10^{-6} units of dissipation.

Due to the QCM-D providing simultaneous frequency and dissipation monitoring, it is considered a useful technique for many biological applications.

The method was applied to pancreatic ductal adenocarcinoma (PDAC) detection through studying the interactions between synthetic phosphorylated and un-phosphorylated α-enolase peptides of healthy and PDAC patients, where synthetic peptides were immobilized on the gold surface of the QCM-D sensor via a self-assembled alkanethiol monolayer [187]. The dissipation factor provides evidence of viscoelastic behaviour, and hence both mass and structural properties of the adsorbed layer can be gauged from this technique [188], [189].

As previously stated, one of the major applications of QCM-D is its ability to measure peptide adsorption in nanograms, as well as being able to determine viscoelastic properties of the deposited layer. For the adsorption of small peptides (in the range of 3-4 KDa in size), there are few techniques that can accurately determine mass adsorbed to such small quantities. Yoshinari et al used the QCM-D to look at the adsorptive behaviour of histatin 5 on PMMA surfaces in the production of biofilms [190]. Protein adsorption of BSA and Fg, as model proteins, were looked at onto hydrophobic and hydrophilic surfaces using the QCM and grazing angle infrared spectroscopy in a large study done by Roach et al in 2005 [191].

However, one of the drawbacks of the QCM-D is that the equipment is sensitive, so it needs to be cleaned thoroughly and trapped dust can become an issue. In addition, due to its sensitivity, consistent results can be another problem. In this thesis, all QCM-D results displayed were taken at least three times, with their averages and errors displayed.

2.3 Dynamic Light Scattering (DLS)

Dynamic light scattering (DLS) is a technique that can be used to determine the size distribution profile of small particles in solution. DLS is a common technique, and one of the few to determine hydrodynamic radii at low concentrations. A laser light will encounter particles in solution, and the light will be scattered in multiple directions due to Rayleigh scattering. The scattering intensity changes over time, due to particles undergoing Brownian motion. Hence, the distance between the particles scattering in solution is constantly changing with time [192]. This scattered light then undergoes interference by the other surrounding particles. From this intensity fluctuation, information about the time scale of movement of the particles that scatter the light can be obtained [193].

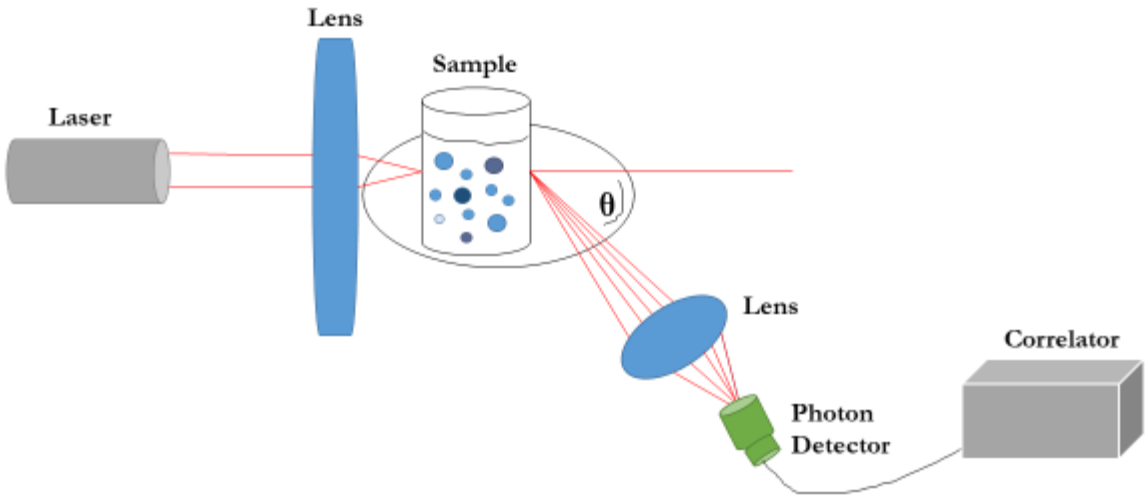

Figure 2.4: Diagrammatic representation of the DLS set up. In this diagram, the sample solution is polydisperse, which is highly likely in a peptide sample.

The hydrodynamic radius of a sphere in the colloidal solution, determined through the Stokes – Einstein equation:

$$D = \frac{kT}{6\pi\eta R_h}$$

Equation 2.3: Where D is the diffusion coefficient, k is Boltzmann's constant, T is the temperature, η is the solvent viscosity, and R_h is the hydrodynamic radius of the particles in solution [194].

Burchard used DLS as a technique to determine the shape and size of synthetic polymers and branched biopolymers [195]. Dynamic light scattering is often used to analyse nanoparticles in solution, as its lower limit can be close to 1-2nm [196]. DLS can also be used for theoretical modelling in viscous media, where particles can only make limited Brownian motion excursions, and hence more accurate theoretical predictions can made [197].

From the above examples, it can be seen that dynamic light scattering is a very useful and widely used technique. However, the technique gives the size distribution of particles, and hence exact sizes of colloidal solutions are difficult to determine. DLS cannot distinguish between a particle of 90 nm or 120 nm and a broad peak and high polydispersity index would appear.

2.4 Zeta Potential

Zeta potential is a quick and easy measurement which is taken to determine the magnitude of a charge on the colloidal solution, and hence can also be a key indicator of the stability of the colloidal dispersion [198]. Zeta potential is an electric potential at the slipping plane of the particle.

An electric field is applied, and the particles in solution move due to their interaction and the applied electric field. The particles movements will have a certain velocity and direction, which are dependent on its charge, the medium and the electric field strength applied. The zeta potential can therefore be found by observing the Doppler shift in the scattered light, which gives particle velocity. Particle velocity is proportional to the electric potential at the shear plane, which is zeta potential. Hence, the optical measurement of the particle motion under an applied field can be used to the determine zeta potential [199].

Particle motion under an applied electric field is known as Doppler electrophoresis. As described above, the zeta potential can be linked to the electrophoretic mobility of the particles through the Henry equation below:

$$\zeta = \frac{U\eta}{\varepsilon f(ka)}$$

Equation 2.4: Zeta potential equation through rearrangement of the Henry equation. U is the electrical mobility, the η is the solvent viscosity, ε is the dielectric constant of the known solvent, f(ka) is the Henry coefficient.

The Henry coefficient for particles in a polar medium can be found by the Smoluchowski model, or by the Hückel approximation for particles in a non-polar medium [200].

In other terms, the zeta potential is the potential difference between the solution in which the particles are dispersed, and the stationary layer of fluid attached to the colloidal particle as it moves [199]. Colloidal stability can be loosely seen to adhere to the DVLO theory, which relies on both electrostatic repulsion and attractive van der Waals forces [201]. The magnitude of the zeta potential indicates the degree of electrostatic repulsion between adjacent, similarly charged particles in a dispersion. For molecules and particles that are small enough, a high zeta potential will confer stability, i.e., the solution or dispersion will resist aggregation [202].

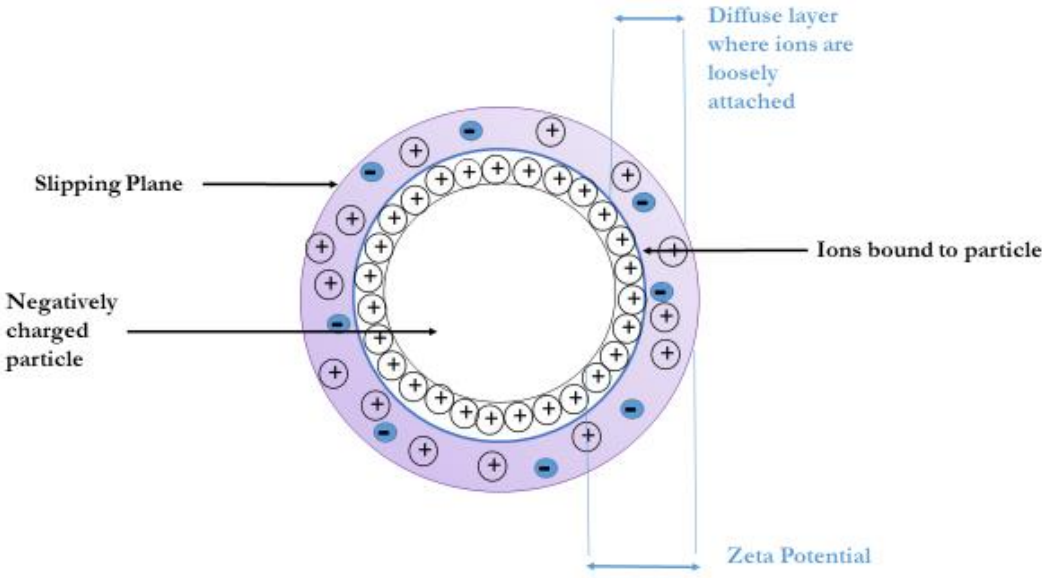

Figure 2.5: Diagrammatic representation of a particle in colloidal conditions and the DL (shown above as the diffuse layer and the inner layer) and the slipping plane, which are found using Zeta potential.

Zeta potential has been widely used for a number of different experimental uses. Wilson et al used zeta potential to assess the surface charge of bacterial cells, which is vital for the maintenance of optimal cell function [203]. Zeta potential measurements are also used in non – biological fields, such as for the adsorption of superplasticizer for cement production [204].

2.5 Electron beam Lithography (EBL)

E-Beam Lithography (EBL) is a nanofabrication technique which has been derived from the first scanning electron microscopes. Similarly to photolithography (PL), EBL uses electrons instead of light to cross-link polymers in the resist, referred to as the e-beam resist [205]. Once the electrons pass over the resist, the remaining polymer can be dissolved presenting the pattern.

The first step in nanofabrication patterning in EBL is to coat the substrate with the e-beam resist, poly(methyl methacrylate) (PMMA). This resist is hardened by baking. In the second step, the e-beam is used to either disrupt the polymer resist (for positive resists) or to cross-link the molecules to produce larger chains (for negative resists) [206]. In this thesis, a positive resist (PMMA) was used and the next steps are explained. Once the e-beam exposes the desired pattern area, the exposed resists polymer chain is disrupted, and hence the now smaller chains can be removed. The previous step is called the development stage, and several solvents can be used to remove the smaller polymer chains [207]. After removing the exposed resist, the following phase of EBL is to deposit a material (for this thesis the material in question is gold) on the substrate. The material is deposited on both the developed area, as well as the unexposed area. The gold deposited on the unexposed area can then be removed by the lift-off process. The lift off process requires a strong solvent to remove the unexposed resist. Once this resist is dissolved, the deposited material on top of the resist can be peeled off, as it's no longer tethered to the substrate. This process is shown in Fig 2.6 below. In this thesis, the E-beam was used as a lithographic technique in order to create different sized nanopatterns on a gold QCM-D, which can then be used to investigate the effect on surface roughness on peptide adsorption.

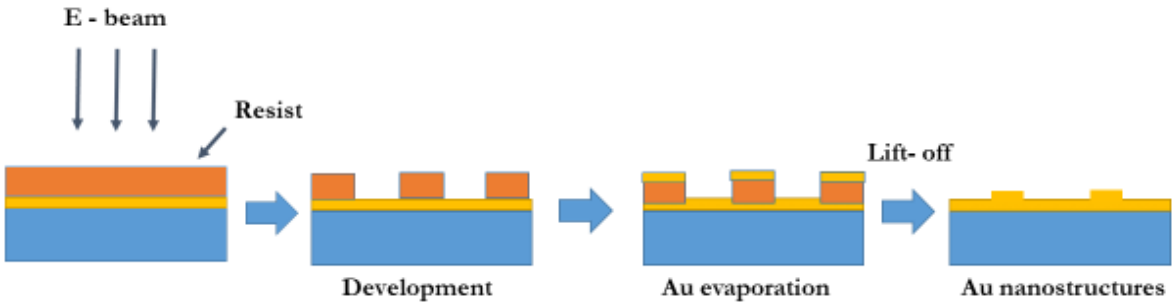

Figure 2.6: The mechanism of e-beam lithography, showing the resist, development, evaporation and lift off stage using a gold substrate to create gold nanostructures.

The electron beam is often used for lithographical purposes for both micro and nanofabrication [208]. However, applications of E-beam range from sterilization of biological materials to cross-linking of PEG based polymers [209], [210]. The primary advantage of electron-beam lithography is that it can create specific surface modifications with sub-10 nm resolution [211]. Yet, this type of lithography has high resolution but a low throughput, limiting its use in large scale development and research [212].

3 Chapter

An investigation of the stability of glucagon, g797, liraglutide and exendin-4 in different solution conditions.

3.1 Introduction

The overall aim of this thesis is to explore the aggregation and adsorption of four therapeutic peptides to a variety of surfaces, in order to better understand how to regulate aggregation. The first critical step in this process was understanding the behaviour of these peptides in solution. This chapter investigates the ability of these four specific peptides to aggregate in solution, to identify potential aggregate structures that they form in solution and to assess peptide stability.

Studies have identified that most, if not all, peptides and proteins are able to form amyloid-like aggregates under appropriate conditions [213]. Amyloid fibrils are associated with numerous diseases, amongst which; Alzheimer 's, transmissible spongiform encephalopathies, and type 2 diabetes [214]–[216].

In this study, we focus on glucagon and human glucagon-like peptide-1 (GLP-1) derivatives due to their importance as drugs for the treatment of type II diabetes, as discussed in Chapter 1. Despite their therapeutic effects, their uses as therapeutic drugs are limited by fast degradation in blood which is catalysed by peptidases, and by their shelf life limitations where peptide-surface interactions are crucial. The lipid chain can play a critical role in aggregation processes by enabling binding with carrier proteins like albumin as well as promoting self-aggregation. Both of these mechanisms are main factors for extending the peptide

half-life following subcutaneous administration [17], [217]. Therefore, one of the focuses of this chapter was to compare and contrast the behaviour of two peptides with lipidated chains (liraglutide and g797) and the two peptides without lipidation (glucagon and exendin-4).

The four peptides investigated in this study were all utilized for similar glucose related functions. Moreover, they all have similar backbones related either to glucagon or GLP-1, and are all comparative in size, as can be seen from Table 3.1 below. The table also displays their exact amino acid sequence and their isoelectric point (pI).

Table 3.1: The properties of the four peptides under investigation in this thesis including their sequence, isoelectric point and their molecular weight in daltons.

Peptide	**Sequence**	**pI**	**MW* (Da)**
Glucagon	HSQGTFTSDYSKYLDSRRAQDFVQ WLMNT	7.30	3485
G797 (lipidated glucagon analogue)	HSQGTFTSDK(gGluPalm)^{10}SEYLDSE RARDFVAWLEAGG-amide	4.28	3727
Exendin-4 (GLP-1 analogue)	HGEGTFTSDLSKQMEEEAVRLFIEW LKNGGPSSGAPPPS-amide	4.20	4186
Liraglutide (lipidated GLP-1 analogue)	HAQGTFTSDVSSYLEGQAAK(gGlu Palm)^{20}EFIAWLVRGRG-acid	4.15	3751

*MW of the peptides are all similar, and hence weight is not taken into account in this study.

Therefore, the four peptides under investigation can be compared to one another. An investigation into the ability of each individual peptide to fibrillate in different conditions is crucial to establish not only the stability of each peptide, but equally to compare and contrast stabilisation mechanisms, aggregation structures, and effects on the function of the peptides. The aim of the chapter

was to gauge the stability of each peptide in extreme conditions, which is established by increasing the concentrations, and changing the pH of the solution. The increase in concentration will lead to denser packing, and hence an increase in peptide association. Different pH conditions will lead to the peptide being either predominantly positively or negatively charged, or carrying little overall charge. Both the concentration and charge of the peptide solution will have a large effect on both the speed of fibrillation and the potential structures formed.

In Chapter 1, each peptide was discussed in terms of function and the reason they are investigated in this thesis. In this chapter, each peptide will be discussed in more detail regarding their structure and secondary structure in different conditions.

3.2 Methods and Materials

For initial aggregation studies, each peptide was put in varying environmental conditions to gauge its intrinsic stability and investigate aggregate formation. The initial peptide concentration studied was 0.5 mg/mL, which is one of the low concentrations commonly used in applications of therapeutic peptides [218]. The concentrations were then increased as follows; 1.0 mg/mL, 2.5 mg/mL and 5.0 mg/mL. These concentrations coincide with concentrations used in the formulation stages of therapeutic peptides [219], [220]. The next step was to investigate the effects of a change in pH. Due to the isoelectric points of the peptides, we can assume they are positively charged in highly acidic conditions, and negatively charged in highly basic conditions. As charge plays a large role in the aggregation of peptides, this is a parameter that is vital to investigate. The overall charges of the peptides in each buffer was also investigated using Zeta Potential.

3.2.1 Peptide preparation

Peptides were purchased from Bachem (> 95% purity), and g797 peptide was made with a peptide synthesizer at AstraZeneca. Hydrochloric acid buffer solution (0.05 M, pH 2.4) was prepared using hydrochloric acid (37%), glycine (> 95%) and HPLC water (resistivity > 18 MΩ/m). Filtered (polypropylene syringe filters, pore size = 0.22 μm, GE Sciences, Whatman) peptide stock solutions of glucagon (3.48 kDa), exendin-4 (4.19 kDa), liraglutide (3.75 kDa), and g797 (3.72 kDa) were each prepared in the same buffer solution (HCl/Glycine, pH 2.4) and then diluted for analysis. Peptide solutions were initially made up at 5.0 mg/mL. Glucagon has been studied extensively in acidic conditions (due to its isoelectric point at 7.4 making it difficult to assess in neutral conditions), and hence all concentration studies were done at a pH of 2.4 unless stated otherwise. Peptide were made at a concentration of 2.5 mg/mL.

All peptide solutions were deposited into 2 mL plastic vials (Vial Shell 2 mL, VWR, UK). Each vial containing peptide solution was then put on the WhirliMixerTM spinner (Fischer, Scientific, UK) for a few minutes, to make the solution as homogenous as possible and to prevent sedimentation. The concentration of the diluted peptide solutions was checked by UV-Vis spectroscopy (Varian Cary® 300 UV-Vis Spectrophotometer, Agilent Technologies, UK) at 280 nm. The absorption spectrum of water and cuvette were deducted from the peptide solution UV spectrum, and the spectrum UV 280 value was corrected for the UV 800 signal. The molar mass M and theoretical extinction coefficient ε of glucagon, exendin–4, g797 and liraglutide were used to calculate the peptide concentration according to the Lambert-Beer law.

The resulting peptide solution was put onto the MaxQ 4450 shaker/incubator (Fisher Scientific, UK) at an rpm of 200 at 37˚C incubation. Aliquots of 4 μL were taken out of each peptide solution (2 mL) at specified time points (t = 0 hrs, t = 2 hrs, t = 4 hrs and every 2 hrs thereafter, until t = ∞) in hours. From the literature, peptides were known to aggregate within the first few hours [221]. Due to restrictions on lab access, t = 12 hrs was the last sample done that day. From t = 12 hrs onwards, samples were then taken every six hours (t = 18 hrs, t = 24 hrs) until t = 96 hrs. After 4 days, each sample was taken once daily. For the purpose of aggregation studies, t = ∞ is the time given for continuously taking samples for 4 weeks at a daily time point.

As each peptide solution was deposited on freshly cleaved mica, left to dry and then imaged using the AFM, it was not possible to do time points every hour.

3.2.2 Change in concentration

For concentration dependent experiments, the peptide stock was made at 5.0 mg/ml and diluted accordingly (2.5 mg/mL, 1.5 mg/mL and 0.5 mg/mL) for each experiment relating to concentration.

As previously stated, all peptide solutions were deposited into 2 mL plastic vials and mixed for a few minutes, to make the solution as homogenous as possible and to prevent sedimentation. The concentration of the diluted peptide solutions was checked by UV-Vis spectroscopy at 280 nm.

The resulting peptide solutions were incubated at 37°C and shaken at an rpm of 200. Aliquots of 4 μL were taken out of each peptide solution (2 mL) at the same specified time points as discussed in the previous section.

3.2.3 Change in pH

Peptide solutions were made as stated in Section 3.2.1. However, for changes in pH, different buffers had to be prepared. Acidic buffer preparation was also described in Section 3.2.1 above.

The neutral buffer used was phosphate buffered saline (PBS) at pH 7.4, and bought from Sigma Aldrich, UK for a 1L solution and diluted to make a 0.05 M buffer solution. Additionally, sodium phosphate buffer solution (0.05 M, pH 10.8) was made using sodium phosphate (anhydrous, < 95%), glycine and HPLC water. Filtered peptide stock solutions glucagon, exendin-4, liraglutide and g797 were each prepared in the same buffer solution (either neutral, acidic or basic depending on experiment) and made up for a concentration of 2.5 mg/mL in 2 mL plastic vials.

The resulting peptide solutions were shaken at an rpm of 200 and incubated at 37°C. Aliquots of 4 μL were taken out of each peptide solution (2 mL) at the same specified time points as discussed in Section 3.2.1.

3.2.4 Atomic Force Microscopy (AFM)

For the experiments regarding both change in concentration and change in pH, Atomic Force Microscope (AFM) was used in order to track the structural changes at different time points of the prepared peptide samples. The theory behind AFM is summarized in Chapter 2, Section 2.2.

For the sample preparation, a 4 μL aliquot was taken out of the vials at specific time points (t = 0 hrs, t = 2 hrs, and every two hours thereafter) for as long as needed until fibrils were seen by the AFM. Fibrillation was defined as finding fibrils in each area investigated by the AFM (for each sample, this was at least 3 separate areas). Conversely, a state is only classified as not containing fibrils if no fibrils are detected in three independent AFM topography maps. The aliquot was deposited on a freshly cleaved mica sheet, which was cleaved with tape to create an even, clean and smooth surface. The sample was left to air dry for 20 minutes under a watch glass to prevent contamination. On occasion, some samples fibrillated very quickly and within a few hours had formed a thick network. Once this was imaged, samples were dispersed in water in up to 100-fold dilutions. As this was a dilution of the fibrous network that had already formed, this did not affect the concentration of the original sample. Once the sample had dried, the mica was put on the sample holder of the AFM.

A PicoPlusTM AFM (Molecular Imaging) with a PicoSPMII controller was used in tapping mode. The AFM probes (HQ:NSC36 /No Al (MikroMasch®, via Windsor Scientific LTD, UK) had a tip radius < 8 nm and force constants between 0.6 and 2.0 N/m. The scanning rate was 0.6 - 0.9 lines per second (depending on the sample) and a maximum imaging area of 9 x 9 μm (for closer detailed images, 3 x 3 μm were used) and resolutions of 512 x 512 or 1024 x 1024 pixels.

To edit images, Gwyddion software was used, a multiform platform to visualise and extract information from AFM images. Through Gwyddion, information

about the lengths, thickness and heights of aggregates can be found, as well as the roughness of surfaces.

3.2.5 Zeta Potential

Zeta Potential was used in order to verify the overall surface charge of the peptides, in different pH conditions.

Peptide solutions were made up at a concentration of 2.5 mg/mL in separate vials. Each peptide solution was made at acidic, neutral and basic conditions. Measurements of the zeta potential of the peptides were made on a Malvern Zetasizer Nano ZS (Malvern Instruments Ltd, UK) with a backscatter detection angle of 173°. The Nano S range uses a He-Ne laser operating at 633 nm. All measurements in the study were taken at a temperature of 25°C ± 0.1°C. Both buffer solutions (previously described) have a viscosity of 0.8952 cP and a reflective index of 1.332, giving no detectable background signals in the instrument and therefore, were used as a negative control during measurements.

3.3 Results

The results presented in this section will tackle the stability and aggregation structures formed by each peptide as the concentration and pH was changed. The formation of fibrils and other aggregates go through three stages on a macroscopic level; the lag phase, the growth phase and the final plateau phase.

Each of these individual phases depends on the changes that are made on the microscopic level; amino acid sequence and solution conditions such as temperature, pH and concentration. Therefore, these results will present information on the aggregation of the four chosen peptides, in differing solution conditions.

The peptide glucagon, which some of the other peptides are based on, is the initial starting point of discussion. This will lead to a detailed analysis of the results of g797, followed by liraglutide stability and aggregation potential, and lastly, exendin-4's stability and aggregation data. Once all four peptides have been discussed in detail, an overview and comparison of the therapeutic peptides was presented.

3.3.1 Glucagon

Glucagon is a peptide hormone, which is produced in the alpha cells of the pancreas. Due to its natural occurrence in the body, the peptide is well tolerated, sparking a trend of glucagon based therapeutic peptides over the past decade [4]. Glucagon has an isoelectric point of 7, making it insoluble at a neutral pH and most neutral conditions. Subsequently, glucagon becomes either negatively or positively charged according to solution conditions. Glucagon equilibrates between a random unordered structure and an α -helical structure in solution. Yet, depending on the pH, salt concentration, temperature and an array of other environmental conditions, this can quickly change to a β-sheet structure, producing amyloid-like fibrils. This, among other reasons, is why glucagon is such an interesting and useful peptide to base research on; many peptides act in a similar fashion - balancing different environmental stresses through their structure [100].

Each amino acid has their own intrinsic property, and hence contributes to glucagon's aggregation and fibrillation structures and mechanisms. For instance, aspartic acid (denoted as Asp), carries a negative charge at isoelectric pH and is known to form electrostatic interactions crucial to glucagon's function as a polypeptide hormone. When Asp was engineered out of the peptide chain, glucagon's activity was lost [222].

Literature dictates that glucagon, with its isoelectric point close to 7, will fibrillate in most conditions above and below its pI and within a short time frame [223], [224]. Due to its natural occurrence in the body, glucagon has been examined for many years. Consequently, the literature on glucagon is vast, yet varied. Glucagon forms fibrils, in differing sizes and structures comprising of alpha helices and beta sheets. Additionally, in the right conditions glucagon also forms oligomers, and aggregates [225]. Full mechanisms of the aggregation of glucagon

are still not fully known, and hence, this chapter will investigate its aggregate structures at specific conditions.

3.3.1.1 Change in concentration

The change in concentration was assessed using AFM imaging. DLS was used to confirm structural size changes (shown in the Appendix).

As described in Section 3.2.2, AFM images were taken at t = 0 hrs, and then every 2 hrs until aggregate structures were found to have formed in all three AFM image panels. In Fig 3.2 below, on the left hand side we can see the initial peptide solution (t = 0 hrs) images at 0.5, 1.0, 2.5 and 5.0 mg/mL on mica. The initial images show no fibrillar structures, but do show small structures. As buffers were always initially checked for contamination, and samples were taken from fully suspended solution and filtered according to protocol, these are likely to be small aggregates. However, the possibility of small amounts of unsuspended peptide causing those structures cannot be ruled out completely.

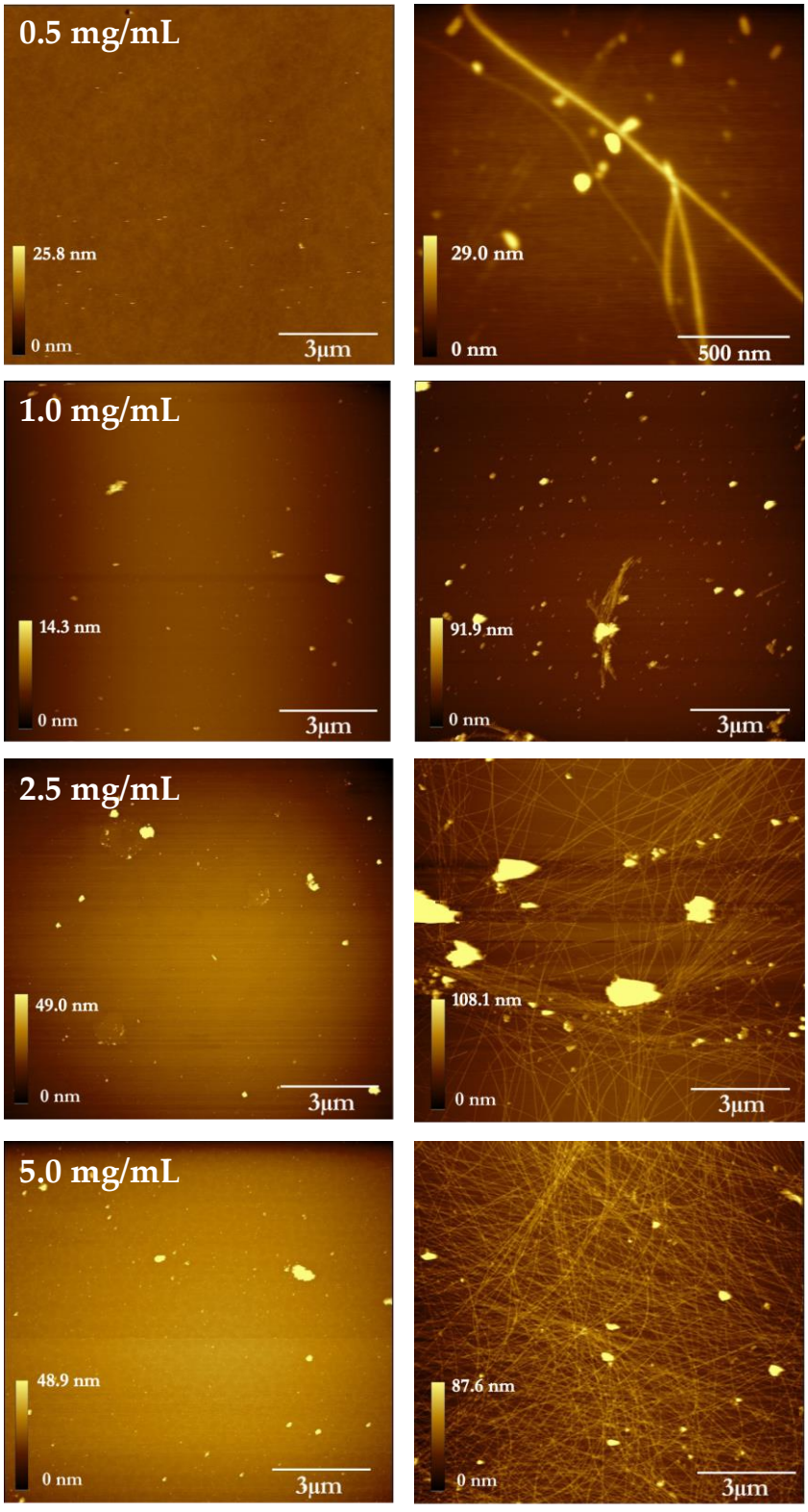

Figure 3.1: Left - AFM images of glucagon at increasing concentrations at t = 0 hrs. **Right -** AFM images of increasing concentrations at t = 4 hrs for the top two images, and t = 2 hrs for all other images. Long and thin fibrils form at all concentrations. Increasing the concentration of the solution increases the density of the fibrils. Images were 9 µm x 9 µm in size, scanning rate 0.84 lines per second and at a resolution of 512 x 512 pixels. Top image was 1 µm x 1 µm in size.

These spherical oligomers vary in size, and are usually considered precursors for fibrillation of glucagon [220]. The structures are typical of early onset aggregation, and have recently been investigated for their toxicity [81]. Additionally, these oligomers contribute to thicker gel like properties, and can make it difficult to use therapeutically.

The right hand side of the panel in Fig 3.1 displays the fibrils at the specified concentrations at a time when fibrils have formed. At both 0.5 mg/mL and 1.0 mg/mL, it took glucagon 4 hrs to show fibrillation in all three independent AFM images. The shape of the fibrils are straight and long and this is congruent at all concentrations. At lower concentrations, fibrils cover on average 10 – 14.5% (± 2.1%) of the surface. The average is taken of all three individual AFM images at one concentration, and lower concentrations are defined as 0.5 mg/mL and 1.0 mg/mL. Initially, fibrils are sparse, and there are also large aggregates formed. From the two top images in Fig 3.1 on the right hand side, fibrils can be seen to be growing from an oligomer nucleation point. Nucleation, as previously described in Chapter 1, is seen as the starting point for fibril formation [226]. However, in recent years, its been suggested that nucleation is not necessarily a one-step reaction to fibrillation, but instead an oligomer can be a precursor for fibrillation, through a nucleated conformational conversion [227], [228]. The nucleation conformational conversion theory seems to be very similar to the images seen in Fig 3.2 above. Thicknesses of the fibrils at low and high concentrations stay similar, between 5 – 10 nm in diameter. At higher concentrations, the density of the fibrils increases, as does the rate of fibrillation. For higher concentrations, fibrils were identified in all three AFM images within 2 hrs. The fibrils that are formed are long and straight (up to around 10 μm), which is concurrent with the literature, and typical of filament formation [221]. At the higher concentrations, the filaments stay straight and show well defined patterns, with a smaller number of large aggregates. From assessing the images

above, and from thorough investigation into the fibrils, it is likely that the filaments grew in a longitudinal direction and not radially. The increase in length but not width adds weight to the theory that some fibrils grow through oligomeric addition to the ever extending fibril [227]. In addition, these straight fibrils are a well-known fibril formation structure presented in literature in acidic conditions [82][229].

With increasing time, the fibrils formed at higher concentrations the density of the fibril networks increases and the structures start stacking upon each other. Fibrils can be tens of μm long, with thicknesses in the range of 8 – 15 nm. This can be seen in Fig 3.2 below, where an AFM image was taken of glucagon at a concentration of 5 mg/mL but left to fibrillate for 48 hrs.

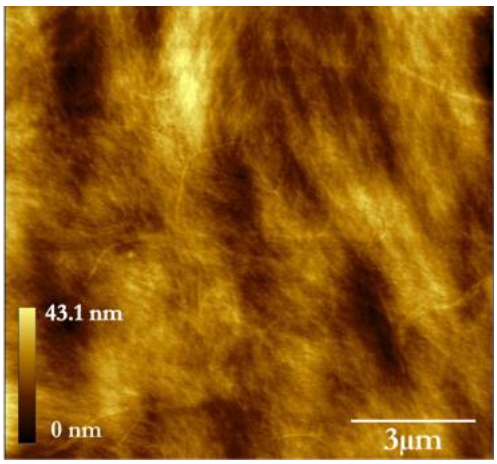

Figure 3.2: An image of a sample of glucagon at 5.0 mg/mL after 48 hours. The captured image was 9 μm x 9 μm in size, at a rate of 0.84 lines a second, and with a resolution of 512 x 512 pixels. As can be seen by the above image, individual fibrils are difficult to identify, and the sample was cloudy, indicating gelation.

In Fig 3.2 above, some differences can be identified compared to the fibrils at just 4 hrs. Firstly, there are no large aggregates after a longer incubation time. Larger aggregates are known to be the precursors of fibrillation, and hence are expected to diminish in number [70], [102]. The AFM images show that the fibrils contain twists, which correlate with their α-helical structure during fibrillation. Alpha – helices are typical of fibrils formed by glucagon, and this finding has been well

documented [229]. Fibrils are formed in acidic conditions due to the highly polarised glucagon at a pH of 2.4. A large number of amino acids will carry a positive charge – only the carboxyl terminus remains slightly negatively charged. These positive charges repel each other and keep the glucagon molecule relatively straight. Therefore, a buffer is needed to overcome these strong charges in order to fibrillate. Glycine/HCl buffer contains both a Cl^- ion and zwitterionic glycine, which shield the strong positive charges and allows for aggregation. Agitation helps aggregation due to the free ends which are created through the shearing of the fibrils, which in turn can result in elongation, as well as increased protein-protein interaction. Secondly, the sample taken in Fig 3.3, which contains a very thick network of fibrils, became cloudy after 48 hrs. The cloudiness of the solution can be seen from looking at the sample vial, and this is how gelation is checked en masse [230]. Gelation was further confirmed by the AFM image. When the fibrils form, the consistency of the sample changes, and by the time a network of fibrils has formed, the sample becomes a gel - this process is called gelation. Glucagon is known to undergo many different pathways of aggregation, and beta sheet formation is one of them, especially in low pH's with agitation [124], [231]. From the image in Fig 3.3, it can be seen that individual fibrils are much more difficult to pinpoint and thick networks of fibrils can be seen, and as the sample get cloudier and gelates, due to β – sheet formation [221]. The process of gelation provides serious concerns in the pharmaceutical industry. As glucagon can be used for emergency medicine as an IV drug for hyperglycaemia, gelation is a major cause for concern. Congealing of the liquid can cause serious problems; the main one being that the drug can no longer be administered, rendering it useless or, even more seriously, that the drug is administered and congeals in the body [232].

From the AFM images above, it can be seen that glucagon forms fibril networks. In addition, the experiments have investigated that the fibrils show a

concentration dependence, and that the speed at which fibrillation occurs also increases with increasing concentration. Fibrils are formed in an array of different concentrations, yet their kinetics and aggregation products vary [233]. Glucagon is well known to aggregate and, in certain conditions, to form fibrils. Why it forms fibrils in certain conditions, and non-fibrillar aggregates in others remains somewhat inconclusive.

Even though fibrillation is concentration dependent, other parameters and aggregation structures of glucagon must also be assessed. Hence, pH dependence was also investigated, as this is a crucial parameter in understanding the role charge plays in aggregation of molecules.

3.3.1.2 Change in pH

a) Zeta Potential

Zeta potential, which is described in Section 2.4, can give the overall charge of the peptide (negative or positive) and can give an indication of the stability of the colloidal solution. It is a useful technique to use alongside an imaging technique, such as the AFM.

Glucagon's stability and charge was confirmed using the Zeta potential, displayed in Fig 3.3 below.

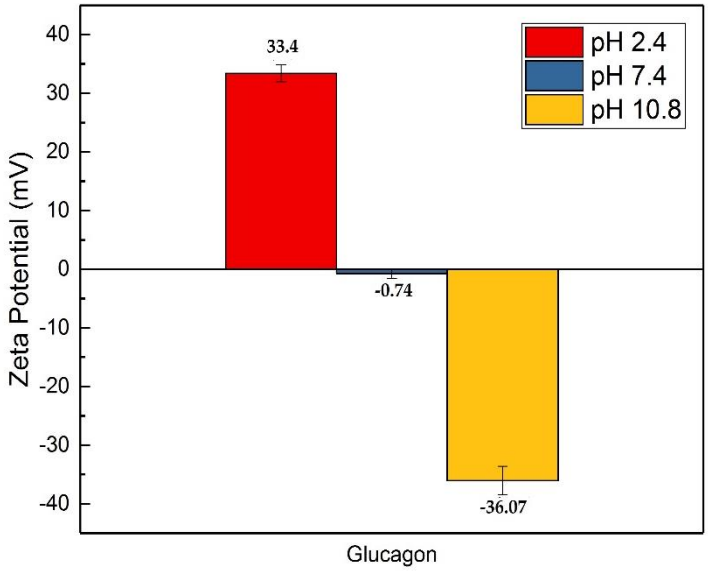

Figure 3.3: Zeta Potential measurements of glucagon in all three differing pH's (0.05 M buffer: Glycine/HCl, PBS and Glycine/NaOH) at a concentration of 2.5 mg/mL. The zeta potential shows that glucagon does indeed carry a large positive charge in acidic conditions, hardly any overall charge in neutral conditions, and a largely negative charge in basic conditions.

The figure above confirms that the charges of the solution are what is expected from the literature and the peptides isoelectric point. Glucagon carries significant positive and negative charges at a pH far from its isoelectric point. At neutral conditions, with a zeta potential very close to 0, glucagon is a highly unstable colloidal solution [199]. At isoelectric point, when the peptides carry no overall charge, they become highly unstable due to their increased peptide – peptide

interactions, and decreased peptide - water interactions due to their lack of charge. This also means they are more likely to precipitate and decreases their colloidal stability [234].

The change in pH of the solution will result in the charge of individual amino acids residues and the overall charge of the peptide changing. As stated in Chapter 1, charge plays a large part in both adsorption and aggregation of the peptide. The AFM was used in order to gauge the exact structures glucagon forms in these highly charged or uncharged conditions.

b) Atomic Force Microscopy (AFM)

In Fig 3.5 to Fig 3.7 below, the pH of the solutions was changed, and images were taken at t = 0 hrs and every 2 hrs for as long as it took for the solution to aggregate. These measurements between pH's varied considerably.

The first solution condition investigated was glucagon aggregation in acidic conditions, at a pH of 2.4, in Fig 3.4 below.

pH 2.4

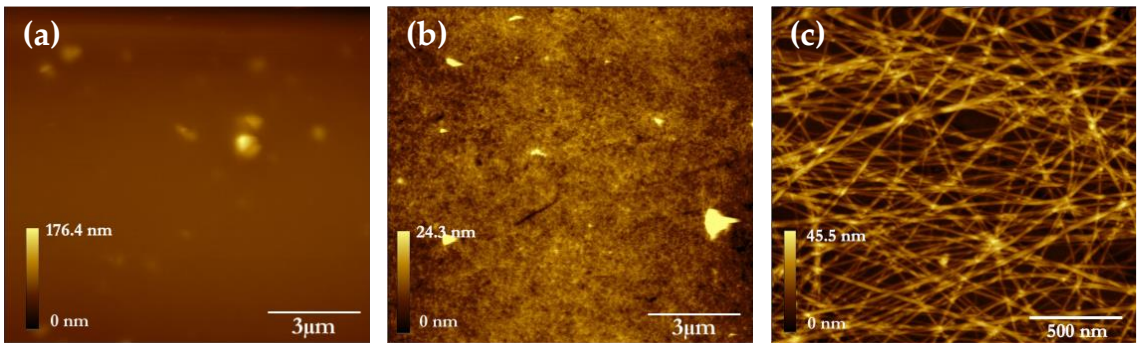

Figure 3.4: Glucagon fibrillation in Glycine/HCl buffer (0.05 M, pH 2.4) at 2.5 mg/mL. (a) At the starting points, T = 0 hrs, when no fibrils have formed. (b) Thick layer of fibrils after 2 hrs. Images (a) and (b) were 9 µm x 9 µm in size and were scanned at a rate of 0.91 lines a second. (c) A 10 fold dilution of the image in the middle, and a zoomed in perspective. Cross linking of fibrils and intricate fibril structure is evident. The captured image was 2 µm x 2 µm in size, at a rate of 0.84 lines a second, and with a resolution of 512 x 512 pixels.

Fig 3.4 above displays glucagon fibrillation in acidic conditions at a concentration of 2.5 mg/mL. As was seen in the previous Section, at the same concentration and pH, fibrils were formed at the same rate. In acidic conditions, at a pH of 2.4, fibrils are formed after two hours, and is concurrent with the literature [235]. At an acidic pH, far removed from glucagon's pI of 7.4, each amino acid in the glucagon sequence will carry five positive charges. However, as mentioned before, the carboxy terminus, with a theoretical pKa of 3, will be slightly negatively charged [225]. The 5+ charge repulsion between the glucagon molecules is large to overcome. In order to stabilize the aggregate structures, however, negatively charged molecules in solution can help, through charge shielding. As previously stated, In Fig 3.5 above, glucagon has been fibrillated in the presence of glycine/HCl buffer (pKa 2.36). At a concentration of 50 mM and at a pH 2.4, this buffer is predicted to contain around 24 mM of Cl^- and 30 mM of zwitterionic glycine, which is capable of shielding some of the 5+ positive charges of glucagon.

After a highly acidic solution, glucagon's aggregation potential was tested in neutral conditions in order to investigate whether the aggregates formed were similar in structure and kinetics.

At neutral conditions, glucagon is insoluble, which let to solutions being mixed for longer than 30 s as from previous experiments. This enhances mixing could have created more nucleation sites, from the free ends of fibrils. The aggregation studies were then performed in neutral conditions, with Fig 3.6 below displaying the results. Due to isoelectric point being very close to neutral pH, the sample was put on the mixer for an extended period of time to enhance solubility.

pH 7.4

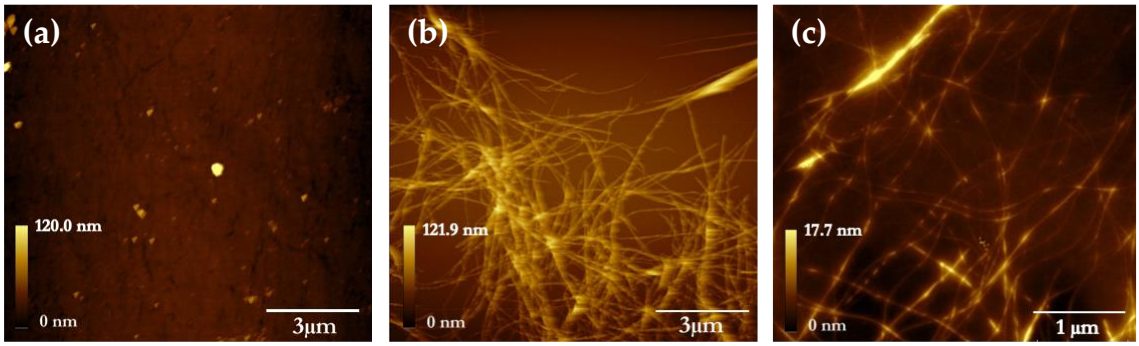

Figure 3.5: Glucagon fibrillation in PBS solution (0.05 M, pH 7.4) at 2.5 mg/mL. (a) T = 0 hrs, very few aggregates have formed, and small structures on the AFM image may be contaminants. (b) Fibril formation at t = 96 hrs. Fibrils have a less ordered structure than in acidic conditions, and at 96 hrs, not yet as thick a layer. Both (a) and (b) were size 9 µm x 9 µm and at a scanning rate of 0.91 lines a second. (c) A zoom of the image, at 3 µm x 3 µm in size, at a rate of 0.84 lines a second, and with a resolution of 512 x 512 pixels.

From Fig 3.5 above, there are a few noteworthy observations. The first interesting result was the time frame of the fibrillation. Having analysed all AFM images taken from three different sample areas, it took 96 hrs to see fibrils in all three areas. This suggests that in neutral conditions, glucagon has a much longer lag phase, due to its structural instability in neutral conditions. The appearance of the formed fibrils is also different to those shown previously in acidic conditions. The fibrils in Fig 3.6 are much less ordered, and not straight as was previously seen. These fibrils are twisted, and contain branching. The branching generates new fibril ends, which can then accept more monomers. The process of end on addition of monomers results in slow exponential growth in which the fibrils formed can grow up to 10 of µm [229]. The difference in structure and sizes of the fibrils suggests differences in both the stability and mechanisms of fibril formation in different pH conditions. The twisted nature of these fibrils are usually found when no agitation has taken place in acidic conditions, as they have a long lag phase [233]. These images show that the long lag phase persists, and similar fibrils are formed in neutral conditions with agitation. In addition, it

must be noted that due to the increased time of mixing, more ends would have been produced which would also have an effect on the structures formed.

As much of the fibril structure in pH 2.4 is related to charge, it was hypothesized that the mechanism and hence structure of the fibrils in neutral pH would be different, as well as the time to fibrillate. The next step was to identify whether fibrils in highly basic conditions would mimic those in acidic conditions, or present a different structure altogether.

Glucagon in a pH of 10.8 was investigated, where peptides carry an overall negative charge and the results shown in Fig 3.6 below.

pH 10.8

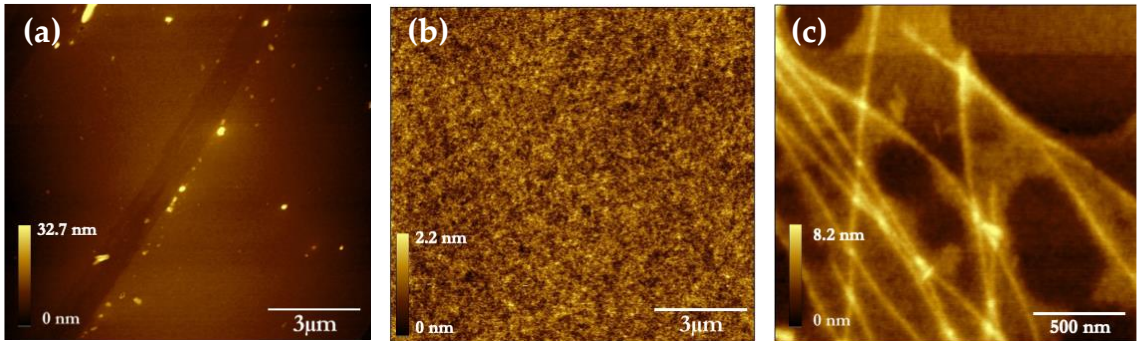

Figure 3.6: Glucagon fibrillation in Glycine/NaOH buffer (0.05 M, pH 10.8) at 2.5 mg/mL. (a) T = 0 hrs, aggregate formation is minimal and the aggregates formed are small in size. (b) A thick layer of fibrils have formed after T = 6 hrs. Both (a) and (b) images were size 9 µm x 9 µm and at a scanning rate of 0.91 lines a second. (c) A ten- fold dilution of a sample at T = 10 hours, and zoomed in at 3 µm x 3 µm in size, at a rate of 0.84 lines a second, and with a resolution of 512 x 512 pixels.

Fig 3.6 above shows the structures formed by glucagon at a highly basic pH. The AFM images presented a few interesting findings. Firstly, the structures formed are very different to both those in acidic conditions and neutral conditions. In basic conditions glucagon will carry an overall negative charge. At low pHs, the three Asp residues on glucagon will become protonated. At high pH levels however, these three residues on the glucagon backbone can function as

'gatekeeper' residues, that will block the formation of the meta stable fibrils formed in acidic conditions [236]. In addition, the Arg residues at position 17 and 18 could also be forming salt bridges with the Asp residues or the C- terminus in basic conditions [237]. Both of these theories could indicate why the fibrillation of glucagon in basic conditions is not only slower but also forms different structures. The fibrils above are highly packed, but disordered compared to those formed in both neutral and acidic conditions. The fibrils seem to be packing more closely, even though the height is only 2.2 nm. The close up also indicates long thin fibrils, much like those formed in acidic conditions, but stacked closer together. This could be due to the fact that glucagon no longer carries an overall 5+ charge, which made peptide-peptide repulsion strong between glucagon molecules. In addition, the close up image was taken after 10 hrs, and the height of the fibrils has increased, indicate close packed stacking of fibril layers. Another observation is that the molecules seem to have a hydration layer around them, indicating that some of the fibrils are surrounded by hydration shells, due to the large electrostatic interactions.

Discussion

Glucagon was investigated in different conditions by varying its concentration and pH. Through the change in conditions, there were significant changes in both the time to reach the lag phase and the structure of aggregates that were formed. This was due to amino acids associating with each other through different mechanisms, depending on individual charges and electrostatic interactions and hence forming different products.

Table 3.2 summarises the aggregation time studies and hence the stability of glucagon in different solution conditions. As stated previously, images were taken every 2 hrs which was unfortunately the maximum resolution of the kinetics study. All solutions were incubated at 37°C and shaken at 200 rpm.

Table 3.2: Summation of glucagon conditions of aggregation. Aggregation was defined as the presence of fibrils in all three different quadrant areas on the AFM.

Glucagon		
Concentration (mg/mL)	Time (hrs)	Structure and size (nm)
0.5	4	Fibrils of 5 – 10 nm in diameter and short at around 1 μm. Oligomers still present as precurors.
1.0	4	Fibrils start extending through monomeric addition, up to 3 μm, with oligomers still present.
2.5	2	Density of fibrils increases, and oligomers decrease. Fibrils extended to 10 μm.
5.0	2	Layer of fibrils, stacking of beta sheets, up to 45 nm thick.
pH		
2.4 (Glycine/HCl)	2	Structured and ordered fibril network, length of 10 μm, diameters of 5 – 10 nm.
7.4 (PBS)	96	Fibrils, long lag phase, very long (up to 12 μm), and thin (average 8 nm diameter)
10.8 (Glycine/NaOH)	6	Fibrils with hydration layer, layers of 2 -9 nm stacking, and shorter fibrils, 1- 2 μm in length.

The results confirm that glucagon fibrillation occurs at all different pHs, even at its isoelectric point, where glucagon exhibits a significantly longer lag phase due to colloidal instability. Timings were very varied, and depend on charge, as well as solution conditions such as concentration. Glucagon aggregation was confirmed to be dependent on both concentration and pH, which is congruent with literature [29][238].

The next peptide investigated was the lipidated version of glucagon, peptide g797.

3.3.2 G797

G797 is an internal AstraZeneca lipidated peptide. It is based on the glucagon structure due to its many advantages regarding peptide sequence, structure and tolerability in the body, discussed in Section 3.1.1 above. Glucagon's main drawback is its short in vivo circulation time before being degraded by dipeptidyl peptidase IV (DPV). Analogues of glucagon which have a longer half-life and/or are not degraded by DPV, have been hailed as the solution. G797 was synthesized with this in mind, and hence has an added lipidated chain.

Due to g797 being a test peptide for AstraZeneca there is no literature on its aggregation or adsorption patterns, hence, an investigation into its basic aggregation mechanisms in solution is vital. Yet, due to its structure and sequence, it is likely to act similar to other lipidated peptides, which have specific properties in solution, such as micelle formation. These properties are further investigated in this chapter and the next chapter, Chapter 4.

G797 is predicted to undergo similar fibrillation time frames to glucagon due to its structural similarity. However, its added fatty acid chain is hypothesized to stabilise the peptide. This is likely to affect both the structures it forms in solution as well as its kinetics, especially in relation to its lag phase, which is predicted to be longer.

3.3.2.1 Change in concentration

Fig 3.9 below shows the fibrillation of peptide g797 in solutions of different concentrations from t = 0 hrs until t = fibrillation, which varies depending on concentration.

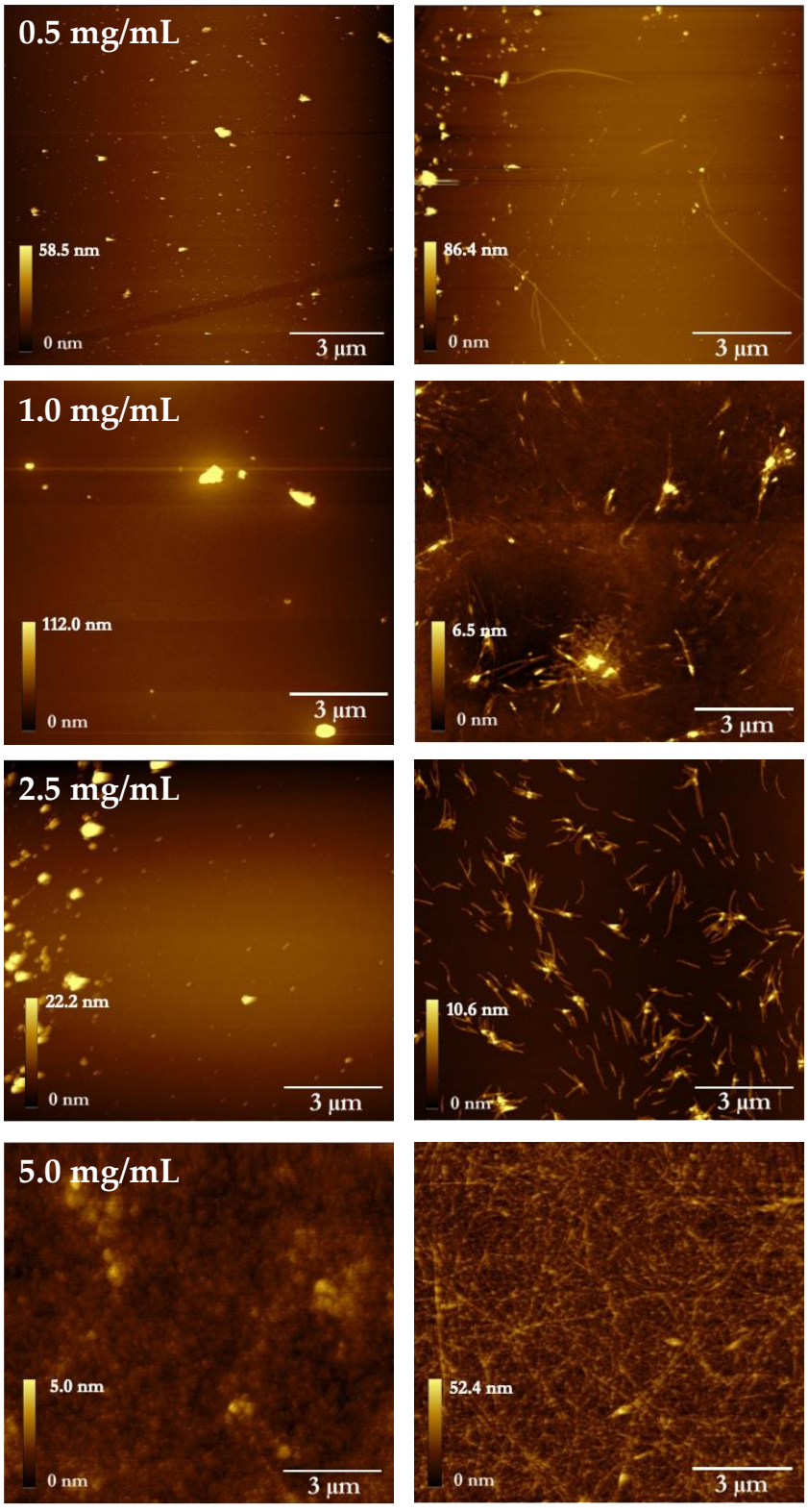

Figure 3.7: Left - AFM images g797 at increasing concentrations at t = 0 hrs. **Right -** AFM images of increasing concentrations at t = 4 hrs for the top two images, and t = 2 hrs for all other images. Increasing the concentration of the solution increases the density of the fibrils. Images were 9 µm x 9 µm in size, scanning rate 0.84 lines per second and at a resolution of 512 x 512 pixels.

From Fig 3.7 above, it can be seen that fibril formation of g797 is different to that of glucagon. The fibrils are shorter and stockier, and show no ordered network of fibrils and instead form a random disordered array. Although the difference is striking, the time taken to fibrillate is very similar. At 0.5 mg/L, g797 started showing fibril formation at just 4 hrs, decreasing to 2 hrs above 1.0 mg/mL. Additionally, at a low concentration, 0.5 mg/mL, fibrils tend to be up to a few μm in length, and as the concentration increases, the fibrils shorten and associate with each other in the y – direction.

In Section 3.3.1, it was deduced that from the appearance and time frame of the fibrillation process of glucagon, it is likely that glucagon takes a pathway where oligomers associated through the addition to the end of the fibril. The fibrils that g797 has produced are likely to undergo a different pathway. Short, stockier fibrils, (average length 100 – 200 nm) which can be referred to as protofibrils, are more likely to be formed according to the HAM (Hierarchal Assembly Model), described in more detail in Chapter 1. This predicts that protofibrils will elongate almost linearly with time initially (less than 10 hrs) and then the growth rate will decrease with time due to the consumption of peptide monomer. The structure of these fibrils is more likely to comprise of several cross-beta sheets which arrange with a head-to-tail arrangement, or by intercoiling of preassembled sheets. Typical amyloid fibrils are between 10 to 20 nm wide and can go up to several μm long, but average distances only reach a few hundred nanometres [239]. Twisting of the individual peptide, or the fibril, is induced through side chain packing restrictions and electrostatic effects. The degree of twisting is reliant on the sequence of the peptide, the number and arrangement of associated sheets, and the solvent conditions (among other environmental factors)[240].

G797 has a mutation which is a palmitic acid residue, which is linked through a glutamic acid, lipidating the original glucagon peptide backbone. This single amino acid mutation is known to drastically increase the peptides therapeutic

half-life. This reasoning is based on liraglutide, a peptide based on the GLP-1 sequence and an added fatty acid chain, the same as g797. The lipidation of the peptide should stabilise the structure, however, as the time studies have shown, g797 still fibrillates in just hours, even at a low concentration. Next, the charge on the peptide was investigated to gauge whether this has a large effect on overall peptide stability, or whether, with its additional palmitoyl chain, the charge will play less of a role.

3.3.2.2 Change in pH

a) Zeta Potential

The change in pH of the solution will result in the overall charge of the peptide, as well as individual amino acid residues, changing. The zeta potential of the peptide in different pH solutions is shown in Fig 3.8 below.

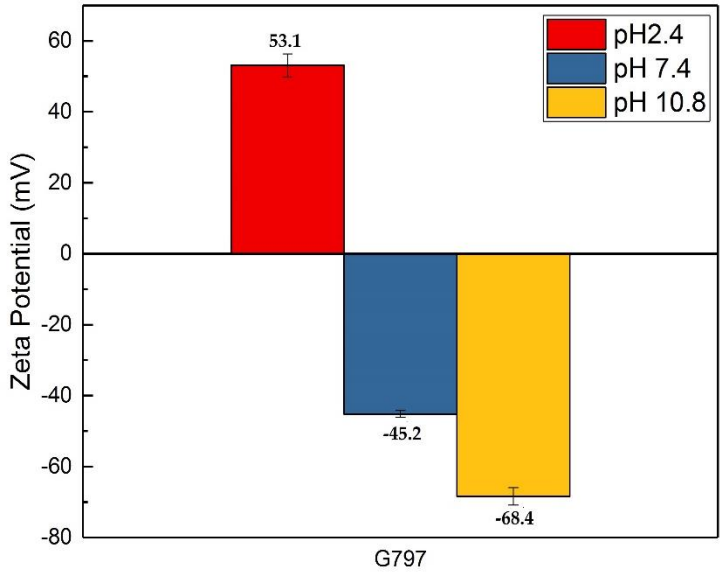

Figure 3.8: Zeta Potential measurements of g797 in all three differing pH's (0.05 M buffer: Glycine/HCl, PBS and Glycine/NaOH) at a concentration of 2.5 mg/mL. The zeta potential shows that g797 carries a large positive charge in acidic conditions, negative charge at a pH of 7.4 and a larger negative charge in basic conditions.

The error bars are the standard deviation for a set of three repeat measurements. The zeta potential has shown that g797 will be either positively or negatively charged in all conditions, even in neutral conditions when it still carries a large negative charge due to its isoelectric point, which unlike glucagon, is closer to 4.

b) Atomic Force Microscopy

First, g797 peptide was investigated in highly acidic conditions at a pH of 2.4. AFM images measured at different time points in the aggregation process are shown in Fig 3.9 below.

pH 2.4

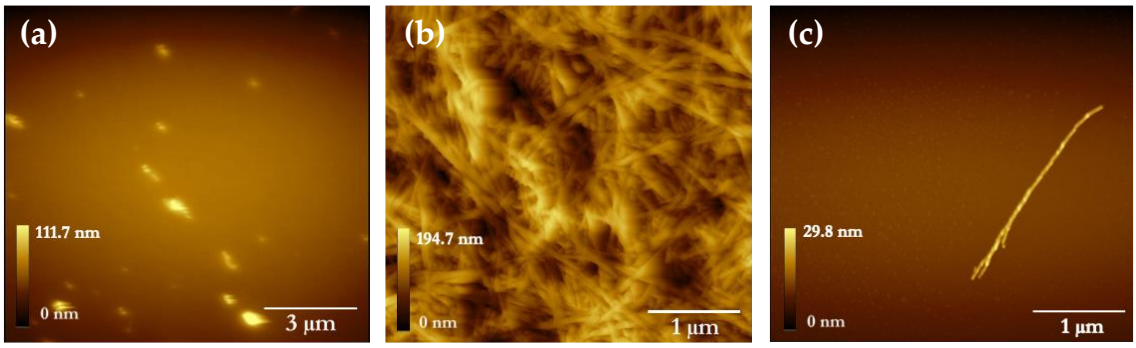

Figure 3.9: Peptide g797 fibrillation in Glycine/HCl solution (0.05 M, pH 2.4) at 2.5 mg/mL. (a) T = 0 hrs, the initial mica with little to no peptide aggregates. Image size 9 µm x 9 µm, rate 0.91 lines a second. (b) Fibril formation shown at t = 24 hrs. (c) A 100 fold dilution of the middle image. Size of 3 µm x 3 µm, at a rate of 0.84 lines a second, and with a resolution of 512 x 512 pixels.

As previously discussed, peptide g797 fibrillated quickly in acidic conditions, in 2 hrs at 2.5 mg/mL. Fig 3.9 shows the layers of fibrils formed after 24 hrs. This is a very thick layer of fibrils, and the fibrils shown are stockier, and thicker than those formed in acidic conditions by glucagon. Additionally, the dilution shows that the fibrils can grow up to 1-2 µm in length, especially as time increases, which corresponds to the fibrils growing according to the HAM theory. This length is also significantly shorter than those found with glucagon fibrils, which can be tens of micrometres long. The stacking of the fibrils is less ordered, and fibrils seem to be very close together, indicating less repulsive interactions between individual fibrils. The height of the stacked layer of fibrils is almost 200 nm in height, indicating many layers of stacking. The thickness of some of the fibrils could indicate association or protofibril formation, which then breaks due to instability creating more free ends for addition [229]. In addition, from the

dilution of the sample, individual fibrils can be seen to be slightly twisted, which could be concurrent with forming α-helices, which is a common structure found in amphiphilic peptide formation [241].

Whether this is a mechanism undergone for g797 in all conditions is not yet clear, and hence g797 was investigated at a pH of 7.4 in Fig 3.10 below.

pH 7.4

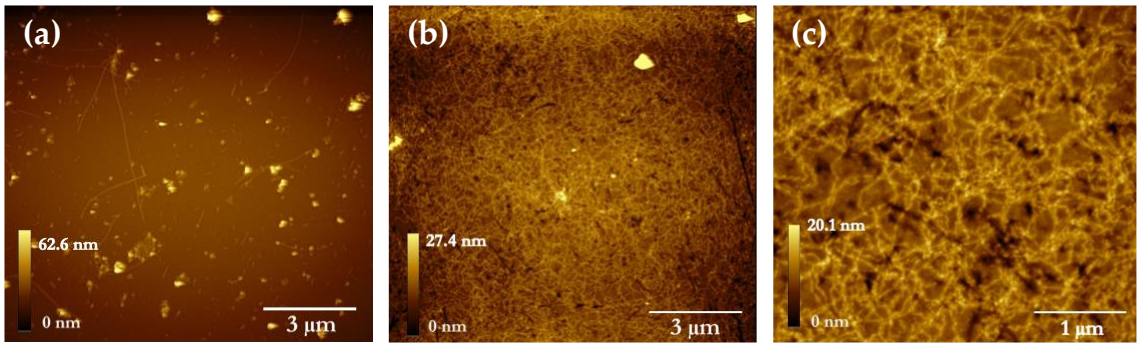

Figure 3.10: Peptide g797 fibrillation in PBS solution (0.05 M, pH 7.4) at 2.5 mg/mL. (a) T = 0 hrs, (b) Fibril formation at t = 12 hrs. Both (a) and (b) were size 9 µm x 9 µm and at a scanning rate of 0.91 lines a second. (c) A zoom of the image, at 3 µm x 3 µm in size, at a rate of 0.84 lines a second, and with a resolution of 512 x 512 pixels.

In Fig 3.10, g797 is shown to form fibrils in neutral conditions, albeit slower than in acidic conditions. At a pH of 7.4, it took fibrils 12 hrs to form. Apart from the stark difference in time to form fibrils, the fibril appearance differs greatly too. The disparity between the aggregate structures formed is a good indication of how environmental conditions can vastly affect the structure of the aggregates formed. The fibrils formed in neutral conditions are twisted and curly, and long in size, and are vastly different in shape. Lengths can be up to tens of µm in size, with diameters of between 10 – 20 nm. Fibrils in acidic conditions are shorter and straighter, and presented after just 2 hrs.

The structures formed in neutral conditions can be described as wormlike micelle formations. These formations are common in lipidated peptides, and are especially favoured by those that have a lipid moiety, which will be centred

inside the structures shielded from the solution [242]. In highly charged conditions, lipidated peptides are likely to form wormlike micelles, as anions will associate strongly with surfactant cations, such as Na^+. These wormlike micelles grow at low surfactant and salt concentrations [56]. As previously discussed in Chapter 1, the shape of the micelles depends strongly on the packing parameters in micellar assembly. The micellar charge is supressed by counter ion binding, in a similar mechanism as the salt conditions in glucagon, and hence decreases the surface area per surfactant molecule. This is done through reducing the electrostatic repulsion between the head groups, which promotes the spherical-to-wormlike micelle transition [243].

The wormlike micelles have been observed in amphiphilic peptides under different conditions, and, as with g797, seen to form different structures dependent on pH [244].

As the structures and kinetics formed by g797 is vastly different depending on pH, it is essential to also look at the aggregation of the peptide in basic conditions, which is shown in Fig 3.11 below.

pH 10.8

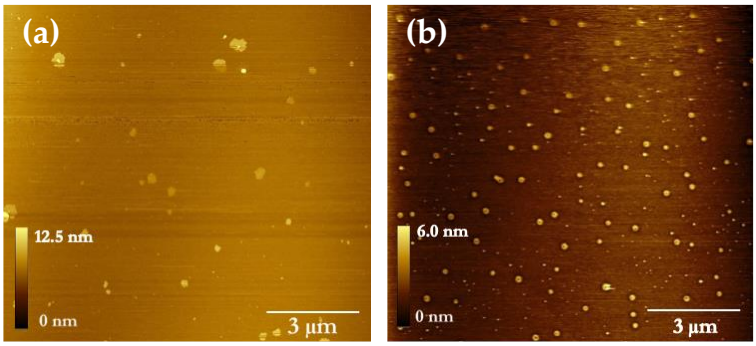

Figure 3.11: Peptide g797 aggregation in Glycine/NaOH solution (0.05 M, pH 10.8) at 2.5 mg/mL. (a) T = 0 hrs. A few small aggregates have formed, but in low amounts and not throughout each image. (b) Small, uniform structures form, which show micelle formation at T = 6 hrs. The images were size 9 µm x 9 µm and at a scanning rate of 0.91 lines a second and with a resolution of 512 x 512 pixels.

Fig 3.11 above displays the images taken of samples in basic conditions, at pH 10.8. From the figure, it can be seen that round micelles are formed after 6 hours. Micelles are driven by hydrophobic interactions, and the shielding of hydrophobic moieties of peptide from the solution [53]. However, electrostatic interactions can also play a part in the formation of specific micelle structures [245]. Due to its charge in basic conditions, its possible g797 only forms micelles as an anion. Unlike general oligomeric aggregates, the micelles are all reproducible in terms of size and structure, with the average diameter of the micelle at 212 nm ± 24.9 nm. The hydrophilic head groups extend from the core into the aqueous solution. The force of repulsion between the head groups is what limits the size to which these micelles can grow [55]. These sizes are also consistent with the sizes seen using DLS, shown in the next chapter. As experiments were done at a concentration of 2.5 mg/mL, this would suggest the CMC of g797 is below that concentration. The CMC for most lipidated peptides is at 1.5 mg/mL, which is in agreement with literature [57], [246].

From the experiments above, some general trends can be observed, which are discussed in the section below.

Discussion

From all the experimental data above, we could conclude that solution conditions give vastly different aggregation products for g797. In each pH condition, different aggregates form; from fibrils, to wormlike micelles and spherical micelles. These structures were formed due to the different electrostatic and/or hydrophobic interactions at play, which, especially with an added lipidation chain, show to have a large effect on the structures produced. From these experiments above, it can be seen that predicting of peptide structures in solution can be difficult.

All the results garnered from the experiments are summarised in Table 3.3 below.

Table 3.3: Summation of g797 conditions of aggregation. Aggregation was defined as the presence of fibrils in all three different quadrant areas on the AFM.

G797		
Concentration (mg/ml)	Time (hrs)	Structure and size (nm)
0.5	4	Thin, long fibrils, up to 1-2 μm in length.
1.0	4	Fibrils start breaking off and becoming shorter, leading to protofibrils, shorter (100 nm) and 20 nm thick.
2.5	2	(Proto) fibrils through HAM theory association, 1-2 μm in length.
5.0	2	At higher concentrations, protofibrils can reach up to 6 μm in length and stacking of 200 nm in height.
pH		
2.4 (Glycine/HCl)	2	(Proto) fibrils, shorter and stockier than normal fibrils, 1 μm in length.
7.4 (PBS)	12	Wormlike micelles, 10 μm length, 10 – 20 nm diameter.
10.8 (Glycine/NaOH)	6	Spherical micelles, 212 nm in diameter.

From the table above, it can be seen that some of the time frames are similar compared to glucagon; such as the concentration dependence. However, when it comes to electrostatic interactions and secondary structure formation, it gets more complex as there isn't just one factor which determines both the time to fibrillation and the structure adopted by the peptide, but a multitude of different factors, which have different degrees of effect on the structure.

In regards to lipidation of the peptides, the following step is to analyse liraglutide in different solution conditions and to determine whether lipidated peptides will follow similar trends.

3.3.3 Liraglutide

Liraglutide, also known as Victoza, is a therapeutic peptide currently on the market for treatment of diabetes. With a very similar structure and weight to G797, Victoza which has a GLP-1 backbone, was made by substitution of Lys34 to Arg, and by addition of palmitoylated fatty acid chain at position C26 using a γ-glutamic acid spacer. This single amino acid mutation and the addition of the C_{16} fatty chain, drastically increases liraglutide's half-life in blood through both the promotion of oligomerization and monomer binding to serum albumin [247].

The added C_{16} fatty acid in liraglutide changes the structure of liraglutide in solution. As a result, it undergoes self-association by forming a heptameric structure. This is one of the reasons why liraglutide is more stable in solution, and therefore, a longer lasting peptide agent.

One of the self-association structures that lipidated peptides form are micelles. Micelle formation shields the hydrophobic patches of the molecules, and expels the hydrophilic parts, which come into contact with the solution, and hence is a mechanism often employed by peptides with long carbon chains.

Due to the breadth of research available, fibrillation of liraglutide has already been investigated. Its additional fatty chain , is a large contributing factor to both the structure of the aggregates formed in solution, as well as its time studies, which are slower than glucagon [42].

3.3.3.1 Change in concentration

Fig 3.12 below shows the images taken at t = 0 hrs on the right hand side and t = fibrillation on the left, for liraglutide at increasing concentrations.

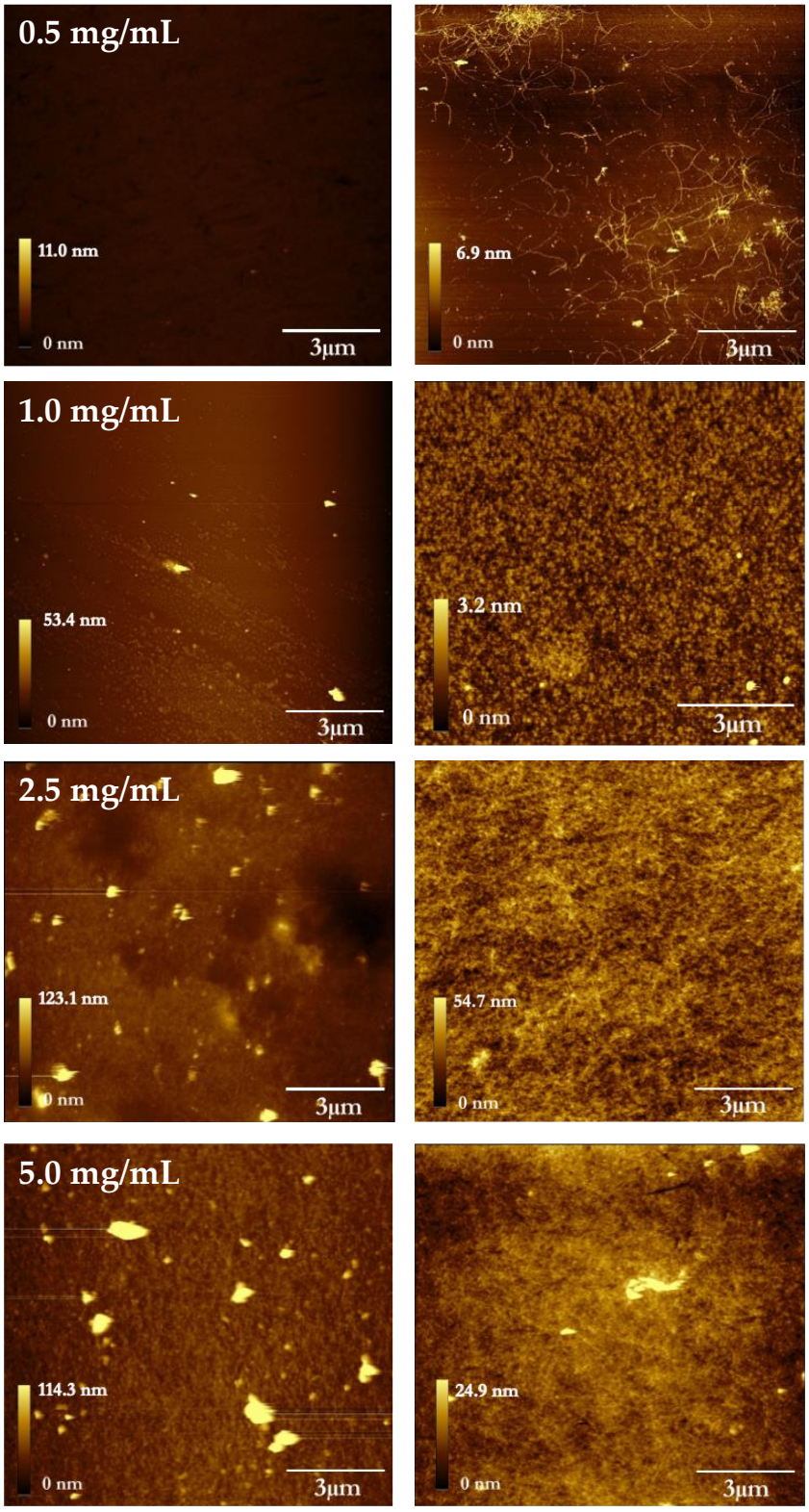

Figure 3.12: Left - AFM images liraglutide at increasing concentrations at t = 0 hrs. **Right -** AFM images of increasing concentrations at t = 6 hrs. Increasing the concentration of the solution increases the density of the fibrils. Images were 9 µm x 9 µm in size, scanning rate 0.84 lines per second and at a resolution of 512 x 512 pixels.

From the figure above, it can be seen that fibrils are initially sprouting out of nucleation points in their growth stage. They centre and cluster around a small oligomer, indicative of secondary nucleation discussed previously. The initial fibrils formed are a few hundred nm to 2 μm in length. These spider- like fibrils can be found to then develop into a thick layer of fibrils. The fibrils produced by liraglutide are 10 to 20 nm wide and can go up to a few micrometres long, but average distances only reach a few hundred nm, and are typical of amyloid fibril formation [90]. As the concentration increases, the layer thickness varies between 25 – 50 nm, indicating that a few layers of fibrils stack upon each other, indicating secondary structure association, such as beta sheets [128]. Another interesting observation is that unlike the other two peptides at high concentrations, liraglutide still has some oligomers present. This further adds to the theory that in acidic conditions, liraglutide can undergo secondary nucleation through oligomers. Furthermore, the increase in concentration did not speed up fibrillation (all concentrations formed fibrils at 6 hrs) as it did with the other two peptides, indicating a different mechanism is at play.

Whether this is the case for liraglutide in other pH conditions is investigated later in this chapter.

3.3.3.2 Change in pH

a) Zeta Potential

The zeta potential was investigated in order to confirm charges of the liraglutide peptide in all three different solution conditions. Fig 3.13 below shows the colloidal stability and the overall charge of the peptide in acidic, neutral and basic conditions.

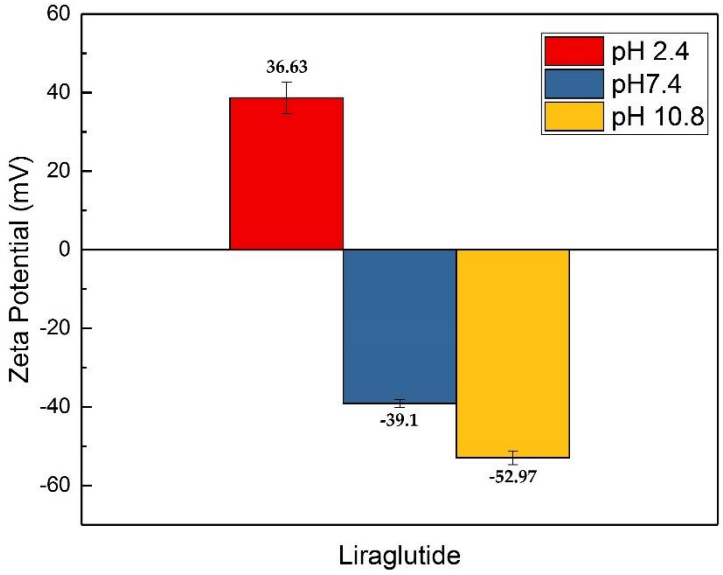

Figure 3.13: Zeta Potential measurements of liraglutide in all three differing pH's (0.05 M buffer: Glycine/HCl, PBS and Glycine/NaOH) at a concentration of 2.5 mg/mL.

The zeta potential shows that liraglutide has a large positive charge in acidic conditions, and as its isoelectric point is between 4 and 5, and carries a negative charge in both neutral and basic conditions.

b) Atomic Force Microscopy

The images of investigation into the aggregation of liraglutide in acidic conditions using the AFM can be seen in Fig 3.14 below.

pH 2.4

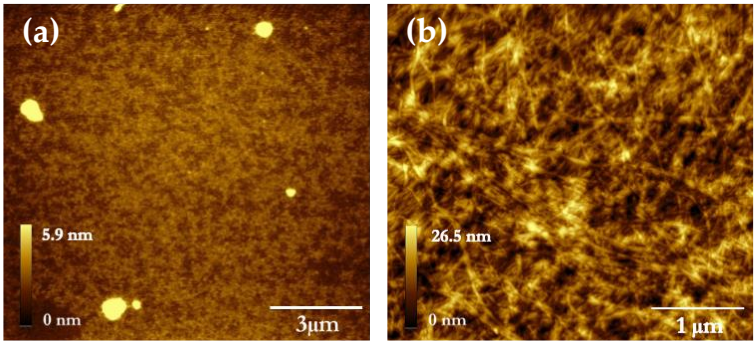

Figure 3.14: Liraglutide fibrillation in Glycine/HCl solution (0.05 M, pH 2.4) at 2.5 mg/mL. (a) T = 0 hrs. Size 9 µm x 9 µm and at a scanning rate of 0.91 lines a second. (b) Fibril formation at t = 6 hrs. Scanning size 3 µm x 3 µm in size, at a rate of 0.84 lines a second, and with a resolution of 512 x 512 pixels.

Fig 3.14 above shows the results of fibrillation studies at an acidic pH at a concentration of 2.5 mg/mL. The image on the right shows a closer look at exactly the type of fibril networks present in acidic conditions. As previously discussed, these fibrils are not as organized as those produced by glucagon. However, they do form a specific network, and fibrils are still straight in shape, up to a few µm in size, and around 10 – 20 nm in diameter. They are shown to have peaks and troughs, which can be either twists or ribbon like formations. Ribbon formations are common in peptides, and are especially favoured by those that show peptides that show intermolecular side-chain interactions, as well as cooperative intermolecular hydrogen bonding between peptide backbones [240]. With liraglutide's added lipidated chain, and its array of different aggregation structures, ribbon formation is likely [247]. The ribbons have been observed in amphiphilic peptides under different conditions and form different structures dependent on pH [249].

To investigate whether this trend persists, AFM images were also taken in neutral conditions, shown in Fig 3.15 below.

pH 7.4

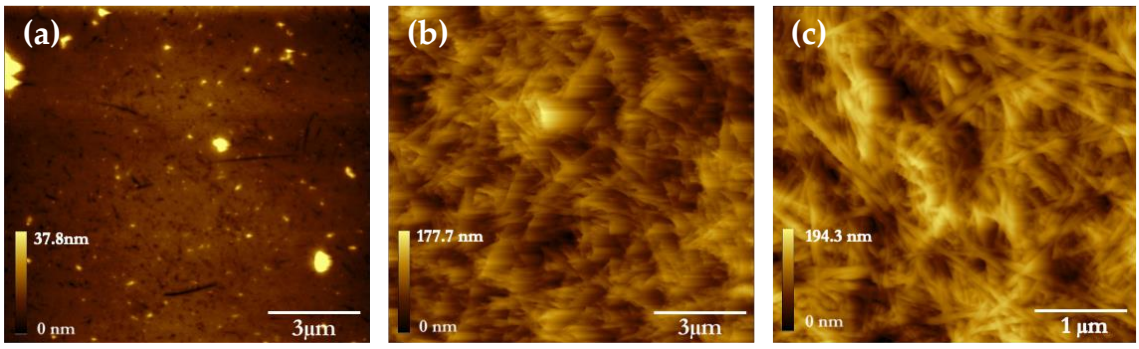

Figure 3.15: Liraglutide fibrillation in PBS solution (0.05 M, pH 7.4) at 2.5 mg/mL. (a) T = 0 hrs, A few small aggregates have formed, but in small amounts and not throughout each image. (b) Fibril formation at t = 24 hrs. Both (a) and (b) were 9 µm x 9 µm in size, and at a scanning rate of 0.91 lines a second. (c) A zoomed in area of image (b) at 3 µm x 3 µm, at a rate of 0.84 lines a second, and with a resolution of 512 x 512 pixels.

Fig 3.15 above shows liraglutide's ability to form different aggregates in different conditions. The fibrils formed in a pH of 7.4 are stockier and shorter fibrils, at an average length of 1 µm and a diameter of 40 nm. In addition to the differences in size, a much thicker layer is formed, with heights of the layer at almost 200 nm compared to 30 – 50 nm in acidic conditions. This indicates that more layers have been stacked on top of one another, which could only be possible if repulsive forces between molecules were minimized. These fibrils are very similar to those formed by g797 in acidic conditions, with comparable measurements for both length, width and height of the formed layers. Hence, it's likely that these fibrils are also formed through the HAM theory, as previously discussed. This is very much concurrent with not only that theory, but in accordance with lipidated peptides [92]. In order to fully investigate the effect of charge on the self-assembly of liraglutide, liraglutide must also be tested in basic conditions, when it carries an overall negative charge.

pH 10.8

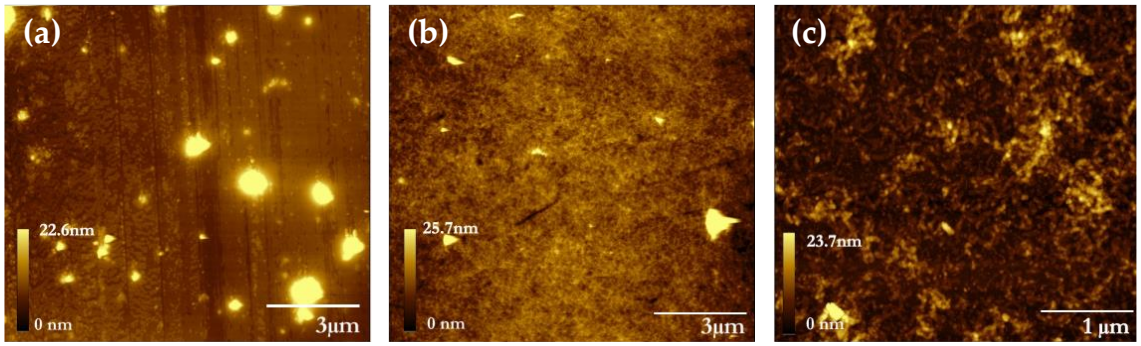

Figure 3.16: Liraglutide fibrillation in Glycine/NaOH solution (0.05 M, pH 10.8) at 2.5 mg/mL. (a) T = 0 hrs, A few small aggregates have formed, but in low amounts and not throughout each image. (b) Fibril formation at t = 72 hrs. Both (a) and (b) were of 9 µm x 9 µm in size and at a scanning rate of 0.91 lines a second. (c) A closer look of aggregation structure at 72 hours, 3 µm x 3 µm in size, at a rate of 0.84 lines a second, and with a resolution of 512 x 512 pixels.

Fig 3.16 shows different aggregation structures and kinetics compared to the previous conditions of liraglutide. Fibrils formed in basic conditions are comparable to those formed in neutral conditions of g797. Especially in image c, where the structure of the aggregates formed can be seen clearly. The worm-like micelle structures are comparable in terms of lengths and thickness of the layer formed, at 20 – 30 nm thick. In addition, the same reasoning that was applied to their formation in neutral conditions of g797 is true for that of liraglutide in basic conditions. Both are lipidated peptides, carrying negative charges and shielding hydrophobic moieties away from the aqueous solution. In addition, liraglutide is known to form spherical micelles, which has been well documented in the literature, especially when in neutral or basic conditions. As previously discussed, liraglutide is known to form octamers and hexamers in solution [250]. The worm like micelles could be precursors to these secondary structures, or could be a thermodynamically stable structure at a relatively high concentration. For liraglutide, its CMC is 1.5 mg/mL, and hence at 2.5 mg/mL, the micelles could have associated to form longer, wormlike micelles [251]. Literature has found

that micelles of liraglutide reorganise dependent on pH and concentration, and hence, the wormlike micelle formation would be concurrent with this [252].

Discussion

The GLP-1 peptide hormone on which liraglutide is based, is known to have a complicated structural landscape including a high propensity to aggregate and form fibrils [253]. GLP-1 has also been shown to have unique pH dependent fibrillation properties [254]. As previously mentioned, peptides undergo fibrillation in a concentration-dependent manner, where increasing peptide concentration results in faster fibrillation [255]. However, GLP-1 shows an inverse concentration dependence at pH < 7, where it has a tendency to form fibrils more rapidly at low concentrations, which could explain the difference in time that liraglutide takes to form aggregate structures compared to the other peptide [248]. Liraglutide has been shown to form different aggregation structures dependent on pH conditions, varying from wormlike micelles, to thick fibril formations and resulting beta sheets.

The overview of the aggregation in each condition for liraglutide is summarised in Table 3.4 below.

Table 3.4: Summary of the aggregation of liraglutide, in different conditions. Aggregation was defined as the presence of fibrils in all three different quadrant areas on the AFM.

Liraglutide		
Concentration (mg/mL)	Time (hrs)	Structure and size (nm)
0.5	6	Oligomer starting points and small thin fibrils, 10- 20 nm wide.
1.0	6	Fibrils grow larger up to 2 μm and increase in density.
2.5	6	Ribbon formation, 3 -4 μm in length, thin firbils, 10 nm thick.
5.0	6	Ribbon formation, with sheet stacking of 25- 50 nm in thickness.
pH		
2.4 (Glycine/HCl)	6	Secondary nucleation mechanism through oligomeric addition. Ribbon like fibrils formed.
7.4 (PBS)	24	Ham theory, (proto) fibril formation, 2 μm long, 40 nm in diameter
10.8 (Glycine/NaOH)	72	Wormlike micelles, 20 – 30 nm in diameter and up to 9 μm.

From the results presented above, a small change in the backbone of the peptide can make a large difference. Some of the mechanisms described above are similar to g797, indicating that even though their backbone sequence is different, there is some rational in the way lipidated peptides behave compared to peptides without added lipid chains. However, times are significantly longer for fibrillation of liraglutide, which also indicates the importance of the placing of the added palmitoyl chain. Exendin-4 was investigated next to explore whether lipidation does indeed have a drastic effect on both the time and the structure of aggregates formed in solution.

3.3.4 Exendin-4

Exendin-4, also referred to as exenatide, is a 39–amino acid peptide incretin mimetic that exhibits glucoregulatory activities similar to the mammalian incretin hormone GLP-1 [37]. Unlike the other peptides, exendin-4 is a synthetic form of the protein found in the saliva of the Gila monster [256].

It is larger in size, and the molecule is also bulkier compared to the other peptides discussed previously. Additionally, exendin-4 has only 54% sequence in common with glucagon, and is also known to be less likely to aggregate [257].

Studies relating to exendin-4 show it as a stable molecule that does not form fibrils [257][258], and is most likely to be found in a stable oligomer, due to its Trp cage. This nine amino acid extension at the C- terminal is not present in any of the other peptides.

In vitro studies have also shown a much higher stability of exendin-4 compared to GLP-1, so this stability will be investigated further in the following section.

3.3.4.1 Change in concentration

Exendin-4 is known for being a very stable molecule. Fig 3.17 below investigated its secondary structure formations in increasing concentrations at a pH of 2.4, and concentration of 2.5 mg/mL.

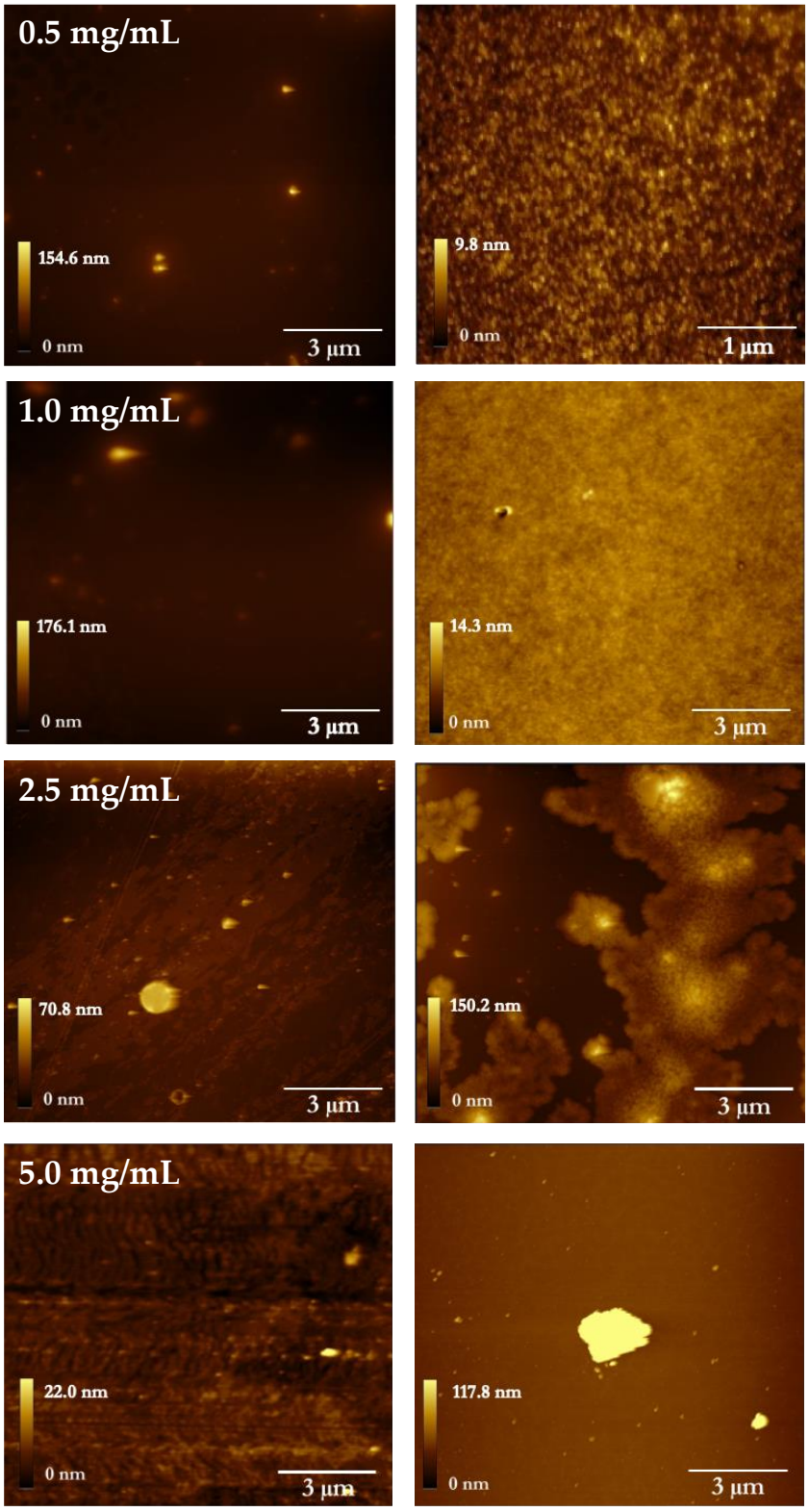

Figure 3.17: **Left -** AFM images exendin-4 at increasing concentrations at t = 0 hrs. **Right -** AFM images of increasing concentrations. At all concentrations, samples were taken for two weeks and no fibrils were formed. Images were 9 µm x 9 µm in size, scanning rate 0.84 lines per second and at a resolution of 512 x 512 pixels. The first image on the right is 3 µm x 3 µm in size.

The figure above shows some interesting formations, or lack thereof. Initially, there are a few aggregates present. In both low concentrations (1.0 mg/mL and under), a monolayer has formed. This layer is between 9 – 15 nm thick, and a serious decrease from the initial larger aggregates, indicating nucleation from the oligomers. However, in this setting, the oligomers are nucleation sites for stable monolayers instead of fibrils. As the concentration increases, so do the sizes of the large oligomers. At a concentration of 2.5 mg/mL, it can be seen that multiple layers have formed, yet no fibrils are seen. Due to exendin-4's added Trp cage for stability, it was predicted that its behaviour in solution would be different. In acidic conditions, the Asp residue is protonated, and hence keeps the cage structure semi- intact through electrostatic interactions. The Trp-cage unfolds partially in protonated conditions, yet due to its high charge, it can partly associate with other molecules, and hence larger oligomers can be formed. It has previously been shown that at increasing concentration in acidic conditions, exendin-4 forms large oligomers [259], which can be seen in Fig 3.17 above.

Exendin-4, like most of the other peptides, is dependent on concentration, as seen in the above figure. The next parameter to investigate was whether the peptide also shows differing structures in different pHs as with the other peptides, or whether the Trp cage stabilises the structure enough to not self-assemble.

3.3.4.2 Change in pH

a) Zeta potential

The charges of exendin-4 in different buffer solutions were confirmed by zeta potential, displayed in Fig 3.18 below.

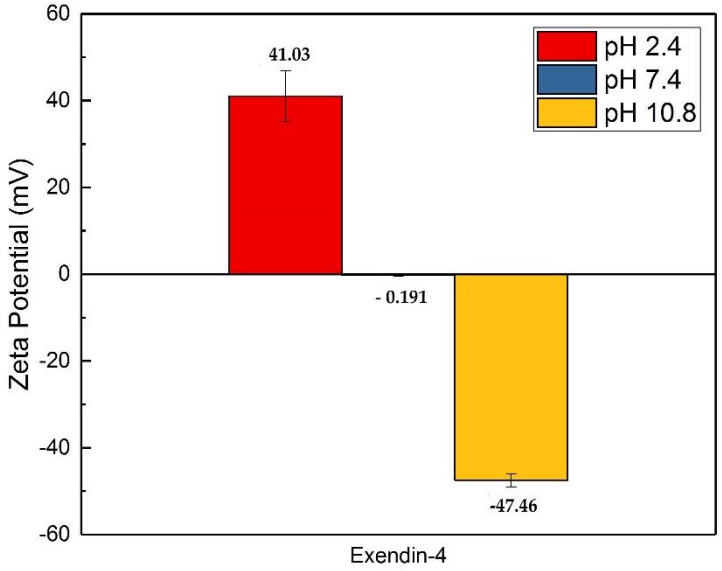

Figure 3.18: Zeta Potential measurements of exendin-4 in all three differing pH's (0.05 M buffer: Glycine/HCl, PBS and Glycine/NaOH) at a concentration of 2.5 mg/mL. The zeta potential shows that exendin-4 has a large positive charge in acidic conditions, almost no charge in neutral conditions, and a largely negative charge in basic conditions.

Interestingly enough, exendin – 4, which has a pI is at 4.2, has no charge in neutral conditions, which is at a pH of 7.4. The buffers were checked with a pH meter before each solution was made.

b) Atomic Force Microscopy

From the Zeta Potential measurements, data has been collected about the charge of the peptide in both acidic, neutral and basic conditions. The AFM is then used as a tool to image the self-association (if there is any) between the peptide monomers in solution, starting at a pH of 2.4, shown in Fig 3.19 below.

pH 2.4

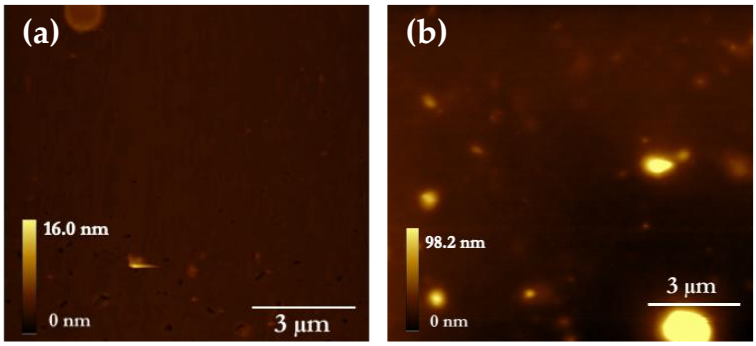

Figure 3.19: Exendin-4 fibrillation in Glycine/HCl solution (0.05 M, pH 2.4) at 2.5 mg/ml. (a) T = 0 hrs, a few small aggregates have formed. (b) Larger aggregates have formed at T = 24 hrs. Both images were size 9 µm x 9 µm and at a scanning rate of 0.91 lines a second.

As previously seen in Figure 3.22, at a concentration of 2.5 mg/mL in acidic conditions, a variety of different structures can be formed. Evidence of multilayers was present, with small multilayers visible in the image on both the right hand side and the left hand side. However, small and larger oligomeric structures have also formed, some as large as 3 µm. This indicates that there is an equilibrium of different thermodynamically favourable structures taken up by exendin-4, which balances between multilayers and oligomers. This coincides with literature, which states that the oligomer–monomer equilibration rates are fast in exendin-4, which means that the peptide switches between monomer and oligomer. Literature also found that even at quite high concentrations (up 600 mM) large aggregates can associate to form particles yet not fibrils [260]. The time between the two images above was at 24 hours, yet no fibrillation was seen. Samples were taken continuously, and there was no change from the image seen above in terms of structure.

However, there is little consistency in their size, and hence further investigation into charge-relationship and self-assembly in exendin-4 was done, starting at investigating the peptide in neutral conditions, shown in Fig 3.20 below.

pH 7.4

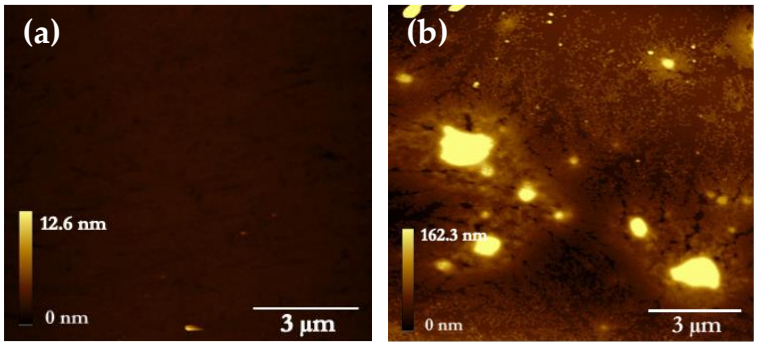

Figure 3.20: Exendin-4 aggregation in PBS solution (0.05 M, pH 7.4) at 2.5 mg/mL. (a) T = 0 hrs, Few little in terms of aggregates can be seen. (b) Large aggregates have formed and can be seen in all images taken. Both images were size 9µm x 9 µm and at a scanning rate of 0.91 lines a second.

From the figure above, a few things can be noted. Firstly, the initial image has little to no aggregates, not unlike the previous initial images seen in acidic conditions. A more indicative image, panel (b), shows more large aggregates than seen in acidic conditions. At a pH of 7.4, the average size of its aggregates are significantly larger (average size 28 µm ± 2.4 µm compared to 2.4 µm ± 0.7 µm) than at acidic conditions previously investigated. As exendin-4 carries little charge at this pH, as shown by Zeta Potential, the colloidal solution is less stable, and hence larger aggregates form. Additionally, when the peptide carries no charge, the Trp-cage will be fully folded and will associate the least with its surrounding solvent, and peptide – peptide interactions will increase, hence the increase in size of the oligomers. The change in size does show that even for a stable molecule like exendin-4, the charge interactions will have an effect on the secondary structure of the peptide. Still, no fibrils are seen, even in unfavourable conditions.

Unlike the other three peptides investigated, exendin-4 shows little to no difference in aggregation structures or time frames at different pH's so far. To see whether this trend also exists at basic conditions, peptide solutions were made at a pH of 10.8, and the AFM images are shown in Fig 3.21 below.

pH 10.8

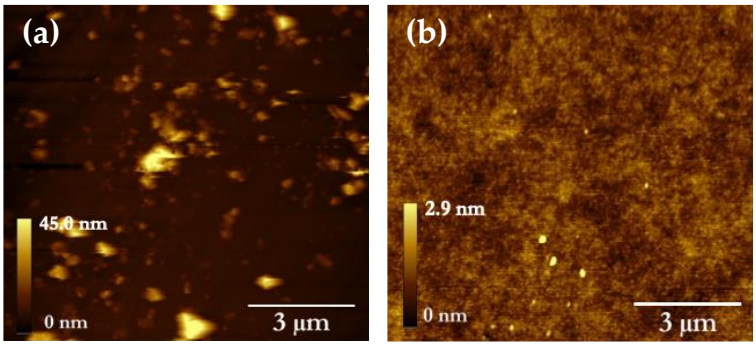

Figure 3.21: Exendin-4 aggregation in Glycine/NaOH (0.05 M, pH 10.8) at 2.5 mg/mL. (a) T = 0 hrs, many smaller aggregates have formed. (b) Small aggregates have decreased and a monolayer has formed. Size 9µm x 9 µm and at a scanning rate of 0.91 lines a second.

Fig 3.26 displays some interesting results, which are similar to those seen in acidic conditions. The initial image shows small aggregates, smaller than 1 µm, but covering much of the surface. The height of the aggregates can be up to 45 nm, and there are clear differences in heights of the oligomers. Over time, the aggregates serve as nucleation points, and a monolayer of exendin-4 is formed. The size and frequency of aggregates decrease as monomer layers are formed. This is in phase with exendin-4 switching between monomer and aggregate formation. This process is likely to be charge related, as in both acidic and basic conditions, exendin-4 will be highly charged. From literature, it has also been hypothesized that exendin-4 prefers charged conditions due to its Asp side chain and Trp cage being able to form multiple hydrogen bonds to the peptide backbone [261].

Discussion

In summation, exendin-4 showed no fibril formation, although monolayer formation, and aggregate formation was seen, with oligomers being potential starting points for secondary nucleation. As previously hypothesized, exendin-4 is the most stable of the peptides investigated, due to its small, and very stable Trp cage, which, especially in charged conditions, keeps the peptide stable.

Exendin-4 does however show differences in sizes of aggregates formed dependent on solution conditions, forming the largest aggregates in neutral conditions (up to 30 μm), when its colloidal stability is at its lowest and hence peptide interactions are at their highest. In all conditions, exendin-4 formed aggregates and oligomers, ranging from a few nm in size in 0.5 mg/mL and in basic conditions, whilst in acidic conditions and neutral conditions, at higher concentrations, oligomers could be found with sizes as large as 10 μm.

3.4 Overview

Therapeutic peptides adsorb and aggregate at surfaces, which causes structural and functional losses, as well as peptide loss [61]. This chapter addresses the solution conditions and the bulk phase of the peptides, through assessing their stability and their aggregate structures in different solution conditions. The morphology of the final aggregates and the extent of their heterogeneity (in terms of diameter, length, and the degree of twisting) depend not only on the amino acid sequence but also on many physiochemical factors. Some of these include; peptide concentration, the absence or presence of agitation, the physical properties of the solution (pH and temperature) and composition of the medium (nature of the buffer and salt concentration) among other factors [24]. From the literature, it can be seen that there isn't a straightforward way to prevent aggregation in solution [6].

The small changes in amino acid sequence can cause changes in charge variance, change in electrostatic interactions between molecules and solution and peptide-peptide interactions and change in hydrophobic and van der Waals forces. Hence, small changes in the backbone of the peptide can cause significant differences in aggregate structure and speed of aggregate formation [262]. The data from all the different peptides is shown in Table 3.6 below.

Table 3.5: Summation of time frames of peptide fibrillation for increasing concentrations starting from 0.5mg/mL.

	Glucagon	G797	Liraglutide	Exendin – 4
Concentration (mg/mL)	Time (hrs)	Time (hrs)	Time (hrs)	Time (hrs)
0.5	4	4	6	N/A
1.0	4	4	6	N/A
2.5	2	2	6	N/A
5.0	2	2	6	N/A

From Table 3.6 above, we can see that glucagon fibrillates fastest and exendin-4 slowest. As exendin-4 also happens to have only 54% similarity in its backbone to glucagon, and has the added stabilisation of the Trp cage, this is unsurprising. Increasing concentration increases the speed of fibrillation. At low concentrations, the concentration is the rate determining factor, whilst at higher concentrations this assumption is no longer upheld, which coincides with the literature [29], [263], [264]. Apart from glucagon and exendin-4, which have very different rates of aggregation depending on concentration, the other peptides are relatively similar in terms of time to form aggregates, only varying with a few hours in acidic conditions. This enhances what we know about increasing concentration; that peptide interactions will increase due to density of the peptide. Yet, other factors, such as the charge that the peptides carry, will also have a large effect on the self-assembly of the peptides. The change in aggregation time as a function of charge is shown in table 3.7 below.

Table 3.6: Summation of pH solution conditions and the time study of each peptide at acidic, neutral and basic conditions at a concentration of 2.5 mg/mL.

	Glucagon	G797	Liraglutide	Exendin – 4
pH	Time (hrs)	Time (hrs)	Time (hrs)	Time (hrs)
2.4	2	2	6	N/A
7.4	96	12	24	N/A
10.8	6	6	72	N/A

As Table 3.7 displays above, stability of the peptides were highly dependent on solution conditions, and highly variable between each peptide. Exendin-4 is the most stable of the peptides, yet all other peptides show large variability depending on their isoelectric points, and the way they self-associate depending on charge. One key finding, however, is that all peptides take significantly longer to show fibrillation in neutral conditions, even with pI's far removed from a pH of 7.4. Most peptides had closer pI's to acidic conditions than neutral. Yet, the structures formed by each peptide was exceedingly varied which was highly dependent on their amino acid backbone. For glucagon, that included its highly charged backbone in acidic conditions, carrying a 5+ charge, which was a large factor to forming its secondary structure. For the lipidated peptides, their added hydrophobic moiety played a large factor in shielding the hydrophobic parts from the solution, changing their structure significantly according to solution conditions and reorganization in solution, from spherical micelles to worm like micelles and ribbon structures; structures not identified in images of non lipidated peptides. For exendin-4, this consisted largely of how the Trp cage would stay intact or unfold, and much of the secondary structure formation was dependent on that.

In solution, aggregation of peptides is dependent on such a range of different factors which can make their fibrillation and stability difficult to predict.

In order to fully understand the behaviour of the peptides, the stability in solution is just one parameter in a plethora of different ways to assess proteins. The methods used in this chapter; the AFM and Zeta Potential, gave both a real time image of the peptide solutions, and measured their charge and stability in solution, in respect to the solution conditions used. This results chapter focused on looking at the bulk solution of the peptides, while the next chapter, Chapter 4, will investigate peptide adsorption at the interface, using both DLS and the QCM-D. The DLS will be used in order to analyse hydrodynamic radii in solution, in order to confirm the secondary structures formed, such as micelles. The QCM-D will be used to investigate the hydrate mass of peptide adsorbed to the surface, as well as the dissipation from the formed layer at the interface. Looking at the adsorption of the peptides at the interface is crucial in order to prevent non-specific adsorption of peptides to primary containers.

4 Chapter

An investigation of peptide adsorption at the interface using QCM-D.

4.1 Introduction

The previous chapter tackled peptide stability in bulk solution. In order to fully investigate peptide aggregation, both aggregation in bulk and at the interface must be investigated. The following chapters focus on the surfaces, how they can influence peptide aggregation and how they can be tailored to change adsorption of peptides.

Amphiphiles, such as peptides, have a pronounced propensity to adsorb to most surfaces [5]. This adsorption depends on a range of factors; from solution conditions such as temperature, pH and concentration, to peptide orientation and specific amino acid sequences and to the nature of the surface, physical and chemical [59], [60]. As peptides are not rigid molecules, adsorption and desorption to interfaces is complex, giving rise to phenomena such as surface aggregation and structural rearrangement. This phenomenological complexity makes for challenging research to affect both fundamental and application specific progress.

Throughout the lifetime of the therapeutic peptide, from the initial storage to transport and delivery, the drug will come in contact with a variety of surfaces [265]. Peptides can be lost from solution due to adsorption to the walls of the container or syringe [113]. Glass is used for both transport and storage purposes, as well as a common delivery tool. A range of plastics are also used, in vials,

syringes and auto injectors [266]. For therapeutic peptides therefore surface adsorption studies are inevitably focused on how to inhibit peptide and protein loss through adsorption to glass and plastic, with limited progress to date [267]. Borosilicate glass is the variety used in both laboratory glassware and pharmaceutical containers. Even though there are in principal methods to reduce the surface binding of peptides, such as addition of Tween20, using high salt concentrations or addition of PEG as a surface coating, these are not always feasible during experiments or later on in the pipeline such as during transportation and drug delivery [268]. Additionally, these additives can change the fundamental properties and function of the therapeutic peptide. Our research is therefore specifically aimed at elucidating the surface interactions of therapeutic peptides directly with pharmaceutically relevant primary containers [269].

At the molecular level the orientation presented at the surface by the peptide is dependent on the local free energy minimum, which in turn is dependent on Coulomb and Van der Waal interactions, hydrogen bonds and the entropy gain from solvent molecule release [270]. The different patches of amino acids at the peptide surface will give rise to spatially varying hydrophilicities and regions of charge. Consequently, on hydrophilic surfaces, peptides will orient to shield hydrophobic patches from the surface. Moreover where there are intrinsic surface charges, peptides tend to adsorb so that a region of opposing charge to that of the surface is presented [185].

As the adsorption increases, single molecule surface interactions develop into monolayer and then multilayer coverage. The packing density of monolayers depends on the strength of the electrostatic attraction between surface adsorbed peptides. Where there is aggregation, the process by which peptides cluster into oligomers of a few monomers or into larger clusters of up to several hundred monomers, the adsorption becomes more complex. The occurrence of aggregates

is thought to be due to either diffusion of surface bound peptides that act as a precursor for aggregation or because of direct adsorption of bulk peptides to other surface bound peptides [271]. Furthermore, cooperative effects can play a large role in the adsorption of peptides. Cooperative effects refer to peptides that are in close proximity to the surface, which are more likely to adsorb if there are already pre-adsorbed peptides present on the surface [272]. In terms of drug storage and delivery, all these adsorption effects can have significant consequences on lifetime, drug efficacy, and potentially drug delivery.

For GLP-1 and glucagon analogues we specifically explore the effect of surface hydrophobicity and hydrophilicity on peptide adsorption and aggregation, and investigate the ability of lipidated and non lipidated peptides to adsorb to a range of surfaces. The aim of the chapter is to explore the effect of different surfaces on the adsorption of the four peptides; glucagon, g797, liraglutide and exendin-4. Each surface is either hydrophobic or hydrophilic, and charged or uncharged, giving a wide range of different surfaces to elucidate mechanisms by which each peptide adsorbs to the surface.

4.2 Materials and Methods

The experimental technique used was quartz crystal microbalance with dissipation monitoring (QCM-D). We first quantify and infer the structure of peptides on hydrophilic surfaces, specifically to investigate whether lipdated peptides undergo self-assembly to form different structures on the surface according to their amino acid sequence. The extreme low and high pH conditions are used due to the insolubility of glucagon at neutral pH [273], and additionally to inspect the hypothesis that adsorption of these peptides is highly electrostatically driven. For these experiments, the peptides must be overwhelmingly positively or negatively charged which we have shown in the last chapter we can control by adjusting the pH. A useful technique for investigating peptide-surface interactions is QCM-D, which quantifies peptide adsorption (and desorption) at an interface in terms of mass adsorption. Furthermore, the dissipation, a measure of the structural properties of an adsorbed layer, can be used as an indicator of the hydration of the layer, and hence it's rigidity [183], [274], [275].

4.2.1 Peptide preparation

Peptides were purchased from Bachem (> 95% purity), and g797 peptide was made with a peptide synthesizer at MedImmune Ltd. Hydrochloric acid buffer solution (0.05 M, pH 2.4) was prepared using hydrochloric acid (37%), glycine (> 95%) and HPLC water (resistivity > 18 MΩ/m). Additionally, sodium phosphate buffer solution (0.05 M, pH 10.8) was made using sodium phosphate (anhydrous, <95%), glycine and HPLC water. Filtered (polypropylene syringe filters, pore size = 0.22μm, GE Sciences, Whatman) peptide stock solutions of glucagon (3.48 kDa), exenatide (4.19 kDa), liraglutide (3.75 kDa), g797 (3.72 kDa) were each prepared in the same buffer solution and then diluted for analysis at the desired concentration, which for all experiments was 2.5 mg/mL. The selected concentration was based on previous studies in the literature done by M. Dong

et al (2006) and E. E.M G, Loomans et al (1997) [219], [220]. The concentration of the diluted peptide solutions was checked by UV-Vis spectroscopy (Varian Cary® 300 UV-Vis Spectrophotometer, Agilent Technologies, UK) at 280 nm.

All buffers were degassed prior to experimentation, as bubbles are a common challenge in the QCM-D apparatus, especially when measuring with hydrophobic surfaces. Buffers were added into a 500 mL glass bottle, degassed using a vacuum pump (Fischerbrand FB70155, at 292mbar) and an ultrasonic bath (Fischerbrand FB15049).

4.2.2 Dynamic Light Scattering (DLS)

Using the protocol for peptide solutions above, the solutions were diluted for experiments ranging from 1.0 mg/mL to 2.5 mg/mL. Each peptide was put into a glass cuvette (2 mL) at the measured concentration and inserted into the machine. Measurements of the hydrodynamic radius of the peptide was made on a Malvern Zetasizer Nano ZS (Malvern Instruments Ltd, UK) with a detection angle of 173°. The Nano S range uses a He-Ne laser operating at 633 nm. All measurements in the study were taken at a temperature of 25°C ± 0.1°C. For each batch, hydrodynamic radii discussed was the mean of three measurements, and values were calculated as the mean of three different batches. The model used for size determination of the particles is a standard regularised non-negative least squares analysis where the regularisation is determined from the L curve. Both buffer solutions (previously described) have a viscosity of 0.8952 cP and a refractive index of 1.332.

4.2.3 Quartz – Crystal Microbalance with Dissipation (QCM-D)

4.2.3.1 Cleaning procedure for the QCM-D apparatus

Before each experiment, the QCM-D machine is thoroughly cleaned to avoid contamination as the apparatus is very sensitive. The nitrogen gun is used to purge all of the tubing before connecting to the main machine. Once all parts are

in place, diluted Hellmanex® (Hellma Analytics, Germany) solution (2% in deionised water) was used to clean the QCM-D tubing and flow cells. After deionised water, 5 mL SDS (5%) is flown through the whole system, followed by 5 mL of ethanol (50%), and lastly, 5 mL more of deionised water. Once the water has cleared the system, it's then dried using the N_2 gun. This ensured the system was clean before chips were put inside the QCM-D.

4.2.3.2 Cleaning procedure for QCM-D chips

a) Gold surfaces (QSX-301)

The gold chips (Q-Sense-Biolin Scientific AB, Sweden) were washed and cleaned prior to use. Firstly, the chips undergo UV/ozone (UV/Ozone ProCleaner™ Plus, Bioforce Nanoscience, US) treatment for 10 minutes. A solution of 10 mL of 5:1:1 mixture of milliQ water, ammonia (25 %) and hydrogen peroxide (30 %) is heated to 75 °C. The sensors are placed in the heated solution for 5 mins. Once taken out, they are rinsed thoroughly with milliQ water and dried with nitrogen gas. They are then put back in the UVO for ten minutes before use.

b) Glass surfaces (QSX 336)

Untreated borosilicate glass sensor chips (Q-Sense-Biolin Scientific AB, Sweden) were used in the QCM-D experiments. Surfaces were cleaned by UVO treatment for 10 mins. They are then fully submerged in a 2% SDS solution for 30 minutes, and rinsed with water immediately afterwards. Once thoroughly rinsed, they are dried with nitrogen gas. The final step is to repeat the first step of UVO treatment for 10 minutes.

c) Silicon Dioxide surfaces (QSX 303)

Untreated silicon dioxide sensor chips (Q-Sense-Biolin Scientific AB, Sweden) were used in the QCM-D experiments. Both surfaces were cleaned by UVO treatment for 10 mins. They are then fully submerged in a 2% SDS solution for

30 mins, and rinsed with water immediately afterwards. Once thoroughly rinsed, they are dried with nitrogen gas. The final step is to repeat the first step of UVO treatment for 10 mins.

d) Polystyrene surfaces

A solution of 1% SDS in milliQ water was made up, and the sensor were immersed in the solution at 30°C for 30 minutes. After this, they were rinsed with milliQ water, and then immersed in a solution of milliQ water for at least 2 hrs. After two hours, the chips are rinsed with 99% ethanol and dried with nitrogen gas. The sensors are then immediately used, to prevent additional contamination such as dust. These sensors are not put under UVO treatments as this can break the PS bonds to the chips.

4.2.4 Functionalization of surfaces

Au chips were functionalized in order to make them hydrophilic (-OH) and hydrophobic ($-CH_3$). This was done using 11-mercapto-1-undecanol, which is used to form hydrophilic self-assembling monolayers or in mixed SAMs as spacers to provide a hydrophilic background, and using 1-undecanethiol to provide hydrophobic surfaces.

The principle of the functionalization of the gold QCM-D chips is based on self-assembly. An alkane chain of typically 10-18 units, is made with a thiol (S-H) head group with a strong preferential adsorption to the substrate, Au. The sulphur head groups bind to the gold as a thiolate (Au-S- (CH_2)nX) bond, which forms a well-structured monolayer with the tail group arranged to position away the surface. For the purpose of this thesis, two SAMs were used, with an –OH and $-CH_3$ tail group.

4.2.4.1 Hydrophilic functionalisation (-OH functionalisation)

QSX- 301 gold sensor chips from Q-sense were used for functionalisation. Gold chips were functionalized using 11-mercapto-1-undecanol (Sigma Aldrich, <97% purity) solution at a 7 mM molarity. Stock solutions of 100 mM were made up using 3.2 mg of 11-mercapto-1-undecanol solution, and 157 μL of pure ethanol. The stock solutions were kept in the fridge at a constant temperature of 4°C and diluted to 7 mM when needed.

The gold QCM-D chips are cleaned following the procedure outlined in Section 4.2.2.2. Once the chips were cleaned, they were put into 1 mL plastic sensor chip holders (which were previously cleaned with ethanol), and 200 μL of 7 mM 11-mercapto-1-undecanol solution was added.

The chips functionalized over 24 hrs, at which point they can be taken out of the holders and used for experiments. Contact angle measurements were done to make sure that the surfaces were adequately functionalised (Appendix).

4.2.4.2 Hydrophobic functionalisation (-CH_3)

QSX- 301 gold sensor chips from Q-sense were used for functionalisation. Gold chips were functionalized using 1-undecanethiol solution (Sigma Aldrich, >98% purity) at a 7 mM molarity. Stock solutions of 100 mM were made up using 3.2 mg of undecane- thiol solution, and 157 μl of pure ethanol. The stock solutions were kept in the fridge at a constant temperature of 4°C and diluted to 7 mM.

The gold QCM-D chips were cleaned as described previously. Once the chips were cleaned, they were put into 1 mL plastic sensor chip holders (which were previously cleaned with ethanol), and 200 μL of 7 mM of 1-undecanethiol solution was added.

The chips functionalize over 24 hrs, when they can be taken out of the holders and used for experiments. Contact angle measurements were done to make sure that the surfaces were adequately functionalised (Appendix).

4.2.4.3 QCM-D apparatus

The QCM-D is a highly sensitive surface mass detector (in nanograms) and was used to look at how all four peptides interact with both glass and silicon dioxide.

The wet mass adsorbed causes a resonance frequency shift, Δf_n, which is directly proportional to the mass adsorbed, m_f. The Sauerbrey equation (shown previously in Section 2.2) is applicable for rigid homogenous layers, and is considered an appropriate model if dissipation is less than 2×10^{-6} [185].

All experiments were performed at a controlled temperature of 25 ± 0.1°C. The system is stabilised by flowing buffer through it at a flow rate of 10 μL/min with a 1.8 mL volume. Stabilisation was achieved when the drift < 2 Hz/hour. The baseline is established by the buffer. Stabilisation usually took between 2-3 hours. Once stabilisation was complete, the experiment was started. The flow rate for the experiment was 100 μL/min, and 0.8 mL was run through the system each time. Initially, buffer is run through the system for 800 seconds, to investigate that the system uses the buffer as the normalised f0. Peptide solution was then passed over the substrate at 800 s, and was run through the system for a further 800 s. Usually, a frequency shift is seen here indicating adsorption of the peptide. After peptide adsorption, 0.8 mL of buffer solution was then passed over the substrate until the surface was saturated, and the frequency usually increases showing desorption of the peptide. From this, both adsorption and desorption of the peptide to the surface could be monitored. The total mass was calculated using the conversion factor C, which is 17.89 ng $Hz^{-1}cm^{-2}$ for a 5MHz QCM-D crystal. Normalized frequencies using the fifth overtone are presented since this overtone usually has the best signal-to-noise ratio.

All QCM-D measurements were repeated at least three times each on QSX 301 (Gold) – OH functionalised, QSX 301 (Gold) – CH_3 functionalised, QSX 305 (Polystyrene), QSX 303 (Silicon Dioxide) and QSX 336 (Borosilicate Glass) sensor chips in both acidic and basic conditions, in order to evaluate peptide adsorption at different overall charges.

The figure below demonstrates an example of raw QCM-D data. As previously described, buffer is used to stabilise the system before measurements are taken. This step ensures the QCM-D system is stable, and that the buffer is the established baseline. Hence, when buffer is initially flown through the system, there is no change in the normalized frequency, as seen up to t = 800 s in Figure 4.1. At 800 s, the solution is changed from the buffer solution to the peptide solution. The resulting decrease in frequency corresponds to peptide adsorption to the surface (m_a), which can be used to calculate hydrated mass adsorbed. After a set amount of time (at t = 1600 s for the figure below), at which the peptide will fully cover the sensor surface, the peptide solution and buffer solution are switched, and buffer once again flows through the system. This corresponds to the increase in frequency, and therefore also decrease in mass, indicated by m_d in the figure below. The system of running buffer first, then peptide, then buffer through the system is specifically designed so that information can be gathered on the amount of peptide adsorbed to the surface, but also the amount of peptide that desorbs once buffer solution is put through the system, garnering information about the strength of the bonds made between the peptide and the surface. The desorption only occurs if the peptide is weakly bound to the surface,

and hence information on the type of surface interactions can be gleaned from this data.

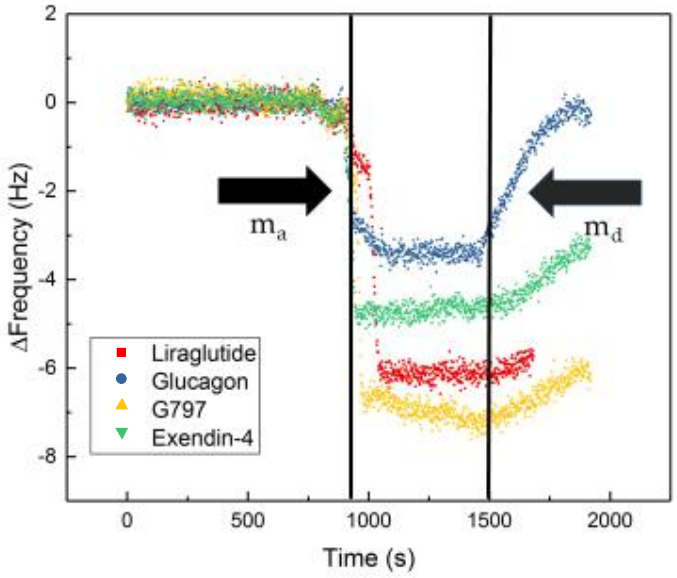

Figure 4.1: An example of QCM-D raw frequency data, with change in frequency on the y-axis vs time on the x-axis. A baseline in buffer is collected up until t = 800 s. The thick black line at t = 950 s marks m_a, the frequency shift that indicates peptide mass adsorption. From t = 950 s to 1500 s, the sensor is exposed to the peptide solution and peptide is available to adsorb and desorb from the surface. At the second black line, the buffer has been run through the system again, and the increase in frequency indicates that mass is desorbing from the surface, m_d.

In addition to the raw frequency data, the average mass adsorbed will also be shown. This was calculated through the conversion factor C, -17.89 Hz, to convert frequency to mass. The average mass adsorbed shown in bar charts is taken from three consecutive repeats, with the standard deviation, at a time of highest mass adsorbed.

4.2.4.4 QCM-D data

The QCM-D data was initially opened using Q-tools software. This software allows for raw data of frequency and dissipation vs time in milliseconds. Per measurement, thousands of data points are taken. The frequency shift (from f0) was analysed and converted to hydrated mass in ng/cm^2. Hence, the control was the frequency at which the buffer was run through the system (f0), and all results are comparative of the control, as shown in Fig 4.1 on the previous page.

For each data set, triplicates were taken, and in the following chapter when stated that results are significant, this is taken to mean a p-value of < 0.001. Results are displayed as histograms of the mean ± standard deviation between the triplicates. All graphing and data analysis was done using Origin Software (8.2).

4.3 Results

Using the QCM-D and DLS, the adsorption of the four peptides to a variety of surfaces in different conditions can be investigated. From Chapter 3, it was determined that at highly acidic and highly basic conditions all peptides carry a charge (a positive charge in acidic conditions, and a negative charge in basic conditions). At pH 7.4, both glucagon and exendin-4 carry no charge, whilst g797 and liraglutide do carry a charge. Therefore, in order to keep experimental factors as consistent as possible, only highly acidic and basic conditions were used. Neutral conditions provides the additional solubility problem, and hence was not tackled in this chapter. The hydrophilicity/hydrophobicity of the surfaces is also investigated, in addition to the effect of charge on the adsorption of peptides to the surface. The DLS was used in order to verify size in solution, and to further investigate the peptide structure – adsorption relationship.

4.3.1 Dynamic Light Scattering (DLS)

Dynamic light scattering was used in order to investigate the changes of hydrodynamic radii shown by the peptides over different concentrations, in order to assess the structures they might form on the surface. Concentrations varying from 0.5 mg/mL to 2.5 mg/mL were used. However, due to the small size of the peptides, and from the structures shown in Chapter 3 at such low concentrations, peptides were not readily detected at 0.5 mg/mL. However, both 1.0 mg/mL and 2.5 mg/mL could be detected, and are displayed in Table 4.1 below.

Table 4.1: The hydrodynamic radii of the peptides in each condition, with varying pH, as well as varying peptide concentration. As previously stated, at concentrations lower than 1.0 mg/mL, the four investigated peptides, of between 3-4 kDa, are difficult to see using DLS.

Size (nm)	**Acidic**		**Basic**	
Peptides	**1.0 mg/mL**	**2.5 mg/mL**	**1.0 mg/mL**	**2.5 mg/mL**
Liraglutide	28.7 ± 12.4	234.5 ± 21.6	75.4 ± 23.6	287.9 ± 36.8
G797	34.6 ± 11.6	286.1 ± 14.4	39.5 ± 12.8	210.8 ± 54.6
Exendin-4	235.9 ± 24.7	456.8 ± 18.9	149.6 ± 37.1	346.7 ± 44.3
Glucagon	134.5 ± 28.1	165 ± 32	31.7 ± 13.7	286.5 ± 17.2

From Table 4.1 above, a few things can be noticed. Primarily, that both glucagon and exendin-4 are significantly larger than the lipidated peptides at 1.0 mg/mL at acidic conditions. From Chapter 3, we know that glucagon fibrillates rapidly, and exendin-4 shows oligomers, even at low concentrations, which could explain the results seen above. Additionally, exendin-4 shows to be even larger in higher concentrations, again confirming that with higher concentrations, exendin-4 shows larger oligomers in both acidic and basic conditions. The lipidated peptides are small at low concentration, and can be seen by their longer lag phase, confirmed in Chapter 3. Both peptides show similar starting sizes, and at high concentration, also show similar results, even though different structures are formed in solution. This DLS data is concurrent with some of the measurements taken with the AFM – g797 micelles are the same size as found using both AFM and DLS. In basic conditions, glucagon shows similar sizes in low and high concentrations to the lipidated peptides, due to its slower kinetics for aggregation. At high concentrations, its been seen in Chapter 3 that larger aggregates do form, which can also make determination of size using DLS

difficult. For all peptides, the hydrodynamic radius of each peptide increases with increasing concentration indicating peptide self-assembly into higher order structures.

The DLS confirms that in solution, and at higher concentrations, peptides will self-assemble into secondary structures. The micelle measurements are consistent with those found using the AFM, as well as the size of oligomeric structures formed by exendin-4.

The next part of the chapter tackles peptide adsorption to a specific set of surfaces, and the interactions and bonds made through tailoring the surface. Firstly, hydrophilic surfaces are investigated in both acidic and basic conditions, followed by hydrophobic surfaces.

4.3.2 Adsorption of Peptides to Hydrophilic surfaces using QCM-D

In an aqueous environment, a peptide will tend to adopt a conformation with its hydrophilic groups positioned externally and hydrophobic groups located internally, as shown in Fig 4.2 below.

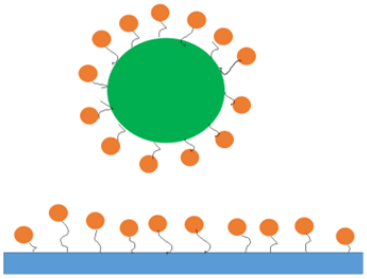

Figure 4.2: Likely mechanism of peptide adsorption on a hydrophilic surface. The surface is blue, while the peptide is green (with hydrophobic patches located internally), and hydrophilic groups are orange, facing the solution.

Proteins could however, be associated with hydrophilic surfaces through entrapment within bound-water layers [32]. These proteins would be reversibly bound and would be expected to wash off when buffer is flown through the system. A likely cause of this type of adsorption is through polar interactions and ionic association. In this case, it's predicted that there is little change to the configuration of the protein, and hence the protein conformation will be similar to that expected whilst in solution. In this section the adsorption of all four peptides in acidic and basic conditions is studied on hydrophilic surfaces.

4.3.2.1 Adsorption of Peptides to Au-OH (QSX 301)

As discussed in Section 4.2.2, Au sensor chips were functionalised with 11-mercapto-1-undecanol in order to create a hydrophilic surface, which was confirmed using contact angle measurements (shown in Appendix). This functionalization makes a surface with –OH groups to create a neutral hydrophilic surface. The O-H bond carries no overall charge, even though both oxygen and hydrogen carry a partially negative and partially positive charge, making the –OH bond polar. The adsorption of the peptides to the –OH functionalized surface will be presented in acidic conditions first, followed by the results of adsorption in basic conditions.

pH 2.4

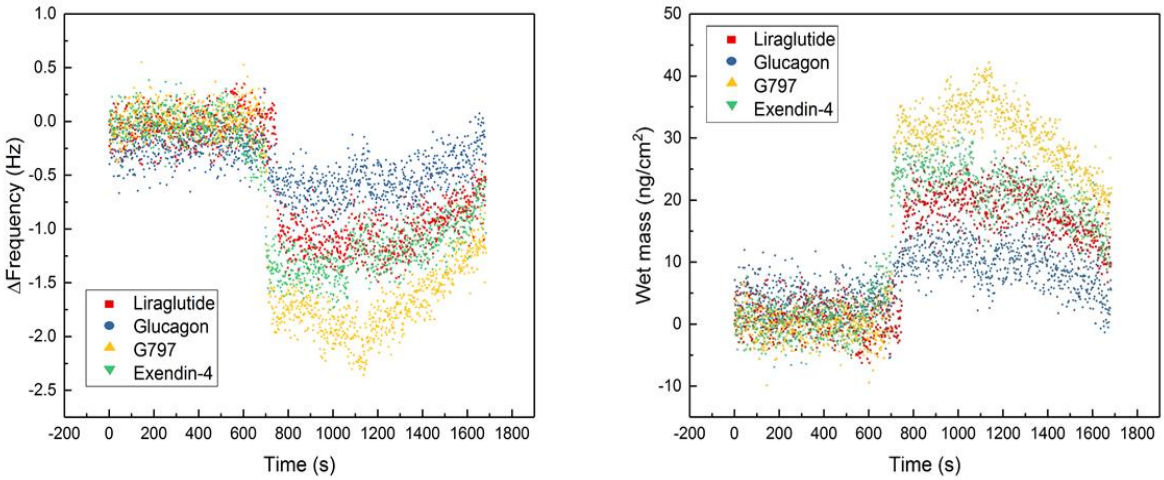

Figure 4.3: Left - QCM-D raw results for glucagon, liraglutide, g797 and exendin-4 adsorption on Au-OH where change in frequency was plotted against time at pH 2.4. **Right -** Frequency is converted to adsorbed mass versus time plot. Glucagon and liraglutide show the lowest mass adsorption on the (QSX-301) Au- OH substrate

Fig 4.3 above shows that only a small amount of peptide adsorbs to Au-OH. The absorbed masses are between 10 – 40 ng/cm^2 for each of the four peptides. These numbers for mass adsorption are small but reproducible over experiments performed in triplicate. This indicates that there is some interaction between the hydrophilic surface and peptides, as clear differences in frequency compared to

the baseline can be observed. Both hydrophilic and neutral surfaces have been studied in detail, and it is well established that peptide adsorption would be minimal [121][124]. The average mass of the experiments shown in Fig 4.3 with its corresponding standard deviation of the three measurements are shown in Fig 4.4 below.

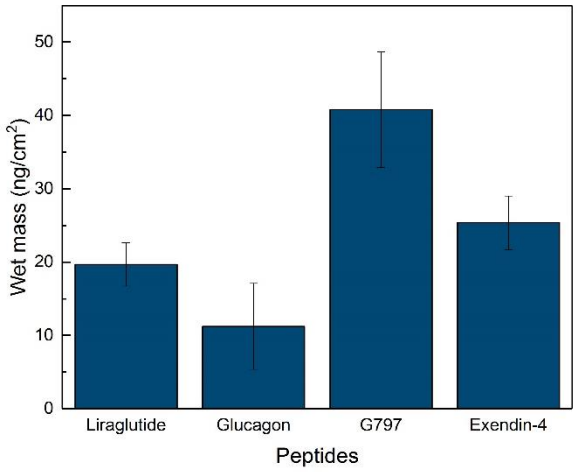

Figure 4.4: Summation of average wet mass adsorbed on Au-OH surface for each peptide in acidic conditions. This was calculated as the difference from the baseline to 1100s, where peptide adsorption has reached its maximum.

Even though all four peptides, glucagon, g797, liraglutide and exendin-4, have slight differences in their amino acid sequence, they follow the same pattern of adsorption on the -OH surface in acidic conditions, when all peptides will carry a positive charge. Interestingly, out of all peptides, g797, a peptide with a glucagon backbone but an additional lipidated chain, adsorbs the most. This is unexpected, as the peptide will try and shield its hydrophobic lipid chain from the –OH hydrophilic surface. However, structural rearrangements of the peptide on the surface could contribute for the small, ± 18.3 ng/cm^2 difference. Due to the small size of wet mass adsorption by all peptides, it can be determined that when peptides are positively charged, they are unlikely to adsorb to a neutral hydrophilic surface.

Whether the peptides follow the same pattern when negatively charged, in basic conditions will be seen in Fig 4.5 below.

pH 10.8

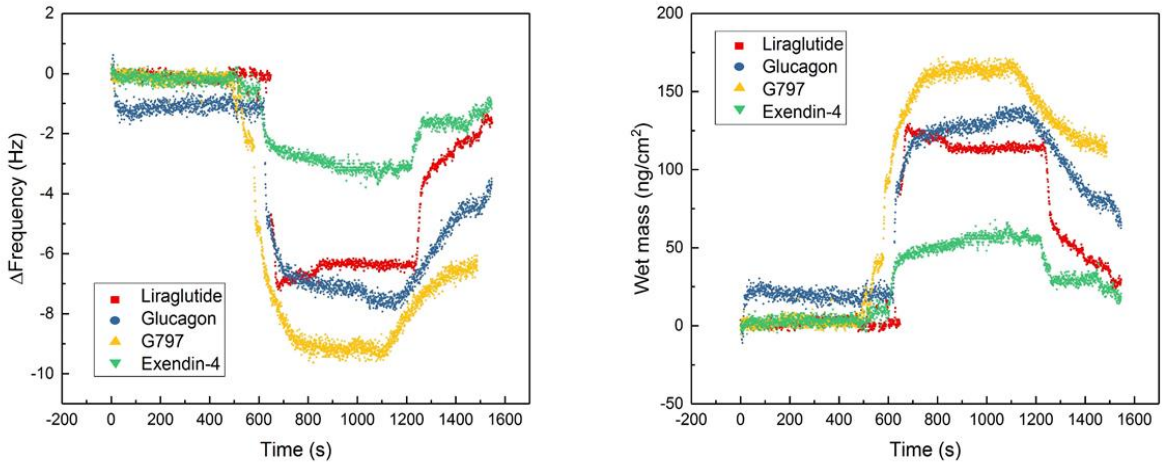

Figure 4.5: Left - QCM-D raw results for glucagon, liraglutide, g797 and exendin-4 adsorption on Au-OH where change in frequency was plotted against time at pH 10.8. **Right -** Frequency is converted to mass versus time plot, using conversion factor C (-17.89Hz^{-1}cm^{-2}).

From the above figure, a pattern for each peptide emerges. Unlike in the previous condition when peptide adsorption was minimal, in basic conditions there is significantly more adsorption, as well as stark differences dependent on individual peptides. G797 adsorb more in basic conditions than any of the other peptides, with glucagon following in second place.

As described in Chapter 3, the size of the charge in highly acidic and highly basic conditions is similar. This could indicate that when negatively charged, amphiphilic peptides tend to adsorb more to hydrophilic surfaces than when positively charged or that the structures formed in basic conditions, previously investigated in Chapter 3, and were more susceptible to adhering to a hydrophilic surface. In addition, the polar surface could form stronger dipole-dipole interactions when peptides are carrying a negative charge. In basic conditions both lipidated peptides formed micelles (spherical or otherwise), which could explain why these g797 peptides is more likely to adsorb. In micellar structures

the hydrophobic part of the peptide is shielded, and hence the hydrophilic moieties will be the main anchors to the hydrophilic surface. Exact peptide masses between acidic and basic conditions vary; with g797 adsorbing 130 ng/cm^2 more in basic conditions, and liraglutide also increasing its adsorbed wet mass by almost 120 ng/cm^2. The averages of the wet mass adsorbed by the peptides in basic conditions is shown in Fig 4.6 below.

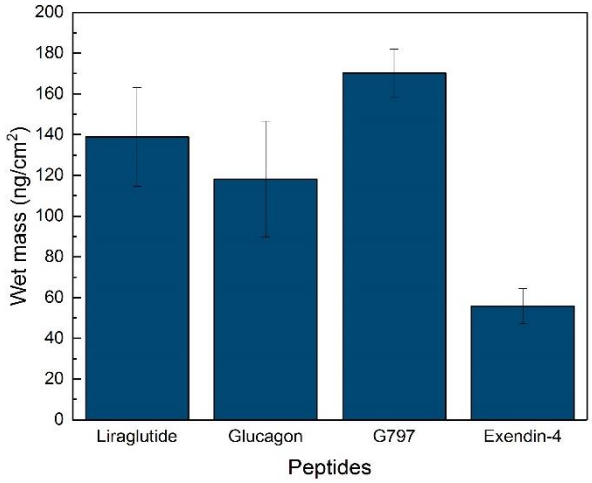

Figure 4.6: A figure summarising the adsorption (in ng/cm^2) of all peptides on Au-OH surface in basic conditions. The error bars represent the standard deviation from all three experimental data sets.

From Fig 4.6 above, it can be seen that all four peptides adsorb more to the –OH surface in basic conditions, even glucagon and exendin-4. The pattern of lipidated peptides adsorbing more to the hydrophilic surface is observed, but unexpected. Unlike g797 and liraglutide, glucagon and exendin-4 do not form micelles. However, glucagon does take longer to form fibrils in basic conditions than in acidic conditions. Perhaps monomeric glucagon is stabilised by adsorption onto hydrophilic surfaces when negatively charged, which could explain its larger wet mass adsorption. Exendin-4 is known to have a stable Trp cage, which will be unaffected in basic conditions on a hydrophilic surface, and hence is unlikely to show much adsorption to the surface, as shown in Fig 4.6 above.

In order to compare the differences in mass adsorption, Table 4.2 summarises the findings of both conditions in table format, as well as the standard deviations established through repetition of experiments at least three times.

Table 4.2: Summation table of peptide adsorption in both acidic and basic conditions, together with their standard deviation.

	Liraglutide (ng/cm^2)	Glucagon (ng/cm^2)	G797 (ng/cm^2)	Exendin-4 (ng/cm^2)
pH 2.4 (+ charge)	19.7 ± 3.0	11.2 ± 5.9	40.8 ± 7.9	25.4 ± 3.7
pH 10.8 (- charge)	138.9 ± 24.2	118.2 ± 27.5	170.3 ± 11.7	55.7 ± 8.6

From Table 4.2 above, peptides adsorb to neutral hydrophilic surfaces when carrying a negative charge, largely due to the structures that each peptide forms in these conditions, and polar interactions. At acidic conditions, however, little peptide adsorption is seen and hence, uncharged hydrophilic surfaces could be useful in preventing adsorption of peptides. However, other factors such as solution conditions and specific amino acid sequence need to be kept in mind, as more surfaces are investigated in the next section.

4.3.2.2 Adsorption of Peptides to Borosilicate Glass (QSX 336)

Borosilicate glass, is a type of glass made from silica and boron trioxide. Its main properties include low thermal expansion coefficients, making borosilicate glass much more resistant to shock and high temperatures than most other glasses. Borosilicate glass is also commonly used in lab ware, as well as, reagent bottles and vials, and hence was used in this thesis as a pharmaceutically relevant surface to be studied.

Borosilicate glass is hydrophilic as is silicon dioxide. Adsorption of the four peptides to borosilicate QCM-D chips is measured in acidic and basic conditions, as presented in the following sections.

Peptide adsorption to the borosilicate glass surface was initially investigated in acidic conditions, when peptides would carry an overall positive charge due to the low isoelectric points of the peptides under investigation, which was previously confirmed in Chapter 3. The hydrophilic surfaces of glass carries a negative charge, however in low acidic pH, this charge diminishes. Studies have assessed the pH at which glass carries no charge, and this is still being investigated. However, the values lie between a pH of 1.7 – 3 [276]–[278]. Therefore, when considering charge interactions between the surface and peptides in this instance, they will be minimal. The experimental results of peptide adsorption on borosilicate glass are shown in acidic conditions in Fig 4.8 below.

pH 2.4

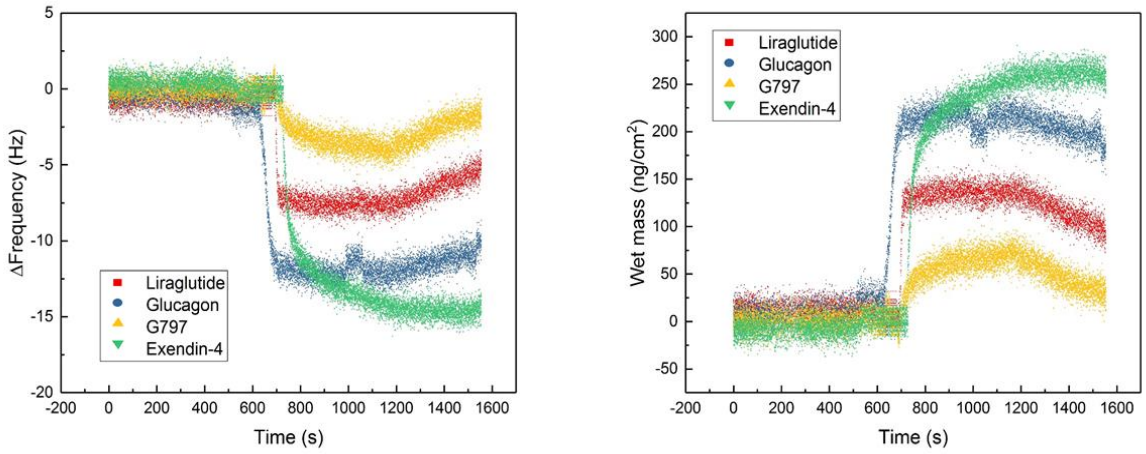

Figure 4.7: Left - QCM-D raw results for glucagon, liraglutide, g797 and exendin-4 adsorption on borosilicate glass where change in frequency was plotted against time at pH 2.4. **Right -** Frequency is converted to mass to give a mass versus time graph. There is a significant m_a step with little to no m_d, indicating strong bond formation between the peptides and the surface.

In Fig 4.7 above, a clear trend can be observed. Firstly, the wet mass adsorption is very high, over 250 ng/cm^2 for exendin-4. Secondly, the two peptides with added C_{16} chains show the least adsorption to the surface. For g797, a lipidated peptide with a glucagon backbone, adsorption in acidic conditions is minimal. In strong acidic conditions, g797 forms fibrils and protofibrils. Hence, the monomeric peptide is stabilising its structure through self-assembly rather than through adsorption to the surface. Liraglutide forms stable hexamers in solution conditions with a pH of 8. However, once the pH drops below 6.9, liraglutide forms an octamer structured micelle [248]. The mass adsorbed follow a trend; g797< liraglutide < exendin-4 ≈ glucagon on the glass surface. Glucagon carries a 5+ charge in acidic conditions, as previously discussed in Chapter 3. This high overall charge could be the reason that glucagon adsorbs well to a slightly charged borosilicate glass. Exendin-4 adsorbs significantly to the glass surface. The Trp cage in exendin-4 becomes protonated in acidic conditions, and hence, its propensity to adsorb and partially unfold [261] to a negatively charged surface (even if small) will be high, stabilising the structure once its adsorbed, which is

confirmed by exendin-4's lack of desorption shown in Fig 4.8 above. The change in secondary structure of the peptides on the surface is further illustrated by the peptides inability to desorb, which is likely due to an alteration of their conformation, and the intramolecular forces within each peptide. A change in secondary structure on a surface can give added thermodynamic stability to the peptide, and desorption would be unfavourable [279].

In order to confirm the results above, the average wet mass adsorbed onto the glass surface was found and plotted in Fig 4.8 below.

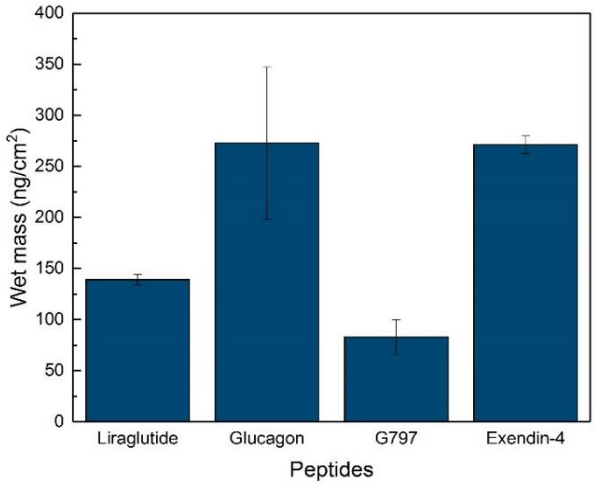

Figure 4.8: The average mass taken from 3 consecutive QCM-D measurements on borosilicate glass surfaces in acidic conditions. The error bars on the graph represent the standard deviation between the three results.

From Fig 4.8, the averages found show the same trend as previously discussed. Glucagon, however, does have large error bars. This could be due to its unstable structure in solution.

The data collected above provides a clearer picture of how peptide sequence plays a large role on their adsorption onto surfaces. Whether these interactions are indeed electrostatically based will be seen in the next section in basic conditions, where, if electrostatic interactions are a large part of the adsorption process, repulsive forces will provide for little peptide adsorption to the surface.

pH 10.8

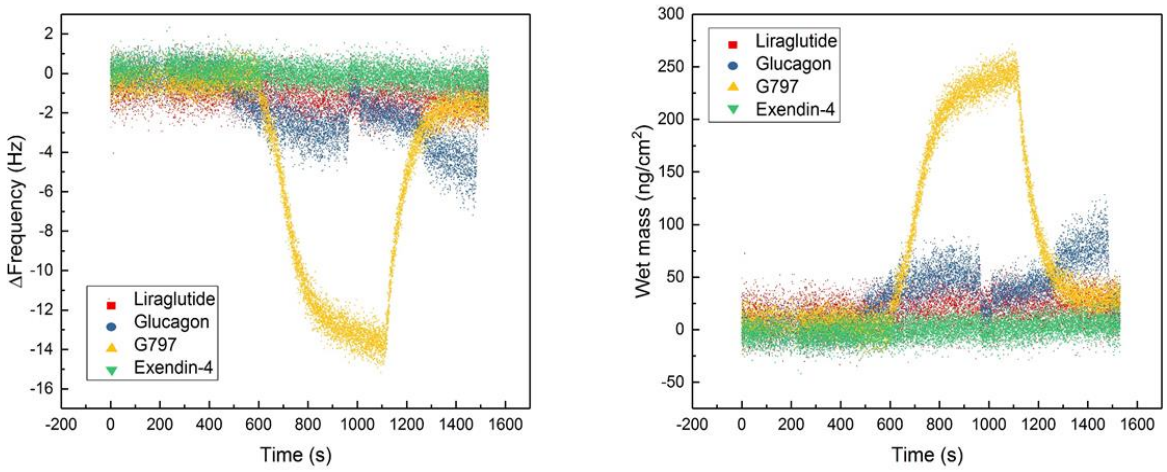

Figure 4.9: **Left** - QCM-D raw results for glucagon, liraglutide, g797 and exendin-4 adsorption on glass where frequency was plotted against time at pH 10.8. At 1100s, glycine buffer is run through for desorption studies, which indicates a weak interaction. **Right -** G797 shows a large mass adsorption to the QSX 336 glass surface in basic conditions, which is inexplicable by electrostatic interactions alone.

Fig 4.9 above shows the adsorption of the four peptides in basic conditions on borosilicate glass. The surface charge at this pH and the overall peptide charge for all peptides are also negative. If the dominant mechanism of peptide adsorption to surfaces was electrostatically driven, little to no adsorption should be seen in this condition. Nevertheless, g797 showed a large frequency shift, which was not seen for glucagon, exendin-4 and liraglutide. G797 completely desorbs once buffer is run through the system, which is shown in Fig 4.10 at 1100s. The implications are that there is a weak interaction between the surface and the peptide, indicating different interactions are at play in comparison to the

interactions in Fig 4.7, where peptides were shown to experience almost no desorption. The average of the three consecutive repeats is shown in Fig 4.10 below.

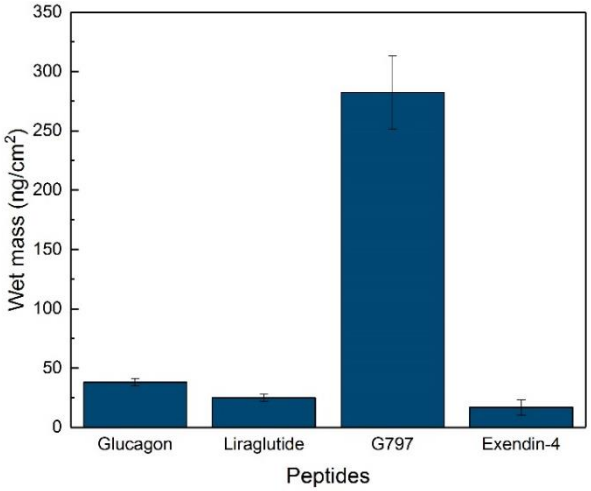

Figure 4.10: The average mass taken from 3 consecutive QCM-D measurements on borosilicate glass surfaces in basic conditions. The error bars on the graph represent the standard deviation between the three results.

Liraglutide is well documented to form micelles, through the palmitoylated side chain. Multiple case studies show the increased longevity of therapeutic peptides through addition of a fatty acid side chain, by means of micelle or higher order structure formations [280], [281]. Peptide g797 has a very different distribution of hydrophobic amino acids compared to liraglutide. Whilst liraglutide has an even distribution of hydrophilic and hydrophobic amino acids in its peptide backbone, g797 has a very predominant hydrophobic C-terminal, and a highly hydrophilic N-terminal. In addition, in Chapter 3 it was observed that in basic conditions, both lipidated peptides formed different structures. For g797, in basic conditions, spherical micelles were formed. The lipidated chain is shielded away from the solution, and possibly some of the charge is too. Whilst for liraglutide, spherical micelles were not observed. The charge, therefore, might not be shielded away as well, causing repulsive forces with the surface. These structures will have an effect on their adsorption to the surface.

The summation of the masses of peptide adsorbed to borosilicate glass in both acidic and basic conditions is tabulated below in Table 4.3.

Table 4.3: The summation of all wet masses of peptide adsorbed to borosilicate glass, in both acidic and basic conditions, with their standard deviations.

	Liraglutide (ng/cm^2)	Glucagon (ng/cm^2)	G797 (ng/cm^2)	Exendin-4 (ng/cm^2)
pH 2.4 (+ charge)	139.1 ± 4.9	272.9 ± 74.4	82.9 ± 16.8	271.2 ± 8.6
pH 10.8 (- charge)	24.9 ± 2.9	38.0 ± 3.0	281.8 ± 30.9	16.8 ± 6.5

From the table above, a few observations can be made. Firstly, there are significant differences in adsorption for all four peptides. Three of the peptides; liraglutide, glucagon and exendin-4, all act similarly and adsorb more in acidic conditions when positively charged. Glucagon and exendin-4 show almost identical masses in acidic conditions, due to their protonation in acidic conditions. Due to borosilicate glass carrying a slight negative charge, a large part of the adsorption will be due to electrostatic attractive interactions, especially with glucagon which is highly charged. Electrostatic interactions play a large part in adsorption, and this is further shown when peptides in basic conditions, carrying a negative charge, are repelled by the negatively charged borosilicate glass. However, this is not the case for g797, which under basic conditions forms micelles. This indicates that the hydrophobic interactions dominate the adsorption mechanism for g797, and can shield some of the negative charge, allowing it to overcome the unfavourable electrostatic interactions. This is not quite the same for liraglutide, the other lipidated peptide. In Chapter 3 it was seen that liraglutide did not form spherical micelles under highly basic conditions in this study and hence the same theory cannot be applied.

4.3.2.3 Silicon Dioxide (QSX 303)

Silicon dioxide surfaces were purchased from Q-sense. These chips were used to investigate the trends seen on borosilicate glass and whether or not they were reproducible on a similarly structured surface.

The silicon- oxygen bond is a strong covalent bond, making both materials strong and relatively inert. Due to the same possible dissociation of the silanol groups, silicon dioxide also carries a negative charge. The charge does however, depend on the solution conditions, and in acidic conditions the overall negative charge of the surface will be smaller than that in basic conditions. Due to the unexpected results shown by g797 in basic conditions, adsorption studies were done on silicon dioxide surfaces as a confirmation for the results found previously for borosilicate glass, as shown in Fig 4.11 below.

pH 2.4

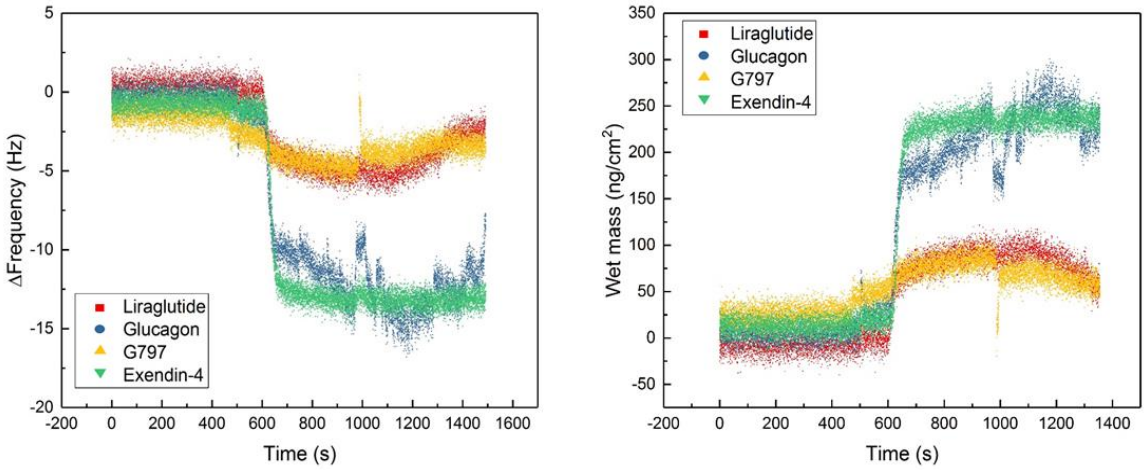

Figure 4.11: Left - QCM-D raw results for glucagon, liraglutide, g797 and exendin-4 adsorption on silicon dioxide where change in frequency was plotted against time at pH 2.4. **Right -** Frequency is converted to mass, shown on the right hand side.

From the figure above, it can be seen that the trends in acidic conditions on borosilicate glass are reproducible on silicon dioxide chips. Both lipidated peptides show less adsorption than their non lipidated counterparts on a charged hydrophilic surface in acidic conditions. Between the two different groups of

peptides, there is roughly a 100 ng/cm^2 difference. This can be accounted for by their fatty acid chains, which causes rearrangement when close to the surface, shielding and diffusing charges compared to glucagon and exendin-4. In addition, exendin-4 shows a similar trend as with borosilicate glass in the same conditions, indicating its stability on the surface at such low pH.

Another interesting observation is that as with borosilicate glass surfaces, the amount of desorption after 1100s is negligible for all peptides, which indicates strong electrostatic interactions.

Both surfaces have similar contact angles, similar hydrophilicities, and comparable structures. Borosilicate glass and silicon dioxide are also slightly negatively charged, which further suggests that there is a significant difference in terms of adsorption for lipidated vs non lipidated peptides in favourable electrostatic interaction conditions, which was not seen on neutral Au – OH surfaces. The averages of the wet mass adsorbed by the four peptides on silicon dioxide are shown in Fig 4. 12 below.

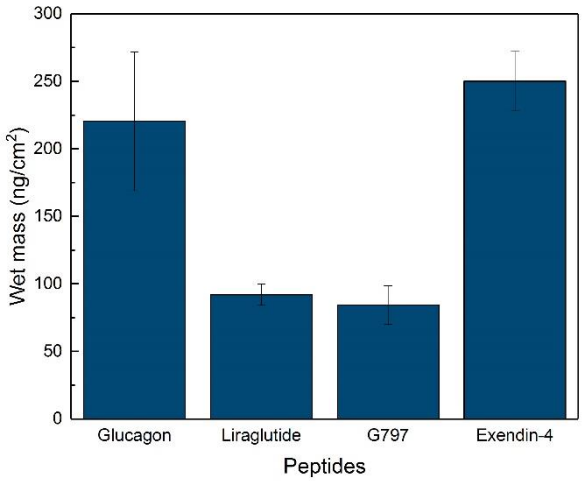

Figure 4.12: The average mass taken from 3 consecutive QCM-D measurements on silicon dioxide surfaces in acidic conditions, showing large error bars for glucagon, which is unstable in highly charged conditions.

All peptides will also carry an overwhelmingly positive charge at this highly acidic pH whilst silicon dioxide will carry a negative charge. With the surface of

opposite charge, peptide adsorption is predicted. However, as the surface is also hydrophilic, it is a play-off of factors; hydrophilic vs hydrophobic and charge interaction, as well as hydrophobic effects, van der Waals interactions and peptide – peptide repulsions. From Fig 4.12, however, we can see that charge does have a significant effect, especially when compared to the adsorption of peptides in acidic conditions on a neutral hydrophilic surface. On both glass and silicon dioxide, peptides adsorb significantly more than on neutral hydrophilic surface, like Au-OH discussed in Section 4.3.1.1

Using this reasoning, peptides were then made up in a basic buffer, where their overall charge would be negative. If peptide adsorption was highly dependent on charge interactions, then with peptides negatively charged, and the surface of a similar charge (and additionally a hydrophilic surface), less adsorption to the surface should occur. In addition, investigation of peptides in basic conditions on silicon dioxide will shed light on whether the results found on borosilicate glass are reproducible. The results of the experiments are shown in Fig 4.13 below.

pH 10.8

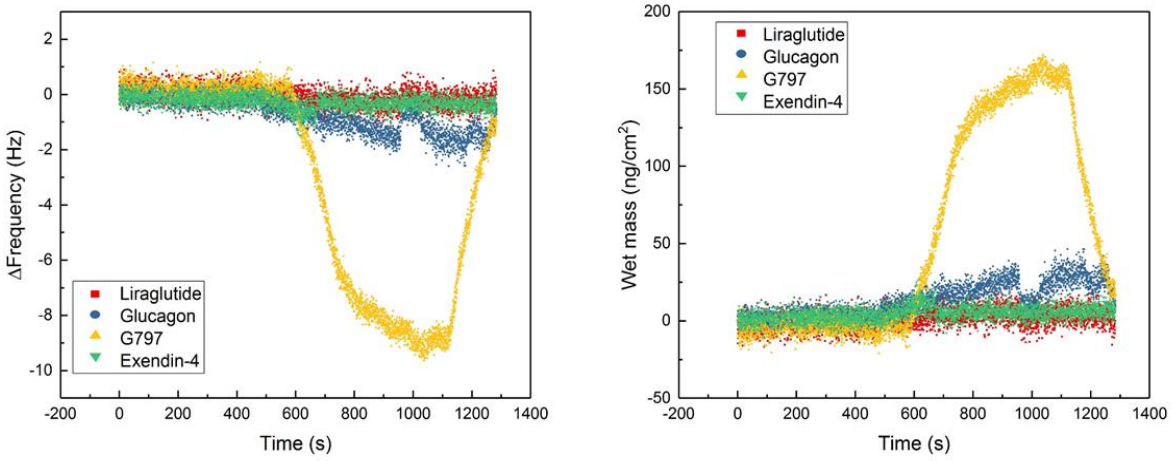

Figure 4.13: Left - QCM-D raw results for glucagon, liraglutide, g797 and exendin-4 adsorption on silicon dioxide where change in frequency was plotted against time at pH 10.8. **Right -** Frequency is converted to mass and it can be seen graphically that g797 and liraglutide show the lowest mass adsorption on the QSX 303 silicon dioxide substrate.

From the figure above, a similar pattern as the adsorption to borosilicate glass is observed. The three therapeutic peptides; glucagon, liraglutide and exendin-4 follow a pattern that indicates charge interactions are a dominant factor when looking at adsorption to interfaces. However, g797 does not follow the trend, and is even shown to adsorb more to the negatively charged surface, when the peptide is carrying a negative charge itself. This unexpected result has previously been discussed in Section 4.3.1.2, as the same effect was seen on borosilicate glass.

Literature has shown that even though peptides and proteins carrying an overall negative charge, they could still adsorb to negative surfaces due to positive amino acid residues rearrangement, and specific pockets of unequal charge distribution. The prime example of this was BSA, which is a much larger molecule, and hence, if few small electrostatic interactions can be a driving force to adsorb for such a large molecule. This reasoning can also be applied to the peptides investigated in this thesis, which could account for the small wet mass

of glucagon adsorbed on the surface, with its Lys residues extending towards the surface [282][283].

The summation of masses adsorbed on silicon dioxide at a pH of 10.8 is shown in Fig 4.14 below, where the average mass of at least three consistent repeats was taken. The trends of the results displayed are comparable to those found on borosilicate glass.

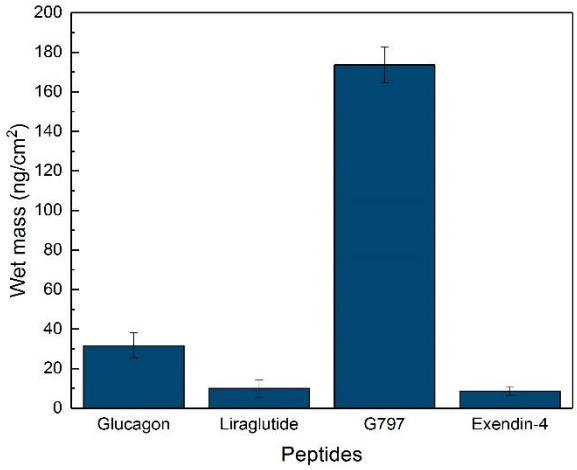

Figure 4.14: The average mass taken from 3 consecutive QCM-D measurements on silicon dioxide surfaces in basic conditions.

Although similar, the average mass on both borosilicate glass and silicon dioxide surfaces do vary; g797 adsorbed significantly more to borosilicate glass (281.8 ng/cm^2) compared to silicon dioxide (173.6 ng/cm^2). Glucagon, however, had a wet mass which was almost identical on both surfaces in basic conditions (38.0 ng/cm^2 to 31.7 ng/cm^2). This same pattern can be seen with liraglutide and exendin-4, who show very similar wet mass adsorption on both surfaces. Borosilicate glass is known to increase NSA, and hence the increase compared to silicon dioxide could be attributed to this [284]. Another noticeable factor about peptide adsorption studies in basic conditions is that peptide g797 desorbs almost completely in just 300s. The fast rate of desorption implies that the interaction between the micelles formed and the surface is weak, and that the interactions at play with g797 are very different to those in acidic conditions,

where almost no desorption is seen. In acidic conditions g797 does not form spherical micelles, and hence different interactions, most likely electrostatic, will be at play especially at low pH when g797 will be highly protonated. The summation of both acidic and basic peptide adsorption studies is shown in Table 4.4 below.

Table 4.4: The summation of peptide adsorption onto silicon dioxide in both acidic and basic conditions, with their standard deviations.

	Liraglutide (ng/cm^2)	Glucagon (ng/cm^2)	G797 (ng/cm^2)	Exendin-4 (ng/cm^2)
pH 2.4 (+ charge)	91.9 ± 7.8	220.3 ± 13.7	84.2 ± 14.3	250.2 ± 22.1
pH 10.8 (- charge)	10.0 ± 4.4	31.7 ± 6.4	173.6 ± 9.0	8.67 ± 2.3

The table above shows that in acidic conditions, exendin-4 shows largest wet mass adsorption, due to its protonated Trp cage, which is semi unfolded due to carrying a large positive charge. This means that it's still stable and keeps its hydrophobic moieties inside the cage, but due to its protonation, can also form strong electrostatic interactions with the surface. Glucagon also shows high mass adsorption in acidic conditions, whilst little mass is adsorbed to the surface in basic conditions due to unfavourable electrostatic interactions. In basic conditions, g797 shows the most adsorption to the silicon dioxide surface due to stabilised micelle formation screening the repulsive negative charges. Liraglutide, on the other hand, has low wet mass adsorption for both conditions, showing a higher affinity for adsorption in acidic conditions when protonated. Much can be learned from looking at the adsorption of the peptides on surface. Using the QCM-D, however, has the added advantage of dissipation measurements. Below, in Fig 4.15, are a cluster of points from all hydrophilic surfaces (peptides have to adsorb, and hence many of the data points from Au-

OH surfaces were discarded). In addition, as peptides did not adsorb (apart from g797) in basic conditions, the figure below is for acidic conditions only. The dissipation of the layer produced on the surface gives an indication of the viscoelastic properties of the adsorbed layer.

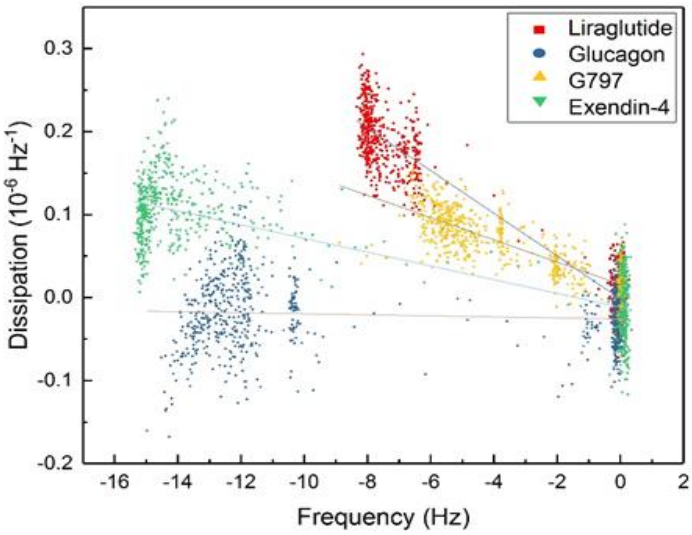

Figure 4.15: A plot of the dissipation against frequency of peptides on hydrophilic surfaces in acidic conditions. Dissipation gives the viscoelastic properties of the adsorbed layer.

All peptides show dissipation less than 2 x 10^{-6} Hz^{-1}, which means that the Sauerbrey equation holds, and hence constant C can be used in order to calculate wet mass adsorbed. This was examined for each set of results as part of the analysis of the data. The slopes of the different peptides give an indication of the types of layers formed on the surface. Both liraglutide and g797 are shown to have higher dissipation than glucagon and exendin-4. Higher dissipation suggests different rigidity in layer formation. This indicates lipidated peptides form layers with higher dissipation, such as ribbon formations seen by the AFM, formed by liraglutide in acidic conditions. Interestingly, in acidic conditions, g797 forms fibrils. However, these fibrils do differ in structure compared to glucagon (and exendin-4 forms monolayers or oligomers). Monolayers, and oligomers such as those formed by exendin-4, show the second lowest dissipation. Glucagon forms the layer with the least dissipation. The fibrils

formed by glucagon in acidic conditions, as seen in Chapter 3, are highly structured and form very tightly packed layers, and hence dissipation of energy from the layers is low. The fibrils formed by the lipidated peptides in acidic conditions are less structured, and hence will dissipate more energy. As both peptides are lipidated, the dissipation assessment further enhances the theory that g797 (and liraglutide) form different structures on the surface compared to glucagon and exendin-4, added to the images taking using the AFM in the previous chapter.

4.3.2.4 Conclusion

For hydrophilic surfaces, peptides in both acidic (pH 2.4) and basic (pH 10.8) conditions were studied. Surfaces were divided into neutral hydrophilic and charged hydrophilic. The QCM-D gives a frequency shift that was monitored and was inversely proportional to wet mass adsorbed, which could be calculated using the constant, C.

From the results seen above, some trends can be observed. The charge of the peptides in solution will have a drastic effect on amount of adsorption, indicating the importance of electrostatic interactions. Yet, peptide self-assembly, such as micelle formation, coupled with its hydrophobic interactions, cannot be discarded. Secondly, that the peptides that do bind to the surface in basic conditions almost immediately desorb once washed with buffer. The reversibility of protein adsorption on hydrophilic surfaces has been studied previously, and it's been found that on hydrophilic surfaces, protein adsorption is more likely to be reversible compared to on hydrophobic surfaces [285].

In most cases, lipidated peptides and non lipidated peptides act differently in the same condition. Also notable is that peptides with similar structures and backbones, can show a wide range of adsorptive patterns, indicating more and more that adsorption to interfaces is difficult to predict and not solely dependent

on one factor. This is very much mirrored by their self-assembly in solution, where peptide secondary structures varied wildly, even between lipidated peptides. Furthermore, adsorption trends are complex as there are many factors at play at the interface. Electrostatic interactions, peptide-peptide repulsions, van der Waals forces, and hydrophobicity are just some of the factors that determine peptide behaviour at interfaces, and generalising a group of peptides in order to characterize behavioural patterns proves difficult.

In order to gather a clearer understanding of all the interactions at play, the four peptides were also studied on a variety of different hydrophobic surfaces. The hydrophobic surfaces chosen were also either charged or neutral, and hence, peptide adsorption to hydrophobic surfaces can also be investigated.

4.3.3 Adsorption of Peptides to Hydrophobic surfaces using QCM-D

Proteins can become irreversibly bound to a hydrophobic surface through dehydration and rearrangement of the protein conformation so that the hydrophobic regions are located at the substrate surface–protein interface and the hydrophilic regions are located at the protein–water interface [63][286].

Dehydration of the surface is energetically favourable on hydrophobic surfaces, but is not favourable for hydrophilic surfaces. As our hydrophobic surfaces are non – polar, other factors must also be kept in mind. Non-polar surfaces can destabilize proteins which would facilitate conformational reorientations, which in turn lead to strong inter-protein and protein– surface interactions, increasing the wet mass adsorbed at the interface [120]. In Fig 4.16, the adsorption of a peptide molecule on a hydrophobic surface is shown.

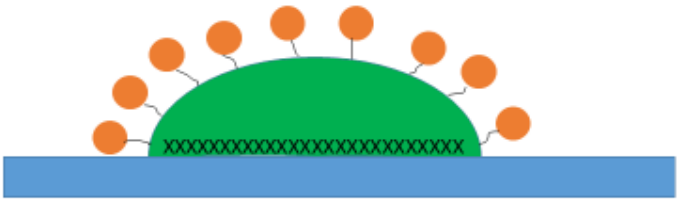

Figure 4.16: Graphical representation of peptides adsorbing to a hydrophobic surface, with xxxxx representing the hydrophobic patch of the peptide, with the hydrophilic groups (orange) facing away from the surface.

However, as previously discussed, there are a plethora of different factors that will contribute to the adsorption on hydrophobic surfaces, which are investigated below.

4.3.3.1 Au-CH_3

As discussed previously, Au sensor chips were functionalised in order to create a hydrophobic surface by addition of a $-CH_3$ group. Its functionalisation and hydrophobicity were confirmed using contact angle measurements shown in the appendix. In Fig 4.17 below, the adsorption of the four peptides to the hydrophobic surface in acidic conditions is shown.

<u>pH 2.4</u>

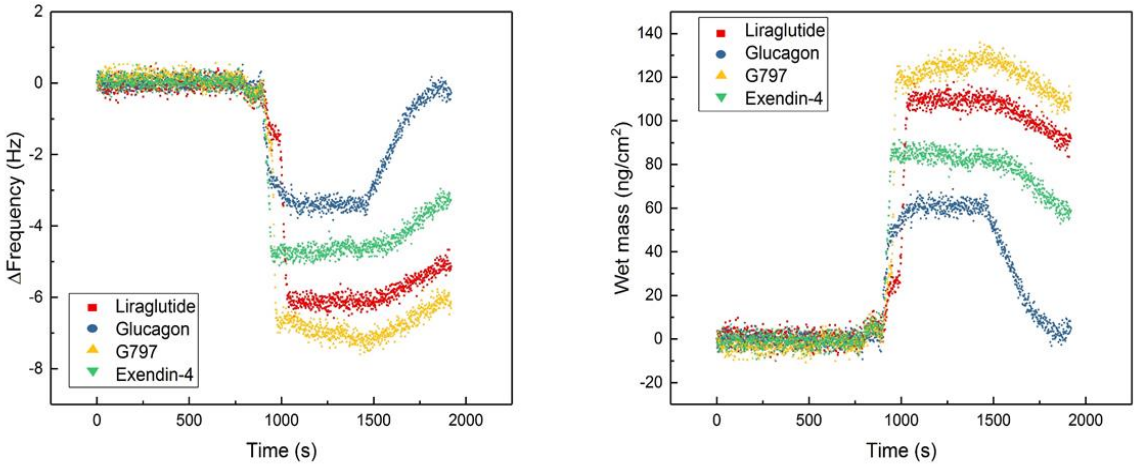

Figure 4.17: Left- QCM-D raw results for glucagon, liraglutide, g797 and exendin-4 adsorption on Au-CH_3 where change in frequency was plotted against time at pH 2.4. **Right -** Frequency is converted to mass and a frequency vs time mass is shown.

From the figure above, we can see clear distinctions between peptides. The amount of adsorption on the hydrophobic surface in acidic conditions can be summed up; glucagon < exendin-4 < liraglutide < g797. From what we know about each peptide, these interactions seem to be hydrophobically driven. Both g797 and liraglutide have the added hydrophobic chain, enabling them to form strong hydrophobic interactions with the surface. This was done through the rearrangement of their lipid chains onto the surface, causing strong interactions. However, both glucagon and exendin-4 still adsorb, which is likely due to also electrostatic interactions, due to their highly charged state. The desorption of the

peptides in solution is also valuable. Glucagon desorbs almost 100%, unlike any of the other peptides, which suggests just weak electrostatic interactions. In this condition, even though exendin-4 does not contain an added lipid chain, its Trp cage stabilises the structure. In acidic conditions, when protonated, it unfolds partially. Both lipidated peptides form strong interactions with the surface, and show little desorption of peptide when the buffer is run through the system.

The averages of the experiments was taken and displayed in Fig 4.18 below, for easier comparison. From the figure it can be seen that there are significant differences between the peptides, especially g797.

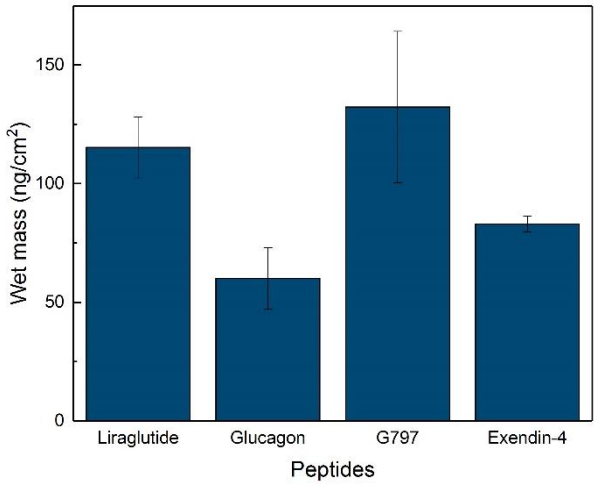

Figure 4.18: The average wet mass of each peptide adsorbed to the Au-CH_3 surface in acidic conditions, with the error bars signifying the standard deviation from three consecutive repeats.

From the repeats of the experiment in acidic conditions on the hydrophobic surface, g797 and liraglutide still show a difference between each peptide, even with their similar structures and added lipid. From chapter 3, both peptides form fibrils in acidic conditions albeit different fibrils. The difference in adsorption indicates that g797 fibrils, formed through HAM structure, are more likely to stabilise through adsorption to the surface than self-assembly. However, both lipidated peptides still show a higher wet mass adsorption than the other two peptides, indicating that the primary force driving the adsorption will be hydrophobic driven.

Exendin-4 and glucagon show very similar values, which can be explained by their structures. At acidic pH, exendin-4's stable Trp cage is semi-folded, and hence a proportion of the hydrophobic moieties are being kept inside the cage like structure, away from the surface. Some of the protonated hydrophobic moieties inside the cage will form hydrophobic bonds to the surface. However, not all hydrophobic parts of the molecule will be available for bonding, destabilising the structure and making it unfavourable for the Trp cage to fully unfold. Glucagon has no added lipid chain, and compared to the other peptides, has the least hydrophobic residues. Its likely mechanism is electrostatic rather than hydrophobic, which explains both the small amount of adsorption, as well as its ability to desorb.

From the results above, hydrophobic interactions seem to dominate the adsorption on hydrophobic surfaces. This was investigated further by exploring the adsorption of the peptides in basic conditions, shown in Fig 4.19 below.

pH 10.8

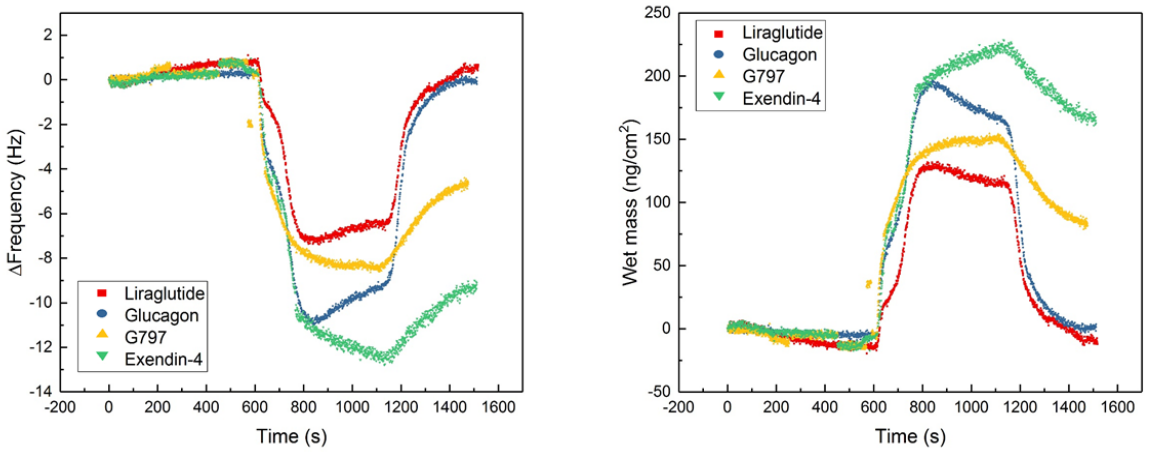

Figure 4.19: Left - QCM-D raw results for glucagon, liraglutide, g797 and exendin-4 adsorption on Au-CH_3 where change in frequency was plotted against time at pH 10.8. **Right -** Frequency is converted to mass, g797 and liraglutide show the lowest mass adsorption on the (QSX 301) Au-CH_3.

At pH 10.8, when peptides will carry an overall negative charge and curiously, the opposite adsorption pattern can be seen compared to acidic conditions. In Fig 4. 19, liraglutide and g797 show the least wet mass adsorption, whilst the two non-lipidated peptides glucagon and exendin-4 show more mass adsorbed, with exendin-4 adsorbing 227.65 ng/cm^{2,}, compared to liraglutide adsorbing 116.98 ng/cm^2. The clear pattern between the two differently charged conditions seems to show that the interactions on the hydrophobic surface are, to some extent electrostatically driven. This is further confirmed by the fact that the peptides show a large amount of desorption, m_d, present at around 1100s. Desorption can be seen when the buffer is flushed through the system, and hence will flush any peptide that is loosely adhered to the surface. All peptides show a large amount of mass desorbed, with both glucagon and liraglutide desorbing completely in just under 300 seconds. Liraglutide showed little desorption in acidic conditions, however glucagon, was shown to desorb in both conditions. In addition, exendin-4 adsorbs the most, even though the Trp cage will be unprotonated, and

hence the molecule should be stable. The Trp cage is structured in such a way that it protects the hydrophobic parts of the peptide away from the solvent. On hydrophobic surfaces the Trp cage has been shown to unfold, due to favourable hydrophobic interactions, which stabilise the molecule in these conditions [287][288]. The unfolding of the peptide cage is possible when the molecule is negatively charged in hydrophobic conditions. However, in the case of exendin-4 structure, this can be outweighed by large protonation in acidic conditions, where the Trp does not unfold fully, even on hydrophobic surfaces.

Even though the mass adsorbed is large, the strength of the peptide-surface interaction is weak. The findings of multiple experiments in these conditions are summarised in Fig 4.20 below.

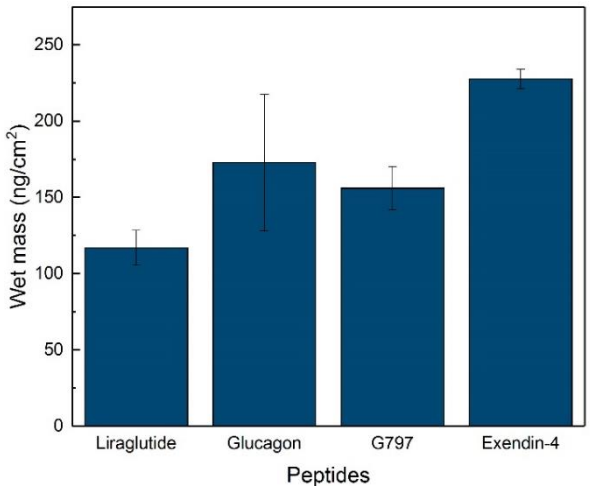

Figure 4.20: The average wet mass of peptides adsorbed in basic conditions on Au-CH_3. The error bars indicate the standard deviation between the three consecutive repeats.

In Fig 4.20 above, the results of the average of three repeats can be seen graphically. The exact opposite trend to the adsorption in acidic conditions can be seen. Exendin-4, which on hydrophobic surfaces will unfold, shows the largest adsorption in basic conditions, where it's unfolding is more favourable due to the large hydrophobic interactions. G797 and liraglutide show interesting

results, as they show only small differences in mass adsorbed to the surface in highly differing conditions.

For easier comparison, Table 4.5 below sums up the masses of peptide adsorbed in both pH 2.4 and pH 10.8 on Au-CH_3.

Table 4.5: Summation of results and their standard deviation of wet mass adsorbed in ng/cm^2 for Au-CH_3 surface in acidic and basic conditions

	Liraglutide	Glucagon	G797	Exendin-4
pH 2.4 (+ charge)	115.5 ± 12.8	60.1 ± 12.9	132.3 ± 31.9	83.1 ± 3.3
pH 10.8 (- charge)	117.0 ± 11.4	172.8 ± 44.8	156.1 ± 14.1	227.7 ± 6.5

One of the first things to notice is that adsorption to the hydrophobic surfaces, shows a smaller variance between some of the peptides in differing conditions. Liraglutide shows almost identical amounts of adsorption in both conditions, and g797 shows a difference of just over whilst 20 ng/cm^2, a very small difference. On the other hand, exendin-4 shows a difference of almost 150 ng/cm^2, and glucagon shows a difference in mass adsorption of almost 100 ng/cm^2. The differences between the masses tells a story; the charge interactions have less of an effect on the lipidated peptides. For the lipidated peptides, it seems that their added hydrophobic chain will be driver for adsorption to hydrophobic surfaces, irrelevant of the charge interactions, which was not always the case on hydrophilic surfaces. Whether this is specific to Au-CH_3 surface or hydrophobic surfaces in general will be investigated next.

4.3.3.2 Polystyrene

Polystyrene was investigated due to its common occurrence in the pharmaceutical industry. Most containers, vials, syringes and other bench materials are in polystyrene, and hence is very relevant to investigate in terms of peptide adsorption. Although its occurrence is widespread, the interfacial region between polystyrene and solution is difficult to investigate [152]. Additionally, polystyrene is very hydrophobic, and hence, prone to contamination from dust and other particles, making experimentation difficult. Polystyrene is also known as a substance that enhances non-specific adsorption (NSA), and hence wet mass adsorbed is expected to be high [267].

Due to its reactivity, polystyrene was difficult to work with, however, consistent results were achieved, with at least three sets of reproducible results. This was done by degassing buffers for at least 20 minutes, and rigorous cleaning without stripping the chip of its polystyrene surface.

Peptide adsorption was investigated on specifically designed polystyrene coated chips, in both acidic and basic conditions. Initially, peptides were investigated in acidic conditions, shown in Fig 4.21 below and compared to findings on Au-CH_3 chips.

pH 2.4

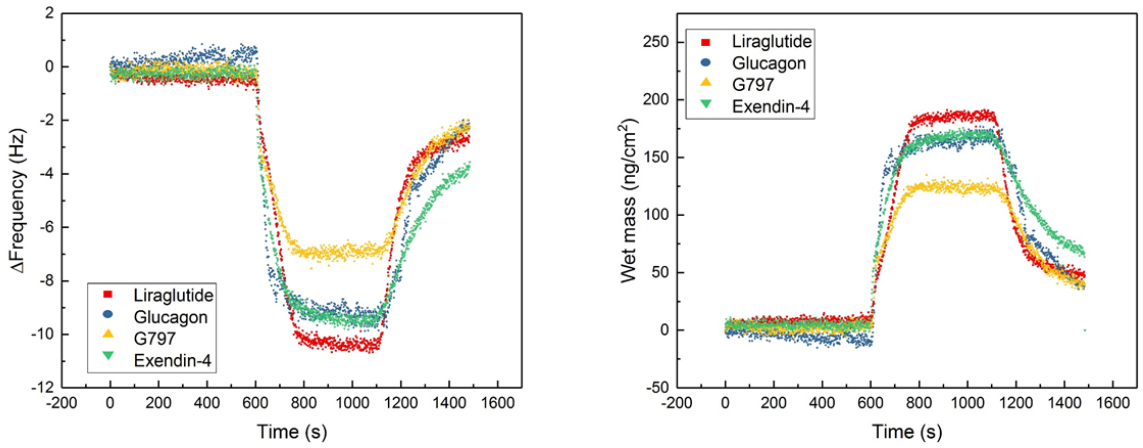

Figure 4.21: Left - QCM-D raw results for glucagon, liraglutide, g797 and exendin-4 adsorption on polystyrene, where change in frequency was plotted against time at pH 2.4. **Right -** Frequency is converted to mass, to give a mass-time graph.

Initially, a few things can be observed from the above figure. Firstly, the difference between individual peptide adsorption is not as large as with Au-CH_3. In addition, the trend of lipidated vs non lipidated peptide adsorption is also no longer valid. The difference between liraglutide, glucagon and exendin-4 is small. The only large outlier is g797 which adsorbs less than the other peptides. These results are not similar to those seen on the previous hydrophobic surface. Both lipidated peptides should be adsorbing more than non lipidated peptides due to the strong hydrophobic interactions. Yet, liraglutide adsorbs significantly more than g797, and so do both glucagon and exendin-4, as previously stated. Exendin-4 adsorption is similar to that seen on Au-CH_3, which could be due to similar interactions at play. G797 could be rearranging onto the polystyrene surface differently so that its hydrophobic chain is no longer in contact with the surface.

The desorption data is also helpful and shows that none of the peptides show strong interactions with the hydrophobic surface. This data is also different to that of Au-CH_3, where only glucagon desorbed significantly from the surface.

With the interesting findings on polystyrene, the experiment was repeated four times, with Fig 4.22 below showing the average of the repeats preformed.

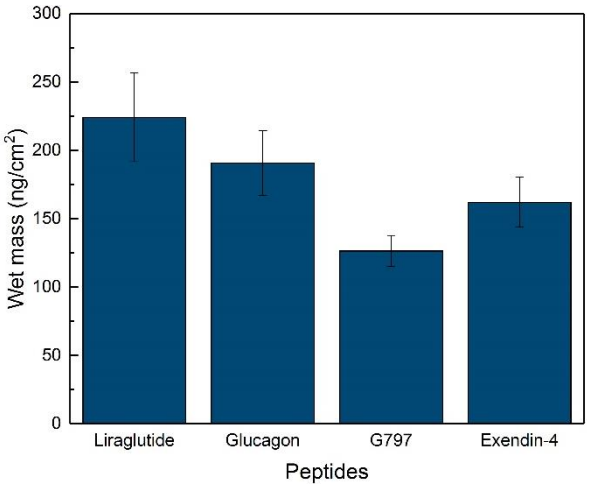

Figure 4.22: The average wet mass of peptides adsorbed in acidic conditions on PS. The error bars indicate the standard deviation between four consecutive repeats.

One of the primary observations is that the errors for liraglutide and glucagon are quite large. As previously described, polystyrene is difficult to work with, and results were averages of four repeats for accuracy. The easily identifiable trend seen for Au-CH_3 is not as clear cut on polystyrene. Liraglutide is seen to adsorb the most, even with a large standard deviation, followed closely by glucagon. There is no pattern in regards to lipidated vs non lipidated peptides, which is surprising, especially considering how hydrophobic the surface is. Compared to Au-CH_3 surfaces, which are also hydrophobic, all peptides adsorb significantly more on polystyrene surfaces. This is anticipated, as polystyrene has the capacity of carrying a charge easily [285]. Therefore, when discussing polystyrene, it is predicted that a surface which is both hydrophobic and charged will be ideal for peptide adsorption to the interfacial surface, and could explain the difference in adsorptive patterns, and the general high masses for all peptides. On neutral hydrophobic surfaces, the peptides able to form more hydrophobic interactions with the surface show a higher tendency to adsorb. Whilst on a charged hydrophobic surface, the distinction isn't as clear, and a

peptide like glucagon, which can carry a large overall positive charge, especially in acidic conditions, can adsorb extensively based on electrostatic interactions.

Following the results from acidic conditions, experiments were also done in basic conditions in order to investigate whether the peptides will show similar trends as on Au-CH_3. The results from the experiments on polystyrene in basic conditions are shown in Fig 4.23 below.

pH 10.8

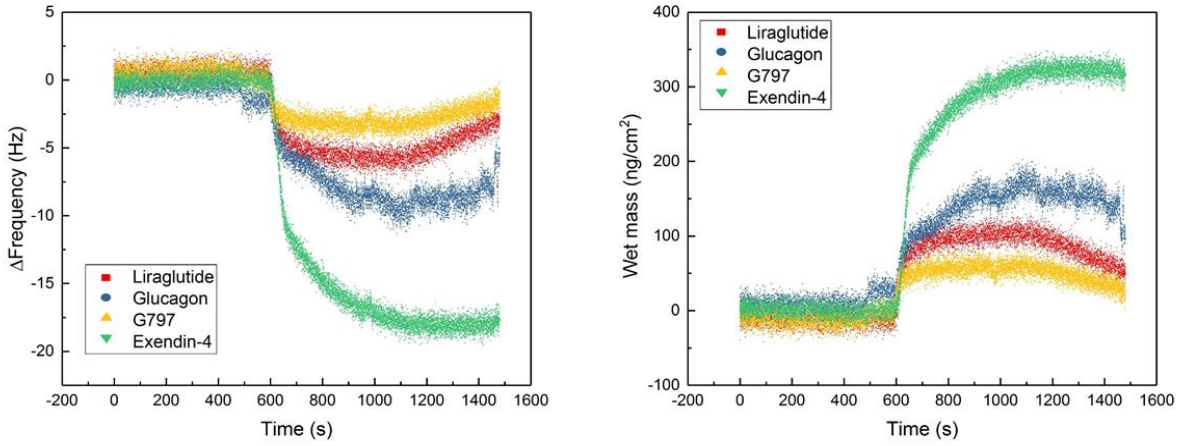

Figure 4.23: Left - QCM-D raw results for glucagon, liraglutide, g797 and exendin-4 adsorption on polystyrene, where change in frequency was plotted against time at pH 10.8. **Right** - Frequency is converted to mass, to give a mass-time graph.

From Fig 4.23 above, it can be seen that there is a significant difference in the mass adsorbed compared to in acidic conditions on the same surface. Result are very similar to Au-CH_3 in basic conditions, with glucagon and exendin-4 adsorbing more (almost 150 ng/cm^2) than g797 and liraglutide. Exendin-4 adsorbs more than all other peptides, due to its favourable unfolding and hydrophobic interactions on the surface in these conditions. The results indicate a clear link between anionic non lipidated peptides and their willingness to adsorb to hydrophobic surfaces. This pattern of adsorption is almost exactly opposite to the adsorption pattern on hydrophilic surfaces in basic conditions, where the lipidated peptides were more likely to adsorb, especially g797.

However, unlike Au-CH_3, the interaction between the polystyrene surface and the peptides is strong – with less mass desorption (m_d) after buffer has been flown through. This suggests the adsorption in basic solution may be irreversible for some peptides, pointing to potentially different interactions at play, and stronger bonding. In some scenarios, when an amphiphilic peptide is adsorbed on a hydrophobic surface, the unfolding of the aggregate structures can be stabilized by strong newly formed hydrophobic interactions resulting from adsorption onto the polystyrene, much like exendin-4. Such a hydrophobic driven adsorption would reduce the interfacial energy by exposing the hydrophobic residues of the interior peptide to the hydrophobic surface [289]. Liraglutide and g797 show some decrease in mass, which indicates that the two lipidated peptides were bound reversibly, as is concurrent with the results found on the Au-CH_3 surface.

Additionally, when both factors such as hydrophobic interactions and charge interactions are added together, this could form strong interactions that is a difficult barrier to overcome. The average of the results are displayed in Fig 4.24 below.

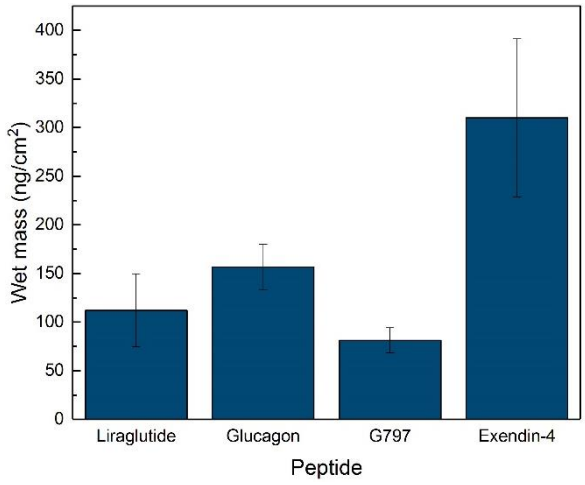

Figure 4.24: The average wet mass of peptides adsorbed in basic conditions on PS. The error bars indicate the standard deviation between the three consecutive repeats.

From the data above, it can be seen that both charge, as well as hydrophobicity play a part in the adsorption of amphiphilic peptides to the interface. If hydrophobicity was the only factor affecting adsorption, the pH of the solution would have negligible effect on the peptide adsorption to the surface, and vice versa for charge. Additionally, the lipidated peptides should show overwhelmingly different results to the non lipidated peptides, which was also not always the case. However, as both the amount of wet mass adsorbed, as well as the trends which are different, indicate a more complicated and less easily definable relationship. This is summed up in Table 4.6 below, where both conditions and the respective wet mass adsorbed on polystyrene is displayed.

Table 4.6: Summation table of all peptide adsorption in ng/cm^2 on polystyrene in both acidic and basic conditions.

	Liraglutide	Glucagon	G797	Exendin-4
pH 2.4 (+ charge)	224.0 ± 32.4	190.7 ± 23.7	126.4 ± 11.3	162.1 ± 18.2
pH 10.8 (- charge)	112.0 ± 37.6	156.3 ± 23.5	81.2 ± 12.9	310.1 ± 81.2

From the above table, some interesting findings can be seen. Firstly, glucagon shows only 50 ng/cm^2 difference in its adsorption to both surfaces, which is half of its difference compared to its adsorption on Au-CH_3. In addition, glucagon showed larger mass adsorption in basic conditions previously. Exendin-4 showed consistent results from both polystyrene and Au-CH_3 surface, both which displayed higher adsorbed masses in basic conditions. Lipidated peptides do not show consistent results on PS compared to Au-CH_3. Both liraglutide and g797 adsorb significantly more in acidic conditions, which was not observed previously. G797 shows low mass adsorption in basic conditions, and liraglutide shows very high mass adsorption in acidic conditions. However, the overall mass adsorbed for liraglutide in basic conditions, and g797 in acidic conditions

is very similar to the masses seen on Au-CH_3. Hence, even though initially the trends differ, the wet mass adsorbed for the peptides is similar in some conditions on hydrophobic surfaces.

4.4 Conclusion

All four peptides; glucagon, liraglutide, g797 and exendin-4 have been investigated on neutral hydrophilic, charged hydrophilic, neutral hydrophobic and charged hydrophobic surfaces. From this, more information was gleamed about the interactions and the factors affecting surface enhanced aggregation.

From the data above, it can be seen that there were some overall trends; adsorption was lowest for neutral hydrophilic substrates, and highest for both polystyrene and glass, the two most common surfaces that peptides will interact with, and two of the surfaces that are known to enhance NSA [115], [290]. In some instances, there were clear patterns such as lipidated vs non lipidated peptides, yet this is not always the case, especially when electrostatic interactions, van der Waals and hydrophobic interactions and individual amino acid residues are all taken into account. The overall trends were based on the amino acid sequence of each peptide, and individual amino acid or lipid chain behaviour. Hence, some trends could be established, but the complexity of peptides is difficult to predict, even with concrete principles of adsorption. As concentration and time were kept constant, the experiments were set up to see initial adsorption, and not diffusion controlled or concentration controlled adsorption.

The conclusions of the findings were summarised for each individual peptide below, in Fig 4.25 – Fig 4.28. Liraglutide will be commented on first, followed by glucagon, g797 and finally exendin-4. For each peptide, a wet mass summation graph of hydrophilic and hydrophobic surfaces is shown.

4.4.1 Liraglutide

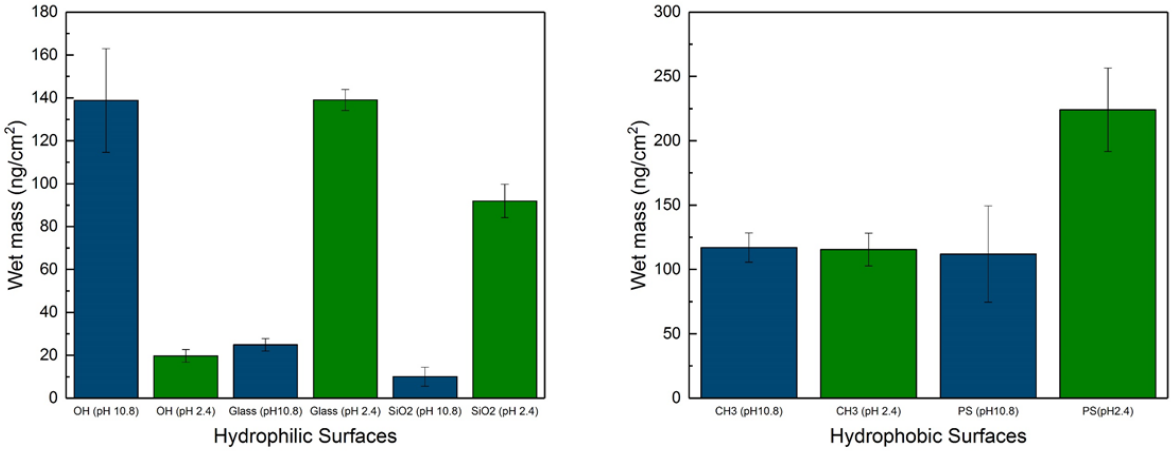

Figure 4.25: The summation of liraglutide adsorption for different surfaces, in ng/cm^2. From the graph, it is clear that in acidic conditions, on polystyrene surface, liraglutide will adsorb the most.

From the above figure, a few things can be noted. Liraglutide adsorbs the most to polystyrene in acidic conditions, when the peptide is positively charged. When liraglutide is in acidic conditions, it will carry a large positive charge. In addition to its large hydrophobic additional side chain, and its large charge, it's unsurprising that liraglutide shows high affinity for the polystyrene surface in these conditions. In basic conditions, liraglutide will form wormlike micelles, which means that even though unfavourable with its large lipid chain, it can still adsorb to hydrophilic surfaces when in basic conditions due to the partial internal stabilisation of shielding hydrophobic moieties.

There is trend of surfaces to avoid, which for liraglutide, are hydrophobic surfaces. Apart from polystyrene in acidic conditions, all other hydrophobic surfaces in differing conditions show almost identical wet mass adsorption. In addition, the Au-OH surface is a significant outlier, as liraglutide shows a large mass adsorption to Au – OH in basic conditions, which can be attributed to the charge of the peptide.

4.4.2 Glucagon

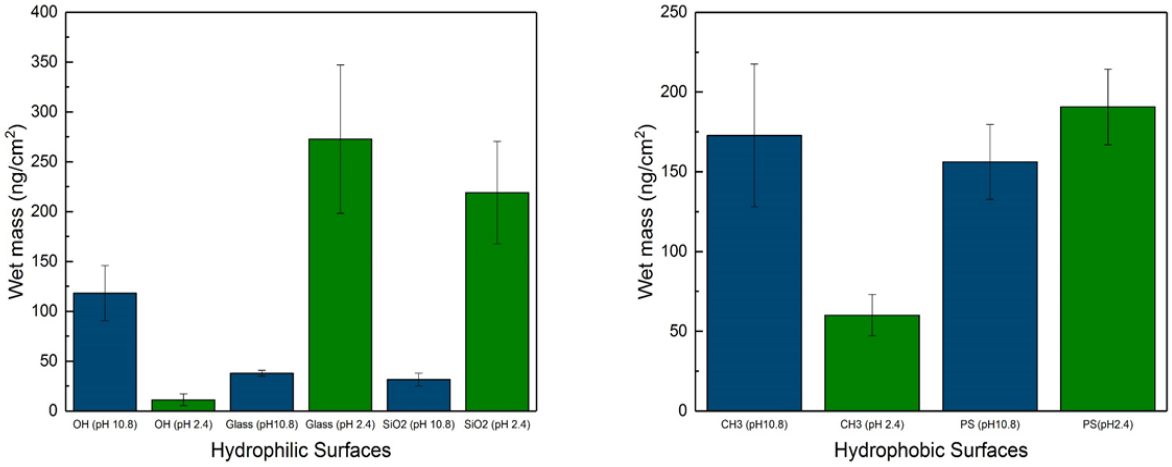

Figure 4.26: The summation of glucagon adsorption for different surfaces, in ng/cm². From the graph, it can be seen that glucagon adsorbs most on both glass and polystyrene.

Glucagon, which is essential for the body and for treatment of T2DM, adsorbs the most to both glass and polystyrene in acidic conditions.

From Fig 4.26 above, at a pH of 2.4 and a pH of 10.8, glucagon will be highly charged, and from the literature and studies done in Chapter 3, is known to aggregate. A general trend emerges, where glucagon adsorbs most on hydrophilic surfaces when positively charged, due to electrostatic interactions with the negatively charged surface. On hydrophobic surfaces, the adsorption pattern isn't as clear cut. Glucagon's high mass adsorption on polystyrene in both acidic and basic conditions is likely to be hydrophobically driven, as PS is a well-known surface which enhances NSA.

The one exception in OH surfaces, in which it adsorbs significantly more when negatively charged, even though the surface is hydrophilic and neutral.

Therefore, for glucagon, its reactivity in solution is very much mirrored on the surface, and the solution conditions have a direct effect on the surface induced aggregation.

4.4.3 G797

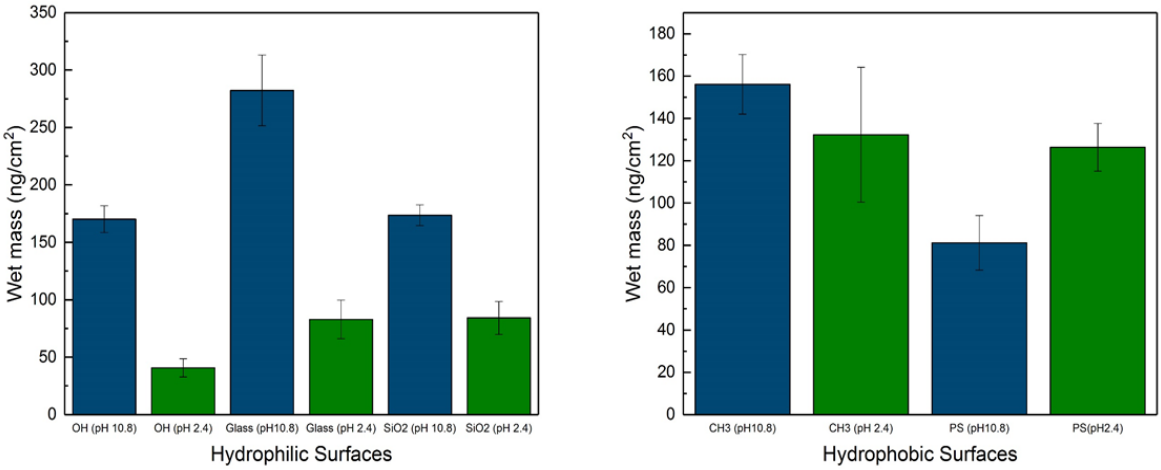

Figure 4.27: The summation of g797 adsorption for different surfaces, in ng/cm^2. G797 adsorbs most on glass in basic conditions.

For G797 we have seen that it can form different higher order structures, ranging from tightly packed fibrils to micelles, and this is very much replicated in results in this chapter.

From Fig 4.27 above, a general trend much like glucagon but mirrored emerges. G797 has a tendency to show high mass adsorption to hydrophilic surfaces in conditions in which it forms micelles and is negatively charged. As the micelles shield away the hydrophobic parts of the peptide, the hydrophilic parts of the peptide will be able to adsorb. This trend was shown on all hydrophilic surfaces, including Au-OH. G797 also absorbs to hydrophobic surfaces, where charge has less of an effect, and overall adsorption is higher than for hydrophilic surfaces due to its lipid chain, on both Au-CH_3 and PS alike.

From the figure above, g797 shows large adsorption to the two most commonly used surfaces in the industry; borosilicate glass and polystyrene.

4.4.4 Exendin-4

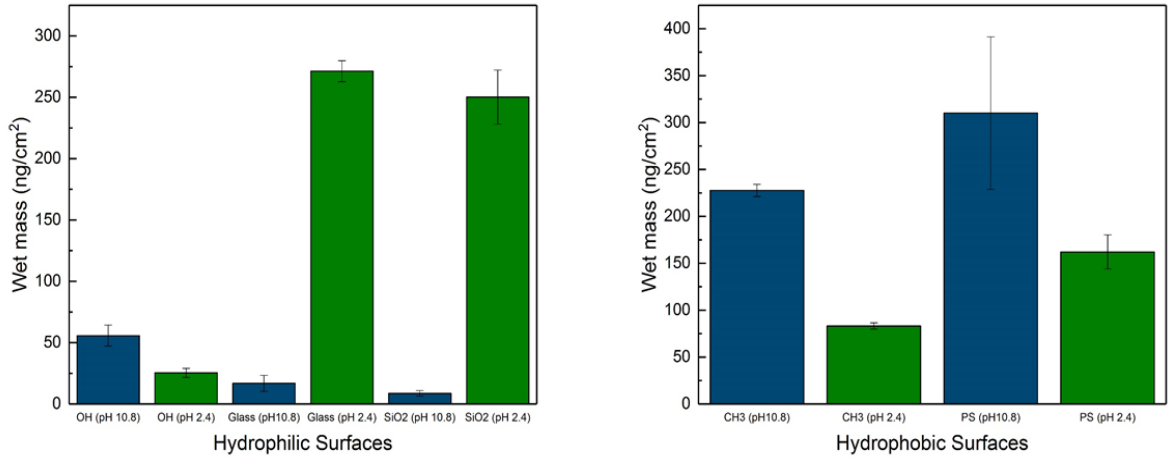

Figure 4.28: The summation of exendin-4 adsorption for different surfaces, in ng/cm^2. Exendin-4 shows large adsorption to hydrophobic surfaces in basic conditions, and hydrophilic in acidic conditions.

Exendin-4, the most stable of the therapeutic peptides under investigation in solution, shows the largest wet mass adsorption of all the peptides on polystyrene in basic conditions due to its unfolding of its stable Trp cage on hydrophobic surfaces, exposing its hydrophobic residues previously held inside the stable cage. The Trp cage only does this on hydrophobic surfaces, and when protonated, the Trp cage remains semi unfolded, which can be seen from the trends on hydrophobic surfaces displayed in Fig 4.28 above.

However, all peptides show a high NSA to polystyrene, and to glass, which were the two highest adsorption peaks for exendin-4. On charged hydrophilic surfaces, the peptide shows higher mass adsorption when positively charged. When carrying a positive charge, the Trp cage is protonated, and semi-folded, hence forming electrostatic interactions with the surface, and the hydrophilic surface does not promote unfolding.

This trend is no longer valid when the looking at Au-OH surface, the uncharged hydrophilic surface, which impedes peptide adsorption.

Although peptide adsorption to surfaces is complex and a number of different factors regarding both bulk solution conditions and interface conditions have to be accounted for, there are some general principles than can be applied to either enhance or prevent surface induced aggregation. Firstly, in general, non - lipidated peptides have adsorption patterns which are more charge driven; when they are positively charged, they adsorb well to negatively charged surfaces and vice versa. Additionally, all peptides show high non-specific adsorption to both plastic and borosilicate glass, which is congruent with the literature [286][114].

The peptides with the additional lipid chain show a very different trend. Lipidation seemingly makes them less susceptible to electrostatic interactions, possibly due to shielding by the added lipid chain, or due to the added hydrophobicity of the chain which will have a larger effect on the adsorption. In addition, lipidated peptides are difficult to compare, as both liraglutide and g797 do act differently on a number of surfaces, such as glass and Au-OH in basic conditions, when they both carry an overall negative charge. This is due to the different structures they form in solution, shown in Chapter 3, and hence the different structures they are likely to form on solid surfaces.

From the results presented above, broad principles of adsorption can be used in order to determine aggregation at the interface. However, keeping amino acid sequence, charges, van der Waals interactions and hydrophobicity in mind is crucial to being able to predict their surface induced aggregation, which is complicated and unpredictable.

Both glass and polystyrene, which are the two most common surfaces that therapeutic peptides will interact with in their lifecycle, are well known to enhance NSA, and hence should not be used as widely as it is in the pharmaceutical industry. Instead, hydrophilic uncharged surfaces, such as functionalised OH, seemed to reduce to adsorption of peptides to the surface, especially in the right conditions.

This chapter has tackled adsorption depending on surface hydrophobicity and charge interactions of the surface and the peptide. The previous chapter tackled peptide structures and secondary structures formed in solution, and the next chapter will assess different methods of changing surface roughness, and the impact of changing surface area to volume ratio on aggregation.

5 Chapter

An investigation into fabrication and application of rough surfaces on peptide adsorption.

The two previous results chapters tackled the bulk solution conditions pertaining to peptide aggregation and surface induced aggregation through adsorption to a variety of different surfaces. Chapter 3 focused on peptide stability in solution, and its dependency on both pH and concentration. Chapter 4 meanwhile, focused on surface induced aggregation, by looking at adsorption of peptides to different surfaces, and how surface hydrophobicity and/or charge has an effect on the amount of peptide adsorbed.

From this, we have gathered data on peptide stability in solution, and how to reduce or enhance surface induced aggregation. The next stage is to look at how surface roughness can affect surface induced aggregation, using the quartz crystal microbalance with dissipation and the atomic force microscope.

This chapter tackles two distinct ways of changing surface topography. The first, through the addition of nanoparticles to the surface, to increase the surface area to volume ratio. The second is to use E- beam lithography to fabricate surfaces with tailored roughness, by creating features ranging from 50 nm to 1 μm.

5.1 Introduction

The adsorption of nanoscale materials to solid surfaces has always been of interest for a broad range of applications ranging from biomedical implants, drug delivery and biosensors [291]–[293]. In relation to this thesis, the interface is crucial to understand aggregation of therapeutic peptides, as surfaces can cause surface induced aggregation, leading to loss of viable drug, as well as toxicity [294].

Having investigated common areas which affect peptide adsorption to surfaces, such as polarity and hydrophobicity, this chapter addresses a more intricate factor, surface roughness.

On biomaterials, for example, increased roughness has been shown to increase cell proliferation, decreasing the chance of rejection of the implant [295][296]. However, the research on roughness in the pharmaceutical industry is lacking in depth analysis and clarity. Moreover, due to the overwhelming evidence that rougher surface increase adsorption of proteins [297][298] and cells [299], the opposing argument is underexplored. There have been some studies that look at roughness and its effect on surface diffusion. For example, Schwartz et al found that rougher nanoscale topography could obstruct surface diffusion of small polymers, creating a physical barrier that small molecules cannot overcome [142]. Surfaces that show slight roughness decelerate the diffusion and therefore slow down the adsorption process, whilst very rough surfaces have been documented to stop the diffusion altogether [143]. In addition to adsorption, surface roughness has been demonstrated to change peptide confirmation in certain cases [300].

A recent study on C60 fullerenes has shown that the highly curved surface enhances enzyme and peptide stability in strongly denaturing environments (such as very low pH's seen in this report). Additionally, it compares the

stabilisation to flat surfaces, and found that the highly curved surfaces stabilised the enzyme and peptides to a much greater extent than the flat surfaces did [144]. Analogous results have been established with other nanoparticles such as silica and gold nanoparticles. The capacity to enhance protein stability by interfacing them with nanoparticles, and quantum dots, could impact a range of fields; from diagnostics to sensors and drug delivery.

However, more often than not, it has been found that surface roughness destabilises the peptide confirmation. Fibrinogen has been shown to alter its conformation when adsorbing to titanium nanopits of 40 nm in diameter [301]. Nanoparticles have been shown to enhance the local concentration of peptides, and hence the peptides form more beta sheets, which stabilises their structure [302]. A very different set of results was found when Denis et al tested protein adsorption to both flat hydrophilic and hydrophobic surfaces and rough hydrophilic and hydrophobic surfaces. Collagen formed the same size layer on both rough and flat surfaces, but no longer formed aggregate structures on rough surfaces, as it did on smooth [303]. Song et al compared the adsorption of Arg-Gly-Asp (RGD) peptide to a perfect crystalline structure of TiO_2, and one which contained nano pits. The rougher surface showed both faster adsorption of the peptide to the nano topographical surface and difference in structure formation of the RGD peptide compared to on the crystalline TiO_2 [304].

From the literature, it is evident that surface roughness and peptide adsorption is an area of interfacial science where there are still many unknowns, where the speed and shape of the product are determined by so many different combined factors that they become very difficult to predict. Surface topography is therefore a vital topic to explore in this chapter.

5.2 Materials and Methods

5.2.1 Peptide solutions

Hydrochloric acid buffer solution (0.05 M, pH 2.4) was prepared using hydrochloric acid (37%), glycine (>95%) and HPLC water (resistivity > 18 MΩ). Filtered (pore size = 0.22 μm) peptide stock solutions glucagon (3.48 KDa) and liraglutide (3.75 KDa) were prepared at a concentration of 2.5 mg/mL. The concentration of the peptide solutions was checked by UV-Vis spectroscopy (Varian Cary® 300 UV-Vis Spectrophotometer, Agilent Technologies, UK) at 280 nm.

Peptides were made in acidic conditions due to isoelectric points being low, resulting in an overall positive charge.

5.2.2 Deposition of 40 nm Au-NPs on QSX 301 gold QCM-D chip

The NPs were purchased from Innova Biosciences as InnovaCoat gold NPs of 40 nm diameter and a concentration of 10 optical density. These nanoparticles have a proprietary coating functionalised with carboxyl end groups.

The protocol used for this experiment is based on the work by Fredriksson et al with minor modifications [305].

Au NPs were deposited on the QCM-D electrode in a stepwise reaction. Firstly, 2% of polydiallyldimethylammonium chloride (PDDA) was drop cast on the QSX 301 sensor chip, and rinsed 5 mins later with DI water and dried. A colloidal solution of Au NPs was then deposited on top of the electrode for 2 hours to reach full saturation. After incubation, the electrode was rinsed thoroughly with water, and dried with nitrogen. The electrode chip was then treated with O_2 plasma, for up to 7 s (Diener, O_2 plasma, 100% power, 0.8 mBar). Modified RCA1 solution was then used to clean the sample for 10 - 15 seconds.

Deposition of Au-NP's was confirmed using the AFM before and after each experiment.

5.2.3 Roughness measurements and imaging using Atomic Force Microscopy

A PicoPlusTM AFM (Molecular Imaging) with a PicoSPMII controller was used in tapping mode. The AFM probes (HQ:NSC36/No Al (MikroMasch®, via Windsor Scientific LTD, UK) had a tip radius < 8 nm and force constants between 0.6 and 2.0 N/m. The scanning rate was 0.6 - 0.9 lines per second (depending on the sample) and a maximum imaging area of 9 x 9 μm (for closer detailed images, 3 x 3 μm size was used) and resolutions of 512 x 512 or 1024 x 1024 pixels.

Gwyddion imaging software was used to extract the mean average roughness of the surfaces, as well as image the surfaces. The surfaces were imaged before and after experiments, in order to assess whether nanoparticles did adhere to the surface even after experimentation and thorough cleaning.

5.2.4 Measuring adsorbed mass using QCM-D

Diluted Hellmanex® (Hellma Analytics, Germany) solution (2% in deionised water) was used to clean the QCM-D tubing. Gold surfaces were cleaned as previously discussed in Chapter 4, Section 4.2.2.

All QCM-D measurements were repeated a minimum of three times on both QSX 301 and QSX 301-NP sensor chips.

5.2.5 E- beam lithography

Electron-beam lithography technique used a focused beam of electrons on a surface to create nano and micro sized structures. Nano structures are created using an electron-sensitive resist, poly methyl methacrylate (PMMA, 950K). When the e-beam resist is exposed by an electron beam, its long chain molecules

are divided into shorter chains, which are easily dissolved in the developer. Features as small as 4 nm can be created using e-beam lithography [306].

Nanopatterned surfaces of the gold QCM-D chip discussed in this chapter were created using e-beam lithography. The e-beam experiments were performed by Dr Atif Aziz, as I was not trained in using the e-beam lithography system.

Before patterning, QCM-D chips was cleaned in order to avoid contamination by dust and other small particles, and the protocol is described in Section 5.2.4.

After cleaning of the chips, the PMMA resist, which had a concentration of 2 wt% in anisole solvent was spin coated on the QCM-D chip at 3000 rpm for 60 seconds. Once the sample was coated, the resist was baked at 200 °C for 5 minutes.

The sample was then exposed to the EBL, using a current of 100 pA and a dose of 500 $\mu C/cm^2$. The sample was developed with DI water-IPA (7:3 volume ratio) developer by immersing it in the solution for one minute. It was then dried with N_2 gun.

5.2.6 Imaging of E-beam surfaces using Ion Microscopy

A Zeiss Orion Nanofab was used to image E-beam lithographic surfaces due to a faulty AFM. James McCleod, a trained technician, was very helpful and aided with the imaging.

The beam current used by the helium ion was 2.4 pA for each individual image (± 0.2 pA), with a scan dwell time of 100 μs and a field of view of 225 μm.

5.3 Results

This results chapter comprises of two sections. The first is the increase of surface roughness through the addition of gold nanoparticles to the surface. A protocol for this was made, tested, and experiments were performed on the surface. The second section tackles the creation of rougher surfaces through E-beam lithography, as a proof of concept study.

5.3.1 Deposition & Characterisation of Gold NP surface

Gold nanoparticles (40 nm) were deposited onto the gold QCM-D chip. The protocol was based on colloidal techniques. A droplet of colloidal solution containing the nanoparticles is placed on top of a surface of opposite charge. The nanoparticles attach to the surface through electrostatic interactions, and their density can be controlled by changing the particle-particle interaction, which can be done by adding salt to the colloidal solution. Once the nanoparticles have been deposited, they are used as a mask for the subsequent evaporation step [307]. The depositing was confirmed using the Atomic Force Microscopy (AFM). The AFM also obtained the diameter of individual NPs, by extracting the maximum height of each nanoparticle, and assuming they are a perfect sphere and the surface is flat, as shown in Fig 5.1 below.

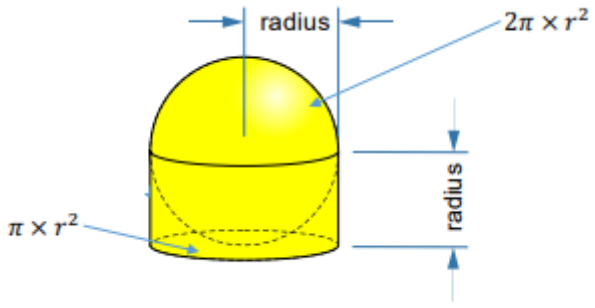

Figure 5.1: A diagram displaying a nanoparticle analysed on the surface. From this figure, an equation was constructed to predict surface area to volume increase after addition of the nanoparticle, by Dr J. A, Rubio. Image used with permission from his thesis.

The AFM was used to image gold QCM-D surfaces before and after the addition of nanoparticles, which had previously been characterised using the DLS. Below in Fig 5.2, is the surface of the gold QCM-D chip before and after addition of nanoparticles, done by the protocol described in Section 5.2.2

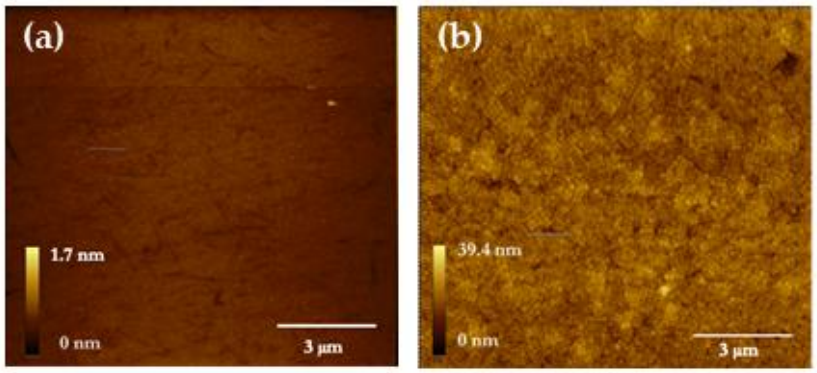

Figure 5.2: (a) AFM image of flat gold sensor surface, QSX 301. Images were 9 µm x 9 µm in size, scanning rate 0.84 lines per second and at a resolution of 512 x 512 pixels. (b) Gold QCM-D chip coated in gold nanoparticles.

From the figure above, it can be seen that the surface roughness has increased to almost 40 nm, in comparison to a little over 1 nm in image (a), the flat gold QSX 301 chip. This result is reproducible; at least three different quadrants of the sample were observed, and the average roughness went from 1.2 ± 0.62 nm to 37.8 nm ± 3.4 nm after the addition of nanoparticles.

From the figure above, it can be seen that the roughness changes, as does the surface. However, individual gold nanoparticles are hard to distinguish, and hence Fig 5.3 below gives a zoomed in perspective of the surface showing the nanoparticle's spherical shapes and their dispersity on the surface. Individual nanoparticles diameter could be measured from the AFM images, and these were used to examine the size of nanoparticles further.

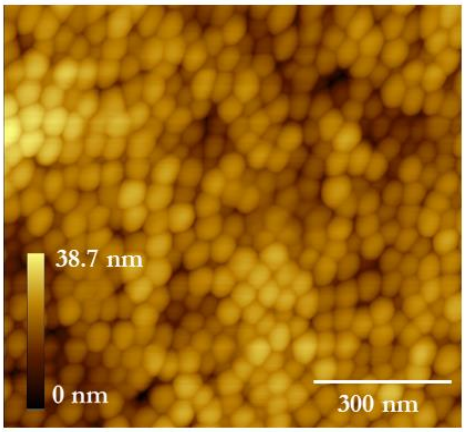

Figure 5.3: Gold QCM-D chip coated in gold nanoparticles, a close up using the AFM. Images were 3 μm x 3 μm in size, scanning rate 0.84 lines per second and at a resolution of 512 x 512 pixels, and edited and analysed in Gwyddion software.

Due to the electrostatic interaction of the positive charge of PMMA, and the negative charge of the carboxyl end group on the Au NPs the nanoparticles adhere to the surface in a relatively structured order.

The AFM was used to determine that the Au-NP particles were between 35 - 39 nm in size, which is compatible with the data from DLS (not shown). The therapeutic peptides used in this study, glucagon and liraglutide, were small in size. In monomeric form the peptides were between 1-2 nm in diameter, and hence the nanoparticle surface created was very rough in comparison to the peptide sizes. However, peptide solutions are made up of monomers, aggregates and fibrils according to solution conditions. As the experiments were done in acidic conditions, using high concentrations (2.5 mg/mL), it's expected that the samples will be a delicate balance of monomer and higher order structures like fibrils and some other aggregates, as investigated in Chapter 3. Initially, one of the ideas was to image the peptides on the nanoparticle surface to see their structure, and whether it had changed compared to on the flat gold surface. However, the peptides were too small in size, so only the nanoparticles on the surface could be seen. As the experiments were performed in a narrow time

frame, in which nucleation of the fibrils will not yet have been complete, as full fibril coverage takes up to 18 hours. Hence, the assumption that the solutions of peptides will contain monomers and small aggregates is maintained. Unfunctionalized gold QCM-D sensor chips were less than 1 nm roughness, and comparable to the size of the monomeric peptide.

Below, in Fig 5.4, are the measurements of the gold nanoparticles diameter, in nm, compared to the gold sensor chip, supplied by Q sense (QSX 301)

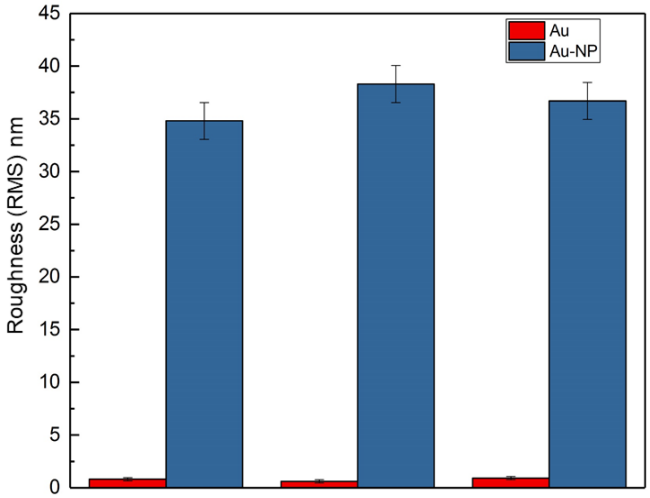

Figure 5.4: Roughness measurements of Gold QSX301 chips, and of QSX301 chips with gold nanoparticles, and their standard deviation as error bars.

The roughness measurements were taken by the AFM, on three different samples, and three measurements per sample. The roughness was taken to be the RMS value, the average roughness. The error bars represent the standard deviation of all the measurements. There is a clear difference in roughness, with the roughness of the gold nanoparticles ranging from between 35 nm – 39 nm. The standard deviation is low, indicating a reproducible technique.

From the data above, through AFM measurements and imaging, the surface addition of nanoparticles to a gold QCM-D chip was successful. The subsequent stage was to identify whether the nanoparticle surfaces could be used during an experiment.

Therefore, an essential part of the newly created NP surface, was to ascertain whether the nanoparticles stay adhered to the surface during the experiment. The premise of the newly formed surface is that the nanoparticle carboxyl group and the PMMA form strong electrostatic interactions. However, the nanoparticles might form stronger interactions with the peptides than with the surface. In order to investigate this avenue, the nanoparticle surface was imaged using the AFM before and after a preformed QCM-D experiment in order to determine consistency of the nanoparticle surface, displayed in Fig 5.5 below.

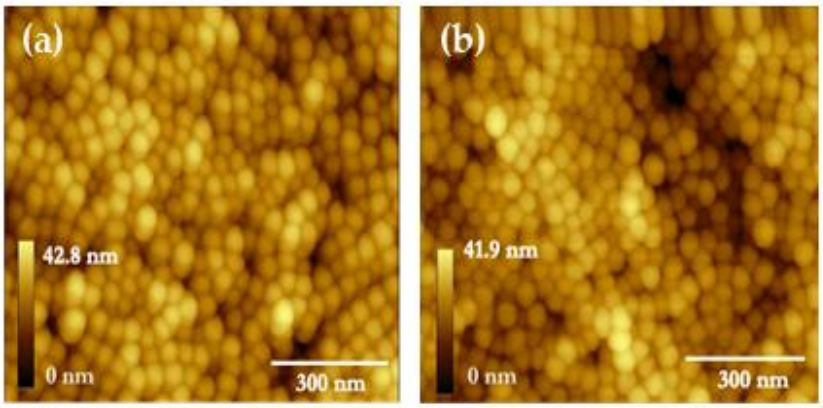

Figure 5.5: (a) The image of the nanoparticle surface taken before a QCM-D adsorption experiment. (b) Image of the nanoparticle surface after a QCM-D adsorption experiment and after a subsequent washing step. Images were 1 μm x 1 μm in size, scanning rate 0.84 lines per second and at a resolution of 512 x 512 pixels, and edited in Gwyddion software.

From Fig 5.5 above it can be seen that the nanoparticles adhere to the surface strongly, and do not desorb and/or form stronger bonds with the therapeutic peptides during the experiment. The structure of the particles are identical, as are their measurements. Additionally, the average mean surface roughness (RMS) was taken before and after the experiment. The average roughness difference between the Au-NP surface before and after the experiment was 2.3 ± 0.7 nm.

After establishing that the Au-NP surfaces were stable and showed no signs of desorption or aggregation of nanoparticles, experiments were performed using flat gold and Au-NP surfaces to investigate the amount of wet mass of therapeutic peptides adsorbed to both surfaces, and to see the effect of roughness on adsorption of peptides.

5.3.2 Glucagon and Liraglutide adsorption to Au and Au-NP surfaces

Adsorption of both glucagon, and lipidated peptide liraglutide, was performed on both gold QCM-D chips and gold nanoparticle QCM-D chips, which were discussed in the previous section.

This section will tackle the difference in mass adsorption between both flat (< 1nm) surfaces and rough (40 nm) surfaces, as well as the variations in adsorption between a non-lipidated peptide and a lipidated peptide.

Here, the increased surface area to volume ratio of the nanoparticle surface is expected to increase the wet mass of peptides adsorbed. From a model derivation done by Dr Juan Lara Rubio (derivation shown in Appendix), if the nanoparticle is larger than two times the size of the peptide, the area increased was calculated to be 2.3 times increase in wet mass adsorption, which could account for the increase in surface area to volume ratio.

Using the QCM-D, adsorption studies were done on both flat gold QCM-D sensors and gold-NP sensors, with Fig 5.6 below showing the results.

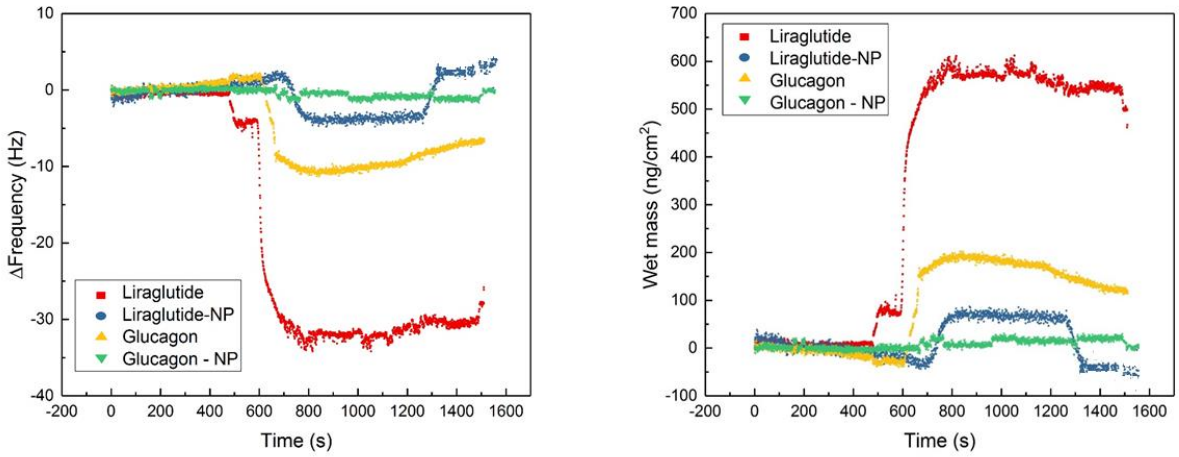

Figure 5.6: Left – Adsorption of glucagon and liraglutide on gold and gold-NP surfaces using QCM-D. The figure shows a large frequency shift for both peptides on flat gold compared to gold nanoparticles. **Right –** The adsorption of the peptides with reference to wet mass vs time, showing relative masses of peptide adsorbed on each surface during a specific time frame.

The above figure shows unexpected results. From Fig 5.6, liraglutide and glucagon adsorb significantly more on gold chips with less than 1 nm roughness, compared to rough gold of 40 nm roughness. As the peptides themselves in monolayer format are very small (even when aggregated or fibrillated, which is likely in highly acidic conditions), the size of the nanoparticles might be too large a barrier to cross and hence prevent the peptides from surface diffusion [141]. In order to verify these results, the experimental procedure was repeated three times, with consistent results. There is a small dip at the end for liraglutide on the nanoparticle surface, which is suggestive of more coming off than initially adsorbed. However, the surfaces were investigated using the AFM, as previously described, and from the three experiments done with consistent results, only this specific experiment showed this peculiarity. Another difference between the peptide reaction on the different surfaces, is their desorption. Liraglutide desorbs completely on nanoparticles, whilst it shows little desorption on the flat gold surface. In addition, glucagon also shows almost no desorption from the flat gold surface, insinuating that the bonds formed between the flat gold surface and the peptides is strong. In Fig 5.7 below, the average mass of

three repeats was taken, and the standard deviation is represented by the error bars.

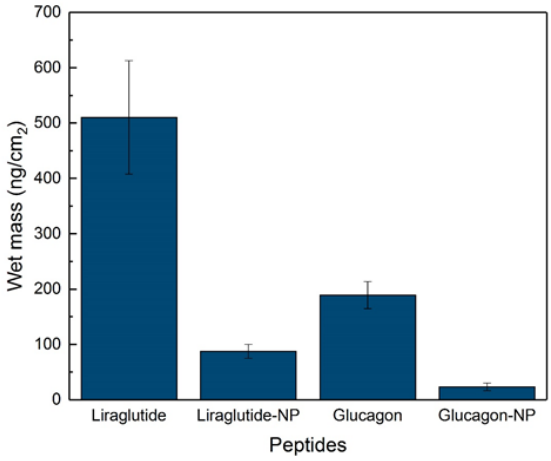

Figure 5.7: Mass summation of three consecutive repeats of glucagon and liraglutide adsorption on gold QCM-D chips and gold-NP QCM-D sensor chips.

The above figure confirms that three consecutive repeats show a stark difference between peptide adsorption on rough and flat gold. The Au-NP surfaces decrease adsorption of both glucagon and liraglutide. Liraglutide shows larger mass adsorption to gold and gold NP compared to glucagon.

The adsorption of both peptides to the gold surfaces will lie in the electrostatic interactions between the surface and the overall positively charged peptides. It should be noted that even on flat gold, peptides adsorb more than on many of the surfaces studied in Chapter 4. This is due to the strong cysteine disulphide bond formed between peptides and gold surfaces, as well as, strong electrostatic interactions due to the highly charged amino acid residues in acidic conditions. Liraglutide shows particularly large mass adsorption, at an average of 500 ng/cm^2. This could be due to its structural rearrangement on gold, providing multiple anchoring points through the lipidated chain [308].

As discussed in Chapter 4, charge plays a significant role in peptide adsorption. The curvature of the surface could make it difficult for the peptides to form attachment points to the surface. Another factor to be explored, which has been previously mentioned, is the size of nanoparticles relative to the peptide size as

previously discussed. As was found by Vertegel in 2004, size of the nanoparticle compared to the peptide or protein will play a large part not just in adsorption but also the structure of the protein on the surface. Here, they explained that the larger the nanoparticle, relative to the protein, the stronger the protein interaction, resulting in more unfolded protein [309]. Change in surface roughness is can be associated with change in peptide structure, and unfolding of the peptide will result in different interactions between the peptide and the surface [310]. This theory is shown diagrammatically in Fig 5.8 below.

Figure 5.8: Diagrammatic representation of a surface with nanoparticles roughly equal to peptide size on the left, and a large nanoparticle, on the right.

From Fig 5.8, it can be seen that on larger NP's, more peptide- peptide interaction due to the dense packing could occur, and hence, the peptides are more likely to form intramolecular bonds. This could indicate that if more peptide-peptide interactions occur, less peptide – surface interactions will occur, and hence, less adsorption. However, due to their high charge in acidic conditions and close packing, repulsive forces will also play a large part in the structure on the surface [302]. As liraglutide has a lipid chain, less peptide – peptide repulsion is expected compared to glucagon, which could account for the difference in adsorption between the two peptides. Yet, the relationship between the roughness of the surface and peptide structure is not always straight forward. For instance, at the edges and corners of gold nanoparticles, the strong Au-S bond density is higher compared to that in the faces because of greater unsaturation of the gold atoms [311]. This means that the peptides that bind to the surface by the Au-S bond at the edges of small gold nanoparticles (5 and 10 nm) can be packed close enough to form an intermolecular H-bond containing β-sheet conformation. With the increase of the size of the NPs, the curvature of the gold atoms at the edges and

corners reduces, which decreases the Au-S bond density and the increase in the intermolecular distance. For gold NP's as large as 40 nm the curvature of the faces is smaller, and the Au-S bond density is relatively comparable to that in the faces [312]. Surface curvature adds more conformational complications into the discussion.

Unlike proteins, peptide do not have set tertiary and quaternary structures. Hence, it can be difficult to investigate the structure formed on the surface. The limits of the AFM are that the nanoparticles are significantly larger, and peptides are too small in comparison to be seen.

However, from the QCM-D, dissipation, or the rigidity of the hydrated layer can also be determined, which can give a suggestion as to the peptide layer formed on the surface of the nanoparticles. Fig 5.9 below shows the dissipation data of both peptides on both gold surfaces (flat gold and gold nanoparticles).

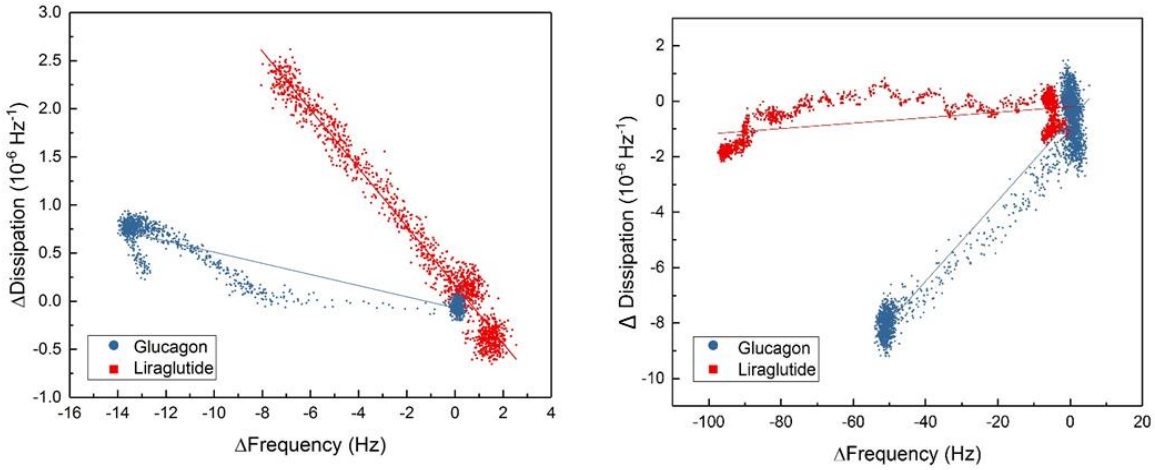

Figure 5.9: Left – Dissipation vs frequency graph of liraglutide and glucagon on the flat gold QCM-D surface. **Right** – Dissipation vs frequency of both peptides on the gold-NP QCM-D surface.

From the figures above, two significant pieces of information can be gathered. Firstly, the dissipation of glucagon and liraglutide is different on flat gold. This

suggests that on flat surfaces, both peptides will form different structures. As liraglutide shows higher dissipation, this suggests it forms a more hydrated, less rigid structure on the surface compared to glucagon. As previously seen in Chapter 3, both peptides will show different aggregate structures in acidic conditions. Glucagon showed very structured and compact fibrils, in an ordered rigid lattice. The fibrils formed by liraglutide were less structured, and formed thicker, unstructured layers, which would dissipate more energy. This is additionally concurrent with the dissipation found in acidic conditions on hydrophilic surfaces for the two peptides, with liraglutide showing higher dissipation than glucagon. Secondly, liraglutide and glucagon show a large difference in dissipation of hydrated layer on the nanoparticles, suggesting different structures are formed on the surface of the nanoparticles too. Glucagon dissipation doesn't increase with decrease in frequency, indicating that the peptide deposited onto the nanoparticle surface is as viscoelastic as the original nanoparticles. Interestingly, liraglutide shows a steady and reproducible decrease in change of dissipation, even though a large increase in mass is seen. This could be explained by a large reorganization of the surface, with liraglutide structures forming a more rigid layer than the original nanoparticle surface or expulsion of water through this reorganisation, as dissipation measures the rigidity of the hydrated layer.

The results gathered from this section indicate that not only is adsorption very specific to structure of surfaces, but there are no set rules on how therapeutic peptides will behave on any given surface. An increase in surface area to volume ratio does not mean that this correlates directly to an increase in mass. Surface curvature also has a large effect on the adsorption of the peptides, and as a result, the next section will look at creating rough surfaces through different means, and how that might impact peptide adsorption.

5.3.3 E- beam lithography for the creation of rough surfaces

The second part of this results chapter investigates e-beam lithography for creating surfaces with high degrees of roughness in a controllable manner.

The roughness of a surface can be changed controllably using different methods. For example, pillars are a common structure made to create a rougher surface through CVD sputtering, whilst holes can be made using E-beam lithography [313]. Most wet chemistry techniques are able to make nanoparticle spheres, such as spheres for the nanoparticle functionalized surfaces described above. Each of these methods will change the surface roughness, but will also have a different shape defect which will also have an effect on the adsorption of the therapeutic peptides. Different shapes of defects will allow for different parts of the peptide to adsorb to the surface, leading to different secondary structures on the surface once adsorbed [314][315]. The peptides will rearrange themselves to 'fit' into the defect, and hence different structures are formed. In addition to the shape of the created defect, size of the defects will also play a significant role in adsorption of the peptides, as previously mentioned.

The measure of roughness most commonly used, is the root mean square (RMS) roughness, which was used in Section 5.3.1 when describing the nanoparticle surface roughness. However, as there is no strict definition of how to measure change in roughness, the parameters themselves are relatively grey. For cell studies, surface gradients are used [316], whilst for physical studies R_a (average roughness) or RMS (root mean square roughness) are the most common.

The RMS is defined as the root mean square of the vertical difference of the profile from the mean line. Ra is the average roughness of individual roughness measurements of the surface.

For this thesis, the RMS was used, as the average roughness is not a sufficient way to measure roughness, as shown in Fig 5.10 below.

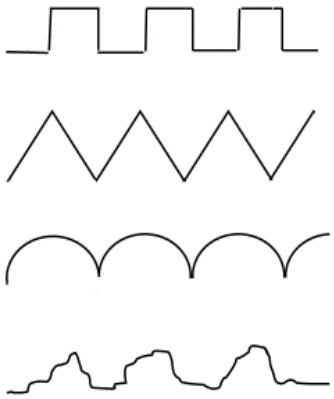

Figure 5.10: Average roughness (R_a) of all of the following surfaces would be the same, and hence, it is an inaccurate way of measuring the roughness of a surface.

The figure above shows that R_a is not an accurate way of measuring the roughness as its measure is only concerned with the relative depth of the profile in the vertical direction. It does not take into account different shapes, slopes, and sizes of the features or the frequency and regularity of the feature occurrence [317]. Hence, the RMS was used as our roughness value, which is more accurate in terms of roughness measurements without modelling, which is outside the scope of this thesis.

Using nanoparticles to create a rougher surface did have its drawbacks. They are difficult to tailor, and getting a homogenous layer can also be challenge. The biggest drawback, however is preventing agglomeration of nanoparticles [318]. Most of these drawbacks can be addressed using the E-beam lithography (EBL). The aim of this part of the project was to create a variety of different sized reproducible pattern defects, from small defects (50 nm) to large ones (1 μm).

5.3.4 Fabrication of nanometre sized holes using E-beam lithography

The E-beam experiment was done on a gold QCM-D chip and the features were made on the gold electrode. The measurements of each individual pattern is shown in Fig 5.11 below, where the diameter of each feature is shown in each square. The field size was 300 μm x 300 μm, and the pitch over diameter was kept constant at a ratio of 4. i.e. for the 50nm diameter holes, the distance between the two centres of the neighbouring disks was 200 nm.

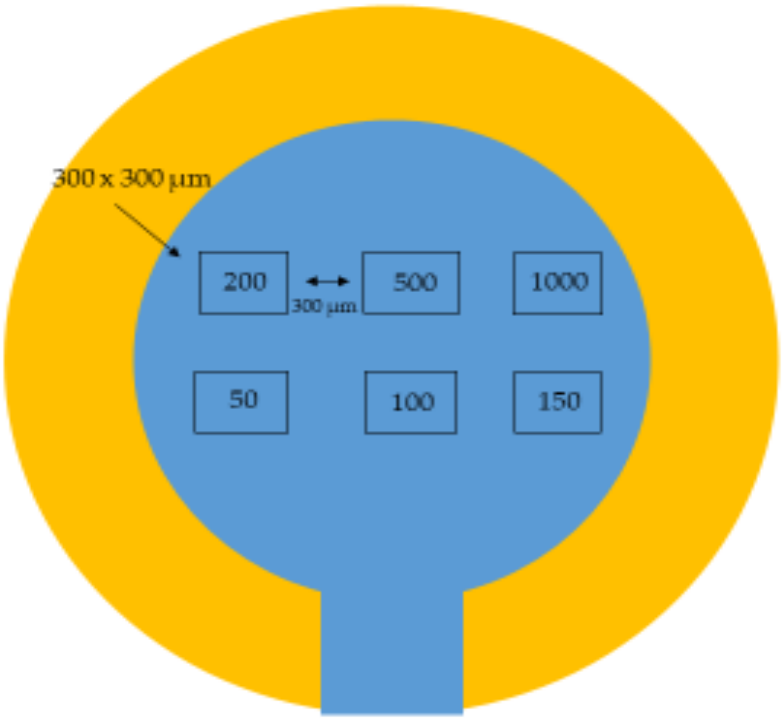

Figure 5.11 : A diagram representing the sizes of the features patterned on a gold QCM-D chip using E-beam lithography, with the light blue featuring the gold electrode.

From the above figure, the sizes of the patterns can be seen. The spherical shapes of the patterns made by the E- beam are seen below in Fig 5.12.

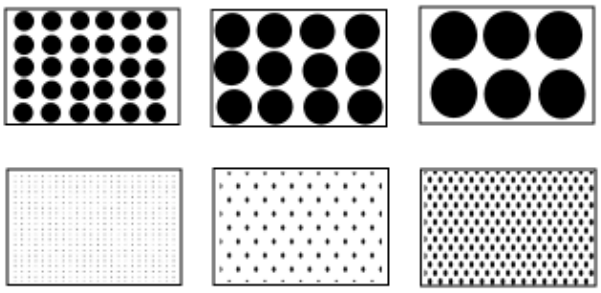

Figure 5.12: The feature patterns made by E- beam lithography in corresponding order to their size. All patterns are the same hole formation but different sizes, as shown in the dimensions in Fig 5.11 above.

The aim of the experiment was to fabricate the above figure, with 6 distinct patterns with different diameters and pitches. The exact protocol in regards to resists and spacers was described in Section 5.2.2. The settings for the production of the patterns were all the same, as the fabrication was done on a single chip. The current used was 100 pA, whilst the dose used was 500 $\mu C/cm^2$. With 60,000 x 60,000 pixels, a dose time was 1.25 μs/pixel.

Table 5.1: Summation of the six features produced on gold QCM-D chip, with their diameter, pitch and pitch/diameter ratio.

Diameter = 200 nm Pitch = 800 nm P/D = 4	Diameter = 500 nm Pitch = 2000 nm (2μm) P/D = 4	Diameter = 1000 nm (1μm) Pitch = 4000 nm (4 μm) P/D = 4
Diameter = 50 nm Pitch = 200 nm P/D = 4	Diameter = 100 nm Pitch = 400 nm P/D = 4	Diameter = 150 nm Pitch = 600 nm P/D = 4

Once the fabrication process was done, the chip was imaged using Zeis Orion Nanofab ion microscope. The imaging of the chip was a crucial step in confirming the fabrication method, and confirming the size of each defect in correspondence with the sizes set out at the beginning of the experiment.

The patterns produced by the e-beam are uniform and spherical, with the only difference being the size of the holes, as described and shown in Fig 5.12 above. The depth is the same for all the patterns produced.

5.3.4 Characterization of E-beam surfaces

Once E-beam lithography was performed, the patterned surface was imaged in order to examine whether the protocol for the formation of different sizes of holes produced by the EBL was successful.

The imaging was done using a Helium- ion microscope, the Zeis Orion Nanofab, This instrument allows imaging up to 0.5 nm, and the distinct patterns for each size can be seen in Fig 5.13 below.

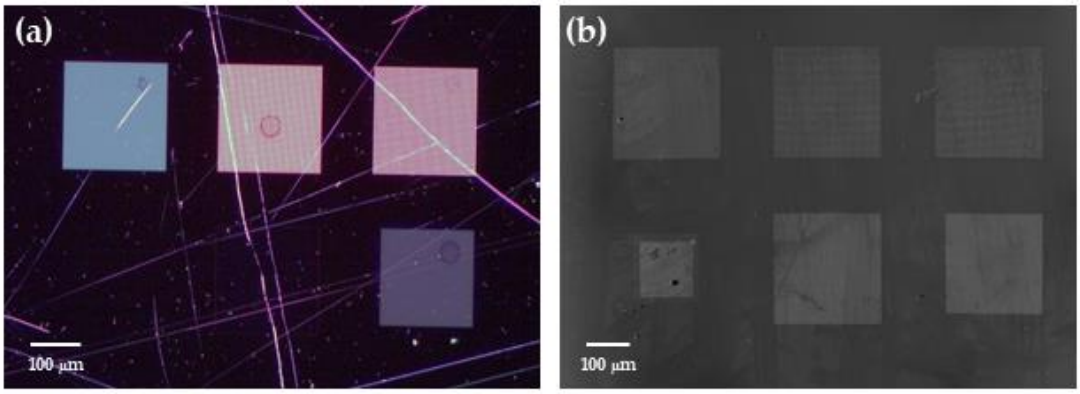

Figure 5.13: The overview of the six different patterns using dark field optical microscopy (A) and He-ion microscope (B).

The surfaces were initially checked using dark field optical microscopy after EBL was performed. The 50 nm patterning on the left hand side, however, was too small to be seen using this microscope and hence, a final image using the He-ion microscope was taken to confirm that the holes were made on the QCM-D gold electrode chip.

Both microscopy methods show that patterns of different sizes were constructed on the gold QCM-D sensor surface. The sizes of the features vary, and in order to determine whether the sizes are correct, each separate feature size was imaged individually using the He-ion microscope. Fig 5.14 below displays a closer look of all six of the patterns produced on the QCM-D chip.

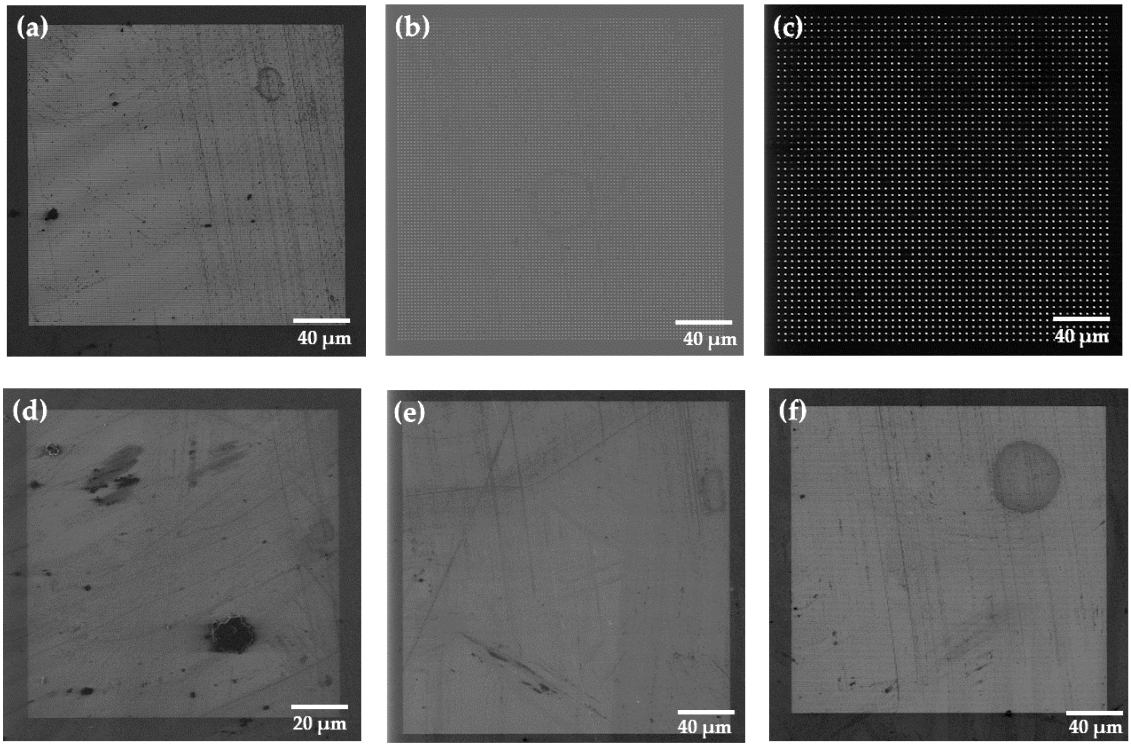

Figure 5.14: Individual images of three fabrication patterns using the Zeiss Nanofab. A – 200 nm diameter pattern, B – 500 nm pattern, C - 1000 nm (1 μm) pattern, D – 50 nm, pattern, E – 100 nm pattern, F - 150 nm pattern.

Even from the Figure 5.14 above, the exact sizes, especially when small, can be difficult to distinguish. However, the sizes were able to be measured, and the figure above confirms that the EBL procedure was successful in creating distinct patterns of different sized holes on a single gold QCM-D chip. This fabrication method could now be used for future peptide related experiments, as it was a relatively quick, accurate and reliable manner of functionalising surfaces on the nanoscale.

5.4 Conclusion

The roughness of the surface will have a profound effect on the adsorption of therapeutic peptides to solid interfaces, from structure of adsorbed peptides, to strength of the bonds formed, and mass of peptide adsorbed. The current literature on the effect of roughness is inconsistent, and lacks universal principles [319], [320].

This chapter tackled two main difficulties presented in the literature; firstly, difficulty in creating surfaces in a consistent, easy and reproducible manner, using two different techniques; nanoparticle addition to surfaces using wet chemistry and E-beam lithography. The largest barrier with nanoparticle surfaces, especially ones that are smaller than 50 nm in size is agglomeration of colloidal particles [321]. However, with the protocol described in this chapter, gold nanoparticles, with a slightly smaller diameter than 40 nm, were added to a gold surface, through carboxyl linkages to the surface. These interactions were stronger than peptide-NP interactions, which led to the gold nanoparticles staying on the gold QCM-D surface, and hence was considered a reproducible and quick method to functionalize and create rough gold surfaces.

The results showed an increase in mass on flat gold surfaces, with a roughness of approximately the same size as the therapeutic peptide monomers. The increased roughness shows a significant decrease in mass adsorbed (over 200 ng/cm^2), which could be due to the difficulty in diffusion due to such a large barrier for the peptides, in size comparison. It could provide difficulty for the peptides to attach as the surface is now significantly more curved, presenting possible problems with reorganization of the peptide.

The Au-NP surfaces provide a surface, with rounded features of a 40 nm size. The decrease could be due to the shape of the surface, and its spherical curvature and not necessarily the roughness. Hence, another method of creating rougher

surfaces had to be found, such as using E-beam lithography to enable comparison of results, and to see how much of an effect the shape of the defect has on peptide adsorption.

E-beam lithography, which uses electron beams to pattern the surface instead of wet chemistry, created holes of different sizes with the same pitch on a single gold QCM-D chip as proof of concept. The lithographic technique was capable of making six different features in 300 μm x 300 μm sized squares on a single gold QCM-D chip in under 12 hours.

This chapter concludes the main results chapters of this thesis. An overview and future works of the project are discussed in the next section.

6 Chapter

Conclusion and Future Works

6.1 The problem

Aggregation of therapeutic peptides is a phenomenon that affects numerous areas of biomedical research; from aggregation of $\alpha\beta$ peptides and their effect on Alzheimer's, to using structural aggregates as a safe, efficient drug delivery device [87], [124], [322]. Much research has been done on the prevention or enhancement of aggregation in solution conditions through biological means, but less research has been done on surface induced aggregation, specifically surfaces of pharmaceutically relevant containers [113]. In the case of this thesis, peptide aggregation was investigated, focusing on surface induction and the part surfaces play on aggregation, primarily on pharmaceutically relevant containers.

The primary aim was to investigate specific peptides for glucose regulation, and their aggregation and adsorption to surfaces in everyday situations, such as transportation or delivery of the investigated therapeutic peptides. This was done through dividing the research into three distinct areas of investigation: peptide stability in different solution conditions, peptide adsorption to hydrophilic, hydrophobic and charged surfaces, and changing roughness of surfaces in order to investigate the adsorption of peptides.

The results achieved in the thesis are summarised in the next section, 6.2.

The results provide clear answers to the problem of surface induced aggregation, experienced by therapeutic peptides in vials, storage containers and syringes.

6.2 Overview of Results

Chapter 3 investigated the stability of the peptides in different solution conditions. Peptides were investigated in varying pH conditions, in order to explore the effect of overall peptide charge on the ability to aggregate and form β-sheets or α-helices. Concentration was also varied, to gauge peptide concentration dependence on aggregation.

Once the stability and conditions of the peptides in bulk solution were determined, this data was used to optimise the solution conditions for experiments at the interface. Hence, the future experiments were done using 200 rpm agitation, using HCl/Glycine buffer (pH 2.4, 0.05 M concentration) at a concentration of 2.5 mg/mL. These conditions were chosen as all peptides carried the same charge at acidic conditions, and aggregate structures formed in these solution conditions were analysed and assessed accordingly. Chapter 3 was vital to lay down the groundwork for peptide interactions in solution, to then focus on their interaction on the surface.

Chapter 4 explored both the adsorption and desorption of therapeutic peptides at surfaces with different polarities and hydrophilicities. The two main conclusions found were that using pharmaceutically relevant surfaces, such as polystyrene and borosilicate glass, increased surface induced aggregation through adsorption of all peptides, even with unfavourable electrostatic interactions. Other surfaces, such as Au-OH, hydrophilic and uncharged, would be a better surface for pharmaceuticals, as it decreased non-specific adsorption compared to the variety of other surfaces investigated. Secondly, peptides that had an added lipidated chain, showed directly opposite trends to peptides without the lipidated chains. This suggested different mechanisms and/or hydrophobic interactions having a large effect on peptide adsorption, as was established in Chapter 3. This was especially true for conditions which were

unfavourable, such as when charge interactions were repulsive between the peptides and the surface.

Chapter 5 explored two different methods of changing surface roughness based on gold QCM-D chips. The first approach used wet chemistry to synthesize gold nanoparticles that could be retained on a surface during and after the experiment, with no change to their size or shape.

Using glucagon and liraglutide would also investigate the effect of lipidation of the peptide on the adsorption to both surfaces. Both liraglutide and glucagon were shown to adsorb the least to the nanoparticles surface, which was unexpected and contrary the literature. Liraglutide did show a large mass adsorption on both surfaces, in part due to its lipidation and possible reorganization of its hydrophobic chain on the surface.

However, as addition of nanoparticles to the surface was only one way of increasing the roughness of the surface, using other methods would be a valuable way to confirm the findings and to investigate how large a part shape of defects plays on the adsorption of the peptides.

The second approach was to use lithography to create a surface with holes of specific sizes. A single QCM-D chip was patterned with six different roughness patterns, ranging from 50 nm to 1 μm using E-beam lithography, showing proof of concept.

From this piece of research there were a few noticeably unexpected results. The initial hypothesis for looking at structurally similar peptides in solution was that due to their similarities, the peptides would show similar time frames for aggregation and similar fibrillation patterns. The peptides, however, underwent such a variety of different pathways and showed such an array of differing structures in solution. The second unexpected result was the large amount of peptide adsorption on borosilicate glass, which to this day, is used in most

pharmaceutical facilities during both transportation, storage and injection. The third, was that peptide adsorption was hindered significantly compared to flat surfaces, which goes against much of the literature on the topic and was the opposite of my hypothesis.

Those three very interesting and unexpected results, led me to the next section, which describes the future work that could be done in order to fully embrace the future potential of the project.

6.3 Future work

This thesis investigated the stability of four therapeutic amphiphilic peptides, assessed different surfaces (hydrophobic, hydrophilic, uncharged and charged) in order to elucidate mechanisms and/or common surfaces to which the peptides adsorb the most to, and evaluated how surface roughness effects peptide adsorption. This was done through an extensive list of different techniques, yet not an exhaustive list. There are plenty more avenues to explore, described in the following section.

6.3.1 Peptide adsorption on E-beam surfaces

Using the E-beam evaporation technique was a proof of concept study detailed in Chapter 5. Hence, the first avenue to explore would be to assess the peptide adsorption of both liraglutide and glucagon on each specific surface created by E-beam lithography. This would be done by creating the specific patterns in each different size, from 50 nm to 1μm on separate QCM-D chips, and doing individual QCM-D experiments on each one, as described in Chapter 4. As similar experiments were run on multiple other surfaces, the same analysis can be used and hence comparisons between different peptides can be made. From this set of experiments, it could be determined whether addition of nanoparticles and e-beam lithography show similar trends relating to peptides adsorbing on rough surfaces, or whether the two different methods also provide two different sets of results. If there are differences, then specific experiments must be done in order to determine whether the differences in adsorption are due to the differences in shapes (ie spheres versus holes) or whether it's the order of magnitude in the roughness compared to the peptide size. From this, some general trends regarding surface roughness and peptide adsorption would emerge.

6.3.2 Peptide adsorption on surfaces in neutral pH

Due to problems with stability and insolubility at neutral pH (for glucagon and exendin-4), experiments in neutral conditions were not performed. This could be helpful in the future to pin point mechanisms of adsorption when peptides are uncharged, and which other possible mechanisms, such as hydrophobic interactions or van der Waals, might be the overarching mechanisms once charge no longer plays a large part in peptide adsorption. However, due to instability this could be difficult, and some basic principles, such as increased peptide-peptide interactions at isoelectric point, have already been established.

6.3.3 Peptide adsorption map

The data and results from this thesis could be expanded upon to create a peptide adsorption map. Once a variety of different surfaces, with different hydrophilicities, roughness and polarity have been investigated, more accurate general patterns would occur. Initially this would be done specifically for diabetes related peptides, such as those studied in this thesis. These same principles can then be applied for a variety of different groups of peptides, to more accurately predict the manner in which they might aggregate in solution and/or adsorb to specific surfaces. However, as can be seen by many of the conclusions above, this would be difficult as each peptide is driven by different principles dependent on their amino acid sequence. In order to create this map, other techniques such as the ones described below can be used to extract more data from the experiments.

6.3.4 Additional Techniques and Future Experiments

In order to thoroughly investigate the surface, QCM-D can be nicely paired with DPI (Dual Polarization Inferometry). As QCM-D provides wet mass adsorbed, this can then be tested using DPI which gives dry mass, and comparisons can be made. From this, water content can be assessed and a more intricate picture of

the layers formed on the surface can be gathered. DPI can also probe the molecular layers, and would be an incredibly useful technique to infer protein conformational changes, as well as getting more thermodynamic data about the change in conformation, as well as kinetic data, which can then be linked to conformations seen in Chapter 3 using the AFM. In addition to this, using DPI could also give a fuller picture of binding interactions, together with more desorption experiments using QCM-D.

A whole array of adsorption/desorption experiments could then be made using both these techniques. It would be really interesting to be able to use both techniques to look at a range of different roughnesses of one material (made through different fabrication methods, like CVD sputtering, wet chemistry and lithographic techniques) and compare the mass adsorbed to the different surfaces. From this, an idea of surface roughness, curvature or surface patterning can be done, and analytical calculations can be made in order to determine which surface roughness provides the best model for future surfaces in order to prevent peptide adsorption.

The AFM, as an imaging technique was a very useful technique and one which was essential to this thesis. However, the AFM can also be used as a tip – sample probe, and with skill, can be used in order to elucidate the strength of binding of molecules to a surface. This would have been in incredibly impressive addition to the thesis, and would have given an additional sound check point to the plethora of techniques already used.

Gauging surface interactions is difficult, but with the breadth of techniques available, more additional experiments could be done to really complete the overall picture of peptide adsorption to surfaces through combining more kinetic and thermodynamic studies.

7 Appendix

7.1 Dynamic Light Scattering

The size of the peptides were investigated in acidic and basic conditions, in order to determine aggregation using light scattering. Average hydrodynamic radii of DLS were shown in Chapter 4. The below figure is the correlation functions, in order to confirm that the data taken from the DLS was accurate in relation to the correlation function. All peptide correlation functions were investigated.

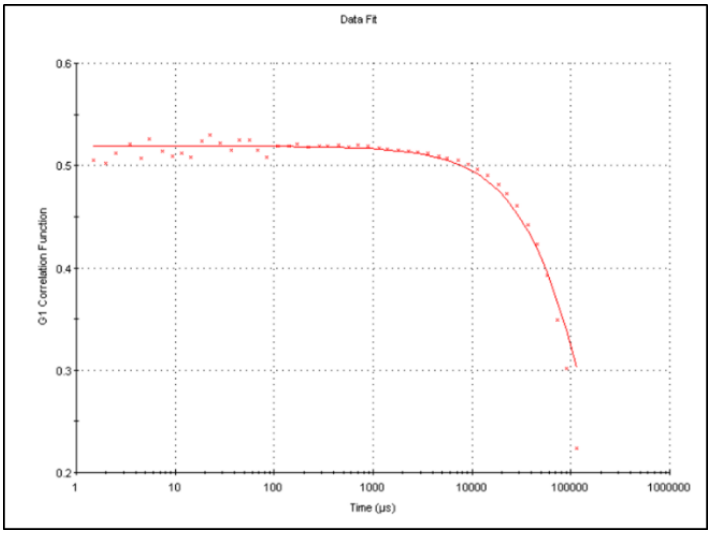

Figure 7.1: The correlation function of Dynamic Light Scattering measurements of glucagon at 1.5 mg/mL. Results were only used when the data correlation function had a data fit synonymous to this curve.

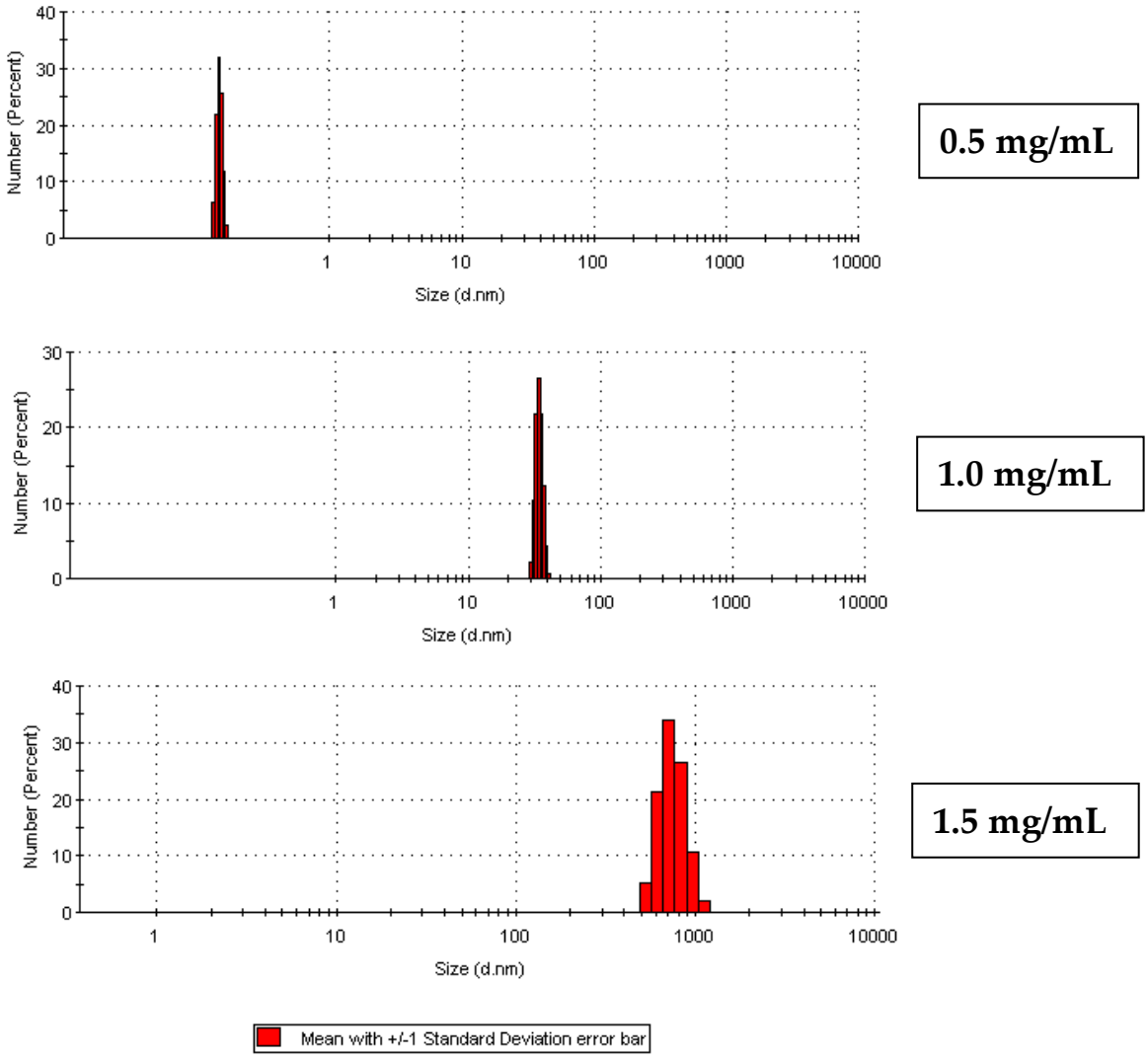

Figure 7.2: Peptide size determination using DLS for g797 (pH2.4, Glycine/HCl buffer) showing how increased concentration shows a much larger hydrodynamic radius, indicating micelle or higher order structure formation above CMC, which for g797 is 1.5 mg/mL. At 0.5 mg/mL, peptides are difficult to see and the lower limit of DLS is around 1 nm.

7.2 Contact Angles

The static water contact angle (θ) was measured for all surfaces described in this thesis using a contact angle goniometer. A drop of water was placed on the selected surface using a micro-syringe. The needle was then removed from the liquid, and the contact angle was noted. Images of the droplet on the surface are shown in Fig 7.3 below. For each sample the reported value is the mean calculated from three measurements at different places on the surface.

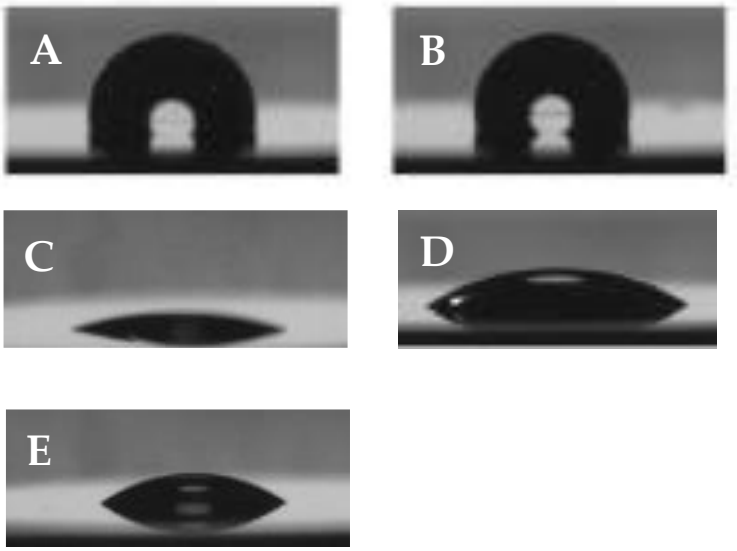

Figure 7.3: Water droplets presented on the five different surfaces used in this thesis. A – Polystyrene, B – CH_3, C – OH, D – SiO_2, E – Borosilicate Glass

Table 7.1: Contact angle measurements using DI water for the surfaces used in the study.

Surface	Contact Angle
Polystyrene	111.2 ± 13.2
-CH_3	107.5 ± 9.5
-OH	12.7 ± 3.4
SiO_2	19. 9 ± 2.8
Borosilicate Glass	24. 8 ± 3.1

7.3 Increased SA/V ratio

From Dr J.A.Rubio's thesis, reproduced with permission.

For a standard BSA protein, it was calculated that the average increase from the SA:V ratio of a 40 nm NP would be 2.3 This was deduced as follows:

The total height of the cylinder available for area increase is the radius of the NP minus the maximum size of the protein (hydrodynamic diameter).

The NP, which sits on a projected circle, must be subtracted from the area increase due to its screening.

$A_{increase} = A_{hemisphere} + A_{Cylinder} - A_{ProjectedCircle}\ A_{increase}$

$2\pi r^2 + 2(r - 2rBSA) - \pi r^2$

$A_{increase} = \pi r^2 + 2(r - 2rBSA)$

The first term of the equation is the area occupied by a projected NP in the SEM image. The whole equation can be written in terms of the projected area:

$A_{increase} = \pi r^2 (1 + 2 - 4rBSAr)$

Where for 43 nm NPs and $rBSA$=3.56 nm the factor for area increase based on the projected area is:

$(1 + 2 - 4rBSAr) = 2.338$

The total area increase can be obtained from the total projected area result from the image analysis using ImageJ and multiplying it by factor from Equation 2.4.

Bibliography

[1] M. W. Pennington, A. Czerwinski, and R. S. Norton, "Peptide therapeutics from venom: Current status and potential," *Bioorg. Med. Chem.*, vol. 26, no. 10, pp. 2738–2758, Jun. 2018, doi: 10.1016/J.BMC.2017.09.029.

[2] N. Sun, S. A. Funke, and D. Willbold, "Mirror image phage display – Generating stable therapeutically and diagnostically active peptides with biotechnological means," *J. Biotechnol.*, vol. 161, no. 2, pp. 121–125, Oct. 2012, doi: 10.1016/J.JBIOTEC.2012.05.019.

[3] P. W. Latham, "Therapeutic peptides revisited," *Nat. Biotechnol.*, vol. 17, p. 755, Aug. 1999.

[4] K. Fosgerau and T. Hoffmann, "Peptide therapeutics: current status and future directions," *Drug Discov. Today*, vol. 20, no. 1, pp. 122–128, Jan. 2015, doi: 10.1016/J.DRUDIS.2014.10.003.

[5] F. Macritchie, "Proteins at Interfaces," *Adv. Protein Chem.*, vol. 32, pp. 283–326, Jan. 1978, doi: 10.1016/S0065-3233(08)60577-X.

[6] K. Trainor, A. Broom, and E. M. Meiering, "Exploring the relationships between protein sequence, structure and solubility," *Curr. Opin. Struct. Biol.*, vol. 42, pp. 136–146, Feb. 2017, doi: 10.1016/J.SBI.2017.01.004.

[7] A. Gerhardt, N. R. Mcgraw, D. K. Schwartz, J. S. Bee, J. F. Carpenter, and T. W. Randolph, "Protein Aggregation and Particle Formation in Prefilled Glass Syringes," *J. Pharm. Sci.*, vol. 103, no. 6, pp. 1601–1612, Jun. 2014, doi: 10.1002/JPS.23973.

[8] V. B. Fainerman and R. Miller, "Surface tension isotherms for surfactant adsorption layers including surface aggregation," *Langmuir*, vol. 12, no. 25, pp. 6011–6014, 1996.

[9] P. Somasundaran and L. Huang, "Adsorption/aggregation of surfactants

and their mixtures at solid–liquid interfaces," *Adv. Colloid Interface Sci.*, vol. 88, no. 1–2, pp. 179–208, 2000.

[10] J. Eastoe, "Surfactant aggregation and adsorption at interfaces," *Colloid Sci.*, pp. 50–76, 2005.

[11] U. R. Aguilar-Parada E, Eisentraut AM, "Pancreatic glucagon secretion in normal and diabetic subjects.," *Am J Med Sci*, vol. 257, no. 6, pp. 415–19, 1969.

[12] B. Ahrén, M. Landin-Olsson, P.-A. Jansson, M. Svensson, A. Schweizer, and D. Holmes, "Inhibition of Dipeptidyl Peptidase-4 Reduces Glycemia, Sustains Insulin Levels, and Reduces Glucagon Levels in Type 2 Diabetes," *J. Clin. Endocrinol. Metab.*, vol. 89, no. 5, pp. 2078–2084, May 2004, doi: 10.1210/jc.2003-031907.

[13] M. Laakso, "Hyperglycemia and cardiovascular disease in type 2 diabetes.," *Diabetes*, vol. 48, no. 5, p. 937, May 1999, doi: 10.2337/diabetes.48.5.937.

[14] D. R. Matthews, J. P. Hosker, A. S. Rudenski, B. A. Naylor, D. F. Treacher, and R. C. Turner, "Homeostasis model assessment: insulin resistance and β-cell function from fasting plasma glucose and insulin concentrations in man," *Diabetologia*, vol. 28, no. 7, pp. 412–419, 1985.

[15] "Peptides Therapeutics Market," *Transparency Market Research*, 2017. [Online]. Available: https://www.transparencymarketresearch.com/peptide-therapeutics-market.html. [Accessed: 19-Apr-2019].

[16] A. Loffet, "Peptides as Drugs: Is There a Market?," *J. Pept. Sci.*, vol. 8, no. 1, pp. 1–7, Jan. 2002, doi: 10.1002/psc.366.

[17] P. Vlieghe, V. Lisowski, J. Martinez, and M. Khrestchatisky, "Synthetic

therapeutic peptides: science and market," *Drug Discov. Today*, vol. 15, no. 1–2, pp. 40–56, Jan. 2010, doi: 10.1016/J.DRUDIS.2009.10.009.

[18] A. Stevenazzi, M. Marchini, G. Sandrone, B. Vergani, and M. Lattanzio, "Amino acidic scaffolds bearing unnatural side chains: An old idea generates new and versatile tools for the life sciences," *Bioorg. Med. Chem. Lett.*, vol. 24, no. 23, pp. 5349–5356, Dec. 2014, doi: 10.1016/J.BMCL.2014.10.016.

[19] J. L. Lau and M. K. Dunn, "Therapeutic peptides: Historical perspectives, current development trends, and future directions," *Bioorg. Med. Chem.*, vol. 26, no. 10, pp. 2700–2707, Jun. 2018, doi: 10.1016/J.BMC.2017.06.052.

[20] A. Hoffman and E. Ziv, "Pharmacokinetic Considerations of New Insulin Formulations and Routes of Administration," *Clin. Pharmacokinet.*, vol. 33, no. 4, pp. 285–301, 1997, doi: 10.2165/00003088-199733040-00004.

[21] D. K. Pettit and W. R. Gombotz, "The development of site-specific drug-delivery systems for protein and peptide biopharmaceuticals.," *Trends Biotechnol.*, vol. 16, no. 8, pp. 343–9, Aug. 1998, doi: 10.1016/S0167-7799(98)01186-X.

[22] A. A. Kaspar and J. M. Reichert, "Future directions for peptide therapeutics development," *Drug Discov. Today*, vol. 18, no. 17–18, pp. 807–817, Sep. 2013, doi: 10.1016/J.DRUDIS.2013.05.011.

[23] A. Padhi, M. Sengupta, S. Sengupta, K. H. Roehm, and A. Sonawane, "Antimicrobial peptides and proteins in mycobacterial therapy: Current status and future prospects," *Tuberculosis*, vol. 94, no. 4, pp. 363–373, Jul. 2014, doi: 10.1016/J.TUBE.2014.03.011.

[24] S. Frokjaer and D. E. Otzen, "Protein drug stability: a formulation challenge," *Nat. Rev. drug Discov.*, vol. 4, no. 4, p. 298, 2005.

[25] Z. Hamrang, N. J. W. Rattray, and A. Pluen, "Proteins behaving badly: emerging technologies in profiling biopharmaceutical aggregation," *Trends Biotechnol.*, vol. 31, no. 8, pp. 448–458, 2013.

[26] S. Runge, B. S. Wulff, K. Madsen, H. Bräuner-Osborne, and L. B. Knudsen, "Different domains of the glucagon and glucagon-like peptide-1 receptors provide the critical determinants of ligand selectivity," *Br. J. Pharmacol.*, vol. 138, no. 5, pp. 787–794, Mar. 2003, doi: 10.1038/sj.bjp.0705120.

[27] Y. Rouillé, S. Kantengwa, J.-C. Irminger, and P. A. Halban, "Role of the Prohormone Convertase PC3 in the Processing of Proglucagon to Glucagon-like Peptide 1," *J. Biol. Chem.*, vol. 272, no. 52, pp. 32810–32816, Dec. 1997, doi: 10.1074/jbc.272.52.32810.

[28] M. Furuta *et al.*, "Severe defect in proglucagon processing in islet A-cells of prohormone convertase 2 null mice," *J. Biol. Chem.*, vol. 276, no. 29, pp. 27197–27202, 2001.

[29] V. J. Hruby, "Structure-conformation-activity studies of glucagon and semi-synthetic glucagon analogs," *Mol. Cell. Biochem.*, vol. 44, no. 1, pp. 49–64, 1982, doi: 10.1007/BF00573846.

[30] K. IMAGAWA *et al.*, "Production of Anti-Glucagon Sera with A C-Terminal Fragment of Pancreatic Glucagon," *Endocrinol. Jpn.*, vol. 26, no. 1, pp. 123–131, 1979, doi: 10.1507/endocrj1954.26.123.

[31] R. R. Banerjee *et al.*, "Regulation of fasted blood glucose by resistin," *Science (80-.).*, vol. 303, no. 5661, pp. 1195–1198, 2004.

[32] D. L. Rothman, I. Magnusson, L. D. Katz, R. G. Shulman, and G. I. Shulman, "Quantitation of hepatic glycogenolysis and gluconeogenesis in fasting humans with 13C NMR," *Science (80-.).*, vol. 254, no. 5031, pp. 573–576, 1991.

[33] R. H. Unger, "Glucagon and the Insulin:Glucagon Ratio in Diabetes and Other Catabolic Illnesses," *Diabetes*, vol. 20, no. 12, p. 834, Dec. 1971, doi: 10.2337/diab.20.12.834.

[34] L. L. Baggio and D. J. Drucker, "Biology of Incretins: GLP-1 and GIP," *Gastroenterology*, vol. 132, no. 6, pp. 2131–2157, May 2007, doi: 10.1053/j.gastro.2007.03.054.

[35] L. Chen, D. Magliano, and P. Z Zimmet, *Chen, L, Magliano, DJ and Zimmet, PZ. The worldwide epidemiology of type 2 diabetes mellitus-present and future perspectives. Nat Rev Endocrinol 8: 228-236*, vol. 8. 2011.

[36] C. Mathieu *et al.*, "A comparison of adding liraglutide versus a single daily dose of insulin aspart to insulin degludec in subjects with type 2 diabetes (BEGIN: VICTOZA ADD-ON)," *Diabetes, Obes. Metab.*, vol. 16, no. 7, pp. 636–644, Jul. 2014, doi: 10.1111/dom.12262.

[37] R. A. DeFronzo, R. E. Ratner, J. Han, D. D. Kim, M. S. Fineman, and A. D. Baron, "Effects of Exenatide (Exendin-4) on Glycemic Control and Weight Over 30 Weeks in Metformin-Treated Patients With Type 2 Diabetes," *Diabetes Care*, vol. 28, no. 5, p. 1092, May 2005, doi: 10.2337/diacare.28.5.1092.

[38] J. W. Neidigh, R. M. Fesinmeyer, K. S. Prickett, and N. H. Andersen, "Exendin-4 and Glucagon-like-peptide-1: NMR Structural Comparisons in the Solution and Micelle-Associated States," *Biochemistry*, vol. 40, no. 44, pp. 13188–13200, Nov. 2001, doi: 10.1021/bi010902s.

[39] C.-Y. Tseng, C.-P. Yu, and H.-C. Lee, "From laws of inference to protein folding dynamics," *Phys. Rev. E. Stat. Nonlin. Soft Matter Phys.*, vol. 82, p. 021914, Aug. 2010, doi: 10.1103/PhysRevE.82.021914.

[40] R. Göke *et al.*, "Exendin-4 is a high potency agonist and truncated exendin-

(9-39)-amide an antagonist at the glucagon-like peptide 1-(7-36)-amide receptor of insulin-secreting beta-cells.," *J. Biol. Chem.*, vol. 268, no. 26, pp. 19650–19655, Sep. 1993.

[41] E. S. Ali *et al.*, "The glucagon-like peptide-1 analogue exendin-4 reverses impaired intracellular Ca2 + signalling in steatotic hepatocytes," *Biochim. Biophys. Acta - Mol. Cell Res.*, vol. 1863, no. 9, pp. 2135–2146, Sep. 2016, doi: 10.1016/J.BBAMCR.2016.05.006.

[42] C. Beglinger and L. Degen, "Gastrointestinal satiety signals in humans–physiologic roles for GLP-1 and PYY?," *Physiol. Behav.*, vol. 89, no. 4, p. 460—464, Nov. 2006, doi: 10.1016/j.physbeh.2006.05.048.

[43] M. Nauck *et al.*, "Efficacy and safety comparison of liraglutide, glimepiride, and placebo, all in combination with metformin, in type 2 diabetes: the LEAD (liraglutide effect and action in diabetes)-2 study," *Diabetes Care*, vol. 32, no. 1, pp. 84–90, Jan. 2009, doi: 10.2337/dc08-1355.

[44] T. Knowles, M. Vendruscolo, and C. M. Dobson, *The physical basis of protein misfolding disorders*, vol. 68. 2015.

[45] T. Abbas, E. Faivre, and C. Hölscher, "Impairment of synaptic plasticity and memory formation in GLP-1 receptor KO mice: Interaction between type 2 diabetes and Alzheimer's disease," *Behav. Brain Res.*, vol. 205, no. 1, pp. 265–271, 2009.

[46] N. Van Gerven, S. E. Van der Verren, D. M. Reiter, and H. Remaut, "The Role of Functional Amyloids in Bacterial Virulence," *J. Mol. Biol.*, vol. 430, no. 20, pp. 3657–3684, Oct. 2018, doi: 10.1016/J.JMB.2018.07.010.

[47] D. M. Fowler, A. V Koulov, C. Alory-Jost, M. S. Marks, W. E. Balch, and J. W. Kelly, "Functional Amyloid Formation within Mammalian Tissue," *PLOS Biol.*, vol. 4, no. 1, pp. e6-, Nov. 2005.

[48] H. Evans, D.F and Wennerstrom, *The Colloidal Domain*. New York: Wiley, 1999.

[49] H. M. McConnell, "Structures and transitions in lipid monolayers at the air-water interface," *Annu. Rev. Phys. Chem.*, vol. 42, no. 1, pp. 171–195, 1991.

[50] C.-H. Chang and E. I. Franses, "Adsorption dynamics of surfactants at the air/water interface: a critical review of mathematical models, data, and mechanisms," *Colloids Surfaces A Physicochem. Eng. Asp.*, vol. 100, pp. 1–45, Jul. 1995, doi: 10.1016/0927-7757(94)03061-4.

[51] M. Ogino, K. and Abe, *Mixed Surfactants Systems.* New York: Dekker, 1993.

[52] M. Blesic, M. H. Marques, N. V Plechkova, K. R. Seddon, L. P. N. Rebelo, and A. Lopes, "Self-aggregation of ionic liquids: micelle formation in aqueous solution," *Green Chem.*, vol. 9, no. 5, pp. 481–490, 2007, doi: 10.1039/B615406A.

[53] C. Tanford, "Theory of micelle formation in aqueous solutions," *J. Phys. Chem.*, vol. 78, no. 24, pp. 2469–2479, Nov. 1974, doi: 10.1021/j100617a012.

[54] C. Tanford, *The hydrophobic effect: formation of micelles and biological membranes 2d ed*. J. Wiley., 1980.

[55] D. J. Mitchell and B. W. Ninham, "Micelles, vesicles and microemulsions," *J. Chem. Soc. Faraday Trans. 2 Mol. Chem. Phys.*, vol. 77, no. 4, pp. 601–629, 1981.

[56] M. E. Cates and S. J. Candau, "Statics and dynamics of worm-like surfactant micelles," *J. Phys. Condens. Matter*, vol. 2, no. 33, p. 6869, 1990.

[57] E. Ruckenstein and R. Nagarajan, "Critical micelle concentration. Transition point for micellar size distribution," *J. Phys. Chem.*, vol. 79, no. 24, pp. 2622–2626, 1975.

[58] P. Mukerjee and K. J. Mysels, "Critical micelle concentrations of aqueous surfactant systems," National Standard reference data system, 1971.

[59] W. Norde, "Adsorption of proteins from solution at the solid-liquid interface," *Adv. Colloid Interface Sci.*, vol. 25, pp. 267–340, Jan. 1986, doi: 10.1016/0001-8686(86)80012-4.

[60] N.-P. Huang *et al.*, "Poly(l-lysine)-g-poly(ethylene glycol) Layers on Metal Oxide Surfaces: Surface-Analytical Characterization and Resistance to Serum and Fibrinogen Adsorption," *Langmuir*, vol. 17, no. 2, pp. 489–498, Jan. 2001, doi: 10.1021/la000736+.

[61] W. Wang, "Advanced protein formulations," *Protein Sci.*, vol. 24, no. 7, pp. 1031–1039, Jul. 2015, doi: 10.1002/pro.2684.

[62] R. Riek and D. S. Eisenberg, "The activities of amyloids from a structural perspective," *Nature*, vol. 539, p. 227, Nov. 2016.

[63] Q. Wei *et al.*, "Protein Interactions with Polymer Coatings and Biomaterials," *Angew. Chemie Int. Ed.*, vol. 53, no. 31, pp. 8004–8031, Jul. 2014, doi: 10.1002/anie.201400546.

[64] M. Ozboyaci, D. B. Kokh, S. Corni, and R. C. Wade, "Modeling and simulation of protein–surface interactions: achievements and challenges," *Q. Rev. Biophys.*, vol. 49, p. e4, 2016, doi: DOI: 10.1017/S0033583515000256.

[65] W. Wang, S. K. Singh, N. Li, M. R. Toler, K. R. King, and S. Nema, "Immunogenicity of protein aggregates—Concerns and realities," *Int. J. Pharm.*, vol. 431, no. 1–2, pp. 1–11, Jul. 2012, doi: 10.1016/J.IJPHARM.2012.04.040.

[66] E. M. Moussa *et al.*, "Immunogenicity of Therapeutic Protein Aggregates," *J. Pharm. Sci.*, vol. 105, no. 2, pp. 417–430, Feb. 2016, doi: 10.1016/j.xphs.2015.11.002.

[67] S. H. White and W. C. Wimley, "Hydrophobic interactions of peptides with membrane interfaces," *Biochim. Biophys. Acta - Rev. Biomembr.*, vol. 1376, no. 3, pp. 339–352, Nov. 1998, doi: 10.1016/S0304-4157(98)00021-5.

[68] T. Gidalevitz, A. Ben-Zvi, K. H. Ho, H. R. Brignull, and R. I. Morimoto, "Progressive Disruption of Cellular Protein Folding in Models of Polyglutamine Diseases," *Science (80-.).*, vol. 311, no. 5766, p. 1471, Mar. 2006, doi: 10.1126/science.1124514.

[69] A. K. Buell *et al.*, "Population of Nonnative States of Lysozyme Variants Drives Amyloid Fibril Formation," *J. Am. Chem. Soc.*, vol. 133, no. 20, pp. 7737–7743, May 2011, doi: 10.1021/ja109620d.

[70] M. Diociaiuti *et al.*, "Native metastable prefibrillar oligomers are the most neurotoxic species among amyloid aggregates," *Biochim. Biophys. Acta - Mol. Basis Dis.*, vol. 1842, no. 9, pp. 1622–1629, Sep. 2014, doi: 10.1016/J.BBADIS.2014.06.006.

[71] O. Sumner Makin and L. C. Serpell, "Structural characterisation of islet amyloid polypeptide fibrils," *J. Mol. Biol.*, vol. 335, no. 5, p. 1279—1288, Jan. 2004, doi: 10.1016/j.jmb.2003.11.048.

[72] K. Sasahara, K. Morigaki, and K. Shinya, "Amyloid aggregation and deposition of human islet amyloid polypeptide at membrane interfaces," *FEBS J.*, vol. 281, no. 11, pp. 2597–2612, Apr. 2014, doi: 10.1111/febs.12807.

[73] H. Hamazaki, "Amyloid P Component Promotes Aggregation of Alzheimer's β-Amyloid Peptide," *Biochem. Biophys. Res. Commun.*, vol. 211, no. 2, pp. 349–353, Jun. 1995, doi: 10.1006/BBRC.1995.1819.

[74] J. Tyedmers, A. Mogk, and B. Bukau, "Cellular strategies for controlling protein aggregation," *Nat. Rev. Mol. Cell Biol.*, vol. 11, p. 777, Oct. 2010.

[75] S. M. Grundy, "Pre-Diabetes, Metabolic Syndrome, and Cardiovascular

Risk," *J. Am. Coll. Cardiol.*, vol. 59, no. 7, pp. 635–643, Feb. 2012, doi: 10.1016/J.JACC.2011.08.080.

[76] T. L. A. R. Group, "The Look AHEAD Study: A Description of the Lifestyle Intervention and the Evidence Supporting It," *Obesity*, vol. 14, no. 5, pp. 737–752, May 2006, doi: 10.1038/oby.2006.84.

[77] T. Tan and S. Bloom, "Gut hormones as therapeutic agents in treatment of diabetes and obesity," *Curr. Opin. Pharmacol.*, vol. 13, no. 6, p. 996—1001, Dec. 2013, doi: 10.1016/j.coph.2013.09.005.

[78] S. A. Sadry and D. J. Drucker, "Emerging combinatorial hormone therapies for the treatment of obesity and T2DM," *Nat. Rev. Endocrinol.*, vol. 9, p. 425, Mar. 2013.

[79] A. to C. C. R. in D. S. Group *et al.*, "Effects of intensive glucose lowering in type 2 diabetes," *N. Engl. J. Med.*, vol. 358, no. 24, pp. 2545–2559, Jun. 2008, doi: 10.1056/NEJMoa0802743.

[80] T. A. Martinek and F. Fülöp, "Side-chain control of β-peptide secondary structures," *Eur. J. Biochem.*, vol. 270, no. 18, pp. 3657–3666, Sep. 2003, doi: 10.1046/j.1432-1033.2003.03756.x.

[81] R. Nelson *et al.*, "Structure of the cross-β spine of amyloid-like fibrils," *Nature*, vol. 435, no. 7043, pp. 773–778, 2005, doi: 10.1038/nature03680.

[82] C. B. Andersen, D. Otzen, G. Christiansen, and C. Rischel, "Glucagon Amyloid-like Fibril Morphology Is Selected via Morphology-Dependent Growth Inhibition," *Biochemistry*, vol. 46, no. 24, pp. 7314–7324, Jun. 2007, doi: 10.1021/bi6025374.

[83] T. Stromer and L. C. Serpell, "Structure and morphology of the Alzheimer's amyloid fibril," *Microsc. Res. Tech.*, vol. 67, no. 3-4, pp. 210–217, Jul. 2005, doi: 10.1002/jemt.20190.

[84] C. M. Dobson, "Protein folding and misfolding," *Nature*, vol. 426, no. 6968, pp. 884–890, 2003, doi: 10.1038/nature02261.

[85] D. Thirumalai, D. K. Klimov, and R. I. Dima, "Emerging ideas on the molecular basis of protein and peptide aggregation," *Curr. Opin. Struct. Biol.*, vol. 13, no. 2, p. 146—159, Apr. 2003, doi: 10.1016/s0959-440x(03)00032-0.

[86] T. P. J. Knowles, M. Vendruscolo, and C. M. Dobson, "The amyloid state and its association with protein misfolding diseases," *Nat. Rev. Mol. Cell Biol.*, vol. 15, p. 384, May 2014.

[87] M. Stefani and C. M. Dobson, "Protein aggregation and aggregate toxicity: new insights into protein folding, misfolding diseases and biological evolution," *J. Mol. Med.*, vol. 81, no. 11, pp. 678–699, 2003, doi: 10.1007/s00109-003-0464-5.

[88] F. Chiti and C. M. Dobson, "Protein Misfolding, Functional Amyloid, and Human Disease," *Annu. Rev. Biochem.*, vol. 75, no. 1, pp. 333–366, Jun. 2006, doi: 10.1146/annurev.biochem.75.101304.123901.

[89] K. Rajagopal and J. P. Schneider, "Self-assembling peptides and proteins for nanotechnological applications," *Curr. Opin. Struct. Biol.*, vol. 14, no. 4, pp. 480–486, Aug. 2004, doi: 10.1016/J.SBI.2004.06.006.

[90] J. Adamcik, J.-M. Jung, J. Flakowski, P. De Los Rios, G. Dietler, and R. Mezzenga, "Understanding amyloid aggregation by statistical analysis of atomic force microscopy images," *Nat. Nanotechnol.*, vol. 5, p. 423, Apr. 2010.

[91] A. W. P. Fitzpatrick *et al.*, "Atomic structure and hierarchical assembly of a cross-β amyloid fibril," *Proc. Natl. Acad. Sci.*, vol. 110, no. 14, p. 5468, Apr. 2013, doi: 10.1073/pnas.1219476110.

[92] K. L. De Jong, B. Incledon, C. M. Yip, and M. R. DeFelippis, "Amyloid fibrils of glucagon characterized by high-resolution atomic force microscopy," *Biophys. J.*, vol. 91, no. 5, pp. 1905–1914, Sep. 2006, doi: 10.1529/biophysj.105.077438.

[93] X. Zhou *et al.*, "Assembly of glucagon (proto)fibrils by longitudinal addition of oligomers," *Nanoscale*, vol. 3, no. 8, pp. 3049–3051, 2011, doi: 10.1039/C1NR10332F.

[94] P. Salahuddin, M. T. Fatima, A. S. Abdelhameed, S. Nusrat, and R. H. Khan, "Structure of amyloid oligomers and their mechanisms of toxicities: Targeting amyloid oligomers using novel therapeutic approaches," *Eur. J. Med. Chem.*, vol. 114, pp. 41–58, May 2016, doi: 10.1016/J.EJMECH.2016.02.065.

[95] Y. Loo, S. Zhang, and C. A. E. Hauser, "From short peptides to nanofibers to macromolecular assemblies in biomedicine," *Biotechnol. Adv.*, vol. 30, no. 3, pp. 593–603, May 2012, doi: 10.1016/J.BIOTECHADV.2011.10.004.

[96] E. Frare, M. F. Mossuto, P. Polverino de Laureto, M. Dumoulin, C. M. Dobson, and A. Fontana, "Identification of the Core Structure of Lysozyme Amyloid Fibrils by Proteolysis," *J. Mol. Biol.*, vol. 361, no. 3, pp. 551–561, Aug. 2006, doi: 10.1016/J.JMB.2006.06.055.

[97] T. P. J. Knowles and M. J. Buehler, "Nanomechanics of functional and pathological amyloid materials," *Nat. Nanotechnol.*, vol. 6, p. 469, Jul. 2011.

[98] J. P Schmittschmitt and J. Martin Scholtz, *Schmittschmitt, J.P. & Scholtz, J.M. The role of protein stability, solubility, and net charge in amyloid fibril formation. Protein Sci. 12, 2374-2378*, vol. 12. 2003.

[99] H. Yang, S.-Y. Fung, M. Pritzker, and P. Chen, "Mechanical-Force-Induced Nucleation and Growth of Peptide Nanofibers at Liquid/Solid Interfaces,"

Angew. Chemie Int. Ed., vol. 47, no. 23, pp. 4397–4400, May 2008, doi: 10.1002/anie.200705404.

[100] S. Ghodke, S. B. Nielsen, G. Christiansen, H. A. Hjuler, J. Flink, and D. Otzen, "Mapping out the multistage fibrillation of glucagon," *FEBS J.*, vol. 279, no. 5, pp. 752–765, 2012.

[101] O. Yavas *et al.*, "Optical and acoustic study of nucleation and growth of bubbles at a liquid-solid interface induced by nanosecond-pulsed-laser heating," *Appl. Phys. A*, vol. 58, no. 4, pp. 407–415, 1994, doi: 10.1007/BF00323618.

[102] P. Arosio, T. P. J. Knowles, and S. Linse, "On the lag phase in amyloid fibril formation," *Phys. Chem. Chem. Phys.*, vol. 17, no. 12, pp. 7606–7618, 2015, doi: 10.1039/C4CP05563B.

[103] T. C. T. Michaels and T. P. J. Knowles, "Mean-field master equation formalism for biofilament growth," *Am. J. Phys.*, vol. 82, no. 5, pp. 476–483, Apr. 2014, doi: 10.1119/1.4870004.

[104] V. Hlady and J. Buijs, "Protein adsorption on solid surfaces," *Curr. Opin. Biotechnol.*, vol. 7, no. 1, pp. 72–77, Feb. 1996, doi: 10.1016/S0958-1669(96)80098-X.

[105] K. Kristensen, J. R. Henriksen, and T. L. Andresen, "Adsorption of Cationic Peptides to Solid Surfaces of Glass and Plastic," *PLoS One*, vol. 10, no. 5, pp. e0122419-, May 2015.

[106] D. E. Chico, R. L. Given, and B. T. Miller, "Binding of cationic cell-permeable peptides to plastic and glass," *Peptides*, vol. 24, no. 1, pp. 3–9, Jan. 2003, doi: 10.1016/S0196-9781(02)00270-X.

[107] M. K. Bernett and W. A. Zisman, "Effect of adsorbed water on wetting properties of borosilicate glass, quartz, and sapphire," *J. Colloid Interface*

Sci., vol. 29, no. 3, pp. 413–423, 1969.

[108] F. Baino, M. Marshall, N. Kirk, and C. Vitale-Brovarone, "Design, selection and characterization of novel glasses and glass-ceramics for use in prosthetic applications," *Ceram. Int.*, vol. 42, no. 1, pp. 1482–1491, 2016.

[109] M. Hasanuzzaman, A. Rafferty, M. Sajjia, and A.-G. Olabi, "Properties of Glass Materials," *Ref. Modul. Mater. Sci. Mater. Eng.*, Jan. 2016, doi: 10.1016/B978-0-12-803581-8.03998-9.

[110] J. A. Sauer and D. E. Kline, "Dynamic mechanical properties of polystyrene, polyethylene, and polytetrafluoroethylene at low temperatures," *J. Polym. Sci.*, vol. 18, no. 90, pp. 491–495, 1955.

[111] J. W. Gilman *et al.*, "Flammability properties of polymer− layered-silicate nanocomposites. Polypropylene and polystyrene nanocomposites," *Chem. Mater.*, vol. 12, no. 7, pp. 1866–1873, 2000.

[112] J. Zhu, A. B. Morgan, F. J. Lamelas, and C. A. Wilkie, "Fire properties of polystyrene− clay nanocomposites," *Chem. Mater.*, vol. 13, no. 10, pp. 3774–3780, 2001.

[113] C. H. Suelter and M. DeLuca, "How to prevent losses of protein by adsorption to glass and plastic," *Anal. Biochem.*, vol. 135, no. 1, pp. 112–119, 1983, doi: https://doi.org/10.1016/0003-2697(83)90738-8.

[114] T. Fukazawa, Y. Yamazaki, and Y. Miyamoto, "Reduction of non-specific adsorption of drugs to plastic containers used in bioassays or analyses," *J. Pharmacol. Toxicol. Methods*, vol. 61, no. 3, pp. 329–333, May 2010, doi: 10.1016/J.VASCN.2009.12.005.

[115] D. Song, L. Hsu, and J. au, *Binding of taxol to plastic and glass containers and protein under in vitro conditions*, vol. 85. 1996.

[116] J. J. Palmgrén, J. Mönkkönen, T. Korjamo, A. Hassinen, and S. Auriola,

"Drug adsorption to plastic containers and retention of drugs in cultured cells under in vitro conditions," *Eur. J. Pharm. Biopharm.*, vol. 64, no. 3, pp. 369–378, 2006.

[117] P. Datta, "Stability of digoxin and digitoxin in specimens collected in blood collection tubes containing serum separator gels," *Clin. Biochem.*, vol. 31, no. 4, pp. 273–275, 1998.

[118] C. A. Lipinski, "Drug-like properties and the causes of poor solubility and poor permeability," *J. Pharmacol. Toxicol. Methods*, vol. 44, no. 1, pp. 235–249, 2000.

[119] M. Gorecki, J. R. Votano, and A. Rich, "Peptide inhibitors of sickle hemoglobin aggregation: effect of hydrophobicity," *Biochemistry*, vol. 19, no. 8, pp. 1564–1568, Apr. 1980, doi: 10.1021/bi00549a005.

[120] G. Anand, S. Sharma, A. K. Dutta, S. K. Kumar, and G. Belfort, "Conformational Transitions of Adsorbed Proteins on Surfaces of Varying Polarity," *Langmuir*, vol. 26, no. 13, pp. 10803–10811, Jul. 2010, doi: 10.1021/la1006132.

[121] J. D. Andrade and V. Hlady, "Protein adsorption and materials biocompatibility: A tutorial review and suggested hypotheses," in *Biopolymers/Non-Exclusion HPLC*, 1986, pp. 1–63.

[122] R. Horvath, J. McColl, G. E. Yakubov, and J. J. Ramsden, "Structural hysteresis and hierarchy in adsorbed glycoproteins," *J. Chem. Phys.*, vol. 129, no. 7, p. 071102, Aug. 2008, doi: 10.1063/1.2968127.

[123] S. Rocha, A. Thünemann, M. do Carmo Pereira, M. Coelho, H. Moehwald, and G. Brezesinski, *Influence of Fluorinated and Hydrogenated Nanoparticles on the Structure and Fibrillogenesis of Amyloid beta-Peptide*, vol. 137. 2008.

[124] J. A. Loureiro, S. Rocha, and M. do C. Pereira, "Charged surfactants induce

a non-fibrillar aggregation pathway of amyloid-beta peptide," *J. Pept. Sci.*, vol. 19, no. 9, pp. 581–587, Sep. 2013, doi: 10.1002/psc.2535.

[125] R. Montserret, M. J. McLeish, A. Böckmann, C. Geourjon, and F. Penin, "Involvement of Electrostatic Interactions in the Mechanism of Peptide Folding Induced by Sodium Dodecyl Sulfate Binding," *Biochemistry*, vol. 39, no. 29, pp. 8362–8373, Jul. 2000, doi: 10.1021/bi000208x.

[126] V. N. Uversky and A. L. Fink, "Conformational constraints for amyloid fibrillation: the importance of being unfolded," *Biochim. Biophys. Acta (BBA)-Proteins Proteomics*, vol. 1698, no. 2, pp. 131–153, 2004.

[127] F. Zhang *et al.*, "Epitaxial Growth of Peptide Nanofilaments on Inorganic Surfaces: Effects of Interfacial Hydrophobicity/Hydrophilicity," *Angew. Chemie Int. Ed.*, vol. 45, no. 22, pp. 3611–3613, May 2006, doi: 10.1002/anie.200503636.

[128] C. Schladitz, E. P. Vieira, H. Hermel, and H. Möhwald, "Amyloid-beta-sheet formation at the air-water interface," *Biophys. J.*, vol. 77, no. 6, pp. 3305–3310, Dec. 1999, doi: 10.1016/S0006-3495(99)77161-4.

[129] B. J. Cargile, D. L. Talley, and J. L. Stephenson Jr., "Immobilized pH gradients as a first dimension in shotgun proteomics and analysis of the accuracy of pI predictability of peptides," *Electrophoresis*, vol. 25, no. 6, pp. 936–945, Mar. 2004, doi: 10.1002/elps.200305722.

[130] C. E. Giacomelli and W. Norde, "Conformational Changes of the Amyloid β-Peptide (1–40) Adsorbed on Solid Surfaces," *Macromol. Biosci.*, vol. 5, no. 5, pp. 401–407, May 2005, doi: 10.1002/mabi.200400189.

[131] P. Hao, J. Qian, Y. Ren, and S. K. Sze, "Electrostatic Repulsion-Hydrophilic Interaction Chromatography (ERLIC) versus Strong Cation Exchange (SCX) for Fractionation of iTRAQ-Labeled Peptides," *J. Proteome Res.*, vol.

10, no. 12, pp. 5568–5574, Dec. 2011, doi: 10.1021/pr2007686.

[132] J. J. Gray, "The interaction of proteins with solid surfaces," *Curr. Opin. Struct. Biol.*, vol. 14, no. 1, pp. 110–115, Feb. 2004, doi: 10.1016/J.SBI.2003.12.001.

[133] W. Norde, "Driving forces for protein adsorption at solid surfaces," in *Macromolecular Symposia*, 1996, vol. 103, no. 1, pp. 5–18.

[134] Y. Lvov, K. Ariga, I. Ichinose, and T. Kunitake, "Assembly of Multicomponent Protein Films by Means of Electrostatic Layer-by-Layer Adsorption," *J. Am. Chem. Soc.*, vol. 117, no. 22, pp. 6117–6123, Jun. 1995, doi: 10.1021/ja00127a026.

[135] C. J. Pike, A. J. Walencewicz, C. G. Glabe, and C. W. Cotman, "In vitro aging of ß-amyloid protein causes peptide aggregation and neurotoxicity," *Brain Res.*, vol. 563, no. 1–2, pp. 311–314, Nov. 1991, doi: 10.1016/0006-8993(91)91553-D.

[136] M. Zhu, P. O. Souillac, C. Ionescu-Zanetti, S. A. Carter, and A. L. Fink, "Surface-catalyzed Amyloid Fibril Formation," *J. Biol. Chem.*, vol. 277, no. 52, pp. 50914–50922, Dec. 2002, doi: 10.1074/jbc.M207225200.

[137] J. Idaszek, E. Kijeńska, M. Łojkowski, and W. Swieszkowski, "How important are scaffolds and their surface properties in regenerative medicine," *Appl. Surf. Sci.*, vol. 388, pp. 762–774, Dec. 2016, doi: 10.1016/J.APSUSC.2016.03.038.

[138] T. P. Kunzler, T. Drobek, M. Schuler, and N. D. Spencer, "Systematic study of osteoblast and fibroblast response to roughness by means of surface-morphology gradients," *Biomaterials*, vol. 28, no. 13, pp. 2175–2182, 2007.

[139] B. Chehroudi, D. McDonnell, and D. M. Brunette, "The effects of micromachined surfaces on formation of bonelike tissue on subcutaneous

implants as assessed by radiography and computer image processing," *J. Biomed. Mater. Res. An Off. J. Soc. Biomater. Japanese Soc. Biomater.*, vol. 34, no. 3, pp. 279–290, 1997.

[140] M. Rabe *et al.*, "On-surface aggregation of α-synuclein at nanomolar concentrations results in two distinct growth mechanisms," *ACS Chem. Neurosci.*, vol. 4, no. 3, pp. 408–417, Dec. 2012, doi: 10.1021/cn3001312.

[141] K. Shezad *et al.*, "Surface Roughness Modulates Diffusion and Fibrillation of Amyloid-β Peptide," *Langmuir*, vol. 32, no. 32, pp. 8238–8244, Aug. 2016, doi: 10.1021/acs.langmuir.6b01756.

[142] D. Wang, C. He, M. P. Stoykovich, and D. K. Schwartz, "Nanoscale Topography Influences Polymer Surface Diffusion," *ACS Nano*, vol. 9, no. 2, pp. 1656–1664, Feb. 2015, doi: 10.1021/nn506376n.

[143] H. Stenberg, J. Maaranen, M. Suvanto, and T. T. Pakkanen, *Solvent-assisted and thermal wrinklings of argon plasma treated polystyrene coatings on silicon substrate*, vol. 238. 2014.

[144] P. Asuri, S. S Karajanagi, A. A Vertegel, J. Dordick, and R. S Kane, *Enhanced Stability of Enzymes Adsorbed onto Nanoparticles*, vol. 7. 2007.

[145] C. Palocci *et al.*, "Lipolytic Enzymes with Improved Activity and Selectivity upon Adsorption on Polymeric Nanoparticles," *Biomacromolecules*, vol. 8, no. 10, pp. 3047–3053, Oct. 2007, doi: 10.1021/bm070374l.

[146] X.-C. Shen, X.-Y. Liou, L.-P. Ye, H. Liang, and Z.-Y. Wang, "Spectroscopic studies on the interaction between human hemoglobin and CdS quantum dots," *J. Colloid Interface Sci.*, vol. 311, no. 2, pp. 400–406, Jul. 2007, doi: 10.1016/J.JCIS.2007.03.006.

[147] W. Norde and C. Giacomelli, "BSA structural changes during homomolecular exchange between the adsorbed and the dissolved states,"

J. Biotechnol., vol. 79, no. 3, pp. 259–268, 2000.

[148] P. N. Lewis, F. A. Momany, and H. A. Scheraga, "Folding of Polypeptide Chains in Proteins: A Proposed Mechanism for Folding," *Proc. Natl. Acad. Sci.*, vol. 68, no. 9, p. 2293, Sep. 1971, doi: 10.1073/pnas.68.9.2293.

[149] P. M. H. Heegaard, U. Boas, and D. E. Otzen, "Dendrimer Effects on Peptide and Protein Fibrillation," *Macromol. Biosci.*, vol. 7, no. 8, pp. 1047–1059, Aug. 2007, doi: 10.1002/mabi.200700051.

[150] C. P. Schneider, D. Shukla, and B. L. Trout, "Effects of Solute-Solute Interactions on Protein Stability Studied Using Various Counterions and Dendrimers," *PLoS One*, vol. 6, no. 11, pp. e27665-, Nov. 2011.

[151] I. Y. Podolski, Z. A. Podlubnaya, and O. V Godukhin, "Fullerenes C60, antiamyloid action, the brain, and cognitive processes," *Biophysics (Oxf).*, vol. 55, no. 1, pp. 71–76, 2010, doi: 10.1134/S0006350910010136.

[152] J. J. Palmgrén, J. Mönkkönen, T. Korjamo, A. Hassinen, and S. Auriola, "Drug adsorption to plastic containers and retention of drugs in cultured cells under in vitro conditions," *Eur. J. Pharm. Biopharm.*, vol. 64, no. 3, pp. 369–378, Nov. 2006, doi: 10.1016/J.EJPB.2006.06.005.

[153] M. Rief, F. Oesterhelt, B. Heymann, and H. E. Gaub, "Single molecule force spectroscopy on polysaccharides by atomic force microscopy," *Science (80-.).*, vol. 275, no. 5304, pp. 1295–1297, 1997.

[154] C. Möller, M. Allen, V. Elings, A. Engel, and D. J. Müller, "Tapping-mode atomic force microscopy produces faithful high-resolution images of protein surfaces," *Biophys. J.*, vol. 77, no. 2, pp. 1150–1158, 1999.

[155] T. Kowalewski and D. M. Holtzman, "In situ atomic force microscopy study of Alzheimer's β-amyloid peptide on different substrates: New insights into mechanism of β-sheet formation," *Proc. Natl. Acad. Sci.*, vol.

96, no. 7, pp. 3688–3693, 1999.

[156] H. K. L. Blackley, G. H. W. Sanders, M. C. Davies, C. J. Roberts, S. J. B. Tendler, and M. J. Wilkinson, "In-situ atomic force microscopy study of β-amyloid fibrillization," *J. Mol. Biol.*, vol. 298, no. 5, pp. 833–840, 2000.

[157] C. Goldsbury, J. Kistler, U. Aebi, T. Arvinte, and G. J. . Cooper, "Watching amyloid fibrils grow by time-lapse atomic force microscopy," *J. Mol. Biol.*, vol. 285, no. 1, pp. 33–39, Jan. 1999, doi: 10.1006/JMBI.1998.2299.

[158] F. Caruso, D. N. Furlong, K. Ariga, I. Ichinose, and T. Kunitake, "Characterization of polyelectrolyte− protein multilayer films by atomic force microscopy, scanning electron microscopy, and Fourier transform infrared reflection− absorption spectroscopy," *Langmuir*, vol. 14, no. 16, pp. 4559–4565, 1998.

[159] T. E. Fisher, A. F. Oberhauser, M. Carrion-Vazquez, P. E. Marszalek, and J. M. Fernandez, "The study of protein mechanics with the atomic force microscope," *Trends Biochem. Sci.*, vol. 24, no. 10, pp. 379–384, 1999.

[160] K. C. Neuman and A. Nagy, "Single-molecule force spectroscopy: optical tweezers, magnetic tweezers and atomic force microscopy," *Nat. Methods*, vol. 5, no. 6, p. 491, 2008.

[161] J. D. Harper, C. M. Lieber, and P. T. Lansbury Jr, "Atomic force microscopic imaging of seeded fibril formation and fibril branching by the Alzheimer's disease amyloid-β protein," *Chem. Biol.*, vol. 4, no. 12, pp. 951–959, 1997.

[162] T. Junno, K. Deppert, L. Montelius, and L. Samuelson, "Controlled manipulation of nanoparticles with an atomic force microscope," *Appl. Phys. Lett.*, vol. 66, no. 26, pp. 3627–3629, 1995.

[163] O. Custance, R. Perez, and S. Morita, "Atomic force microscopy as a tool for atom manipulation," *Nat. Nanotechnol.*, vol. 4, no. 12, p. 803, 2009.

[164] N. Oyabu, O. Custance, I. Yi, Y. Sugawara, and S. Morita, "Mechanical vertical manipulation of selected single atoms by soft nanoindentation using near contact atomic force microscopy," *Phys. Rev. Lett.*, vol. 90, no. 17, p. 176102, 2003.

[165] G. Binnig, C. F. Quate, and C. Gerber, "Atomic Force Microscope," *Phys. Rev. Lett.*, vol. 56, no. 9, pp. 930–933, Mar. 1986, doi: 10.1103/PhysRevLett.56.930.

[166] F. J. Giessibl, "Advances in atomic force microscopy," *Rev. Mod. Phys.*, vol. 75, no. 3, pp. 949–983, Jul. 2003, doi: 10.1103/RevModPhys.75.949.

[167] N. Jalili and K. Laxminarayana, "A review of atomic force microscopy imaging systems: application to molecular metrology and biological sciences," *Mechatronics*, vol. 14, no. 8, pp. 907–945, 2004.

[168] B. Cappella and G. Dietler, "Force-distance curves by atomic force microscopy," *Surf. Sci. Rep.*, vol. 34, no. 1–3, pp. 1–104, 1999.

[169] E. Jensen, "Types of Imaging, Part 3: Atomic Force Microscopy," *Anat. Rec.*, vol. 296, no. 2, pp. 179–183, Feb. 2013, doi: 10.1002/ar.22605.

[170] S. Naeem, Y. Liu, H.-Y. Nie, W. M. Lau, and J. Yang, "Revisiting atomic force microscopy force spectroscopy sensitivity for single molecule studies," *J. Appl. Phys.*, vol. 104, no. 11, p. 114504, 2008.

[171] J. L. Hutter and J. Bechhoefer, "Calibration of atomic-force microscope tips," *Rev. Sci. Instrum.*, vol. 64, no. 7, pp. 1868–1873, 1993.

[172] T. Junno, S. Anand, K. Deppert, L. Montelius, and L. Samuelson, "Contact mode atomic force microscopy imaging of nanometer-sized particles," *Appl. Phys. Lett.*, vol. 66, no. 24, pp. 3295–3297, 1995.

[173] D. Rugar and P. Hansma, "Atomic force microscopy," *Phys. Today*, vol. 43, no. 10, pp. 23–30, 1990.

[174] Y. Sugawara, M. Ohta, H. Ueyama, and S. Morita, "Defect motion on an InP (110) surface observed with noncontact atomic force microscopy," *Science (80-.).*, vol. 270, no. 5242, pp. 1646–1648, 1995.

[175] S. Kitamura and M. Iwatsuki, "Observation of 7× 7 reconstructed structure on the silicon (111) surface using ultrahigh vacuum noncontact atomic force microscopy," *Jpn. J. Appl. Phys.*, vol. 34, no. 1B, p. L145, 1995.

[176] G. Meyer and N. M. Amer, "Novel optical approach to atomic force microscopy," *Appl. Phys. Lett.*, vol. 53, no. 12, pp. 1045–1047, 1988.

[177] J. P. Cleveland, B. Anczykowski, A. E. Schmid, and V. B. Elings, "Energy dissipation in tapping-mode atomic force microscopy," *Appl. Phys. Lett.*, vol. 72, no. 20, pp. 2613–2615, 1998.

[178] 4PK Hansma *et al.*, "Tapping mode atomic force microscopy in liquids," *Appl. Phys. Lett.*, vol. 64, no. 13, pp. 1738–1740, 1994.

[179] P. Eaton and P. West, *Atomic force microscopy*. Oxford university press, 2010.

[180] R. V Lapshin, "Automatic drift elimination in probe microscope images based on techniques of counter-scanning and topography feature recognition," *Meas. Sci. Technol.*, vol. 18, no. 3, p. 907, 2007.

[181] R. V Lapshin, "Automatic lateral calibration of tunneling microscope scanners," *Rev. Sci. Instrum.*, vol. 69, no. 9, pp. 3268–3276, 1998.

[182] R. P. Richter and A. Brisson, "QCM-D on Mica for Parallel QCM-DAFM Studies," *Langmuir*, vol. 20, no. 11, pp. 4609–4613, May 2004, doi: 10.1021/la049827n.

[183] S. M. Notley, M. Eriksson, and L. Wågberg, "Visco-elastic and adhesive properties of adsorbed polyelectrolyte multilayers determined in situ with QCM-D and AFM measurements," *J. Colloid Interface Sci.*, vol. 292, no. 1, pp. 29–37, 2005.

[184] K. Sittel, P. E. Rouse Jr, and E. D. Bailey, "Method for Determining the Viscoelastic Properties of Dilute Polymer Solutions at Audio-Frequencies," *J. Appl. Phys.*, vol. 25, no. 10, pp. 1312–1320, 1954.

[185] B. D. Vogt, C. L. Soles, H.-J. Lee, E. K. Lin, and W. Wu, "Moisture Absorption and Absorption Kinetics in Polyelectrolyte Films: Influence of Film Thickness," *Langmuir*, vol. 20, no. 4, pp. 1453–1458, Feb. 2004, doi: 10.1021/la035239i.

[186] A. Dolatshahi-Pirouz, K. Rechendorff, M. B. Hovgaard, M. Foss, J. Chevallier, and F. Besenbacher, "Bovine serum albumin adsorption on nano-rough platinum surfaces studied by QCM-D," *Colloids Surfaces B Biointerfaces*, vol. 66, no. 1, pp. 53–59, 2008.

[187] M. Bianco *et al.*, "Quartz crystal microbalance with dissipation (QCM-D) as tool to exploit antigen–antibody interactions in pancreatic ductal adenocarcinomadetection," *Biosens. Bioelectron.*, vol. 42, pp. 646–652, Apr. 2013, doi: 10.1016/J.BIOS.2012.10.012.

[188] C. Satriano, M. E. Fragalà, G. Forte, A. M. Santoro, D. La Mendola, and B. Kasemo, "Surface adsorption of fibronectin-derived peptide fragments: the influence of electrostatics and hydrophobicity for endothelial cells adhesion," *Soft Matter*, vol. 8, no. 1, pp. 53–56, 2012.

[189] C. Ayela, F. Roquet, L. Valera, C. Granier, L. Nicu, and M. Pugniere, "Antibody–antigenic peptide interactions monitored by SPR and QCM-D: A model for SPR detection of IA-2 autoantibodies in human serum," *Biosens. Bioelectron.*, vol. 22, no. 12, pp. 3113–3119, 2007.

[190] M. Yoshinari *et al.*, "Adsorption behavior of antimicrobial peptide histatin 5 on PMMA," *J. Biomed. Mater. Res. Part B Appl. Biomater. An Off. J. Soc. Biomater. Japanese Soc. Biomater. Aust. Soc. Biomater. Korean Soc. Biomater.*, vol. 77, no. 1, pp. 47–54, 2006.

[191] P. Roach, D. Farrar, and C. C. Perry, "Interpretation of Protein Adsorption: Surface-Induced Conformational Changes," *J. Am. Chem. Soc.*, vol. 127, no. 22, pp. 8168–8173, Jun. 2005, doi: 10.1021/ja042898o.

[192] C. M. Hoo, N. Starostin, P. West, and M. L. Mecartney, "A comparison of atomic force microscopy (AFM) and dynamic light scattering (DLS) methods to characterize nanoparticle size distributions," *J. Nanoparticle Res.*, vol. 10, no. 1, pp. 89–96, 2008, doi: 10.1007/s11051-008-9435-7.

[193] B. J. Berne and R. Pecora, *Dynamic light scattering: with applications to chemistry, biology, and physics*. Courier Corporation, 2000.

[194] R. Pecora, "Dynamic Light Scattering Measurement of Nanometer Particles in Liquids," *J. Nanoparticle Res.*, vol. 2, no. 2, pp. 123–131, 2000, doi: 10.1023/A:1010067107182.

[195] W. Burchard, "Static and dynamic light scattering from branched polymers and biopolymers," in *Light scattering from polymers*, Springer, 1983, pp. 1–124.

[196] M. Kaszuba, D. McKnight, M. T. Connah, F. K. McNeil-Watson, and U. Nobbmann, "Measuring sub nanometre sizes using dynamic light scattering," *J. Nanoparticle Res.*, vol. 10, no. 5, pp. 823–829, 2008, doi: 10.1007/s11051-007-9317-4.

[197] P. N. Pusey and W. Van Megen, "Dynamic light scattering by non-ergodic media," *Phys. A Stat. Mech. its Appl.*, vol. 157, no. 2, pp. 705–741, Jun. 1989, doi: 10.1016/0378-4371(89)90063-0.

[198] J. D. Clogston and A. K. Patri, "Zeta potential measurement," in *Characterization of nanoparticles intended for drug delivery*, Springer, 2011, pp. 63–70.

[199] R. J. Hunter, *Zeta potential in colloid science: principles and applications*, vol. 2.

Academic press, 2013.

[200] B. J. Kirby and E. F. Hasselbrink Jr., "Zeta potential of microfluidic substrates: 1. Theory, experimental techniques, and effects on separations," *Electrophoresis*, vol. 25, no. 2, pp. 187–202, Jan. 2004, doi: 10.1002/elps.200305754.

[201] T. Missana and A. Adell, "On the applicability of DLVO theory to the prediction of clay colloids stability," *J. Colloid Interface Sci.*, vol. 230, no. 1, pp. 150–156, 2000.

[202] S. Bhattacharjee, "DLS and zeta potential – What they are and what they are not?," *J. Control. Release*, vol. 235, pp. 337–351, Aug. 2016, doi: 10.1016/J.JCONREL.2016.06.017.

[203] W. W. Wilson, M. M. Wade, S. C. Holman, and F. R. Champlin, "Status of methods for assessing bacterial cell surface charge properties based on zeta potential measurements," *J. Microbiol. Methods*, vol. 43, no. 3, pp. 153–164, Jan. 2001, doi: 10.1016/S0167-7012(00)00224-4.

[204] J. Plank and C. Hirsch, "Impact of zeta potential of early cement hydration phases on superplasticizer adsorption," *Cem. Concr. Res.*, vol. 37, no. 4, pp. 537–542, Apr. 2007, doi: 10.1016/J.CEMCONRES.2007.01.007.

[205] C. Vieu *et al.*, "Electron beam lithography: resolution limits and applications," *Appl. Surf. Sci.*, vol. 164, no. 1–4, pp. 111–117, Sep. 2000, doi: 10.1016/S0169-4332(00)00352-4.

[206] A. A. Tseng, K. Chen, C. D. Chen, and K. J. Ma, "Electron beam lithography in nanoscale fabrication: recent development," *IEEE Trans. Electron. Packag. Manuf.*, vol. 26, no. 2, pp. 141–149, 2003.

[207] X.-M. Zhao, Y. Xia, and G. M. Whitesides, "Soft lithographic methods for nano-fabrication," *J. Mater. Chem.*, vol. 7, no. 7, pp. 1069–1074, 1997.

[208] G. Brewer, *Electron-beam technology in microelectronic fabrication*. Elsevier, 2012.

[209] T. L. Odland, "Electron beam sterilization of biological tissues." Google Patents, 20-Mar-2001.

[210] K. L. Christman, E. Schopf, R. M. Broyer, R. C. Li, Y. Chen, and H. D. Maynard, "Positioning Multiple Proteins at the Nanoscale with Electron Beam Cross-Linked Functional Polymers," *J. Am. Chem. Soc.*, vol. 131, no. 2, pp. 521–527, Jan. 2009, doi: 10.1021/ja804767j.

[211] S. Y. Chou, P. R. Krauss, and P. J. Renstrom, "Imprint lithography with 25-nanometer resolution," *Science (80-.).*, vol. 272, no. 5258, pp. 85–87, 1996.

[212] T. Ito and S. Okazaki, "Pushing the limits of lithography," *Nature*, vol. 406, no. 6799, p. 1027, 2000.

[213] C. M. Dobson, "Protein misfolding, evolution and disease," *Trends Biochem. Sci.*, vol. 24, no. 9, pp. 329–332, 1999.

[214] J. D. Harper and P. T. Lansbury Jr, "Models of amyloid seeding in Alzheimer's disease and scrapie: mechanistic truths and physiological consequences of the time-dependent solubility of amyloid proteins," *Annu. Rev. Biochem.*, vol. 66, no. 1, pp. 385–407, 1997.

[215] S. B. Prusiner, "Prions," *Proc. Natl. Acad. Sci.*, vol. 95, no. 23, pp. 13363–13383, 1998.

[216] G. J. Cooper, A. C. Willis, A. Clark, R. C. Turner, R. B. Sim, and K. B. Reid, "Purification and characterization of a peptide from amyloid-rich pancreases of type 2 diabetic patients," *Proc. Natl. Acad. Sci.*, vol. 84, no. 23, pp. 8628–8632, 1987.

[217] A. K. Sato, M. Viswanathan, R. B. Kent, and C. R. Wood, "Therapeutic peptides: technological advances driving peptides into development,"

Curr. Opin. Biotechnol., vol. 17, no. 6, pp. 638–642, Dec. 2006, doi: 10.1016/J.COPBIO.2006.10.002.

[218] C. Soto, E. M. Sigurdsson, L. Morelli, R. Asok Kumar, E. M. Castaño, and B. Frangione, "β-sheet breaker peptides inhibit fibrillogenesis in a rat brain model of amyloidosis: Implications for Alzheimer's therapy," *Nat. Med.*, vol. 4, no. 7, pp. 822–826, 1998, doi: 10.1038/nm0798-822.

[219] E. E. M. G. Loomans, T. A. M. Beumer, K. C. S. Damen, M. A. Bakker, and W. J. G. Schielen, "Real-Time Monitoring of Peptide–Surface and Peptide–Antibody Interaction by Means of Reflectometry and Surface Plasmon Resonance," *J. Colloid Interface Sci.*, vol. 192, no. 1, pp. 238–249, Aug. 1997, doi: 10.1006/JCIS.1997.5008.

[220] M. Dong, M. B. Hovgaard, S. Xu, D. E. Otzen, and F. Besenbacher, "AFM study of glucagon fibrillation via oligomeric structures resulting in interwoven fibrils," *Nanotechnology*, vol. 17, no. 16, pp. 4003–4009, 2006, doi: 10.1088/0957-4484/17/16/001.

[221] K. L. De Jong, B. Incledon, C. M. Yip, and M. R. DeFelippis, "Amyloid Fibrils of Glucagon Characterized by High-Resolution Atomic Force Microscopy," *Biophys. J.*, vol. 91, no. 5, pp. 1905–1914, Sep. 2006, doi: 10.1529/BIOPHYSJ.105.077438.

[222] C. G. Unson, C.-R. Wu, C. P. Cheung, and R. B. Merrifield, "Positively charged residues at positions 12, 17, and 18 of glucagon ensure maximum biological potency," *J. Biol. Chem.*, vol. 273, no. 17, pp. 10308–10312, 1998.

[223] J. S. Pedersen, D. Dikov, J. L. Flink, H. A. Hjuler, G. Christiansen, and D. E. Otzen, "The changing face of glucagon fibrillation: structural polymorphism and conformational imprinting," *J. Mol. Biol.*, vol. 355, no. 3, pp. 501–523, 2006.

[224] M. A. Jackson, N. Caputo, J. R. Castle, L. L. David, C. T. Roberts, and W. K. Ward, "Stable liquid glucagon formulations for rescue treatment and bi-hormonal closed-loop pancreas," *Curr. Diab. Rep.*, vol. 12, no. 6, pp. 705–710, 2012.

[225] C. L. P. Oliveira, M. A. Behrens, J. S. Pedersen, K. Erlacher, D. Otzen, and J. S. Pedersen, "A SAXS study of glucagon fibrillation," *J. Mol. Biol.*, vol. 387, no. 1, pp. 147–161, 2009.

[226] A. Lomakin, D. S. Chung, G. B. Benedek, D. A. Kirschner, and D. B. Teplow, "On the nucleation and growth of amyloid beta-protein fibrils: detection of nuclei and quantitation of rate constants," *Proc. Natl. Acad. Sci.*, vol. 93, no. 3, pp. 1125–1129, 1996.

[227] J. Lee, E. K. Culyba, E. T. Powers, and J. W. Kelly, "Amyloid-β forms fibrils by nucleated conformational conversion of oligomers," *Nat. Chem. Biol.*, vol. 7, no. 9, p. 602, 2011.

[228] E. Chatani and N. Yamamoto, "Recent progress on understanding the mechanisms of amyloid nucleation," *Biophys. Rev.*, vol. 10, no. 2, pp. 527–534, Apr. 2018, doi: 10.1007/s12551-017-0353-8.

[229] J. S. Pedersen, "The nature of amyloid-like glucagon fibrils." SAGE Publications, 2010.

[230] G. R. Ziegler and E. A. Foegeding, "The Gelation Of Proteins," *Adv. Food Nutr. Res.*, vol. 34, pp. 203–298, Jan. 1990, doi: 10.1016/S1043-4526(08)60008-X.

[231] P. Salahuddin, M. T. Fatima, A. S. Abdelhameed, S. Nusrat, and R. H. Khan, "Structure of amyloid oligomers and their mechanisms of toxicities: Targeting amyloid oligomers using novel therapeutic approaches," *Eur. J. Med. Chem.*, vol. 114, pp. 41–58, May 2016, doi:

10.1016/J.EJMECH.2016.02.065.

[232] A. F. Miller, "Gelation of misfolded proteins," in *Macromolecular Symposia*, 2005, vol. 222, no. 1, pp. 109–114.

[233] F. Macchi *et al.*, "Mechanical stress affects glucagon fibrillation kinetics and fibril structure," *Langmuir*, vol. 27, no. 20, pp. 12539–12549, 2011.

[234] C. Tanford, *Physical chemistry of macromolecules*. Wiley, 1961.

[235] A. Staub, L. Sinn, and O. K. Behrens, "Purification and crystallization of glucagon," *J Biol Chem*, vol. 214, no. 2, pp. 619–632, 1955.

[236] D. E. Otzen, O. Kristensen, and M. Oliveberg, "Designed protein tetramer zipped together with a hydrophobic Alzheimer homology: A structural clue to amyloid assembly," *Proc. Natl. Acad. Sci.*, vol. 97, no. 18, p. 9907, Aug. 2000, doi: 10.1073/pnas.160086297.

[237] A. P. Pawar, K. F. DuBay, J. Zurdo, F. Chiti, M. Vendruscolo, and C. M. Dobson, "Prediction of 'Aggregation-prone' and 'Aggregation-susceptible' Regions in Proteins Associated with Neurodegenerative Diseases," *J. Mol. Biol.*, vol. 350, no. 2, pp. 379–392, 2005, doi: https://doi.org/10.1016/j.jmb.2005.04.016.

[238] L. L. Baggio and D. J. Drucker, "Biology of Incretins: GLP-1 and GIP," *Gastroenterology*, vol. 132, no. 6, pp. 2131–2157, May 2007, doi: 10.1053/J.GASTRO.2007.03.054.

[239] P. Marek *et al.*, "Aromatic interactions are not required for amyloid fibril formation by islet amyloid polypeptide but do influence the rate of fibril formation and fibril morphology," *Biochemistry*, vol. 46, no. 11, pp. 3255–3261, 2007.

[240] A. Aggeli *et al.*, "Hierarchical self-assembly of chiral rod-like molecules as a model for peptide β-sheet tapes, ribbons, fibrils, and fibers," *Proc. Natl.*

Acad. Sci., vol. 98, no. 21, pp. 11857–11862, 2001.

[241] B. Forood, E. J. Feliciano, and K. P. Nambiar, "Stabilization of alpha-helical structures in short peptides via end capping.," *Proc. Natl. Acad. Sci.*, vol. 90, no. 3, pp. 838–842, 1993.

[242] T. Shimada, S. Lee, F. S. Bates, A. Hotta, and M. Tirrell, "Wormlike Micelle Formation in Peptide-Lipid Conjugates Driven by Secondary Structure Transformation of the Headgroups," *J. Phys. Chem. B*, vol. 113, no. 42, pp. 13711–13714, Oct. 2009, doi: 10.1021/jp901727q.

[243] Z. Lin, J. J. Cai, L. E. Scriven, and H. T. Davis, "Spherical-to-Wormlike Micelle Transition in CTAB Solutions," *J. Phys. Chem.*, vol. 98, no. 23, pp. 5984–5993, Jun. 1994, doi: 10.1021/j100074a027.

[244] W. Lin, Z. Yang, J. Wang, T. Chen, and X. Shi, "Wormlike micelles with pH-induced rheological property formed by cationic surfactant/anthranilic acid mixed aqueous solution," *J. Mol. Liq.*, vol. 224, pp. 333–337, Dec. 2016, doi: 10.1016/J.MOLLIQ.2016.10.011.

[245] S. . Shah, N. . Jamroz, and Q. . Sharif, "Micellization parameters and electrostatic interactions in micellar solution of sodium dodecyl sulfate (SDS) at different temperatures," *Colloids Surfaces A Physicochem. Eng. Asp.*, vol. 178, no. 1–3, pp. 199–206, Mar. 2001, doi: 10.1016/S0927-7757(00)00697-X.

[246] V. Bhardwaj, P. Sharma, M. S. Chauhan, and S. Chauhan, "Micellization, interaction and thermodynamic study of butylated hydroxyanisole (synthetic antioxidant) and sodium dodecyl sulfate in aqueous-ethanol solution at 25, 30 and 35 °C," *J. Saudi Chem. Soc.*, vol. 20, pp. S109–S114, Sep. 2016, doi: 10.1016/J.JSCS.2012.09.008.

[247] J. R. Bothe, A. Andrews, K. J. Smith, L. A. Joyce, Y. Krishnamachari, and S.

Kashi, “Peptide Oligomerization Memory Effects and Their Impact on the Physical Stability of the GLP-1 Agonist Liraglutide,” *Mol. Pharm.*, vol. 16, no. 5, pp. 2153–2161, May 2019, doi: 10.1021/acs.molpharmaceut.9b00106.

[248] Y. Wang, A. Lomakin, S. Kanai, R. Alex, and G. B. Benedek, “Transformation of Oligomers of Lipidated Peptide Induced by Change in pH,” *Mol. Pharm.*, vol. 12, no. 2, pp. 411–419, Feb. 2015, doi: 10.1021/mp500519s.

[249] P. E. Fraser *et al.*, “Conformation and fibrillogenesis of Alzheimer Aβ peptides with selected substitution of charged residues,” *J. Mol. Biol.*, vol. 244, no. 1, pp. 64–73, 1994.

[250] Y. Chen *et al.*, “Controlled release of liraglutide using thermogelling polymers in treatment of diabetes,” *Sci. Rep.*, vol. 6, p. 31593, 2016.

[251] L. Zhang and G. Bulaj, “Converting peptides into drug leads by lipidation,” *Curr. Med. Chem.*, vol. 19, no. 11, pp. 1602–1618, 2012.

[252] I. Guryanov *et al.*, “Innovative chemical synthesis and conformational hints on the lipopeptide liraglutide,” *J. Pept. Sci.*, vol. 22, no. 7, pp. 471–479, 2016.

[253] S. Poon, N. R. Birkett, S. B. Fowler, B. F. Luisi, C. M. Dobson, and J. Zurdo, “Amyloidogenicity and aggregate cytotoxicity of human glucagon-like peptide-1 (hGLP-1),” *Protein Pept. Lett.*, vol. 16, no. 12, pp. 1548–1556, 2009.

[254] K. L. Zapadka *et al.*, “A pH-induced switch in human glucagon-like peptide-1 aggregation kinetics,” *J. Am. Chem. Soc.*, vol. 138, no. 50, pp. 16259–16265, 2016.

[255] L. Nielsen *et al.*, “Effect of environmental factors on the kinetics of insulin fibril formation: elucidation of the molecular mechanism,” *Biochemistry*, vol. 40, no. 20, pp. 6036–6046, 2001.

[256] L. L. Nielsen, A. A. Young, and D. G. Parkes, “Pharmacology of exenatide

(synthetic exendin-4): a potential therapeutic for improved glycemic control of type 2 diabetes," *Regul. Pept.*, vol. 117, no. 2, pp. 77–88, Feb. 2004, doi: 10.1016/J.REGPEP.2003.10.028.

[257] G. M. Bray, "Exenatide," *Am. J. Heal. Pharm.*, vol. 63, no. 5, pp. 411–418, 2006.

[258] F. Qi *et al.*, "Preparation of uniform-sized exenatide-loaded PLGA microspheres as long-effective release system with high encapsulation efficiency and bio-stability," *Colloids Surfaces B Biointerfaces*, vol. 112, pp. 492–498, 2013.

[259] N. H. Andersen, Y. Brodsky, J. W. Neidigh, and K. S. Prickett, "Medium-dependence of the secondary structure of exendin-4 and glucagon-like-peptide-1," *Bioorg. Med. Chem.*, vol. 10, no. 1, pp. 79–85, 2002.

[260] F. M. Hudson and N. H. Andersen, "Exenatide: NMR/CD evaluation of the medium dependence of conformation and aggregation state," *Pept. Sci. Orig. Res. Biomol.*, vol. 76, no. 4, pp. 298–308, 2004.

[261] C. A. Jimenez-Cruz, G. I. Makhatadze, and A. E. Garcia, "Protonation/deprotonation effects on the stability of the Trp-cage miniprotein," *Phys. Chem. Chem. Phys.*, vol. 13, no. 38, pp. 17056–17063, 2011.

[262] A.-M. Fernandez-Escamilla, F. Rousseau, J. Schymkowitz, and L. Serrano, "Prediction of sequence-dependent and mutational effects on the aggregation of peptides and proteins," *Nat. Biotechnol.*, vol. 22, no. 10, p. 1302, 2004.

[263] H. Levine III, "Thioflavine T interaction with synthetic Alzheimer's disease β-amyloid peptides: Detection of amyloid aggregation in solution," *Protein Sci.*, vol. 2, no. 3, pp. 404–410, 1993.

[264] X. Hu, S. L. Crick, G. Bu, C. Frieden, R. V Pappu, and J.-M. Lee, "Amyloid seeds formed by cellular uptake, concentration, and aggregation of the amyloid-beta peptide," *Proc. Natl. Acad. Sci.*, vol. 106, no. 48, pp. 20324–20329, 2009.

[265] T. A. Horbett and J. L. Brash, "Proteins at Interfaces: Current Issues and Future Prospects," in *Proteins at Interfaces*, vol. 343, American Chemical Society, 1987, pp. 1–33.

[266] C.-S. C. Wu and G. C. Chen, "Adsorption of proteins onto glass surfaces and its effect on the intensity of circular dichroism spectra," *Anal. Biochem.*, vol. 177, no. 1, pp. 178–182, Feb. 1989, doi: 10.1016/0003-2697(89)90036-5.

[267] C. H. Suelter and M. DeLuca, "How to prevent losses of protein by adsorption to glass and plastic," *Anal. Biochem.*, vol. 135, no. 1, pp. 112–119, Nov. 1983, doi: 10.1016/0003-2697(83)90738-8.

[268] R. A. Messing, "Adsorption of proteins on glass surfaces and pertinent parameters for the immobilization of enzymes in the pores of inorganic carriers," *J. Non. Cryst. Solids*, vol. 19, pp. 277–283, Dec. 1975, doi: 10.1016/0022-3093(75)90093-9.

[269] M. Goebel-Stengel, A. Stengel, Y. Taché, and J. R. Reeve, "The importance of using the optimal plasticware and glassware in studies involving peptides," *Anal. Biochem.*, vol. 414, no. 1, p. 38—46, Jul. 2011, doi: 10.1016/j.ab.2011.02.009.

[270] K. Kristensen, J. R. Henriksen, and T. L. Andresen, "Adsorption of cationic peptides to solid surfaces of glass and plastic," *PLoS One*, vol. 10, no. 5, p. e0122419, 2015.

[271] M. G. E. G. Bremer, J. Duval, W. Norde, and J. Lyklema, "Electrostatic interactions between immunoglobulin (IgG) molecules and a charged

sorbent," *Colloids Surfaces A Physicochem. Eng. Asp.*, vol. 250, no. 1–3, pp. 29–42, Dec. 2004, doi: 10.1016/J.COLSURFA.2004.05.026.

[272] M. Wahlgren and T. Arnebrant, "Protein adsorption to solid surfaces," *Trends Biotechnol.*, vol. 9, no. 1, pp. 201–208, 1991.

[273] S. S. Steiner, M. Li, R. Hauser, and R. Pohl, "Stabilized glucagon formulation for bihormonal pump use," *J. Diabetes Sci. Technol.*, vol. 4, no. 6, pp. 1332–1337, Nov. 2010, doi: 10.1177/193229681000400606.

[274] A. A. Feiler, A. Sahlholm, T. Sandberg, and K. D. Caldwell, "Adsorption and viscoelastic properties of fractionated mucin (BSM) and bovine serum albumin (BSA) studied with quartz crystal microbalance (QCM-D)," *J. Colloid Interface Sci.*, vol. 315, no. 2, pp. 475–481, 2007.

[275] Z. Feldötö, T. Pettersson, and A. Dėdinaitė, "Mucin− electrolyte interactions at the solid− liquid interface probed by QCM-D," *Langmuir*, vol. 24, no. 7, pp. 3348–3357, 2008.

[276] D. P. J. Barz, M. J. Vogel, and P. H. Steen, "Determination of the zeta potential of porous substrates by droplet deflection. I. The influence of ionic strength and pH value of an aqueous electrolyte in contact with a borosilicate surface," *Langmuir*, vol. 25, no. 3, pp. 1842–1850, 2009.

[277] B. J. Kirby and E. F. Hasselbrink Jr, "Zeta potential of microfluidic substrates: 1. Theory, experimental techniques, and effects on separations," *Electrophoresis*, vol. 25, no. 2, pp. 187–202, 2004.

[278] K. Bourikas, J. Vakros, C. Kordulis, and A. Lycourghiotis, "Potentiometric mass titrations: experimental and theoretical establishment of a new technique for determining the point of zero charge (PZC) of metal (hydr) oxides," *J. Phys. Chem. B*, vol. 107, no. 35, pp. 9441–9451, 2003.

[279] J. D. Andrade, V. Hlady, and A. P. Wei, "Adsorption of complex proteins

at interfaces," *Pure Appl. Chem.*, vol. 64, no. 11, pp. 1777–1781, Nov. 2007, doi: 10.1351/pac199264111777.

[280] A. Banerjee and H. Onyuksel, "Peptide delivery using phospholipid micelles," *Wiley Interdiscip. Rev. Nanomedicine Nanobiotechnology*, vol. 4, no. 5, pp. 562–574, Sep. 2012, doi: 10.1002/wnan.1185.

[281] J. Han, Y. Fei, F. Zhou, X. Chen, W. Zheng, and J. Fu, "Micellar Nanomedicine of Novel Fatty Acid Modified Xenopus Glucagon-like Peptide-1: Improved Physicochemical Characteristics and Therapeutic Utilities for Type 2 Diabetes," *Mol. Pharm.*, vol. 14, no. 11, pp. 3954–3967, Nov. 2017, doi: 10.1021/acs.molpharmaceut.7b00632.

[282] K. Kubiak-Ossowska, B. Jachimska, and P. A. Mulheran, "How Negatively Charged Proteins Adsorb to Negatively Charged Surfaces: A Molecular Dynamics Study of BSA Adsorption on Silica," *J. Phys. Chem. B*, vol. 120, no. 40, pp. 10463–10468, Oct. 2016, doi: 10.1021/acs.jpcb.6b07646.

[283] B. Jachimska, K. Tokarczyk, M. Łapczyńska, A. Puciul-Malinowska, and S. Zapotoczny, "Structure of bovine serum albumin adsorbed on silica investigated by quartz crystal microbalance," *Colloids Surfaces A Physicochem. Eng. Asp.*, vol. 489, pp. 163–172, Jan. 2016, doi: 10.1016/J.COLSURFA.2015.10.033.

[284] A. M. Yahya, J. C. McElnay, and P. F. D'Arcy, "Drug sorption to glass and plastics.," *Drug Metabol. Drug Interact.*, vol. 6, no. 1, pp. 1–45, 1988.

[285] M. M. Browne, G. V. Lubarsky, M. R. Davidson, and R. H. Bradley, "Protein adsorption onto polystyrene surfaces studied by XPS and AFM," *Surf. Sci.*, vol. 553, no. 1–3, pp. 155–167, Mar. 2004, doi: 10.1016/J.SUSC.2004.01.046.

[286] D. Horinek *et al.*, "Peptide adsorption on a hydrophobic surface results from an interplay of solvation, surface, and intrapeptide forces," *Proc. Natl.*

Acad. Sci., vol. 105, no. 8, p. 2842, Feb. 2008, doi: 10.1073/pnas.0707879105.

[287] Z. Cai and Y. Zhang, "Hydrophobicity-driven unfolding of Trp-cage encapsulated between graphene sheets," *Colloids Surfaces B Biointerfaces*, vol. 168, pp. 103–108, Aug. 2018, doi: 10.1016/J.COLSURFB.2018.03.039.

[288] K. A. Marino and P. G. Bolhuis, "Confinement-Induced States in the Folding Landscape of the Trp-cage Miniprotein," *J. Phys. Chem. B*, vol. 116, no. 39, pp. 11872–11880, Oct. 2012, doi: 10.1021/jp306727r.

[289] O. Mermut, D. C. Phillips, R. L. York, K. R. McCrea, R. S. Ward, and G. A. Somorjai, "In Situ Adsorption Studies of a 14-Amino Acid Leucine-Lysine Peptide onto Hydrophobic Polystyrene and Hydrophilic Silica Surfaces Using Quartz Crystal Microbalance, Atomic Force Microscopy, and Sum Frequency Generation Vibrational Spectroscopy," *J. Am. Chem. Soc.*, vol. 128, no. 11, pp. 3598–3607, Mar. 2006, doi: 10.1021/ja056031h.

[290] J. J. Palmgrén, J. Mönkkönen, T. Korjamo, A. Hassinen, and S. Auriola, "Drug adsorption to plastic containers and retention of drugs in cultured cells under in vitro conditions," *Eur. J. Pharm. Biopharm.*, vol. 64, no. 3, pp. 369–378, Nov. 2006, doi: 10.1016/J.EJPB.2006.06.005.

[291] A. Janshoff, H.-J. Galla, and C. Steinem, "Piezoelectric Mass-Sensing Devices as Biosensors—An Alternative to Optical Biosensors?," *Angew. Chemie Int. Ed.*, vol. 39, no. 22, pp. 4004–4032, Nov. 2000, doi: 10.1002/1521-3773(20001117)39:22<4004::AID-ANIE4004>3.0.CO;2-2.

[292] R. P. Richter and A. Brisson, "Characterization of lipid bilayers and protein assemblies supported on rough surfaces by atomic force microscopy," *Langmuir*, vol. 19, no. 5, pp. 1632–1640, 2003.

[293] J. Y. Martin *et al.*, "Effect of titanium surface roughness on proliferation, differentiation, and protein synthesis of human osteoblast-like cells

(MG63)," *J. Biomed. Mater. Res.*, vol. 29, no. 3, pp. 389–401, 1995.

[294] M. Rabe, D. Verdes, and S. Seeger, "Understanding protein adsorption phenomena at solid surfaces," *Adv. Colloid Interface Sci.*, vol. 162, no. 1–2, pp. 87–106, Feb. 2011, doi: 10.1016/J.CIS.2010.12.007.

[295] R. A. Gittens *et al.*, "The effects of combined micron-/submicron-scale surface roughness and nanoscale features on cell proliferation and differentiation," *Biomaterials*, vol. 32, no. 13, pp. 3395–3403, 2011.

[296] D. D. Deligianni, N. D. Katsala, P. G. Koutsoukos, and Y. F. Missirlis, "Effect of surface roughness of hydroxyapatite on human bone marrow cell adhesion, proliferation, differentiation and detachment strength," *Biomaterials*, vol. 22, no. 1, pp. 87–96, 2000.

[297] K. Rechendorff, M. B. Hovgaard, M. Foss, V. P. Zhdanov, and F. Besenbacher, "Enhancement of protein adsorption induced by surface roughness," *Langmuir*, vol. 22, no. 26, pp. 10885–10888, 2006.

[298] P. E. Scopelliti *et al.*, "The effect of surface nanometre-scale morphology on protein adsorption," *PLoS One*, vol. 5, no. 7, p. e11862, 2010.

[299] M. Lampin, R. Warocquier-Clérout, C. Legris, M. Degrange, and M. F. Sigot-Luizard, "Correlation between substratum roughness and wettability, cell adhesion, and cell migration," *J. Biomed. Mater. Res. An Off. J. Soc. Biomater. Japanese Soc. Biomater.*, vol. 36, no. 1, pp. 99–108, 1997.

[300] M. Berglin, E. Pinori, A. Sellborn, M. Andersson, M. Hulander, and H. Elwing, "Fibrinogen adsorption and conformational change on model polymers: novel aspects of mutual molecular rearrangement," *Langmuir*, vol. 25, no. 10, pp. 5602–5608, 2009.

[301] D. S. Sutherland, M. Broberg, H. Nygren, and B. Kasemo, "Influence of nanoscale surface topography and chemistry on the functional behaviour

of an adsorbed model macromolecule," *Macromol. Biosci.*, vol. 1, no. 6, pp. 270–273, 2001.

[302] M. Zaman, E. Ahmad, A. Qadeer, G. Rabbani, and R. H. Khan, "Nanoparticles in relation to peptide and protein aggregation," *Int. J. Nanomedicine*, vol. 9, pp. 899–912, Feb. 2014, doi: 10.2147/IJN.S54171.

[303] F. A. Denis *et al.*, "Protein adsorption on model surfaces with controlled nanotopography and chemistry," *Langmuir*, vol. 18, no. 3, pp. 819–828, 2002.

[304] D.-P. Song, M.-J. Chen, Y.-C. Liang, Q.-S. Bai, J.-X. Chen, and X.-F. Zheng, "Adsorption of tripeptide RGD on rutile TiO2 nanotopography surface in aqueous solution," *Acta Biomater.*, vol. 6, no. 2, pp. 684–694, Feb. 2010, doi: 10.1016/J.ACTBIO.2009.07.032.

[305] H. Fredriksson *et al.*, "Hole–mask colloidal lithography," *Adv. Mater.*, vol. 19, no. 23, pp. 4297–4302, 2007.

[306] C. Vieu *et al.*, "Electron beam lithography: resolution limits and applications," *Appl. Surf. Sci.*, vol. 164, no. 1–4, pp. 111–117, 2000.

[307] P. Hanarp, D. S. Sutherland, J. Gold, and B. Kasemo, "Control of nanoparticle film structure for colloidal lithography," *Colloids Surfaces A Physicochem. Eng. Asp.*, vol. 214, no. 1–3, pp. 23–36, 2003.

[308] M. Ozboyaci, D. B. Kokh, and R. C. Wade, "Three steps to gold: mechanism of protein adsorption revealed by Brownian and molecular dynamics simulations," *Phys. Chem. Chem. Phys.*, vol. 18, no. 15, pp. 10191–10200, 2016.

[309] A. A. Vertegel, R. W. Siegel, and J. S. Dordick, "Silica nanoparticle size influences the structure and enzymatic activity of adsorbed lysozyme," *Langmuir*, vol. 20, no. 16, pp. 6800–6807, 2004.

[310] E. Roduner, "Size matters: why nanomaterials are different," *Chem. Soc. Rev.*, vol. 35, no. 7, pp. 583–592, 2006.

[311] A. C. Templeton, W. P. Wuelfing, and R. W. Murray, "Monolayer-protected cluster molecules," *Acc. Chem. Res.*, vol. 33, no. 1, pp. 27–36, 2000.

[312] H. S. Mandal and H.-B. Kraatz, "Effect of the Surface Curvature on the Secondary Structure of Peptides Adsorbed on Nanoparticles," *J. Am. Chem. Soc.*, vol. 129, no. 20, pp. 6356–6357, May 2007, doi: 10.1021/ja0703372.

[313] M. S. Lord, M. Foss, and F. Besenbacher, "Influence of nanoscale surface topography on protein adsorption and cellular response," *Nano Today*, vol. 5, no. 1, pp. 66–78, 2010.

[314] J. Feng, J. M. Slocik, M. Sarikaya, R. R. Naik, B. L. Farmer, and H. Heinz, "Influence of the shape of nanostructured metal surfaces on adsorption of single peptide molecules in aqueous solution," *Small*, vol. 8, no. 7, pp. 1049–1059, 2012.

[315] Y. Kim, J.-H. Park, H. Lee, and J.-M. Nam, "How do the size, charge and shape of nanoparticles affect amyloid β aggregation on brain lipid bilayer?," *Sci. Rep.*, vol. 6, p. 19548, 2016.

[316] A. Ranella, M. Barberoglou, S. Bakogianni, C. Fotakis, and E. Stratakis, "Tuning cell adhesion by controlling the roughness and wettability of 3D micro/nano silicon structures," *Acta Biomater.*, vol. 6, no. 7, pp. 2711–2720, Jul. 2010, doi: 10.1016/J.ACTBIO.2010.01.016.

[317] B. Bhushan, "Surface roughness analysis and measurement techniques," in *Modern Tribology Handbook, Two Volume Set*, CRC press, 2000, pp. 79–150.

[318] I. M. Tucker *et al.*, "Laser Doppler Electrophoresis applied to colloids and surfaces," *Curr. Opin. Colloid Interface Sci.*, vol. 20, no. 4, pp. 215–226, Aug. 2015, doi: 10.1016/J.COCIS.2015.07.001.

[319] V. Puddu and C. C. Perry, "Peptide adsorption on silica nanoparticles: evidence of hydrophobic interactions," *ACS Nano*, vol. 6, no. 7, pp. 6356–6363, 2012.

[320] W. Song and H. Chen, "Protein adsorption on materials surfaces with nano-topography," *Chinese Sci. Bull.*, vol. 52, no. 23, pp. 3169–3173, 2007.

[321] J. Jiang, G. Oberdörster, and P. Biswas, "Characterization of size, surface charge, and agglomeration state of nanoparticle dispersions for toxicological studies," *J. Nanoparticle Res.*, vol. 11, no. 1, pp. 77–89, 2009.

[322] G. T. Dolphin, M. Ouberai, P. Dumy, and J. Garcia, "Designed Amyloid β Peptide Fibril—A Tool for High-Throughput Screening of Fibril Inhibitors," *ChemMedChem Chem. Enabling Drug Discov.*, vol. 2, no. 11, pp. 1613–1623, 2007.